JOURNAL OF MATHEMATICAL SCIENCES AND MODELLING

ISSN: 2636-8692

VOLUME I
ISSUE II

VOLUME I ISSUE II
ISSN 2636-8692

September 2018
http://dergipark.gov.tr/jmsm

JOURNAL OF MATHEMATICAL SCIENCES AND MODELLING

Editors

Editorial Board of Journal of Mathematical Sciences and Modelling

Contents

1 **Proximal vortex cycles and vortex nerve structures. Non-concentric, nesting, possibly overlapping homology cell complexes**
James F. Peters **56-72**

2 **On fourth-order jacobsthal quaternions**
Gamaliel Cerda-Morales **73-79**

3 **Improved semi-local convergence of the Gauss-Newton method for systems of equations**
Ioannis K Argyros, Santhosh George **80-85**

4 **On convolution surfaces in Euclidean 3-space**
Selin Aydöner, Kadri Arslan **86-92**

5 **On the influence of far-field model reduction techniques using a coupled FEM-SBFEM approach in time domain**
Marco Schauer **93-104**

6 **Generalized Lie-algebraic structures related to integrable dispersionless dynamical systems and their application**
Oksana E. Hentosh, Yarema A. Prykarpatski, Denis Blackmore, Anatolij Prykarpatski **105-130**

7 **Caustics of wave fronts reflected by a surface**
Alexander Yampolsky, Oleksandr Fursenko **131-137**

Journal of Mathematical Sciences and Modelling, 1 (2) (2018) 80-85

Journal of Mathematical Sciences and Modelling

Journal Homepage: www.dergipark.gov.tr/jmsm
ISSN 2636-8692

Proximal vortex cycles and vortex nerve structures. Non-concentric, nesting, possibly overlapping homology cell complexes

James F. Peters[ab*]

[a]*Computational Intelligence Laboratory, University of Manitoba, WPG, MB, R3T 5V6, Canada*
[b]*Department of Mathematics, Faculty of Arts and Sciences, Adiyaman University, 02040 Adiyaman, Turkey*
[*]*Corresponding author E-mail: james.peters3@umanitoba.ca*

Article Info

Keywords: *Connectedness Proximity, CW Topology, Vortex Cycle, Vortex Nerve*
2010 AMS: *68U05, 55R40, 54E05.*
Received: *18 May 2018*
Accepted: *17 July 2018*
Available online: *30 September 2018*

Abstract

This article introduces proximal planar vortex 1-cycles, resembling the structure of vortex atoms introduced by William Thomson (Lord Kelvin) in 1867 and recent work on the proximity of sets that overlap either spatially or descriptively. Vortex cycles resemble Thomson's model of a vortex atom, inspired by P.G. Tait's smoke rings. A vortex cycle is a collection of non-concentric, nesting 1-cycles with nonempty interiors (*i.e.*, a collection of 1-cycles that share a nonempty set of interior points and which may or may not overlap). Overlapping 1-cycles in a vortex yield an Edelsbrunner-Harer nerve within the vortex. Overlapping vortex cycles constitute a vortex nerve complex. Several main results are given in this paper, namely, a Whitehead CW topology and a Leader uniform topology are outcomes of having a collection of vortex cycles (or nerves) equipped with a connectedness proximity and the case where each cluster of closed, convex vortex cycles and the union of the vortex cycles in the cluster have the same homotopy type.

1. Introduction

This paper introduces vortex cycles restricted to the Euclidean plane. Each vortex cycle A (denoted by $\mathrm{vcyc}A$) is a collection of non-concentric, nesting 1-cycles with nonempty interiors. A 1-cycle is a finite, collection of vertices (0-cells) connected by oriented edges (1-cells) that define a simple, closed path so that there is a path between any pair of vertices in each 1-cycle. A path is simple, provided it has no self-intersections.

Let $\mathrm{vcyc}A$ be a finite region of the Euclidean plane (denoted by $\mathbb{R}^2$). Also, let $\mathrm{bdy}(\mathrm{vcyc}A)$ be a set of boundary points of $\mathrm{vcyc}A$. Then, for every vortex cycle, there is a collection of functions $f : \mathrm{bdy}(\mathrm{vcyc}A) \longrightarrow \mathbb{R}^2$ such that each function maps a $\mathrm{vcyc}A$ boundary point to an interior fixed point shared by the 1-cycles in the vortex. The physical analogue of a vortex cycle is a collection of non-concentric, nesting equipotential curves in an electric field [3, §5.1, pp. 96-97]. This view of vortex cycles befits a proximal physical geometry approach to the study of vortices in the physical world [37].

Oriented 1-cycles by themselves in vortex cycles are closed braids [5] with nonempty interiors. The study of vortex cycles and their spatial as well as descriptive proximities is important in isolating distinctive shape properties such as vertex area, cycle overlap count, hole count, nerve count, perimeter, diameter over surface shape sub-regions. A finite, bounded *planar shape* A (denoted by $\mathrm{sh}A$) is a finite region of the Euclidean plane bounded by a simple closed curve and with a nonempty interior [40]. In effect, a vortex cycle is a system of shapes within a shape[1]

[1]Many thanks to M.Z. Ahmad for pointing this out.

***Email address*:** **james.peters3@umanitoba.ca (J. F. Peters)**

The geometry of vortex cycles is related to the study shape signatures [39], the study of Edelsbrunner-Harer nerves on tessellated, finite, bounded planar regions [32] and the geometry of photon vortices by N.M. Litchinitser [26], overlapping vortices by E. Adelberger, G. Dvali and A. Gruzinov [14], vortex properties of photons and electromagnetic vortices formed by photons by I.V. Dzedolik [13] and vortex atoms introduced by Kelvin [24].

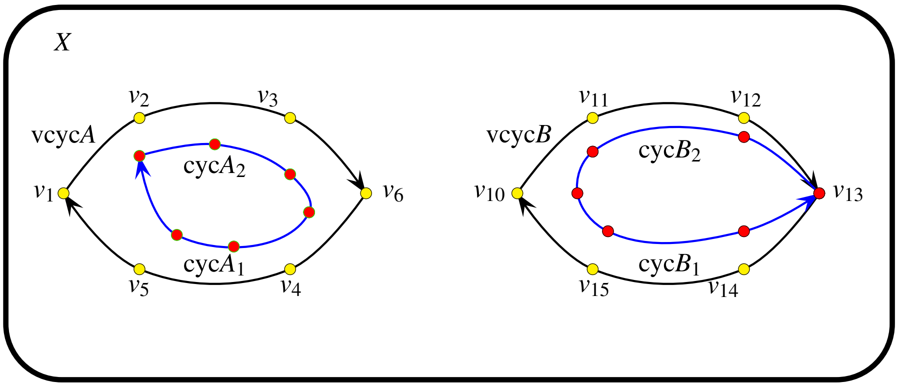

Figure 1: Pair of Two Different Vortex Cycles

Overlapping 1-cycles in a vortex constitute an Edelsbrunner-Harer nerve within the vortex. Let F be a finite collection of sets. An *Edelsbrunner-Harer nerve* [15, §III.2, p. 59] consists of all nonempty subcollections of F (denoted by Nrv$F$) whose sets have nonempty intersection, *i.e.*,

$$\mathrm{Nrv}F = \left\{ X \subseteq F : \bigcap X \neq \emptyset \right\} \text{ (Edelsbrunner-Harer Nerve).}$$

Example 1. Two Forms of Vortex Cycles.
Two different vortex cycles vcyc$A$, vcyc$B$ are shown in Fig. 1. Vortex vcyc$A$ contains a pair of non-overlapping 1-cycles cycA_1, cycA_2. By contrast, vortex vcyc$B$ in Fig. 1 contains a pair of overlapping 1-cycles cycB_1, cycB_2 with a common vertex, namely, v_{13}. Let F be a collection of sets of edges in cycB_1, cycB_2. The pair of 1-cycles in vortex vcyc$B$ constitute an Edelsbrunner-Harer nerve, since cyc$B_1 \cap$ cyc$B_2 = v_{13}$, i.e., *the intersection of 1-cycles cycB_1, cycB_2 is nonempty. The edges of the cycles in both forms of vortices define closed convex curves.* ■

A number of simple results for vortex cycles come from the Jordan Curve Theorem.

Theorem 1. [Jordan Curve Theorem [23]].
A simple closed curve lying on the plane divides the plane into two regions and forms their common boundary.

Proof. For the first complete proof, see O. Veblen [50]. For a simplified proof via the Brouwer Fixed Point Theorem, see R. Maehara [28]. For an elaborate proof, see J.R. Mundres [29, §63, 390-391, Theorem 63.4]. □

Lemma 1. *A finite planar shape contour separates the plane into two distinct regions.*

Proof. The boundary of each planar shape is a finite, simple closed curve. Hence, from Theorem 1, a finite, planar shape separates the plane into two regions, namely, the region outside the shape boundary and the region in the shape interior. □

Theorem 2. *A finite planar vortex cycle is a collection of non-concentric, nesting shapes within a shape.*

Proof. Each 1-cycle in a finite planar vortex cycle is a simple, closed curve. By definition, a vortex cycle is a collection of non-concentric 1-cycles nesting within a 1-cycle, each with a nonempty interior. From Theorem 1, each vortex 1-cycle separates the plane into two regions. Hence, from Lemma 1, a finite planar vortex is a collection of planar shapes within a shape. □

A darkened region in a planar shape represents a hole in the interior of the shape. In cellular homology, a cell complex K is a Hausdorff space and a sequence of subspaces called skeletons [8] (also called a CW complex or Closure-finite Weak topology complex [22]). Minimal planar skeletons are shown in Table 1.

Table 1 includes a $K_{1.5}$ skeleton, which is a filled triangle with a 2-hole in its interior. The fractional dimension of a $K_{1.5}$ skeleton signals the fact such a skeleton has a partially filled interior, punctured with one or more holes. A 2-*hole* is a planar region with a boundary and an empty interior. For example, a finite simple, closed curve that is the boundary of a planar shape defines a 2-hole.
For a recent graphics study of polygons with holes in their interiors, see H. Boomari, M. Ostavari and A. Zarei [20]. Also, from Table 1, it is apparent from the grey shading that a K_2 skeleton is the intersection of three half planes that form a filled triangle. Similarly, a 6-sided 1-cycle such as cycA_2 in vortex cycle vcyc$A$ in Fig. 1 is the intersection of six half planes that construct a 6-gon with a nonempty interior. Recall that a polytope is the intersection of finitely-many closed half planes [53]. In general, a 1-cycle is an n-sided polytope that is the intersection of n half planes.

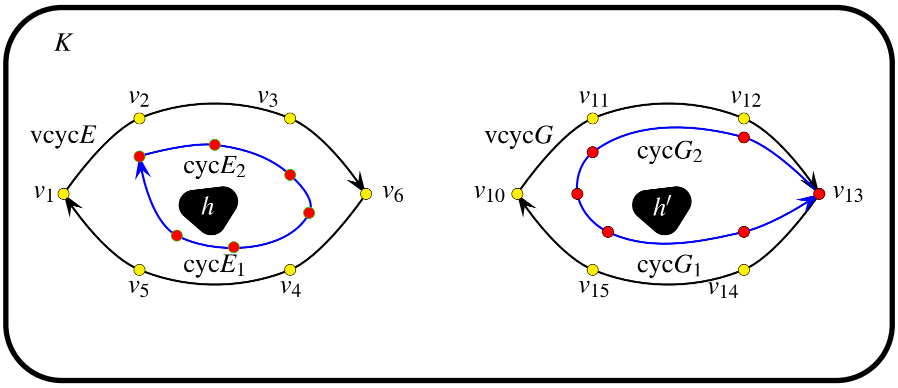

Figure 2: Pair of Two Different Vortex Cycles With Holes

Table 1: Minimal Planar Cell Complex Skeletons

Minimal Skeleton	$K_i, i = 0, 1, 1.5, 2$	Planar Geometry	Interior
	K_0	Vertex	nonempty
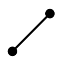	K_1	Line segment	nonempty
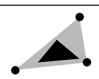	$K_{1.5}$	Partially filled triangle containing a 2-hole	nonempty
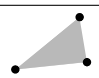	K_2	Filled triangle	nonempty

Problem 1. *How many 2-holes are needed to destroy a 1-cycle, making it a shape boundary with an empty interior?*

Problem 2. *The diameter of a 2-hole is the maximum distance between a pair of points on the boundary of the 2-hole. What is the diameter of a 2-hole in a filled, planar n-sided polytope that destroys a 1-cycle, making it a shape boundary with an empty interior?*

Example 2. Vortex Cycles with Holes.
Two different vortex cycles with holes are shown in Fig. 2, namely, $\mathrm{vcyc}E, \mathrm{vcyc}G$. *The vortex cycle* $\mathrm{vcyc}E$ *is an example of a 1-cycle within a 1-cycle (*i.e., $\mathrm{cyc}E_2$ *within* $\mathrm{cyc}E_1$*) in which* $\mathrm{cyc}E_2$ *has a 2-hole h in its interior. The vortex cycle* $\mathrm{vcyc}G$ *is an example of intersecting 1-cycles (*i.e., $\mathrm{cyc}G_2$ *within* $\mathrm{cyc}G_1$*) that form a vortex nerve in which* $\mathrm{cyc}G_2$ *has a 2-hole* h' *in its interior. In both cases, each inner 1-cycle is in the interior of an outer 1-cycle. Hence, the 2-hole in the interior of the inner 1-cycle is common to the interiors of both 1-cycles in each vortex. For example, 2-hole* h' *in vortex nerve* $\mathrm{vcyc}G$ *is common to both of its 1-cycles.* ■

Theorem 3. *Let K be a collection of skeletons in a planar cell complex.*
1^o In K, skeletons K_0, K_1, K_2 are planar shapes.
2^o A $K_{1.5}$ skeleton is a planar shape.
3^o A 1-cycle cycA with a hole $h \in int(cycA)$ that is a proper subset in the interior of cycA is a planar shape.
4^o A planar vortex cycle with a hole is a collection of overlapping 1-cycles, each with a hole.
5^o A planar vortex cycle with a hole is a collection of concentric planar shapes.

Proof.

1^o: By definition, every member of K is a skeleton. Each of the skeletons K_0, K_1, K_2 has a boundary with nonempty interior. Hence, these skeletons are planar shapes.
2^o: By definition, a $K_{1.5}$ skeleton is a closed 3-sided polytope that has a nonempty interior with a hole. That is, let $h \in \mathrm{int}(cycA)$ be a 2-hole that is a proper subset in the interior of a $K_{1.5}$ skeleton. In that case, the nonempty part of interior of the $K_{1.5}$ skeleton $\mathrm{int}(cycA)$ equals $\mathrm{int}(cycA) \setminus h$. In effect, $cycA$ is a planar shape.
3^o: That a 1-cycle $cycA$ with a hole that is a proper subset in the interior of $cycA$ is a planar shape, follows from Part 2.
4^o: Immediate from Part 3.
5^o: Immediate from Part 3 and Theorem 2.

□

Let (K, δ_Φ) be a collection of planar vortex cycles equipped with a descriptive proximity δ_Φ [6, §4], [35, §1.8], based on the descriptive intersection $\underset{\Phi}{\cap}$ of nonempty sets A and B [33, §3]. With respect to vortex cycles $\mathrm{vcyc}E, \mathrm{vcyc}G$ in K, for example, we consider $\mathrm{vcyc}E \underset{\Phi}{\cap} \mathrm{vcyc}G$, *i.e.*, the set of descriptions common to a pair of vortex cycles. A vortex cycle description is a mapping $\Phi : 2^K \longmapsto \mathbb{R}^n$ (an n-dimensional feature space). For each given vortex cycle vcyc$E$, find all vortex cycles vcyc$G$ in K that have nonempty descriptive intersection with vcyc$E$, *i.e.*, cyc$A \underset{\Phi}{\cap}$ cyc$B \neq \emptyset$ such that $\Phi(\text{vcyc}G) = \Phi(\text{vcyc}E)$. This results in a Leader uniform topology on H_1 [25].

2. Preliminaries

This section briefly presents the axioms for connectedness, strong and descriptive proximity. A nonempty set P is a proximity space, provided the closeness or remoteness of any two subsets in P can be determined.

2.1. Cech Proximity Space

A proximity space P is sometimes called a δ-space [44], provided P is equipped with a relation δ that satisfies, for example, the following Čech axioms for sets $A,B,C \in 2^P$ [48, §2.5, p. 439].

Čech axioms
P1 All subsets in P are far from the empty set.
P2 $A\ \delta\ B \implies B\ \delta\ A$, *i.e.*, A close to B implies B is close to A.
P3 $A\ \delta\ (B \cup C) \Leftrightarrow A\ \delta\ B$ or $A\ \delta\ C$.
P4 $A \cap B \neq \emptyset \implies A\ \delta\ B$.

A space P equipped with the Čech proximity (denoted by (P,δ)) is called a Čech proximity space. We adopt the convention for a proximity metric $\delta : 2^P \times 2^P \longrightarrow \{0,1\}$ introduced by Ju. M. Smirnov [44, §1, p. 8]. We write $\delta(A,B) = 0$, provided subsets $A,B \in 2^P$ are close and $\delta(E,H) = 1$, provided subsets $A,B \in 2^P$ are not close, *i.e.*, there is a non-zero distance between E and H. Let $A,B,C \in 2^P$. Then a proximity space satisfies the following properties.

Smirnov Proximity Space Properties
Q1 If $A \subseteq B$, then for any C, $\delta(A,C) \geq \delta(B,C)$.
Q2 Any sets which intersect are close.
Q3 No set is close to the empty set.

In a Čech proximity space, Smirnov proximity space property Q3 is satisfied by axiom $P1$ and property $Q2$ is satisfied by axioms P2-P4, *i.e.*, any subsets of P are close, provided the subsets have nonempty intersection. That is, A close to B implies B is close to A (axiom P2). Similarly, A close to $B \cup C$ implies A is close to B or A is close to C (axiom P3) or A is close to $B \cap C$ (axiom P4). Let $A \cap C = \emptyset$. Then $\delta(A,C) = 1$, since A has no points in common with C. Similarly, assume $B \cap C = \emptyset$. Then, $\delta(B,C) = 1$, since B and C have no points in common. Hence, property Q1 is satisfied, since

$$\delta(A,C) = \delta(B,C) = 1 \Rightarrow \delta(A,C) \geq \delta(B,C).$$

For $A \subset B$ and $C \subset B$, we have $\delta(A,C) = 0$, since A and C have points in common. Similarly, $\delta(B,C) = 0$. Hence, $\delta(A,C) = \delta(B,C) = 0 \Rightarrow \delta(A,C) \geq \delta(B,C)$.

2.2. Connectedness Proximity Space

Let K be a collection of skeletons in a planar cell complex and let A,B,C be subsets containing skeletons in K equipped with the relation $\overset{conn}{\delta}$. The pair A,B is connected, provided $A \cap B \neq \emptyset$, *i.e.*, there is a skeleton in A that has at least one vertex in common a skeleton in B. Otherwise, A and B are disconnected.
Let X be a nonempty set and let $A,B \in 2^X$, nonempty subsets in the collection of subsets 2^X. A and B are mutually separated, provided $A \cap B = \emptyset$, *i.e.*, A and B have no points in common [52, §26.4, p. 192]. From the notion of separated sets, we obtain the following result for connected spaces.

Theorem 4. *[52]*
If $X = \bigcup\limits_{n-1}^{\infty} X_n$, *where each* $X_n \in 2^X$ *is connected and* $X_{n-1} \cap X_n \neq \emptyset$ *for each* $n \geq 2$, *then space* X *is connected.*

Proof. The proof is given by S. Willard [52, §26.4, p. 193]. For a new kind of connectedness in which nonempty intersection is replaced by strong nearness, see C. Guadagni [19, p. 72] and in J.F. Peters [35, §1.16]. □

In this work, connectedness is defined in terms of the connectedness proximity $\overset{conn}{\delta}$ and overlap connectedness $\overset{\Lsh}{\overset{conn}{\delta}}$ in Section 2.5. In both cases, nonempty intersection is replaced by a connectedness proximity in the study of connected cell complex spaces populated by connected skeletons. For connected sets $A,B \subset K$, we write $A\ \overset{conn}{\delta}\ B$. In effect, for each pair of skeletons A,B in K, $A\ \overset{conn}{\delta}\ B$, provided there is a path between at least one vertex in A and one or more vertices in B. A *path* is sequence of edges between a pair of vertices.

Equivalently, $A \cap B \neq \emptyset$ implies $A \overset{conn}{\delta} B$. If the sets of skeletons $A, B \in K$ are separated (*i.e.*, A, B have no vertices in common), we write $A \overset{conn}{\not\delta} B$. This view of connectedness
Then the Čech axiom P4 is replaced by

P4conn $A \cap B \neq \emptyset \Leftrightarrow A \overset{conn}{\delta} B$.

By replacing δ with $\overset{conn}{\delta}$ in the remaining Čech axioms, we obtain

Connectedness proximity axioms.

P1conn $A \cap B = \emptyset \Leftrightarrow A \overset{conn}{\not\delta} B$, *i.e.*, the sets of skeletons A and B are not close (A and B are far from each other).
P2conn $A \overset{conn}{\delta} B \implies B \overset{conn}{\delta} A$, *i.e.*, A close to B implies B is close to A.
P3conn $A \overset{conn}{\delta} (B \cup C) \implies A \overset{conn}{\delta} B$ or $A \overset{conn}{\delta} C$.
P4conn $A \cap B \neq \emptyset \Leftrightarrow A \overset{conn}{\delta} B$ (Connectedness Axiom).

A connectedness proximity space is denoted by $(K, \overset{conn}{\delta})$. For $A, B \in K$, the Smirnov metric $\delta(A, B) = 0$ means that there is a path between any two vertices in $A \cup B$ and $\delta(A, B) = 1$ means that there is no path between any two vertices in $A \cup B$.

Lemma 2. *Let K be a collection of skeletons in a planar cell complex equipped with the relation $\overset{conn}{\delta}$. Then $A \overset{conn}{\delta} B$ implies $A \cap B \neq \emptyset$.*

Proof. $A \overset{conn}{\delta} B$, provided there is a path between any pair of vertices in skeletons A and B, *i.e.*, A, B are connected, provided there is a vertex common to A and B. Consequently, $A \cap B \neq \emptyset$. □

Lemma 3. *Let K be a connectedness space containing a collection of skeletons in a planar cell complex equipped with the relation $\overset{conn}{\delta}$. The space K is a proximity space.*

Proof. Let $A, B, C \in K$. Smirnov proximity space property Q3 is satisfied by axiom *P1conn* and property *Q*2 is satisfied by axioms **P2conn-P4conn**, *i.e.*, any sets of skeletons that are close, are connected. Let $C \subset A \cup B$ (C is part of the skeleton $A \cup B \in K$). For any vertex p in A or B, there is a path between p and any vertex $q \in C$. Then $A \overset{conn}{\delta} C$ and $B \overset{conn}{\delta} C$. Consequently, $\delta(A, C) = 0 = \delta(B, C)$, Hence, $\delta(A, C) \geq \delta(B, C)$. If $(A \cup B) \cap C = \emptyset$ (the skeletons in A and B have no vertices in common with C), then $\delta(A, C) = 1 = \delta(B, C)$ and $\delta(A, C) \geq \delta(B, C)$. From axiom **P4conn**, we have

$$(A \cup B) \overset{conn}{\not\delta} C \Leftrightarrow (A \cup B) \cap C = \emptyset \Leftrightarrow \delta(A, C) = 1 = \delta(B, C) \Rightarrow \delta(A, C) \geq \delta(B, C).$$

Smirnov property Q1 is satisfied. Hence, $(K, \overset{conn}{\delta})$ is a proximity space. □

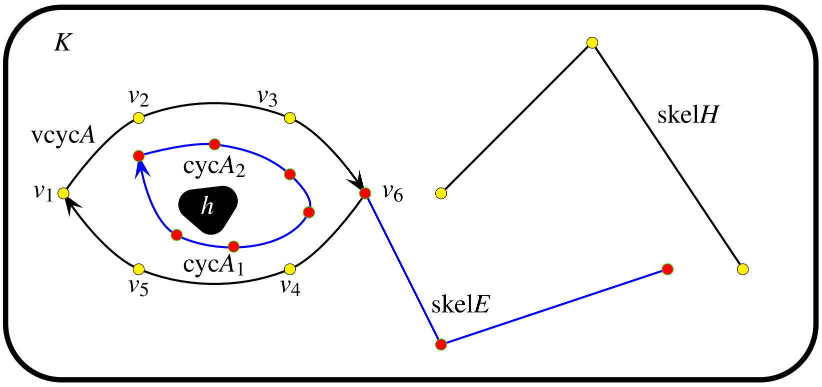

Figure 3: Collection of Skeletons, including a Vortex Cycle with a Hole

Example 3. Connectedness Proximity Space.

Let K be a collection of skeletons represented in Fig. 3, equipped with the proximity $\overset{conn}{\delta}$. A pair of skeletons in K are close, provided the skeletons have at least one vertex in common. For example, vortex cycle vcycA and skeleton skelE have vertex v_6 in common. Hence, from axiom **P4conn**, *we have*

$$v_6 \in vcycA \cap skelE \Leftrightarrow vcycA \overset{conn}{\delta} skelE$$

Skeletons that are not close have no vertices in common. For example, in Fig. 3,

$$skelE \ \overset{conn}{\delta} \ skelH,$$

since the pair of skeletons $skelE, skelH$ have no vertices in common. ■

Theorem 5. *Let K be a collection of vortex cycles in a planar cell complex. The space K equipped with the relation $\overset{conn}{\delta}$ is a proximity space.*

Proof. A vortex cycle is a collection of concentric 1-cycles. Each 1-cycle is a skeleton. Then vortex cycle is a collection of skeletons and each collection of vortex cycles is also a collection of skeletons. Hence, from Lemma 3, K is a connectedness proximity space. □

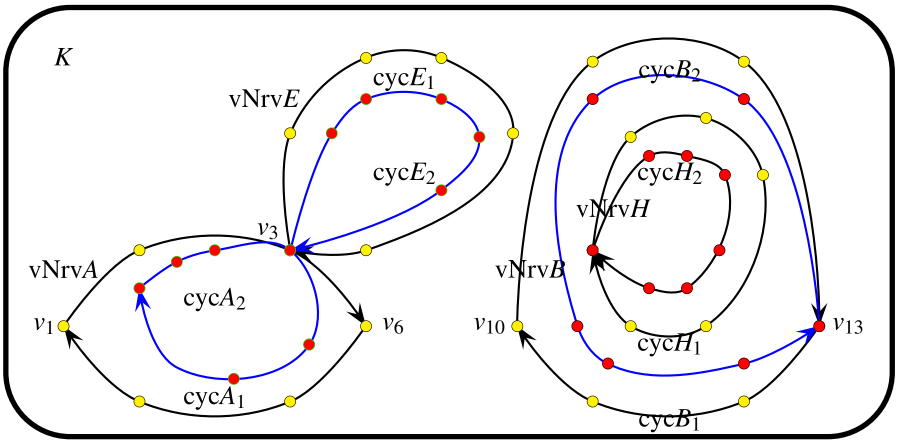

Figure 4: Collection of Proximal Vortex Nerves

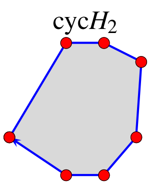

Figure 5: cycH_2 $\in$ vNrv$H$ $\in$ vNrv$B$ in Fig. 4

2.3. Vortex Nerves Proximity space

A vortex cycle vcyc$A$ containing 1-cycles with a common vertex is an example of a vortex nerve (denoted by $vNrvA$). A collection of vortex nerves equipped with the $\overset{conn}{\delta}$ proximity is a connectedness proximity space.

Theorem 6. *Let K be a collection of vortex nerves in a planar cell complex. The space K equipped with the relation $\overset{conn}{\delta}$ is a proximity space.*

Proof. Each vortex nerve is a collection of intersecting 1-cycles, which are skeletons. The results follows from Lemma 3, since K is also a collection of skeletons equipped with the proximity $\overset{conn}{\delta}$. □

Example 4. Vortex Nerves Proximity Space.
Three vortex nerves $vNrvA, vNrvE$ attached to $vNrvA, vNrvB, vNrvH$ in the interior of $vNrvB$ in a cell complex K are represented in Fig. 4. The filled interior of a 1-cycle in a vortex that appears in Fig. 4 is represented with a shaded interior in $cycH_2 \in vNrvH \in vNrvB$ in Fig. 5. For simplicity, the filled interiors of the 1-cycles in Fig. 4 are hidden (not shaded). Let the collection of vortex nerves K be equipped with the proximity $\overset{conn}{\delta}$. Vortex nerves are close, provided the nerves have nonempty intersection. For example, $vNrvA \ \overset{conn}{\delta} \ vNrvE$, i.e., *$\delta(vNrvA, vNrvE) = 0$. Hence, Smirnov property Q2 is satisfied by $\left(K, \overset{conn}{\delta}\right)$. Vortex nerves are far (not close), provided the vortex nerves have empty intersection. For example, $vNrvA \ \overset{conn}{\delta} \ vNrvE$,* i.e., *$\delta(vNrvA, vNrvE) = 1$ (Smirnov property Q3). We also have, for example,*

$$\delta(vNrvA, vNrvH) = 1 = \delta(vNrvB, vNrvH) \text{ non-intersecting nerves are far},$$
$$\delta(vNrvH, vNrvE) = 1 \text{ and } \delta(vNrvA, vNrvE) = 0$$
$$\Leftrightarrow \delta(vNrvH, vNrvE) \geq \delta(vNrvA, vNrvE).$$

In effect, Smirnov property Q1 is satisfied. Hence, $\left(K, \overset{conn}{\delta}\right)$ is a connectedness proximity space. ■

Example 5. Spacetime Vortex Nerves Proximity Space.
Spacetime vortex nerves (overlapping vortex cycles) have been observed in recent studies of ground vortex aerodynamics by J.P. Murphy and D.G. MacManus [30] and in the vortex flows of overlapping jet streams in ground proximity by J.M.M. Barata, N. Bernardo, P.J.C.T. Santos and A.R.R. Silva [4] and by A.R.R. Silva, D.F.G. Durão, J.M.M. Barata, P. Santos S. Ribeiro [43]. Physical vortex nerves can be observed in the representation of the contours of overlapping turbulence velocity vortices in, for example, Figure 6 in [43, p. 8] and systems of vortex in Figure 7 in P.R. Spalart, M. Kh. Strelets, A.K. Travin and M.L. Slur [42]. ■

The presence of holes in the interiors of vortex nerves in a cell complex equipped with the proximity $\overset{conn}{\delta}$ gives us the following result.

Corollary 1. *Let K be a collection of vortex nerves containing holes in their interiors in a planar cell complex. The space K equipped with the relation $\overset{conn}{\delta}$ is a proximity space.*

Proof. Immediate from Theorem 6, since the relationships between vortex nerves in K are unaffected by the presence of holes in the interiors of the nerves. □

Example 6. *A pair of disjoint vortex nerves containing holes in their interiors is represented in Fig. 6.* ■

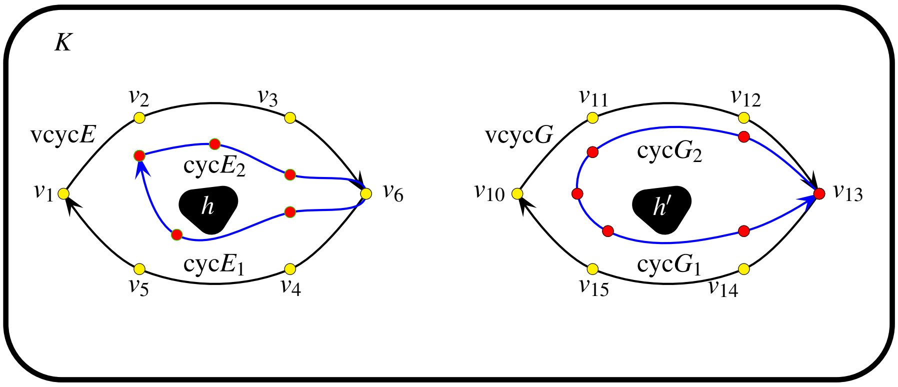

Figure 6: Pair of Disjoint Vortex Nerves With Holes

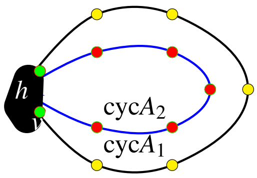

Figure 7: $(\mathrm{cyc}A_1 \cup \mathrm{cyc}A_2) \cap h$

Problem 3. *Let K be a collection of vortex nerves so that the boundary of each of the holes has more than one vertex that is in the intersection 1-cycles in each of the nerves in a planar cell complex. For an example of vortex cycles that overlap vertices on the boundary of a hole, see Fig. 7. Prove that a vortex nerve is destroyed by a hole whose boundary overlaps the nerve cycles in more than one vertex.*

Problem 4. *Let K be a collection of vortex nerves so that the boundary of each of the holes has a single vertex that is in the intersection of the 1-cycles in each of the nerves in a planar cell complex. Also let K be equipped the proximity $\overset{conn}{\delta}$. Prove that K is a connectedness proximity space.*

2.4. Neighbourhoods, Set Closure, Boundary, Interior and CW Topology

The interior of a nonempty set is considered, here. It is the interior of a vortex cycle that leads to strong forms of connectedness proximity on a shapes in cell complex in which the interiors of vortices overlap either spatially or descriptively. Let A be a nonempty set of vertices, $p \in A$ in a bounded region X of the Euclidean plane. An *open ball* $B_r(p)$ with radius r is defined by

$$B_r(p) = \{q \in X : \|p - q\| < r\}.$$

The *closure* of A (denoted by cl$A$) is defined by

$$\mathrm{cl}A = \{q \in X : B_r(q) \subset A \text{ for some } r\} \text{ (Closure of set } A).$$

The *boundary* of A (denoted by bdy$A$) is defined by

$$\mathrm{bdy}A = \{q \in X : B(q) \subset A \cap X \setminus A\} \text{ (Boundary of set } A).$$

Of great interest in the study of the closeness of vortex cycles is the interior of a shape, found by subtracting the boundary of a shape from its closure. In general, the *interior* of a nonempty set $A \subset X$ (denoted by int$A$) defined by

$$\text{int}A = \text{cl}A - \text{bdy}A \text{ (Interior of set } A).$$

Let the cell complex K be a Hausdorff space. Let A be a cell (skeleton) in K. Each cell decomposition $A, B \in K$ is called a CW complex, provided

Closure Finiteness Closure of every cell (skeleton) cl$A$ intersects on a finite number of other cells.
Weak topology $A \in 2^K$ is closed ($A = \text{bdy}A \cup \text{int}A$), provided $A \cap \text{cl}B$ is closed, *i.e.*,
$A \cap \text{cl}B = \text{bdy}(A \cap \text{cl}B) \cup Int(A \cap \text{cl}B)$.

K has a topology τ that is a CW topology [51], [39, §2.4, p. 81], provided τ has the closure finiteness and weak topology properties.

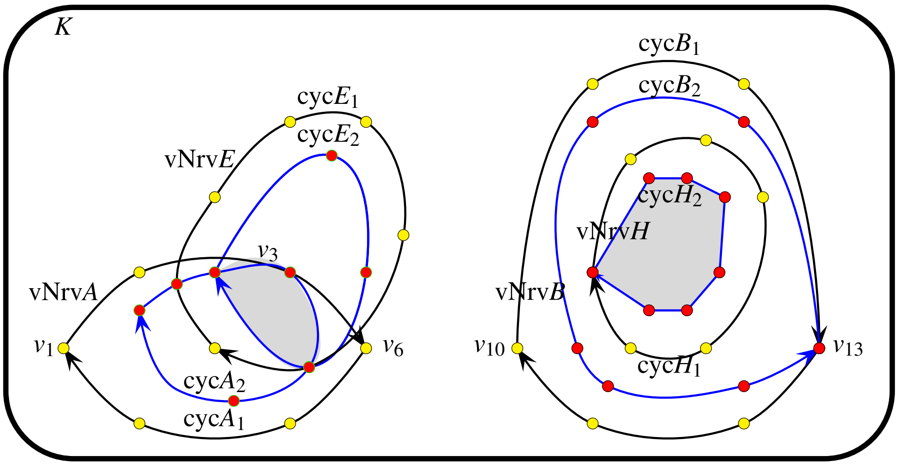

Figure 8: Vortex Nerves with Overlapping Interiors

2.5. Overlap Connectedness Proximity Space

In this section, weak and strong connectedness proximities of skeletons arise when we consider pairs of vortex cycles with overlapping interiors. Let K be a collection of vortex cycles equipped with the proximity $\overset{\curlywedge}{\overset{\mathit{conn}}{\delta}}$, which is a form of the strong proximity $\overset{\curlywedge}{\delta}$ [35, §1.9, pp. 28-30]. The weak and strong forms of $\overset{\curlywedge}{\overset{\mathit{conn}}{\delta}}$ satisfy the following axioms.

P4overlap [weak option] $\text{int}A \cap \text{int}B \neq \emptyset \Rightarrow A \overset{\curlywedge}{\overset{\mathit{conn}}{\delta}} B$.

P5overlap [strong option] $A \overset{\curlywedge}{\overset{\mathit{conn}}{\delta}} B \Rightarrow A \cap B \neq \emptyset$

Axiom **P4overlap** is a rewrite of the Čech axiom **P4** and axiom **P5overlap** is addition to the usual Čech axioms. It is easy to see that $\overset{\curlywedge}{\delta}$ satisfies the remaining Čech axioms after replacing δ with $\overset{\curlywedge}{\delta}$. Let $A, B, C \in K$, a cell complex space equipped with the proximity $\overset{\curlywedge}{\overset{\mathit{conn}}{\delta}}$, which satisfies the following axioms.

Overlap Connectedness proximity axioms.

P1intConn $A \cap B = \emptyset \Leftrightarrow A \overset{\curlywedge}{\overset{\mathit{conn}}{\delta}} B$, *i.e.*, the sets of skeletons A and B are not close (A and B are far from each other).

P2intConn $A \overset{\curlywedge}{\overset{\mathit{conn}}{\delta}} B \implies B \overset{\curlywedge}{\overset{\mathit{conn}}{\delta}} A$, *i.e.*, A overlaps (is close to) B implies B overlaps (is close to) A.

P3intConn $A \overset{\curlywedge}{\overset{\mathit{conn}}{\delta}} (B \cup C) \implies A \overset{\curlywedge}{\overset{\mathit{conn}}{\delta}} B$ or $A \overset{\curlywedge}{\overset{\mathit{conn}}{\delta}} C$.

P4intConn $\text{int}A \cap \text{int}B \neq \emptyset \Rightarrow A \overset{\curlywedge}{\overset{\mathit{conn}}{\delta}} B$ (Weak Overlap Connectedness Axiom).

P5intConn $A \overset{\curlywedge}{\overset{\mathit{conn}}{\delta}} B \Rightarrow A \cap B \neq \emptyset$ (Strong Overlap Connectedness Axiom). ■

An overlap connectedness space is denoted by $\left(K, \overset{\Cap}{\underset{}{\overset{conn}{\delta}}}\right)$. Skeletons A, B in K are close, provided the interior int$A$ has nonempty intersection with the interior int$A$.

Theorem 7. *Let K be a collection of vortex nerves in a planar cell complex. The space K equipped with the relation $\overset{\Cap}{\overset{conn}{\delta}}$ is a proximity space.*

Proof. The result follows from Lemma 3, since K is also a collection of skeletons equipped with the proximity $\overset{conn}{\delta}$. □

Example 7. Overlapping Vortex Nerves.

Two pairs of overlapping vortex nerves are represented in Fig. 8, namely, $vNrvA \overset{\Cap}{\overset{conn}{\delta}} vNrvE$ and $vNrvB \overset{\Cap}{\overset{conn}{\delta}} vNrvH$. In the case of the pair of vortex nerves $vNrvA, vNrvE$, the gray region for these nerves in Fig. 8 represents the nonempty intersection of the interior of the 1-cycle $intcycA_2 \in vNrvA$ and the interior of the 1-cycle $intcycE_2 \in vNrvE$. From axiom P4intConn, we have

$$\begin{aligned} intcycA_2 \cap intcycE_2 \neq \emptyset \Rightarrow\ & cycA_2 \overset{\Cap}{\overset{conn}{\delta}} cycE_2 \\ \Rightarrow\ & vNrvA \overset{\Cap}{\overset{conn}{\delta}} vNrvE, \text{ Axiom P5intConn, we have} \end{aligned}$$

$$vNrvA \overset{\Cap}{\overset{conn}{\delta}} vNrvE \Rightarrow intcycA_2 \cap intcycE_2 \neq \emptyset.$$

Concentric vortex nerves $vNrvB, vNrvH$ are also represented in Fig. 8, The interior $IntcycH_2$ is represented in Fig. 5in the vortex nerve $vNrvH$, which is in the interior of vortex nerve $vNrvB$. Again, from axiom P4intConn, we have

$$intvNrv\ B \cap int\ vNrv\ H \neq \emptyset \Rightarrow vNrv\ B \overset{\Cap}{\overset{conn}{\delta}} vNrv\ H, \text{ and from Axiom P5intConn, we have}$$

$$vNrvB \overset{\Cap}{\overset{conn}{\delta}} vNrvH \Rightarrow intvNrv\ B \cap int\ vNrv\ H \neq \emptyset. \quad \blacksquare$$

Example 8. Spacetime Vortex Cycles: Overlapping Electromagnetic Vortices.
I.V. Dzedolik observes that an electromagnetic vortex is formed by photons that possess some net angular momentum about the longitudinal axis of a dielectric waveguide [12, p. 135]. Photons are almost massless objects that carry energy from an emitter to an absorber [49]. Modeling spiraling vortices as vortex cycles equipped with the $\overset{\Cap}{\overset{conn}{\delta}}$ proximity suggests the possibility of obtaining an expanded range of measurements in vortex optics. N.M. Litchinitser observes that vortex-preshaped femtosecond laser pulses indicate the possibility of achieving repeatable and predictable spatial and temporal distribution in using metamaterials in light filamentation [27, p. 1055]. The overlap connectedness proximity space approach to characterizing, analysing and modelling neighboring photons gains strength by considering recent work by M. Hance on isolating and comparing different forms of photons (and photon vortical flux) [21, §4, pp. 8-11]. ■

2.6. Descriptive Connectedness Proximity

In this section, weak and strong descriptive connectedness proximities of skeletons arise when we consider pairs of vortex cycles with matching description. A vortex cycle description is a feature vector that contains features values extracted from vortices with what are known as probe functions. Let K be a collection of vortex cycles equipped with the descriptive proximity $\overset{\Cap}{\overset{conn}{\delta_\Phi}}$, which is an extension of the descriptive proximity $\overset{\Cap}{\delta_\Phi}$ [7, §3-4, pp. 95-98]. The mapping $\Phi : K \longrightarrow \mathbb{R}^n$ yields an n-dimensional feature vector in Euclidean space $\mathbb{R}^n$ either a vortex cyc$A \in K$ (denoted by $\Phi(\text{cyc}A)$) or a vortex cycle vcyc$E$ in K (denoted by $\Phi(\text{vcyc}E)$) or a vortex nerve vNrv$H$ in K (denoted by $\Phi(\text{vNrv}H)$). For the axioms for a descriptive proximity, the usual set intersection is replaced by descriptive intersection [34, §3] (denoted by $\underset{\Phi}{\cap}$) defined by

$$A \underset{\Phi}{\cap} B = \{x \in A \cup B : \Phi(x) \in \Phi(A),\ \Phi(x) \in \Phi(B)\}.$$

The descriptive closure of A (denoted by cl$_\Phi A$) [35, §1.4, p. 16] is defined by

$$\text{cl}_\Phi A = \left\{ x \in K : x \overset{\Cap}{\overset{conn}{\delta_\Phi}} A \right\}.$$

The weak and strong forms of $\overset{\Cap}{\overset{conn}{\delta_\Phi}}$ satisfy the following axioms.

P$_\Phi$4 [weak option] $\text{int}A \underset{\Phi}{\cap} \text{int}B \neq \emptyset \ \Rightarrow \ A \ \overset{\overset{\Cap}{conn}}{\delta_{\Phi}} \ B.$

P$_\Phi$5 option] $A \ \overset{\overset{\Cap}{conn}}{\delta_{\Phi}} \ B \Rightarrow A \underset{\Phi}{\cap} B \neq \emptyset$

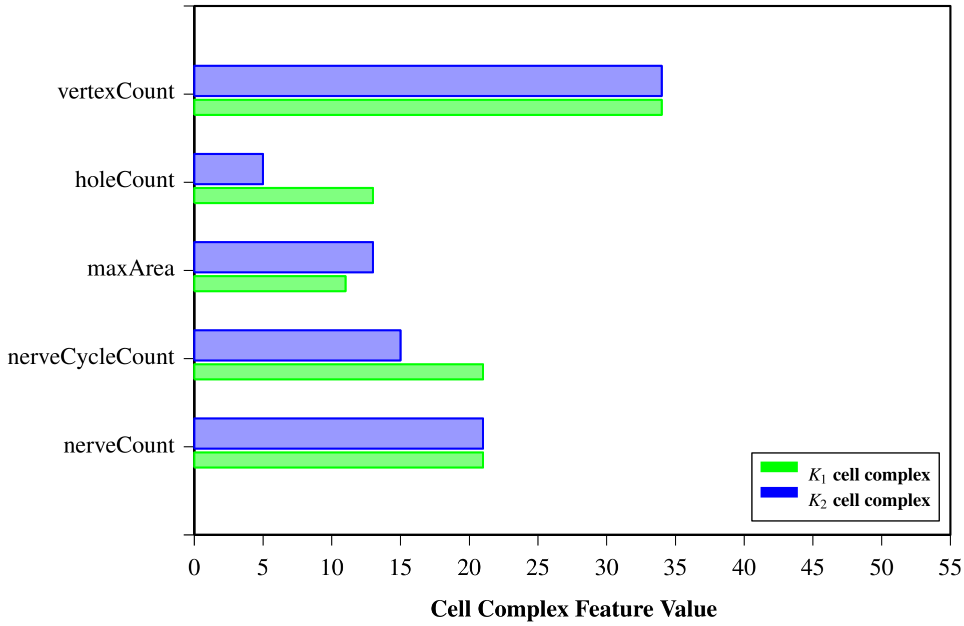

Figure 9: Comparison of Cell Complex Feature Values

Axiom **P$_\Phi$4** is a rewrite of the Čech axiom **P4** and axiom **P$_\Phi$5** is an addition to the usual Čech axioms. It is easy to see that $\overset{\overset{\Cap}{conn}}{\delta_{\Phi}}$ satisfies the remaining Čech axioms after replacing δ with $\overset{\overset{\Cap}{conn}}{\delta_{\Phi}}$. Let $A,B,C \in K$, a cell complex space equipped with the proximity $\overset{\overset{\Cap}{conn}}{\delta_{\Phi}}$, which satisfies the following axioms.

Descriptive Overlap Connectedness proximity axioms.

P$_\Phi$1dConn $A \underset{\Phi}{\cap} B = \emptyset \ \Leftrightarrow A \ \overset{\overset{\Cap}{conn}}{\not\delta_{\Phi}} \ B$, *i.e.*, the sets of skeletons A and B are not descriptively close (A and B are far from each other).

P$_\Phi$2dConn $A \ \overset{\overset{\Cap}{conn}}{\delta_{\Phi}} \ B \ \Longrightarrow \ B \ \overset{\overset{\Cap}{conn}}{\delta_{\Phi}} \ A$, *i.e.*, A is descriptively close to B implies B is descriptively close to A.

P$_\Phi$3dConn $A \ \overset{\overset{\Cap}{conn}}{\delta_{\Phi}} \ (B \cup C) \ \Longrightarrow \ A \ \overset{\overset{\Cap}{conn}}{\delta_{\Phi}} \ B$ or $A \ \overset{\overset{\Cap}{conn}}{\delta_{\Phi}} \ C$.

P$_\Phi$4dConn $\text{int}A \underset{\Phi}{\cap} \text{int}B \neq \emptyset \ \Rightarrow \ A \ \overset{\overset{\Cap}{conn}}{\delta_{\Phi}} \ B$ (Weak Descriptive Connectedness Axiom).

P$_\Phi$5dConn $A \ \overset{\overset{\Cap}{conn}}{\delta_{\Phi}} \ B \Rightarrow A \underset{\Phi}{\cap} B \neq \emptyset$ (Strong Descriptive Connectedness Axiom). ■

A descriptive overlap connectedness space is denoted by $\left(K, \overset{\overset{\Cap}{conn}}{\delta_{\Phi}}\right)$. Skeletons A,B in K are close descriptively, provided the interior int$A$ has nonempty descriptive intersection with the interior int$A$. This form of proximity has many applications, since we often want to compare objects such as 1-cycles by themselves or vortex cycles or the more complex vortex nerves that do not overlap spatially or at the same time.

Example 9. Descriptive Connectedness Overlap of Disjoint Vortex Cycles in Spacetime.

Let $vcycA, vcycB$ be a pair of vortex cycles in a collection of vortex cycles equipped with the proximities $\overset{\overset{\Cap}{conn}}{\delta}$ and $\overset{\overset{\Cap}{conn}}{\delta_{\Phi}}$. Assume these

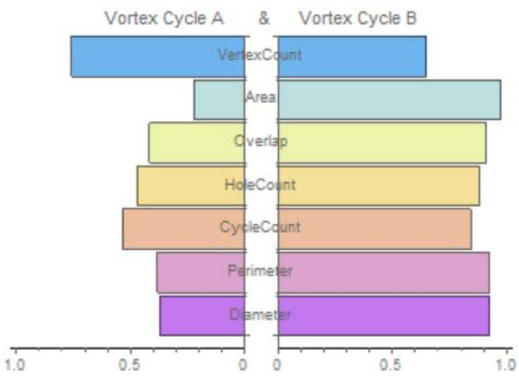

Figure 10: Comparison of Vortex Cell Feature Values

vortices represent non-overlapping electromagnetic vortexes that have matching descriptions in spacetime, e.g., $\Phi(vcycA) = \Phi(vcycB) =$ *(persistence duration). That is, the length of time that vcycA persists equals the duration of vcycB. In that case, vcycA* $\overset{\wedge\!\!\wedge}{\overset{conn}{\delta_{\Phi}}}$ *vcycB.* ■

Example 10. Descriptive Connectedness Overlap of Cell Complexes.
The bar graph[2] *in Fig. 9 compares feature values for a pair of cell complexes, namely, vertex count, hole count, maximum vortex cycle area, nerve cycle count and nerve count. From the bar graph,* $K_1 \overset{\wedge\!\!\wedge}{\overset{conn}{\delta_{\Phi}}} K_2$*, since*

$$\Phi(K_1 vertexCount) = \Phi(K_2 vertexCount) = 35, \text{ and}$$
$$\Phi(K_1 nerveCount) = \Phi(K_2 nerveCount) = 21.$$

This is the case, even though the hole count and nerve cycle count are far apart. ■

Example 11. Absence of Descriptive Connectedness of Sample Vortex Cycles.
The bar graph in Fig. 10 compares normalized feature values for a pair of sample vortex cycles vcycA, vcycB, namely, vertex count, vortex cycle area, overlap (i.e., *number of overlapping 1-cycles in a vortex cycle), hole count, cycle count, perimeter* (i.e., *length of the boundary of a vortex cycle), diameter* (i.e., *maximum distance between a pair of vertices on the boundary of a vortex cycle). From the bar graph, it is apparent that vcycA* $\overset{\wedge\!\!\wedge}{\overset{conn}{\delta_{\Phi}}}$ *vcycB, since there are no matching feature values for the sample pair of vortex cycles.* ■

Theorem 8. *Let K be a collection of vortex cycles in a planar cell complex. The space K equipped with the relation* $\overset{\wedge\!\!\wedge}{\overset{conn}{\delta_{\Phi}}}$ *is a proximity space.*

Proof. The result follows from Lemma 3, since each vortex cycle in K is also a collection of skeletons equipped with the proximity $\overset{\wedge\!\!\wedge}{\overset{conn}{\delta_{\Phi}}}$. □

Corollary 2. *Let K be a collection of vortex nerves in a planar cell complex. The space K equipped with the relation* $\overset{\wedge\!\!\wedge}{\overset{conn}{\delta_{\Phi}}}$ *is a proximity space.*

Proof. The result follows from Theorem 8, since each vortex nerve in K is also a collection of intersecting vortex cycles equipped with the proximity $\overset{\wedge\!\!\wedge}{\overset{conn}{\delta_{\Phi}}}$. □

Example 12. Non-Overlapping Vortex Nerve with Matching Descriptions.

Let K_{vNrv} *be a collection of vortex nerves in a planar cell complex the proximities* $\overset{conn}{\delta}$ *and* $\overset{\wedge\!\!\wedge}{\overset{conn}{\delta_{\Phi}}}$*. Let vNrvA be a vortex nerve and let* $\Phi(vNrvA) =$ *(number of 1-cycles) be a description of the nerve based on one feature, namely, the number of 1-cycles in the nerve. Pairs of*

[2] Many thanks to M.Z. Ahmad for the LaTeX script used to display this bar graph, which does not depend on an external file.

non-overlapping vortex nerves with matching descriptions are represented in Fig. 8, namely,

$$
\begin{aligned}
&vNrvA \ \overset{conn}{\delta} \ vNrvB \ (Nerves\ vNrvA, vNrvB\ do\ not\ overlap),\\
&vNrvA \ \overset{\wedge\!\!\wedge}{\overset{conn}{\delta_{\Phi}}} \ vNrvB,\ since\ \Phi vNrvA) = \Phi(vNrvB) = (2),\\
&vNrvA \ \overset{conn}{\delta} \ vNrvH \ (Nerves\ vNrvA, vNrvH\ do\ not\ overlap),\\
&vNrvA \ \overset{\wedge\!\!\wedge}{\overset{conn}{\delta_{\Phi}}} \ vNrvH\ since\ \Phi(vNrvA) = \Phi(vNrvH) = (2),\\
&vNrvE \ \overset{conn}{\delta} \ vNrvB \ (Nerves\ vNrvE, vNrvB\ do\ not\ overlap),\\
&vNrvE \ \overset{\wedge\!\!\wedge}{\overset{conn}{\delta_{\Phi}}} \ vNrvB\ since\ \Phi(vNrvE) = \Phi(cycH_1) = (2),\\
&vNrvE \ \overset{conn}{\delta} \ vNrvH \ (Nerves\ vNrvE, vNrvH\ do\ not\ overlap),\\
&vNrvE \ \overset{\wedge\!\!\wedge}{\overset{conn}{\delta_{\Phi}}} \ vNrvH\ since\ \Phi(vNrvE) = \Phi(vNrvH) = (2). \quad \blacksquare
\end{aligned}
$$

Example 13. Non-Overlapping Vortex Nerve Cycles with Matching Descriptions.

Let K_{cyc} be a collection of 1-cycles in a planar cell complex the proximities $\overset{conn}{\delta}$ and $\overset{\wedge\!\!\wedge}{\overset{conn}{\delta_{\Phi}}}$. Let cycA be a 1-cycle in a vortex cycle and let $\Phi(cycA) = (number\ of\ vertices)$ be a description of the cycle based on one feature, namely, the number of vertices in the cycle. Pairs of non-overlapping vortex nerves containing 1-cycles with matching descriptions are represented in Fig. 8, namely,

$$
\begin{aligned}
&cycA_2 \ \overset{conn}{\delta} \ cycH_1 \ (Cycles\ cycA_2, cycH_1\ do\ not\ overlap),\\
&cycA_2 \ \overset{\wedge\!\!\wedge}{\overset{conn}{\delta_{\Phi}}} \ cycH_1,\ since\ \Phi(cycA_2) = \Phi(cycH_1) = (6),\\
&cycA_2 \ \overset{conn}{\delta} \ cycB_2 \ (Cycles\ cycA_2, cycB_2\ do\ not\ overlap),\\
&cycA_2 \ \overset{\wedge\!\!\wedge}{\overset{conn}{\delta_{\Phi}}} \ cycB_2\ since\ \Phi(cycA_2) = \Phi(cycB_2) = (6),\\
&cycA_1 \ \overset{conn}{\delta} \ cycH_1 \ (Cycles\ cycA_1, cycH_1\ do\ not\ overlap),\\
&cycA_1 \ \overset{\wedge\!\!\wedge}{\overset{conn}{\delta_{\Phi}}} \ cycH_1\ since\ \Phi(cycA_1) = \Phi(cycH_1) = (6),\\
&cycA_1 \ \overset{conn}{\delta} \ cycB_2 \ (Cycles\ cycA_1, cycB_2\ do\ not\ overlap),\\
&cycA_1 \ \overset{\wedge\!\!\wedge}{\overset{conn}{\delta_{\Phi}}} \ cycB_2\ since\ \Phi(cycA_1) = \Phi(cycB_2) = (6). \quad \blacksquare
\end{aligned}
$$

2.7. Vortex Cycle Spaces Equipped with Proximal Relators

This section introduces a connectedness proximal relator [36] (denoted by $\mathscr{R}$), an extension of a Száz relator [45], which is a non-void collection of connectedness proximity relations on a nonempty cell complex K. A space equipped with a proximal relator $\mathscr{R}$ is called a proximal relator space (denoted by $(K, \mathscr{R})$).

Example 14. Proximal Relator Space. *Example 12 introduces a proximal relator space $\left(K_{vNrv}, \left\{\overset{conn}{\delta}, \overset{\wedge\!\!\wedge}{\overset{conn}{\delta_{\Phi}}}\right\}\right)$, useful in measuring, comparing, and classifying collections of vortex nerves that either have or do not have matching descriptions. Similarly, Example 13 introduces a proximal relator $\left(K_{cyc}, \left\{\overset{conn}{\delta}, \overset{\wedge\!\!\wedge}{\overset{conn}{\delta_{\Phi}}}\right\}\right)$, useful in the study of collections of 1-cycles that either have or do not have matching descriptions.* $\blacksquare$

The connection between $\overset{\wedge\!\!\wedge}{\delta}$ and δ is summarized in Lemma 4.

Lemma 4. *Let $\left(K, \left\{\overset{\wedge\!\!\wedge}{\overset{conn}{\delta_{\Phi}}}, \overset{\wedge\!\!\wedge}{\overset{conn}{\delta}}, \overset{conn}{\delta}\right\}\right)$ be a proximal relator space K, $A, B \subset K$. Then*

1º $A \ \overset{\wedge\!\!\wedge}{\overset{conn}{\delta}} \ B \Rightarrow A \ \overset{conn}{\delta} \ B.$

2º $A \ \overset{\wedge\!\!\wedge}{\overset{conn}{\delta}} \ B \Rightarrow A \ \overset{\wedge\!\!\wedge}{\overset{conn}{\delta_{\Phi}}} \ B.$

Proof.

1^o: From Axiom P5conn, $A \overset{\wedge\!\!\wedge}{\overset{conn}{\delta}} B$ implies $A \cap B \neq \emptyset$, which implies $A \overset{conn}{\delta} B$. From Lemma 2, $A \overset{conn}{\delta} B$ implies $A \cap B \neq \emptyset$, which implies $A\ \delta\ B$ (from Čech Axiom P4).
2^o: From (1), there are cyc $x \in A$, cyc $y \in B$ common to A and B. Hence, $\Phi(\text{cyc } x) = \Phi(\text{cyc } y)$, which implies $A \underset{\Phi}{\cap} B \neq \emptyset$. Then, from the descriptive connectedness Axiom P_Φ4conn, $A \underset{\Phi}{\cap} B \neq \emptyset \Rightarrow A \overset{\wedge\!\!\wedge}{\overset{conn}{\delta_\Phi}} B$. This gives the desired result. □

Let vNrv$A$ be a vortex nerve. By definition, vNrv$A$ is collection of 1-cycles with nonempty intersection. The boundary of vNrv$A$ (denoted by bdyvNrv$A$) is a sequence of connected vertices. That is, for each pair of vertices $v, v' \in$ bdyvNrv$A$, there is a sequence of edges, starting with vertex v and ending with vertex v'. There are no loops in bdyvNrv$A$. Consequently, bdyvNrv$A$ defines a simple, closed polygonal curve. The interior of bdyvNrv$A$ is nonempty, since Nrv$A$ is a collection of filled polytopes. Hence, by definition, a vNrv$A$ is also a nerve shape.

Theorem 9. *Let* $\left(K, \left\{\overset{\wedge\!\!\wedge}{\overset{conn}{\delta_\Phi}}, \overset{\wedge\!\!\wedge}{\overset{conn}{\delta}}\right\}\right)$ *be a proximal relator space with nerve vortices vNrvA, vNrvB* $\in K$. *Then*

1^o vNrvA $\overset{\wedge\!\!\wedge}{\overset{conn}{\delta}}$ *vNrvB implies vNrvA* $\overset{\wedge\!\!\wedge}{\overset{conn}{\delta_\Phi}}$ *vNrvB.*
2^o A 1-cycle cycE $\in$ *vNrvA* $\cap$ *vNrvB implies cycE* $\in$ *vNrvA* $\underset{\Phi}{\cap}$ *vNrvB.*
3^o A 1-cycle cycE $\in$ *vNrvA* $\cap$ *vNrvB implies vNrvA* $\overset{\wedge\!\!\wedge}{\overset{conn}{\delta_\Phi}}$ *vNrvB.*

Proof.
1^o: Immediate from part (2) of Lemma 4.

2^o: By definition, vNrv$A$, vNrv$B$ are nerve shapes. From Axioms **P4conn, P5conn**, cyc$E \in$ vNrv$A \cap$ vNrv$B$, if and only if vNrv$A$ $\overset{\wedge\!\!\wedge}{\overset{conn}{\delta_\Phi}}$ vNrv$B$. Consequently, cyc$E$ is common to vNrv$A$, vNrv$B$. Then there is a cycle cyc$E \in$ Nrv$A$ with the same description as a cycle cyc$E \in$ vNrv$B$. Let $\Phi(\text{cyc}E)$ be a description of cyc$E$. Then, $\Phi(\text{cyc}E) \in \Phi(\text{vNrv}A) \& \in \Phi(\text{cyc}E) \in \Phi(\text{vNrv}B)$, since cyc$E \in$ vNrv$A \cap$ vNrv$B$. Hence, cyc$E \in$ vNrv$A \underset{\Phi}{\cap}$ vNrv$B$.
3^o: Immediate from (2) and Lemma 4. □

3. Main Results

This section gives some main results for collections of proximal vortex cycles and proximal vortex nerves.

3.1. Topology on Vortex Cycle Spaces

This section introduces the construction of topology (homology) classes of vortex cycles and vortex nerves. Topology classes have proved to be useful in classifying physical objects such as quasi-crystals [11] and in knowledge extraction [17]. Such classes provide a basis for knowledge extraction about proximal vortex cycles and nerves. A strong beneficial side-effect of the construction of such classes is the ease with which the persistence of homology class objects can be computed (see, *e.g.*, [16], [2]). More importantly, the construction of topology classes leads to problem size reduction (see, *e.g.*, [31, §3.1, p. 5]).

Lemma 5. *Let K be a nonempty collection of finite skeletons on a finite cell complex K that is a Hausdorff space equipped the proximity* $\overset{conn}{\delta}$. *From the pair* $\left(K, \overset{conn}{\delta}\right)$, *a Whitehead Closure Finite Weak (CW) Topology can be constructed.*

Proof.
From Lemma 3, $\left(K, \overset{conn}{\delta}\right)$ is a connectedness proximity space. Let sk$A$, sk$B$ be skeletons in a finite cell complex K. The closure cl(sk$A$) is finite and includes the connected vertices on the boundary bdy(sk$A$) and in the interior bdy(sk$A$) of sk$A$. Since K is finite, cl(sk$A$) intersects a only a finite number of other skeletons in K. The intersection sk$A \cap$ sk$B \neq \emptyset$ is itself a finite skeleton, which can be either a single vertex or a set of edges common to sk$A$, sk$B$. In that case, sk$A \overset{conn}{\delta}$ sk$B$. By definition, sk$A \cap$ sk$B$ is a skeleton in K. Consequently, whenever sk$A \overset{conn}{\delta}$ sk$B$, then sk$A \cap$ sk$B \in K$. Hence, $\left(K, \overset{conn}{\delta}\right)$ defines a Whitehead CW topology. □

Theorem 10. *Let K be a nonempty collection of finite skeletons on a finite cell complex K that is a Hausdorff space equipped the proximity* $\overset{\wedge\!\!\wedge}{\overset{conn}{\delta}}$. *From the pair* $\left(K, \overset{\wedge\!\!\wedge}{\overset{conn}{\delta}}\right)$, *a Whitehead Closure Finite Weak (CW) Topology can be constructed.*

Proof.
Immediate from Lemma 5. □

Next, we construct a Leader uniform topology on a collection of vortex cycles equipped with the descriptive connectedness proximity $\overset{\wedge\!\!\wedge}{\overset{conn}{\delta_\Phi}}$.

Definition 1. *Let X be a nonempty set. For each given set $A \in 2^X$, form a cluster containing all subsets $B \in 2^X$ such that $A \cap B \neq \emptyset$. The intersection as well as the union of clusters belong to K, defining a Leader uniform topology on K, namely, the collection of all uniform clusters on K.* ■

Theorem 11. *Let K be a finite collection of vortex cycles equipped the proximity $\overset{\curlywedge}{\overset{conn}{\delta}}$ and let τ be a Leader uniform topology on the proximity space $\left(K, \overset{\curlywedge}{\overset{conn}{\delta}}\right)$. Then each cluster of vortex cycles $E \in \tau$ has a CW topology on E.*

Proof.

Each $E \in \tau$ is a finite collection of vortex cycles equipped with the proximity $\overset{\curlywedge}{\overset{conn}{\delta_\Phi}}$. Each closure $\mathrm{cl}(\mathrm{vcyc}H) \in E$ intersects with a finite number of other vortex cycles in E, since E is finite (closure finiteness property). Let $\mathrm{cl}(\mathrm{vcyc}A), \mathrm{cl}(\mathrm{vcyc}B) \in E$. For $\mathrm{int}(\mathrm{vcyc}A) \cap \mathrm{int}(\mathrm{vcyc}B) \neq \emptyset \Rightarrow \mathrm{cl}(\mathrm{vcyc}A) \overset{\curlywedge}{\overset{conn}{\delta}} \mathrm{cl}(\mathrm{vcyc}B)$, from Axiom P4intConn (weak topology property). Hence, E has a CW topology. □

For descriptive proximity spaces, the construction of Leader uniform topologies is accomplished by considering the descriptive intersection $\underset{\Phi}{\cap}$ and descriptive union $\underset{\Phi}{\cup}$ of nonempty sets of vortex cycles. Let K be a nonempty collection of vortex cycles, $A, B \in K$. Then descriptive union $\underset{\Phi}{\cup}$ is defined by

$A \underset{\Phi}{\cup} B = \{E \in K : \Phi(E) \in \Phi(A \cup B)\}$ (**Descriptive union of sets of vortex cycles**).

Lemma 6. *Let K be a nonempty collection of vortex cycles on a finite cell complex K equipped the proximity $\overset{\curlywedge}{\overset{conn}{\delta_\Phi}}$. From the pair $\left(K, \overset{\curlywedge}{\overset{conn}{\delta_\Phi}}\right)$, a Leader uniform topology can be constructed.*

Proof.
We have $\Phi(K) = \{\Phi(\mathrm{vcyc}A) : \mathrm{vcyc}A \in K\}$, the feature space for K. Let $\mathrm{vcyc}A \underset{\Phi}{\cap} \mathrm{vcyc}B \neq \emptyset$ be descriptive intersection of a pair of vortex cycles $\mathrm{vcyc}A, \mathrm{vcyc}B$ in K. From Axiom P_Φ4conn, $\mathrm{vcyc}A \overset{\curlywedge}{\overset{conn}{\delta_\Phi}} \mathrm{vcyc}B$. For each given $\mathrm{vcyc}A$, find all vortex cycles $\mathrm{vcyc}B \in K$ with nonempty intersection $\mathrm{vcyc}A \underset{\Phi}{\cap} \mathrm{vcyc}B \in \Phi(K)$ (intersection property), *i.e.*, all vortex cycles $\mathrm{vcyc}B$ such that $\mathrm{vcyc}A \overset{\curlywedge}{\overset{conn}{\delta_\Phi}} \mathrm{vcyc}B$. Let $A \underset{\Phi}{\cup} B = G$ be a descriptive union of sets of vortex cycles $A, B \in K$. By definition, $\Phi(G) \in \Phi(A \cup B)$ (union property). This gives the desired result. □

Theorem 12. *Let K be a nonempty finite collection of vortex nerves equipped the proximity $\overset{\curlywedge}{\overset{conn}{\delta}}$. The proximity space $\left(K, \overset{\curlywedge}{\overset{conn}{\delta}}\right)$ constructs a Leader uniform topology.*

Proof.
Immediate from Lemma 6. □

From what we have observed so far, a form of problem reduction results from the construction of CW topology on a cluster in a Leader uniform topology.

Theorem 13. *Let $\mathscr{C}$ be a Leader uniform topology cluster in a collection of skeletons K equipped the proximity $\overset{conn}{\delta}$. The proximity space $\left(\mathscr{C}, \overset{conn}{\delta}\right)$ constructs a CW topology.*

Proof.
Immediate from Lemma 5. □

Corollary 3. *Let $\mathscr{C}$ be a Leader uniform topology cluster in a collection of skeletons K equipped the proximity $\overset{\curlywedge}{\overset{conn}{\delta}}$. The proximity space $\left(\mathscr{C}, \overset{\curlywedge}{\overset{conn}{\delta}}\right)$ constructs a CW topology.*

Proof.
Immediate from Theorem 13. □

Corollary 4. *Let $\mathscr{C}$ be a Leader uniform topology cluster in a collection of vortex cycles K equipped the proximity $\overset{\curlywedge}{\overset{conn}{\delta}}$. The proximity space $\left(\mathscr{C}, \overset{\curlywedge}{\overset{conn}{\delta}}\right)$ constructs a CW topology.*

Proof.
Immediate from Theorem 13. □

Corollary 5. *Let $\mathscr{C}$ be a Leader uniform topology cluster in a collection of vortex nerves K equipped the proximity $\overset{\curlywedge}{\overset{conn}{\delta}}$. The proximity space $\left(\mathscr{C}, \overset{\curlywedge}{\overset{conn}{\delta}}\right)$ constructs a CW topology.*

Proof.
Immediate from Theorem 13. □

3.2. Homotopic Types of Vortex Cycles and Vortex Nerves

Theorem 14. [15, §III.2, p. 59] *Let $\mathscr{F}$ be a finite collection of closed, convex sets in Euclidean space. Then the nerve of $\mathscr{F}$ and the union of the sets in $\mathscr{F}$ have the same homotopy type.*

Lemma 7. *Let cycA be a vortex cycle in a finite collection of closed, convex skeletons in a cell complex K. Then vortex cycle cycA and the union of the skeletons in cycA have the same homotopy type.*

Proof. From Theorem 14, we have that the union of the skeletons $\mathrm{sk}E \in \mathrm{cyc}A$ and $\mathrm{cyc}A$ have the same homotopy type. □

Theorem 15. *Let K be a finite collection of vortex cycles equipped the proximity $\overset{\curlywedge}{\overset{conn}{\delta}}$ and let τ be a Leader uniform topology on the proximity space $\left(K, \overset{\curlywedge}{\overset{conn}{\delta}}\right)$. Then each cluster of closed, convex vortex cycles $\mathscr{C} \in \tau$ and the union of vortex cycles in $\mathscr{C}$ have the same homotopy type.*

Proof. Each vortex cycle vcyc$A$ in $\mathscr{C}$ is constructed from a collection of closed, convex skeletons in the cell complex K. Consequently, $\mathscr{C}$ is a collection of closed, convex vortex cycles. Hence, from Lemma 7, we have that the union of the vortex cycles $\mathrm{cyc}A \in \mathscr{C}$ and $\mathscr{C}$ have the same homotopy type. □

Corollary 6. *Let K be a finite collection of vortex nerves equipped the proximity $\overset{\curlywedge}{\overset{conn}{\delta}}$ and let τ be a Leader uniform topology on the proximity space $\left(K, \overset{\curlywedge}{\overset{conn}{\delta}}\right)$. Then each cluster of closed, convex vortex nerves $\mathscr{N} \in \tau$ and the union of vortex nerves in $\mathscr{N}$ have the same homotopy type.*

Proof.
Immediate from Theorem 15, since vortex nerve is a collection of intersecting closed convex vortex cycles in K. □

3.3. Open Problems

This section identifies open problems emerging from the study of proximal vortex cycles and proximal vortex nerves. Vortex cycles can either be spatially close (overlapping vortex cycles have one or more common vertices) or descriptively close (pairs of vortex cycles that intersect descriptively). For such cell complexes, we have the following open problems.

open-1^o Vortex photons can be spatially close (overlap). From Theorem 11, a CW topology can be constructed on each cluster of vortex photons in a uniform Leader topology on a collection of vortex photons. In that case, the problem of considering the spatial closeness of vortex photons for classification and analysis purposes, is simplified by considering a CW topology on each cluster of intersecting vortex photons. This is a form of problem reduction, which has not yet been attempted.

open-2^o The space between the spiraling flux of vortex photons can be viewed as holes. Modelling vortex photons with holes using a combination of connectedness proximity and CW topology on clusters of such photons for classification and analysis purposes, is an open problem. This is a form of knowledge extraction.

open-3^o It is well-known that real elementary particles can have the form of knots [18], which have various forms in knot theory [46]. Vortex cycles can be viewed as collections of intersecting knots. The collection of all possible configurations of spatially close vortex cycles is an open problem.

open-4^o A class of elementary particles known as glueballs exist as knotted chromodynamics flux lines [18]. Vortex nerves can be viewed as collections of intersecting (overlapping) glueballs. The collection of all possible configurations of spatially close vortex nerves is an open problem.

open-5^o From what has been observed in this paper, vortex cycles can be spatially close (overlap) vortex nerves. The collection of all possible configurations of vortex cycles spatially close to vortex nerves is an open problem.

open-6^o Let the cell complex K be a Hausdorff space equipped with $\overset{\curlywedge}{\overset{conn}{\delta_{\Phi}}}$ and descriptive closure cl_{Φ}. Let A be a cell (skeleton) in K. A descriptive CW complex can be defined on each cell decomposition $A, B \in K$, if and only if

descriptive Closure Finiteness Closure of every cell (skeleton) $\mathrm{cl}_{\Phi}A$ intersects on a finite number of other cells.
descriptive Weak topology $A \in 2^K$ is descriptively closed ($A = \mathrm{cl}_{\Phi}A$), provided $A \underset{\Phi}{\cap} \mathrm{cl}_{\Phi}B$ is closed, *i.e.*, $A \underset{\Phi}{\cap} \mathrm{cl}B = \mathrm{cl}_{\Phi}(A \cap \mathrm{cl}B)$.

Prove that K has a topology τ that is a descriptive CW topology, provided τ has the descriptive closure finiteness and descriptive weak topology properties.

open-7^o Let K be a finite collection of vortex cycles that is a Hausdorff space equipped the proximity $\overset{\Lambda\!\!\Lambda}{\overset{conn}{\delta_{\Phi}}}$ and descriptive closure cl_{Φ} and let τ be a Leader uniform topology on the proximity space $\left(K, \overset{\Lambda\!\!\Lambda}{\overset{conn}{\delta_{\Phi}}}\right)$. Prove that each cluster of vortex cycles $E \in \tau$ has a descriptive CW topology on E.

open-8^o Let K be a finite collection of vortex nerves that is a Hausdorff space equipped the proximity $\overset{\Lambda\!\!\Lambda}{\overset{conn}{\delta_{\Phi}}}$ and descriptive closure cl_{Φ} and let τ be a Leader uniform topology on the proximity space $\left(K, \overset{\Lambda\!\!\Lambda}{\overset{conn}{\delta_{\Phi}}}\right)$. Prove that each cluster of vortex cycles $E \in \tau$ has a descriptive CW topology on E.

open-9^o Inner and outer contours on maximal nucleus clusters (MNCs) on tessellated digital images [38, §8.9-8.2] form vortex cycles. An open problem is to construct a CW topology on collections of MNC vortex cycles equipped with the relator $\left\{\overset{conn}{\delta}, \overset{\Lambda\!\!\Lambda}{\overset{conn}{\delta}}, \overset{\Lambda\!\!\Lambda}{\overset{conn}{\delta_{\Phi}}}\right\}$.

open-10^o An open problem is to construct a Leader uniform topology on a collection of MNC vortex cycles equipped with the relator $\left\{\overset{conn}{\delta}, \overset{\Lambda\!\!\Lambda}{\overset{conn}{\delta}}, \overset{\Lambda\!\!\Lambda}{\overset{conn}{\delta_{\Phi}}}\right\}$ and a CW topology on a Leader uniform topology cluster.

open-11^o Brain tissue tessellation shows an absence of canonical microcircuits [41]. For related work on donut-like trajectories along preferential brain railways, shaped as a torus, see, *e.g.*, [47]. An open problem is to construct a CW topology on a Leader uniform topology cluster (equipped with the proximity $\overset{\Lambda\!\!\Lambda}{\overset{conn}{\delta}}$ or with $\overset{\Lambda\!\!\Lambda}{\overset{conn}{\delta_{\Phi}}}$) that results from a brain tissue tessellation. This is an application of the result from Problem 9.

open-12^o **Vortex Cat in spacetime**. By tessellating a video frame showing a cat, finding the maximum nucleus cluster MNC on the tessellated frame, and constructing fine and coarse contours surrounding the MNC nucleus, we obtain a vortex cycle. By repeating these steps over a sequence of frames in a video, we obtain a vortex cat cycle in spacetime. See, for example, the sample vortex cat cycles in [9] and [10]. An open problem is the construction of a Leader uniform topology on the collection of video frame vortex cat cycles equipped with the proximity $\overset{\Lambda\!\!\Lambda}{\overset{conn}{\delta}}$ and to track the persistence of a Leader uniform topology cluster over a video frame sequence.

open-13^o **Čech nerve contours**. Contours on Čech nerve nuclei are introduced in [1, §4.3.2, p. 119ff]. An open problem is to construct a descriptive CW topology on a collection of Čech nerve contours equipped with the proximity $\overset{\Lambda\!\!\Lambda}{\overset{conn}{\delta_{\Phi}}}$. ■

Acknowledgement

Many thanks are extended to the anonymous reviewers for their astute, very helpful suggestions and corrections. The research has been supported by the Natural Sciences & Engineering Research Council of Canada (NSERC) discovery grant 185986, Scientific and Technological Research Council of Turkey (TÜBİTAK) Scientific Human Resources Development (BIDEB) under grant no: 2221-1059B211402463, and Instituto Nazionale di Alta Matematica (INdAM) Francesco Severi, Gruppo Nazionale per le Strutture Algebriche, Geometriche e Loro Applicazioni grant 9 920160 000362, n.prot U 2016/000036.

References

[1] M.Z. Ahmad and J.F. Peters, *Proximal Čech complexes in approximating digital image object shapes. Theory and application*, Theory and Applications of Math. & Comp. Sci. **7** (2017), no. 2, 81–123, MR3769444.

[2] V.A. Baikov, R.R. Gilmanov, I.A. Taimanov, and A.A. Yakovlev, *Topological characteristics of oil and gass reservoirs and their applications*, Integrative Machine Learning, LNAI 10344 (A. Halzinger et. al., ed.), Springer, Berlin, 2017, pp. 182–193.

[3] D. Baldomir and P. Hammond, *Geometry of electromagnetic systems*, Oxford,UK, Clarendon Press, 1996, xi+239 pp., Zbl 0919.76001.

[4] J.M.M. Barata, P.J.C.T. Santos N. Bernardo, and A.R.R. Silva, *Experimental study of a ground vortex: the effect of the crossflow velocity*, 49th AIAA Aerospace Sciences Meeting, AIAA, 2011, pp. 1–9.

[5] J.S. Birman and W.W. Menasco, *Studying links via closed braids. V: the unlink*, Trans. Amer. Math. Soc. **329** (1992), no. 2, 585–606.

[6] A. Di Concilio, C. Guadagni, J.F. Peters, and S. Ramanna, *Descriptive proximities I: Properties and interplay between classical proximities and overlap*, arXiv **1609** (2016), no. 06246v1, 1–12, Math. in Comp. Sci. 2017, `https://doi.org/10.1007/s11786-017-0328-y`, in press.

[7] ______, *Descriptive proximities. properties and interplay between classical proximities and overlap*, Math. Comput. Sci. **12** (2018), no. 1, 91–106, MR3767897.

[8] G.E. Cooke and R.L. Finney, *Homology of cell complexes. based on lectures by norman e. steenrod*, Princeton University Press; University of Tokyo Press, Tokyo, Princeton, New Jersey, 1967, xv+256 pp., MR0219059.

[9] E. Cui, *Video vortex cat cycles part 1*, Tech. report, University of Manitoba, Computational Intelligence Laboratory, Deparment of Electrical & Computer Engineering, U of MB, Winnipeg, MB R3T 5V6, Canada, 2018, `https://youtu.be/rVGmkGTm40c`.

[10] ______, *Video vortex cat cycles part 2*, Tech. report, University of Manitoba, Computational Intelligence Laboratory, Deparment of Electrical & Computer Engineering, U of MB, Winnipeg, MB R3T 5V6, Canada, 2018, `https://youtu.be/yJBCdLhgcqk`.

[11] A. Dareau, E. Levy, M.B. Aguilera, R. Bouganne, E. Akkermans, F. Gerbier, and J. Beugnon, *Revealing the topology of quasicrystals with a diffraction experiment*, arXiv, Physical Review Letters **1607** (2017), no. 00901v2, 1–7, `doi.org/10.1103/PhysRevLett.119.215304`.

[12] I.V. Dzedolik, *Vortex properties of a photon flux in a dielectic waveguide*, Technical Physics **75** (2005), no. 1, 137–140.

[13] ______, *Vortex properties of a photon flux in a dielectric waveguide*, Technical Physics [trans. from Zhurnal Tekhnicheskol Fiziki] **50** (2005), no. 1, 135–138.

[14] G. Dvali E. Adelberger and A. Gruzinov, *Structured light meets structured matter*, Phys. Rev. Letters **98** (2007), 010402–1–010402–4.

[15] H. Edelsbrunner and J.L. Harer, *Computational topology. An introduction*, Amer. Math. Soc., Providence, RI, 2010, xii+241 pp. ISBN: 978-0-8218-4925-5, MR2572029.
[16] M. Fermi, *Persistent topology for natural data analysis - a survey*, arXiv **1706** (2017), no. 00411v2, 1–18.
[17] ———, *Why topology for machine learning and knowledge extraction*, Machine Learning & Knowledge Extraction **1** (2018), no. 6, 1–6, https://doi.org/10.3390/make1010006.
[18] A. Flammini and A. Stasiak, *Natural classification of knots*, Proc. R. Soc. Lond. Ser. A Math. Phys. Eng. Sci. **463** (2017), no. 2078, 569–582, MR2288834.
[19] C. Guadagni, *Bornological convergences on local proximity spaces and ω_μ-metric spaces*, Ph.D. thesis, Università degli Studi di Salerno, Salerno, Italy, 2015, Supervisor: A. Di Concilio, 79pp.
[20] M. Ostavari H. Boomari and A. Zarei, *Recognizing visibility graphs of polygons with holes and internal-external visibility graphs of polygons*, arXiv **1804** (2018), no. 05105v1, 1–16.
[21] M. Hance, *Algebraic structures on nearness approximation spaces*, Ph.D. thesis, University of Pennsylvania, Department of Physics and Astronomy, 2015, supervisor: H.H. Williams, vii+113pp.
[22] A. Hatcher, *Algebraic topology*, Cambridge University Press, Cambridge, UK, 2002, xii+544 pp. ISBN: 0-521-79160-X, MR1867354.
[23] C. Jordan, *Cours d'analyse de l'École polytechnique, tome i-iii*, Éditions Jacques Gabay, Sceaux, 1991, reprint of 1915 edition, Tome I: MR1188186,Tome II: MR1188187, Tome III: MR1188188.
[24] W. Thomson (Lord Kelvin), *On vortex atoms*, Proc. Roy. Soc. Edin. **6** (1867), 94–105.
[25] S. Leader, *On clusters in proximity spaces*, Fundamenta Mathematicae **47** (1959), 205–213.
[26] N.M. Litchinitser, *Structured light meets structured matter*, Science, New Series **337** (2012), no. 6098, 1054–1055.
[27] ———, *Structured light meets structured matter*, Science, New Series **337** (2012), no. 6098, 1054–1055.
[28] R. Maehara, *The Jordan curve theorem via the Brouwer fixed point theorem*, Amer. Math. Monthly **91** (1984), no. 10, 641–643, MR0769530.
[29] J.R. Munkres, *Topology, 2^{nd} ed.*, Prentice-Hall, Englewood Cliffs, NJ, 2000, xvi + 537 pp., 1^{st} Ed. in 1975,MR0464128.
[30] J.P. Murphy and D.G. MacManus, *Ground vortex aerodynamics under crosswind conditions*, Experiments in Fluids **50** (2011), no. 1, 109–124.
[31] M. Pellikka, S. Suuriniemi, and L. Kettunen, *Homology in electromagnetic boundary value problems*, Boundary Value Problems **2010** (2010), no. 381953, 1–18, doi:10.1155/2010/381953.
[32] J. F. Peters and E. İnan, *Strongly proximal Edelsbrunner-Harer nerves*, Proc. Jangjeon Math. Soc. **19** (2016), no. 3, 1–20, MR3618825, zbMATH Zbl 1360.54021.
[33] J.F. Peters, *Local near sets: Pattern discovery in proximity spaces*, Math. in Comp. Sci. **7** (2013), no. 1, 87–106, DOI 10.1007/s11786-013-0143-z, MR3043920, ZBL06156991.
[34] ———, *Local near sets: pattern discovery in proximity spaces*, Math. Comput. Sci. **7** (2013), no. 1, 87–106, MR3043920, ZBL06156991.
[35] ———, *Computational proximity. Excursions in the topology of digital images.*, Intelligent Systems Reference Library **102** (2016), xxviii + 433pp, ISBN: 978-3-319-30260-7; 978-3-319-30262-1; DOI: 10.1007/978-3-319-30262-1; zbMATH Zbl 1382.68008;MR3727129.
[36] ———, *Proximal relator spaces*, Filomat **30** (2016), no. 2, 469–472, doi:10.2298/FIL1602469P, MR3497927.
[37] ———, *Two forms of proximal, physical geometry. Axioms, sewing regions together, classes of regions, duality and parallel fibre bundles*, Advan. in Math: Sci. J **5** (2016), no. 2, 241–268, Zbl 1384.54015, reviewed by D. Leseberg, Berlin.
[38] ———, *Foundations of computer vision. Computational geometry, visual image structures and object shape recognition*, Intelligent Systems Ref. Library 124, Springer International Pub. AG, Cham, Switzerland, 2017, xvii+431 pp., ISBN: 978-3-319-52483-2; 978-3-319-52481-8; DOI 10.1007/978-3-319-52483-2; MR3769444.
[39] ———, *Proximal planar shape signatures. Homology nerves and descriptive proximity*, Advan. in Math: Sci. J **6** (2017), no. 2, 71–85, Zbl 06855051.
[40] ———, *Proximal planar shapes. Correspondence between shape and nerve complexes*, arXiv **1708** (2017), no. 04147v1, 1–12, Bulletin of the Allahabad Math. Soc., Dharma Prokash Gupta Memorial Volume, 2018 *in press*.
[41] J.F. Peters, A. Tozzi, and S. Ramanna, *Brain tissue tessellation shows absence of canonical microcircuits*, Neuroscience Letters **626** (2016), 99–105, http://dx.doi.org/10.1016/j.neulet.2016.03.052.
[42] A.K. Travin P.R. Spalart, M. Kh. Strelets and M.L. Slur, *Modeling the interaction of a vortex pair with the ground*, Fluid Dynamics **36** (1999), no. 6, 899–908.
[43] A.R.R. Silva, D.F.G. Dur ao, J.M.M. Barata, P. Santos, and S. Ribeiro, *Laser-doppler analysis of the separation zone of a ground vortex flow*, 14th Symp on Applications of Laser Techniques to Fluid Mechanics, Lisbon, Portugal, Universidade Beira Interior, 2008, pp. 7–10.
[44] Ju. M. Smirnov, *On proximity spaces*, American Math. Soc. Translations, Series 2, vol. 38 (AMS, ed.), Amer. Math. Soc., Providene, RI, 1964, pp. 3–36.
[45] Á Száz, *Basic tools and mild continuities in relator spaces*, Acta Math. Hungar. **50** (1987), no. 3-4, 177–201, MR0918156.
[46] S. De Toffoli and V. Giardino, *Forms and roles of diagrams in knot theory*, Erkenntnis **79** (2014), no. 4, 829–842, MR3260948.
[47] A. Tozzi, J.F. Peters, and E. Deli, *Towards plasma-like collisionless trajectories in the brain*, Neuroscience Letters **662** (2018), 105–109.
[48] E. Čech, *Topological spaces*, John Wiley & Sons Ltd., London, 1966, fr seminar, Brno, 1936-1939; rev. ed. Z. Frolik, M. Katětov. Scientific editor, Vlastimil Pt 'ak. Editor of the English translation, Charles O. Junge Publishing House of the Czechoslovak Academy of Sciences, Prague; Interscience Publishers John Wiley & Sons, London-New York-Sydney 1966 893 pp., MR0211373.
[49] H. van Leunen, *The hilbert book model project*, Tech. report, Deparment of Applied Physics, Technische Universiteit Eindhoven, 2018, https://www.researchgate.net/project/The-Hilbert-Book-Model-Project.
[50] O. Veblen, *Theory on plane curves in non-metrical analysis situs*, Transactions of the American Mathematical Society **6** (1905), no. 1, 83–98, MR1500697.
[51] J.H.C. Whitehead, *Combinatorial homotopy. I.*, Bulletin of the American Mathematical Society **55** (1949), no. 3, 213–245, Part 1, MR0030759.
[52] S. Willard, *General topology*, Dover Pub., Inc., Mineola, NY, 1970, xii + 369pp, ISBN: 0-486-43479-6 54-02, MR0264581.
[53] G.M. Ziegler, *Lectures on polytopes*, Springer, Berlin, 2007, x+370 pp. ISBN: 0-387-94365-X, MR1311028.

Journal of Mathematical Sciences and Modelling, 1 (2) (2018) 73-79

Journal of Mathematical Sciences and Modelling

Journal Homepage: www.dergipark.gov.tr/jmsm
ISSN 2636-8692

On fourth-order jacobsthal quaternions

Gamaliel Cerda-Morales[a*]

[a]*Instituto de Matemáticas, Pontificia Universidad Católica de Valparaíso, Blanco Viel 596, Cerro Barón, Valparaíso, Chile.*
[*]*Corresponding author E-mail: gamaliel.cerda@usm.cl*

Article Info

Keywords: *Fourth-order Jacobsthal number, Jacobsthal number, quaternion, Recurrence relation*
2010 AMS: *11B39, 11R52, 20G20*
Received: *18 June 2018*
Accepted: *2 August 2018*
Available online: *30 September 2018*

Abstract

In this paper, we present for the first time a sequence of quaternions of order 4 that we will call the fourth-order Jacobsthal and the fourth-order Jacobsthal-Lucas quaternions. In particular, we are interested in the generating function, Binet formula, explicit formula and some interesting results for fourth-order Jacobsthal quaternions and fourth-order Jacobsthal-Lucas quaternions. This generalizes some previous results given by Szynal-Liana and Włoch in [13], Torunbalci Aydin and Yüce in [14] and Cerda-Morales in [2].

1. Introduction

The Jacobsthal numbers have many interesting properties and applications in many fields of science (see, e.g. [1, 4, 12, 9]). In [1], Barry investigated a Jacobsthal decomposition of Pascal's triangle. In [4], Deveci et. al. defined the generalized order-k Jacobsthal sequences modulo m. In [12], Köken and Bozkurt showed that the Jacobsthal numbers are also generated by a special matrix. The Jacobsthal numbers J_n are defined [9] by the recurrence relation

$$J_0=0,\ J_1=1,\ J_{n+2}=J_{n+1}+2J_n,\ n\geq 0. \tag{1.1}$$

Another important sequence is the Jacobsthal-Lucas sequence. This sequence is defined by the recurrence relation

$$j_0=2,\ j_1=1,\ j_{n+2}=j_{n+1}+2j_n,\ n\geq 0. \tag{1.2}$$

In [3] the Jacobsthal recurrence relation is extended to higher order recurrence relations and the basic list of identities provided by Horadam [9] is expanded and extended to several identities for some of the higher order cases. Furthermore, the authors generalized the Jacobsthal recursion as

$$J_{n+r}^{(r)}=\sum_{s=1}^{r-1}J_{n+r-s}^{(r)}+2J_n^{(r)}. \tag{1.3}$$

with $n\geq 0$ and initial conditions $J_0=0$ and $J_s=1$ for $s=1,\ldots,r-1$. For the n-th order-r Jacobsthal-Lucas numbers $j_n^{(r)}$ we use the same recursion with initial conditions $j_s^{(r)}=j_s^{(r-1)}$ for $s=1,\ldots,r-1$.

In this work we consider the particular case $r=4$, the fourth-order Jacobsthal numbers $\{J_n^{(4)}\}_{n\geq 0}$ and the fourth-order Jacobsthal-Lucas numbers $\{j_n^{(4)}\}_{n\geq 0}$ are defined by

$$J_{n+4}^{(4)}=J_{n+3}^{(4)}+J_{n+2}^{(4)}+J_{n+1}^{(4)}+2J_n^{(4)},\ J_0^{(4)}=0,\ J_1^{(4)}=J_2^{(4)}=J_3^{(4)}=1 \tag{1.4}$$

and

$$j_{n+4}^{(4)}=j_{n+3}^{(4)}+j_{n+2}^{(4)}+j_{n+1}^{(4)}+2j_n^{(4)},\ j_0^{(4)}=2,\ j_1^{(4)}=1,\ j_2^{(4)}=5,\ j_3^{(4)}=10, \tag{1.5}$$

respectively.

Email addresses: **gamaliel.cerda@usm.c (G. Cerda-Morales)**

The first fourth-order Jacobsthal numbers and fourth-order Jacobsthal-Lucas numbers are presented in the following table.

s	0	1	2	3	4	5	6	7	8	9	10	11	12	...
$J_s^{(4)}$	0	1	1	1	3	7	13	25	51	103	205	409	819	...
$j_s^{(4)}$	2	1	5	10	20	37	77	154	308	613	1229	2458	4916	...

On the other hand, Horadam [7] introduced the n-th Fibonacci and the n-th Lucas quaternion as follows

$$Q_n = F_n + iF_{n+1} + jF_{n+2} + kF_{n+3} \tag{1.6}$$

and

$$Q_n = L_n + iL_{n+1} + jL_{n+2} + kL_{n+3}, \tag{1.7}$$

respectively. Here F_n and L_n are the n-th Fibonacci and n-th Lucas numbers, respectively. Furthermore, the basis i, j, k satisface the following rules:

$$i^2 = j^2 = k^2 = -1,\ ijk = -1. \tag{1.8}$$

Furthermore, the rules (1.8) imply $ij = -ji = k$, $jk = -kj = i$ and $ki = -ik = j$. In general, a quaternion is a hyper-complex number and is defined by $Q = q_r + iq_i + jq_j + kq_k$, where i, j, k are as in (1.8) and $\{q_r, q_i, q_j, q_k\} \subset \mathbb{R}$. Note that we can write $Q = q_r + V_Q$ where $V_Q = iq_i + jq_j + kq_k$. The conjugate of the quaternion Q is denoted by $\overline{Q} = q_r - V_Q$. The norm of a quaternion Q is defined by $Nr(Q) = Q\overline{Q} = q_r^2 + q_i^2 + q_j^2 + q_k^2 \in \mathbb{R}$.
Many interesting properties of Fibonacci and Lucas quaternions can be found in [5, 6, 7, 8, 10]. In [6], Halici investigated complex Fibonacci quaternions. In [8] Horadam mentioned the possibility of introducing Pell quaternions and generalized Pell quaternions. In [13], the authors defined the Jacobsthal quaternions and the Jacobsthal-Lucas quaternions. Recently, in [2] the author defined the third-order Jacobsthal quaternions and mentioned the possibility of introducing higher order Jacobsthal quaternions.
In this paper, we introduce and study the fourth-order Jacobsthal quaternions and the fourth-order Jacobsthal-Lucas quaternions. In particular, we give generating function, Binet formula and some interesting results for the fourth-order Jacobsthal quaternions and fourth-order Jacobsthal-Lucas quaternions.
For fourth-order Jacobsthal and fourth-order Jacobsthal-Lucas numbers some identities are given, see [3]. In this paper we need some of them.

$$j_n^{(4)} - 6J_n^{(4)} = \begin{cases} 2 & \text{if} \quad n \equiv 0 \pmod 4 \\ -5 & \text{if} \quad n \equiv 1 \pmod 4 \\ -1 & \text{if} \quad n \equiv 2 \pmod 4 \\ 4 & \text{if} \quad n \equiv 3 \pmod 4 \end{cases}, \tag{1.9}$$

$$6J_n^{(4)} + j_n^{(4)} - j_{n+1}^{(4)} = \begin{cases} 1 & \text{if} \quad n \equiv 0,2 \pmod 4 \\ 2 & \text{if} \quad n \equiv 1 \pmod 4 \\ -4 & \text{if} \quad n \equiv 3 \pmod 4 \end{cases}, \tag{1.10}$$

$$J_{n+2}^{(4)} - J_n^{(4)} - j_{n-1}^{(4)} = \begin{cases} 0 & \text{if} \quad n \equiv 0 \pmod 4 \\ -2 & \text{if} \quad n \equiv 1 \pmod 4 \\ 1 & \text{if} \quad n \equiv 2,3 \pmod 4 \end{cases} \quad (n \geq 1), \tag{1.11}$$

$$\sum_{s=0}^{n} J_s^{(4)} = \begin{cases} J_{n+1}^{(4)} - 1 & \text{if} \quad n \equiv 0 \pmod 4 \\ J_{n+1}^{(4)} & \text{if} \quad n \equiv 1,3 \pmod 4 \\ J_{n+1}^{(4)} + 1 & \text{if} \quad n \equiv 2 \pmod 4 \end{cases} \tag{1.12}$$

and

$$\sum_{s=0}^{n} j_s^{(4)} = \begin{cases} j_{n+1}^{(4)} - 2 & \text{if} \quad n \not\equiv 0 \pmod 3 \\ j_{n+1}^{(4)} + 1 & \text{if} \quad n \equiv 0 \pmod 3 \end{cases}. \tag{1.13}$$

Using standard techniques for solving recurrence relations, the auxiliary equation, and its roots are given by

$$x^4 - x^3 - x^2 - x - 2 = 0;\ x = 2,\ x = -1, \text{ and } x = \pm i.$$

Note that the latter two are the complex conjugate quartic roots of unity. Call them ω_1 and ω_2, respectively. Thus the Binet formulas can be written as

$$J_n^{(4)} = \frac{1}{5}\left(2^n - \left(\frac{1+3i}{2}\right)\omega_1^n - \left(\frac{1-3i}{2}\right)\omega_2^n\right) \tag{1.14}$$

and

$$j_n^{(4)} = \frac{3}{10}\left(2^{n+2} + \frac{5}{3}(-1)^n + \left(\frac{1+3i}{2}\right)\omega_1^n + \left(\frac{1-3i}{2}\right)\omega_2^n\right), \tag{1.15}$$

respectively.
Now, we use the notation

$$H_n^{(4)}(a,b) = \frac{A\omega_1^n - B\omega_2^n}{\omega_1 - \omega_2} = \begin{cases} a & \text{if} \quad n \equiv 0 \pmod 4 \\ b & \text{if} \quad n \equiv 1 \pmod 4 \\ -a & \text{if} \quad n \equiv 2 \pmod 4 \\ -b & \text{if} \quad n \equiv 3 \pmod 4 \end{cases}, \tag{1.16}$$

where $A = b - a\omega_2$ and $B = b - a\omega_1$, in which ω_1 and ω_2 are the complex conjugate quartic roots of unity (i.e. $\omega_1^4 = \omega_2^4 = 1$). Furthermore, note that for all $n \geq 0$ we have

$$H_{n+2}^{(4)}(a,b) = -H_n^{(4)}(a,b), \tag{1.17}$$

where $H_0^{(4)}(a,b) = a$ and $H_1^{(4)}(a,b) = b$.
From the Binet formulas (1.14), (1.15) and Eq. (1.16), we have

$$\begin{aligned} J_n^{(4)} &= \frac{1}{5}\left(2^n - V_n^{(4)}\right), \\ j_n^{(4)} &= \frac{3}{10}\left(2^{n+2} + \frac{5}{3}(-1)^n + V_n^{(4)}\right), \end{aligned} \tag{1.18}$$

where $V_n^{(4)} = H_n^{(4)}(1,-3)$.

2. The fourth-order jacobsthal quaternions

The n-th fourth-order Jacobsthal quaternion $JQ_n^{(4)}$ and the n-th fourth-order Jacobsthal-Lucas quaternion $jQ_n^{(4)}$ can be defined as

$$JQ_n^{(4)} = J_n^{(4)} + iJ_{n+1}^{(4)} + jJ_{n+2}^{(4)} + kJ_{n+3}^{(4)} \tag{2.1}$$

and

$$jQ_n^{(4)} = j_n^{(4)} + i\,j_{n+1}^{(4)} + j\,j_{n+2}^{(4)} + k\,j_{n+3}^{(4)}, \; n \geq 0, \tag{2.2}$$

respectively. Here $J_n^{(4)}$ and $j_n^{(4)}$ are the n-th fourth-order Jacobsthal and n-th fourth-order Jacobsthal-Lucas numbers, respectively. Furthermore, the basis i, j, k satisface the rules in (1.8).
The function $G(t) = \sum_{n\geq 0} JQ_n^{(4)} t^n$ is called the generating function for the sequence $\{JQ_n^{(4)}\}$. In [3], the authors found a generating function for fourth-order Jacobsthal numbers. In the following theorem, we established the generating function for fourth-order Jacobsthal and fourth-order Jacobsthal-Lucas quaternions.

Theorem 2.1. *The generating function for fourth-order Jacobsthal-Lucas quaternion is*

$$\sum_{n\geq 0} jQ_n^{(4)} t^n = \frac{\left\{ \begin{array}{c} 2+i+5j+10k+t(-1+4i+5j+10k)+t^2(2+4i+5j+7k) \\ +t^3(2+4i+2j+10k) \end{array} \right\}}{1-t-t^2-t^3-2t^4}. \tag{2.3}$$

Proof. Assuming that the generating function of the quaternion $\{jQ_n^{(4)}\}_{n\geq 0}$ has the form $G(t) = \sum_{n\geq 0} jQ_n^{(4)} t^n$, we obtain that

$$\begin{aligned} (1-t-t^2-t^3-2t^4)G(t) &= \left(jQ_0^{(4)} + jQ_1^{(4)}t + \cdots\right) - \left(jQ_0^{(4)}t + jQ_1^{(4)}t^2 + \cdots\right) - \cdots \\ &= jQ_0^{(4)} + t\left(jQ_1^{(4)} - jQ_0^{(4)}\right) + t^2\left(jQ_2^{(4)} - jQ_1^{(4)} - jQ_0^{(4)}\right) + t^3\left(jQ_3^{(4)} - jQ_2^{(4)} - jQ_1^{(4)} - jQ_0^{(4)}\right), \end{aligned}$$

since $jQ_{n+4}^{(4)} = jQ_{n+3}^{(4)} + jQ_{n+2}^{(4)} + jQ_{n+1}^{(4)} + 2jQ_n^{(4)}$ $(n \geq 0)$ and the coefficients of t^n for $n \geq 4$ are equal to zero. In equivalent form is

$$G(t) = \frac{\left\{ \begin{array}{c} jQ_0^{(4)} + t\left(jQ_1^{(4)} - jQ_0^{(4)}\right) + t^2\left(jQ_2^{(4)} - jQ_1^{(4)} - jQ_0^{(4)}\right) \\ +t^3\left(jQ_3^{(4)} - jQ_2^{(4)} - jQ_1^{(4)} - jQ_0^{(4)}\right) \end{array} \right\}}{1-t-t^2-t^3-2t^4}.$$

Thus, the proof is completed. □

Thus, the Binet formula for $jQ_n^{(4)}$ can be given in the following theorem.

Theorem 2.2. *If $jQ_n^{(4)} = j_n^{(4)} + i\,j_{n+1}^{(4)} + j\,j_{n+2}^{(4)} + k\,j_{n+3}^{(4)}$ be the n-th fourth-order Jacobsthal-Lucas quaternion. Then,*

$$\begin{aligned} jQ_n^{(4)} &= \frac{3}{10}\left[2^{n+2}\alpha + \frac{5}{3}(-1)^n\beta + \left(\frac{1+3i}{2}\right)\omega_1^n\underline{\omega_1} + \left(\frac{1-3i}{2}\right)\omega_2^n\underline{\omega_2}\right] \\ &= \frac{3}{10}\left[2^{n+2}\alpha + \frac{5}{3}(-1)^n\beta + VQ_n^{(4)}\right], \end{aligned} \tag{2.4}$$

where ω_1, ω_2 are the complex conjugate quartic roots of unity. Furthermore, $\alpha = 1+2i+4j+8k$, $\beta = 1-i+j-k$ and $VQ_n^{(4)} = V_n^{(4)} + iV_{n+1}^{(4)} + jV_{n+2}^{(4)} + kV_{n+3}^{(4)}$.

Proof. Let $V_n^{(4)}=H_n^{(4)}(1,-3)$. Using the relation (1.18), we have

$$\begin{aligned}\frac{10}{3}\cdot jQ_n^{(4)} &= \frac{10}{3}\left(j_n^{(4)}+ij_{n+1}^{(4)}+jj_{n+2}^{(4)}+kj_{n+3}^{(4)}\right)\\ &= \left(2^{n+2}+\frac{5}{3}(-1)^n+V_n^{(4)}\right)+i\left(2^{n+3}-\frac{5}{3}(-1)^n+V_{n+1}^{(4)}\right)+j\left(2^{n+4}+\frac{5}{3}(-1)^n+V_{n+2}^{(4)}\right)+k\left(2^{n+5}-\frac{5}{3}(-1)^n+V_{n+3}^{(4)}\right)\\ &= 2^{n+2}(1+2i+4j+8k)+\frac{5}{3}(-1)^n(1-i+j-k)+VQ_n^{(4)},\end{aligned}$$

where $VQ_n^{(4)}=V_n^{(4)}+iV_{n+1}^{(4)}+jV_{n+2}^{(4)}+kV_{n+3}^{(4)}$. Furthermore,

$$\begin{aligned}VQ_n^{(4)} &= \left(\left(\frac{1+3i}{2}\right)\omega_1^n+\left(\frac{1-3i}{2}\right)\omega_2^n\right)+i\left(\left(\frac{1+3i}{2}\right)\omega_1^{n+1}+\left(\frac{1-3i}{2}\right)\omega_2^{n+1}\right)\\ &+ j\left(\left(\frac{1+3i}{2}\right)\omega_1^{n+2}+\left(\frac{1-3i}{2}\right)\omega_2^{n+2}\right)+k\left(\left(\frac{1+3i}{2}\right)\omega_1^{n+3}+\left(\frac{1-3i}{2}\right)\omega_2^{n+3}\right)\\ &= \left(\frac{1+3i}{2}\right)\omega_1^n\underline{\omega_1}+\left(\frac{1-3i}{2}\right)\omega_2^n\underline{\omega_2},\end{aligned}$$

with $\underline{\omega_1}=1+\omega_1 i-j-\omega_1 k$ and $\underline{\omega_2}=1+\omega_2 i-j-\omega_2 k$, since $\omega_1^2=\omega_2^2=-1$. So, the theorem is proved. □

In a similar way, using the Eqs. (2.3) and (2.4) one can easily prove the following theorem.

Theorem 2.3. *If $JQ_n^{(4)}=J_n^{(4)}+iJ_{n+1}^{(4)}+jJ_{n+2}^{(4)}+kJ_{n+3}^{(4)}$ be the n-th fourth-order Jacobsthal quaternion. Then,*

$$\sum_{n\geq 0} JQ_n^{(4)}t^n=\frac{\begin{pmatrix} i+j+k+t(1+2k)\\ +t^2(-i+j+3k)+t^3(-1+2j+2k)\end{pmatrix}}{1-t-t^2-t^3-2t^4}, \tag{2.5}$$

$$JQ_n^{(4)}=\frac{1}{5}\left[2^n\alpha-VQ_n^{(4)}\right], \tag{2.6}$$

where $\alpha=1+2i+4j+8k$ and $VQ_n^{(4)}=V_n^{(4)}+iV_{n+1}^{(4)}+jV_{n+2}^{(4)}+kV_{n+3}^{(4)}$.

3. Some identities for the fourth-order jacobsthal quaternions

By some elementary calculations we find the following recurrence relations for the fourth-order Jacobsthal and fourth-order Jacobsthal-Lucas quaternions from (2.1) and (2.2):

$$\begin{aligned}&JQ_{n+2}^{(4)}+JQ_{n+1}^{(4)}+JQ_n^{(4)}+2JQ_{n-1}^{(4)}\\ &\quad=(J_{n+2}^{(4)}+iJ_{n+3}^{(4)}+jJ_{n+4}^{(4)}+kJ_{n+5}^{(4)})+(J_{n+1}^{(4)}+iJ_{n+2}^{(4)}+jJ_{n+3}^{(4)}+kJ_{n+4}^{(4)})\\ &\quad\quad+(J_n^{(4)}+iJ_{n+1}^{(4)}+jJ_{n+2}^{(4)}+kJ_{n+3}^{(4)})+2(J_{n-1}^{(4)}+iJ_n^{(4)}+jJ_{n+1}^{(4)}+kJ_{n+2}^{(4)})\\ &\quad=(J_{n+2}^{(4)}+J_{n+1}^{(4)}+J_n^{(4)}+2J_{n-1}^{(4)})+(J_{n+3}^{(4)}+J_{n+2}^{(4)}+J_{n+1}^{(4)}+2J_n^{(4)})i\\ &\quad\quad+(J_{n+4}^{(4)}+J_{n+3}^{(4)}+J_{n+2}^{(4)}+2J_{n+1}^{(4)})j+2(J_{n+5}^{(4)}+J_{n+4}^{(4)}+J_{n+3}^{(4)}+2J_{n+2}^{(4)})k\\ &\quad=J_{n+3}^{(4)}+iJ_{n+4}^{(4)}+jJ_{n+5}^{(4)}+kJ_{n+6}^{(4)}\\ &\quad=JQ_{n+3}^{(4)}\end{aligned} \tag{3.1}$$

and similarly $jQ_{n+3}^{(4)}=jQ_{n+2}^{(4)}+jQ_{n+1}^{(4)}+jQ_n^{(4)}+2jQ_{n-1}^{(4)}$, for $n\geq 1$.

Now, we give some interesting results for the fourth-order Jacobsthal quaternions $\{JQ_n^{(4)}\}_{n\geq 0}$ and the fourth-order Jacobsthal-Lucas quaternions $\{jQ_n^{(4)}\}_{n\geq 0}$.

Theorem 3.1. *Let $n\geq 0$ integer. Then, we have*

$$jQ_n^{(4)}-6JQ_n^{(4)}=\begin{cases} 2-5i-j+4k & \text{if } n\equiv 0 \pmod 4\\ -5-i+4j+2k & \text{if } n\equiv 1 \pmod 4\\ -1+4i+2j-5k & \text{if } n\equiv 2 \pmod 4\\ 4+2i-5j-k & \text{if } n\equiv 3 \pmod 4\end{cases}. \tag{3.2}$$

Proof. To prove Eq. (3.2) we need the Eq. (1.9). In fact, it suffices to take the Binet's formula of $J_n^{(4)}$ and $j_n^{(4)}$ in (1.18). Then,

$$\begin{aligned}j_n^{(4)}-6J_n^{(4)} &= \frac{3}{10}\left(2^{n+2}+\frac{5}{3}(-1)^n+V_n^{(4)}\right)-\frac{6}{5}\left(2^n-V_n^{(4)}\right)\\ &= \frac{1}{2}\left((-1)^n+3V_n^{(4)}\right).\end{aligned}$$

For definitions (2.1) and (2.2), we have $JQ_n^{(4)} = J_n^{(4)} + iJ_{n+1}^{(4)} + jJ_{n+2}^{(4)} + kJ_{n+3}^{(4)}$ and $jQ_n^{(4)} = j_n^{(4)} + ij_{n+1}^{(4)} + jj_{n+2}^{(4)} + kj_{n+3}^{(4)}$. Then, if we consider $n \equiv 0 (\bmod\ 4)$, we obtain

$$\begin{aligned} jQ_n^{(4)} - 6JQ_n^{(4)} &= \left(j_n^{(4)} + ij_{n+1}^{(4)} + jj_{n+2}^{(4)} + kj_{n+3}^{(4)}\right) - 6\left(J_n^{(4)} + iJ_{n+1}^{(4)} + jJ_{n+2}^{(4)} + kJ_{n+3}^{(4)}\right) \\ &= \left(j_n^{(4)} - 6J_n^{(4)}\right) + i\left(j_{n+1}^{(4)} - 6J_{n+1}^{(4)}\right) + j\left(j_{n+2}^{(4)} - 6J_{n+2}^{(4)}\right) + k\left(j_{n+3}^{(4)} - 6J_{n+3}^{(4)}\right) \\ &= 2 - 5i - j + 4k, \end{aligned}$$

since $j_{n+1}^{(4)} - 6J_{n+1}^{(4)} = -5$, $j_{n+2}^{(4)} - 6J_{n+2}^{(4)} = -1$ and $j_{n+3}^{(4)} - 6J_{n+3}^{(4)} = 4$. The other identities are clear from equations (1.9) and (1.18). □

Theorem 3.2. *Let $n \geq 0$ integer. Then,*

$$Nr(JQ_n^{(4)}) = \begin{cases} \frac{1}{5}\left(17 \cdot 2^{2n} - 6 \cdot 2^n + 4\right) & \text{if} \quad n \equiv 0,1 \pmod 4 \\ \frac{1}{5}\left(17 \cdot 2^{2n} + 6 \cdot 2^n + 4\right) & \text{if} \quad n \equiv 2,3 \pmod 4 \end{cases}. \tag{3.3}$$

Proof. To prove Eq. (3.3), we use definition of norm for the fourth-order Jacobsthal quaternion $JQ_n^{(4)}$,

$$Nr(JQ_n^{(4)}) = \left(J_n^{(4)}\right)^2 + \left(J_{n+1}^{(4)}\right)^2 + \left(J_{n+2}^{(4)}\right)^2 + \left(J_{n+3}^{(4)}\right)^2.$$

Then, by the Binet formula (1.18) we have

$$\begin{aligned} Nr(JQ_n^{(4)}) &= \frac{1}{25}\left(\begin{array}{c} \left(2^n - V_n^{(4)}\right)^2 + \left(2^{n+1} - V_{n+1}^{(4)}\right)^2 \\ + \left(2^{n+2} - V_{n+2}^{(4)}\right)^2 + \left(2^{n+3} - V_{n+3}^{(4)}\right)^2 \end{array}\right) \\ &= \frac{1}{25}\left(\begin{array}{c} 85 \cdot 2^{2n} - 2^{n+1}\left(V_n^{(4)} + 2V_{n+1}^{(4)} + 4V_{n+2}^{(4)} + 8V_{n+3}^{(4)}\right) \\ + \left(V_n^{(4)}\right)^2 + \left(V_{n+1}^{(4)}\right)^2 + \left(V_{n+2}^{(4)}\right)^2 + \left(V_{n+3}^{(4)}\right)^2 \end{array}\right) \\ &= \frac{1}{25}\left(85 \cdot 2^{2n} + 3 \cdot 2^{n+1}\left(V_n^{(4)} + 2V_{n+1}^{(4)}\right) + 20\right) \\ &= \frac{1}{5}\left(17 \cdot 2^{2n} + 3 \cdot 2^{n+1} U_{n+1}^{(4)} + 4\right), \end{aligned} \tag{3.4}$$

where $U_n^{(4)} = H_n^{(4)}(1,-1)$. Then, if $n \equiv 0,1 (\bmod\ 4)$, we obtain $U_{n+1}^{(4)} = -1$ and $Nr(JQ_n^{(4)}) = \frac{1}{5}\left(17 \cdot 2^{2n} - 3 \cdot 2^{n+1} + 4\right)$. The other identities are clear from equations (3.4) and (1.16). □

In a similar way, using the Eqs. (1.10) and (1.11) one can easily prove the following theorem.

Theorem 3.3. *Let $n \geq 0$ integer. Then,*

$$6JQ_n^{(4)} - jQ_n^{(4)} - jQ_{n+1}^{(4)} = \begin{cases} 1 + 2i + j - 4k & \text{if} \quad n \equiv 0 \pmod 4 \\ 2 + i - 4j + k & \text{if} \quad n \equiv 1 \pmod 4 \\ 1 - 4i + j + 2k & \text{if} \quad n \equiv 2 \pmod 4 \\ -4 + i + 2j + k & \text{if} \quad n \equiv 3 \pmod 4 \end{cases}, \tag{3.5}$$

$$JQ_{n+2}^{(4)} - JQ_n^{(4)} - jQ_{n-1}^{(4)} = \begin{cases} -2i + j + k & \text{if} \quad n \equiv 0 \pmod 4 \\ -2 + i + j & \text{if} \quad n \equiv 1 \pmod 4 \\ 1 + i - 2k & \text{if} \quad n \equiv 2 \pmod 4 \\ 1 - 2j + k & \text{if} \quad n \equiv 3 \pmod 4 \end{cases}, \ (n \geq 1). \tag{3.6}$$

The following is a result for the sum of fourth-order Jacobsthal quaternions.

Theorem 3.4. *Let $n \geq 0$ integer. Then,*

$$\sum_{s=0}^{n} JQ_s^{(4)} = \begin{cases} JQ_{n+1}^{(4)} - (1 + 2k) & \text{if} \quad n \equiv 0 \pmod 4 \\ JQ_{n+1}^{(4)} + (i - j - 3k) & \text{if} \quad n \equiv 1 \pmod 4 \\ JQ_{n+1}^{(4)} + (1 - 2j - 2k) & \text{if} \quad n \equiv 2 \pmod 4 \\ JQ_{n+1}^{(4)} - (i + j + k) & \text{if} \quad n \equiv 3 \pmod 4 \end{cases}. \tag{3.7}$$

Proof. Using equality (1.12), we have

$$\sum_{s=0}^{n} J_s^{(4)} = \begin{cases} J_{n+1}^{(4)} - 1 & \text{if} \quad n \equiv 0 \pmod 4 \\ J_{n+1}^{(4)} & \text{if} \quad n \equiv 1,3 \pmod 4 \\ J_{n+1}^{(4)} + 1 & \text{if} \quad n \equiv 2 \pmod 4 \end{cases}.$$

Furthermore, if $n\equiv 0(\text{mod } 4)$, $\sum_{s=0}^{n} J_s^{(4)} = J_{n+1}^{(4)} - 1$, $\sum_{s=0}^{n+1} J_s^{(4)} = J_{n+2}^{(4)}$, $\sum_{s=0}^{n+2} J_s^{(4)} = J_{n+3}^{(4)} + 1$ and $\sum_{s=0}^{n+3} J_s^{(4)} = J_{n+4}^{(4)}$. Then,

$$\begin{aligned}\sum_{s=0}^{n} JQ_s^{(4)} &= \sum_{s=0}^{n} J_s^{(4)} + i\sum_{s=0}^{n} J_{s+1}^{(4)} + j\sum_{s=0}^{n} J_{s+2}^{(4)} + k\sum_{s=0}^{n} J_{s+3}^{(4)} \\ &= \sum_{s=0}^{n} J_s^{(4)} + i\left(\sum_{s=0}^{n+1} J_s^{(4)}\right) + j\left(\sum_{s=0}^{n+2} J_s^{(4)} - 1\right) + k\left(\sum_{s=0}^{n+3} J_s^{(4)} - 2\right) \\ &= \left(J_{n+1}^{(4)} - 1\right) + i\left(J_{n+2}^{(4)}\right) + j\left(J_{n+3}^{(4)}\right) + k\left(J_{n+4}^{(4)} - 2\right) \\ &= JQ_{n+1}^{(4)} - (1+2k).\end{aligned}$$

If $n\equiv 1(\text{mod } 4)$, we have $\sum_{s=0}^{n+1} J_s^{(4)} = J_{n+2}^{(4)} + 1$, $\sum_{s=0}^{n+2} J_s^{(4)} = J_{n+3}^{(4)}$ and $\sum_{s=0}^{n+3} J_s^{(4)} = J_{n+4}^{(4)} - 1$, then $\sum_{s=0}^{n} JQ_s^{(4)} = JQ_{n+1}^{(4)} + (i-j-3k)$. The proof is similar for the cases $n\equiv 2,3(\text{mod } 4)$. Thus, the proof is completed. □

There are three well-known identities for Fibonacci numbers, namely, Catalan's, Cassini's, and d'Ocagne's identities. The proofs of these identities are based on Binet formulas. We can obtain these types of identities for fourth-order Jacobsthal quaternions using the Binet formulas derived above. We use the notation

$$\begin{aligned} HQ_n^{(4)}(a,b) &= \frac{A\omega_1^n \underline{\omega_1} - B\omega_2^n \underline{\omega_2}}{\omega_1-\omega_2} \\ &= \begin{cases} a+bi-aj-bk & \text{if} \quad n\equiv 0 \pmod 4 \\ b-ai-bj+ak & \text{if} \quad n\equiv 1 \pmod 4 \\ -a-bi+aj+bk & \text{if} \quad n\equiv 2 \pmod 4 \\ -b+ai+bj-ak & \text{if} \quad n\equiv 3 \pmod 4 \end{cases}, \end{aligned} \tag{3.8}$$

where $A = b - a\omega_2$ and $B = b - a\omega_1$, in which $\underline{\omega_1} = 1+\omega_1 i - j - \omega_1 k$ and $\underline{\omega_2} = 1+\omega_2 i - j - \omega_2 k$ are the complex conjugate quartic roots of unity (i.e. $\omega_1^2=\omega_2^2=-1$). Furthermore, note that for all $n\geq 0$ we have

$$HQ_{n+2}^{(4)}(a,b) = -HQ_n^{(4)}(a,b), \tag{3.9}$$

where $HQ_0^{(4)}(a,b) = a+bi-aj-bk$ and $HQ_1^{(4)}(a,b) = b-ai-bj+ak$.
The following theorem gives d'Ocagne's identities for fourth-order Jacobsthal quaternion.

Theorem 3.5. *If $JQ_n^{(4)} = J_n^{(4)} + iJ_{n+1}^{(4)} + jJ_{n+2}^{(4)} + kJ_{n+3}^{(4)}$ be the n-th fourth-order Jacobsthal quaternion. Then, for any integers n and m, we have*

$$JQ_m^{(4)} JQ_{n+1}^{(4)} - JQ_{m+1}^{(3)} JQ_n^{(4)} = \frac{1}{5}\left\{ \begin{array}{c} 2^m \alpha UQ_n^{(4)} - 2^n UQ_m^{(4)}\alpha \\ -i\left(\omega_1^{m-n}\underline{\omega_1}\,\underline{\omega_2} - \omega_2^{m-n}\underline{\omega_2}\,\underline{\omega_1}\right) \end{array} \right\} \tag{3.10}$$

where $\alpha = 1+2i+4j+8k$, $\underline{\omega_1} = 1+\omega_1 i - j - \omega_1 k$, $\underline{\omega_2} = 1+\omega_2 i - j - \omega_2 k$ and $UQ_n^{(4)} = HQ_n^{(4)}(-1,-1)$.

Proof. Using the Binet formula for the fourth-order Jacobsthal quaternions and $VQ_n^{(4)} = HQ_n^{(4)}(1,-3)$ in (3.8) gives

$$\begin{aligned} & JQ_m^{(4)} JQ_{n+1}^{(4)} - JQ_{m+1}^{(4)} JQ_n^{(4)} \\ &= \frac{1}{25}\left(\begin{array}{c} \left(2^m\alpha - VQ_m^{(4)}\right)\left(2^{n+1}\alpha - VQ_{n+1}^{(4)}\right) \\ -\left(2^{m+1}\alpha - VQ_{m+1}^{(4)}\right)\left(2^n\alpha - VQ_n^{(4)}\right) \end{array}\right) \\ &= \frac{1}{25}\left(\begin{array}{c} -2^m\alpha VQ_{n+1}^{(4)} - 2^{n+1}VQ_m\alpha + 2^{m+1}\alpha VQ_n^{(4)} + 2^n VQ_{m+1}^{(4)}\alpha \\ +VQ_m^{(4)}VQ_{n+1}^{(4)} - VQ_{m+1}^{(4)}VQ_n^{(4)} \end{array}\right) \\ &= \frac{1}{5}\left(2^m\alpha UQ_n^{(4)} - 2^n UQ_m^{(4)}\alpha - i\left(\omega_1^{m-n}\underline{\omega_1}\,\underline{\omega_2} - \omega_2^{m-n}\underline{\omega_2}\,\underline{\omega_1}\right)\right), \end{aligned} \tag{3.11}$$

where $UQ_n^{(4)} = \frac{1}{5}\left(2VQ_n^{(4)} - VQ_{n+1}^{(4)}\right) = HQ_n^{(4)}(1,-1)$. □

Taking $m=n+1$ in this theorem and using the identity

$$-i\left(\omega_1\underline{\omega_1}\,\underline{\omega_2} - \omega_2\underline{\omega_2}\,\underline{\omega_1}\right) = \underline{\omega_1}\,\underline{\omega_2} + \underline{\omega_2}\,\underline{\omega_1} = -4(1+j),$$

we obtain Cassini's identities for fourth-order Jacobsthal quaternions.

Corollary 3.6. *For any integer $n\geq 0$, we have*

$$\left(JQ_{n+1}^{(4)}\right)^2 - JQ_{n+2}^{(3)} JQ_n^{(4)} = \frac{1}{5}\left(2^n\left(2\alpha UQ_n^{(4)} - UQ_{n+1}^{(4)}\alpha\right) - 4(1+j)\right). \tag{3.12}$$

We will give an example in which we check in a particular case the Cassini-like identity for fourth-order Jacobsthal quaternions.

Example 3.7. *Let $\{JQ_s^{(4)} : s = 0,1,2,3\}$ be the fourth-order Jacobsthal quaternions such that $JQ_0^{(4)} = i + j + k$, $JQ_1^{(4)} = 1 + i + j + 3k$, $JQ_2^{(4)} = 1 + i + 3j + 7k$ and $JQ_3^{(4)} = 1 + 3i + 7j + 13k$. In this case,*

$$\begin{aligned}
\left(JQ_1^{(4)}\right)^2 - JQ_2^{(4)}JQ_0^{(4)} &= (1+i+j+3k)^2 - (1+i+3j+7k)(i+j+k) \\
&= (-10+2i+2j+6k) - (-11-3i+7j-k) \\
&= 1+5i-5j+7k \\
&= \frac{1}{5}\left(\left(2\alpha UQ_0^{(4)} - UQ_1^{(4)}\alpha\right) - 4(1+j)\right).
\end{aligned}$$

and

$$\begin{aligned}
\left(JQ_2^{(4)}\right)^2 - JQ_3^{(4)}JQ_1^{(4)} &= (1+i+3j+7k)^2 - (1+3i+7j+13k)(1+i+j+3k) \\
&= (-58+2i+6j+14k) - (-48+12i+12j+12k) \\
&= -10-10i-6j+2k \\
&= \frac{1}{5}\left(2\left(2\alpha UQ_1^{(4)} - UQ_2^{(4)}\alpha\right) - 4(1+j)\right).
\end{aligned}$$

4. Conclusions

In this work, some known identities of the sequence of Jacobsthal numbers have continued to be generalized with the use of the quaternion ring. The main motivation is based on the study of the non-commutative properties of the quaternions, and how we can solve friendly cases with sequences of recursive numbers. In particular, the ideas of finding rules of commutativity, matrix representation of quaternion sequences and their study in a wider class of rings, say in octonions or in any power associative ring.

Acknowledgements

The author also thanks the suggestions sent by the reviewer, which have improved the final version of this article.

References

[1] P. Barry, *Triangle geometry and Jacobsthal numbers*, Irish Math. Soc. Bulletin 51 (2003), 45–57.
[2] G. Cerda-Morales, *Identities for Third Order Jacobsthal Quaternions*, Adv. Appl. Clifford Algebras 27(2) (2017), 1043–1053.
[3] C.K. Cook and M.R. Bacon, *Some identities for Jacobsthal and Jacobsthal-Lucas numbers satisfying higher order recurrence relations*, Annales Mathematicae et Informaticae 41 (2013), 27–39.
[4] O. Deveci, E. Karaduman and G. Sağlam, *The Jacobsthal sequences in finite groups*, Bull. Iranian Math. Soc. 42(1) (2016), 79–89.
[5] S. Halici, *On Fibonacci quaternions*, Adv. Appl. Clifford Algebras 22 (2012), 321–327.
[6] S. Halici, *On complex Fibonacci quaternions*, Adv. Appl. Clifford Algebras 23 (2013), 105–112.
[7] A.F. Horadam, *Complex Fibonacci numbers and Fibonacci quaternions*, Am. Math. Month. 70 (1963), 289–291.
[8] A.F. Horadam, *Quaternion recurrence relations*, Ulam Quarterly 2 (1993), 23–33.
[9] A.F. Horadam, *Jacobsthal representation numbers*, Fibonacci Quarterly 34 (1996), 40–54.
[10] M.R. Iyer, *A note on Fibonacci quaternions*, Fibonacci Quaterly 7(3) (1969), 225–229.
[11] D. Kalman, *Generalized Fibonacci numbers by matrix methods*, Fibonacci Quaterly 20(1) (1982), 73–76.
[12] F. Köken and D. Bozkurt, *On the Jacobsthal numbers by matrix methods*, Int. J. Contemp. Math. Sci. 3 (2008), 605–614.
[13] A. Szynal-Liana and I. Włoch, *A Note on Jacobsthal Quaternions*, Adv. Appl. Clifford Algebras 26 (2016), 441–447.
[14] F. Torunbalci Aydin and S.Yüce, *A new approach to Jacobsthal quaternions*, FILOMAT 31 (2017), 5567–5579.

Journal of Mathematical Sciences and Modelling, 1 (2) (2018) 80-85

Journal of Mathematical Sciences and Modelling

Journal Homepage: www.dergipark.gov.tr/jmsm
ISSN 2636-8692

Improved semi-local convergence of the Gauss-Newton method for systems of equations

Ioannis K. Argyros[a] **and Santhosh George**[b*]

[a] *Department of Mathematical Sciences, Cameron University, Lawton, OK 73505, USA*
[b] *Department of Mathematical and Computational Sciences, National Institute of Technology Karnataka, India-575 025*
[*] *Corresponding author E-mail: sgeorge@nitk.ac.in*

Article Info

Keywords: *Gauss- Newton method, Newton's method, Semi-local convergence, Least squares problem*
2010 AMS: *65H10, 65G99, 65K10, 47H17, 49M15*
Received: *8 June 2018*
Accepted: *13 September 2018*
Available online: *30 September 2018*

Abstract

Our new technique of restricted convergence domains is employed to provide a finer convergence analysis of the Gauss-Newton method in order to solve a certain class of systems of equations under a majorant condition. The advantages are obtained under the same computational cost as in earlier studies such as [5, 14]. Special cases and a numerical example are also given in this study.

1. Introduction

Let $\Omega \subseteq \mathbb{R}^n$ be open. Let $F : \Omega \to \mathbb{R}^m$ be continuously Fréchet- differentiable. The problem of approximating least squares solutions x^* of the nonlinear problem

$$\min_{x\in\Omega} \|F(x)\|^2, \tag{1.1}$$

is very important in computational mathematics. The least squares solutions of (1.1) are stationary points of $Q(x) = \|F(x)\|^2$. A lot of problems arising in applied sciences and in engineering can be expressed in a form like (1.1). For example in data fitting n is the number of parameters and m is the number of observations. Other examples can be found in [6, 16, 19] and the references therein. The famous Gauss-Newton method defined by

$$x_{k+1} = x_k - F'(x_k)^\dagger F(x_k), \text{ for each } k = 0, 1, \cdots, \tag{1.2}$$

where x_0 is an initial point and $F'(x_k)^\dagger$ the Moore-Penrose inverse of the linear operator $F'(x_k)$ has been used extensively to generate a sequence $\{x_k\}$ converging to x^* [1]–[6], [8, 10, 20, 14, 15, 17].

In the present paper, we are motivated by the work of Goncalves and Oliveira in [14] (see also [12], [13]) and our works in [1, 2, 3, 4, 6, 7, 8]. These authors presented a semi-local convergence analysis for the Gauss-Newton method (1.2) for systems of nonlinear equations where the function F satisfies

$$\|F'(y)^\dagger (I_{\mathbb{R}^m} - F'(x)F'(x)^\dagger)F(x)\| \leq k\|x-y\| \text{ for each } x \text{ and } y \in \Omega,$$

where $k \in [0,1)$ and $I_{\mathbb{R}^m}$ denotes the identity operator on $\mathbb{R}^m$. Their semilocal- convergence analysis is based on the construction of a majorant function (see condition (h_3)). Their results unify the classical results for functions involving Lipschitz derivative [6, 7, 16, 18] with results for analytical functions ($\alpha-$theory or $\gamma-$theory) [9, 11, 15, 17, 19, 20].

We introduce a center majorant function (see (c_3)) which is a special case of the majorant function that can provide more precise estimates on the distances $\|F'(x)^\dagger\|$. Then, we find a domain where the iterates lie which is more precise than in the aformentioned studies. This leads to "smaller" majorant functions yielding to weaker sufficient convergence conditions; more precise error estimates on the distances $\|x_{k+1} - x_k\|, \|x_k - x^*\|$ and an at least as precise information on the location of the solution.

The rest of the paper is organized as follows: The semi-local convergence analysis of the Gauss-Newton method is presented in Section 2. Special cases and numerical examples are given in the concluding Section 3.

Email addresses: iargyros@cameron.edu (I. K. Argyros), sgeorge@nitk.ac.in (S. George)

2. Semi-local convergence analysis

In this section we present the semi-local convergence analysis of the Gauss-Newton method. Let $R > 0$. Denote by $B(x_0,R),\bar{B}(x_0,R)$ the open and closed balls in $\mathbb{R}^n$, respectively with center $x_0 \in \mathbb{R}^n$ and radius R. We shall use the hypotheses denoted by $(\mathscr{C})$.
(c_0) Let $B(x_0,R) \subseteq \mathbb{R}^n$ and $F : B(x_0,R) \to \mathbb{R}^m$ be continuously Fréchet- differentiable.
(c_1) continuously differentiable functions $f_0 : [0,R) \longrightarrow \mathbb{R}$, $f : [0,R^*) \to \mathbb{R}$

$$\|F'(x_0)^{\dagger}\|\|F'(x) - F'(x_0)\| \leq f_0'(\|x - x_0\|) - f_0'(0) \text{ for each } \ x \in B(x_0,R)$$

and

$$\|F'(x_0)^{\dagger}\|\|F'(y) - F'(x)\| \leq f'(\|y - x\| + \|x - x_0\|) - f'(\|x - x_0\|) \text{ for each } \ x,y \in B(x_0,R^*)$$

with $\|y - x\| + \|x - x_0\| < R^*$ where $R_0 := \sup\{t \in [0,R] : f_0'(t) < 0\}$. Set

$$R^* := \min\{R_0,R\}.$$

(c_2)

$$\|F'(y)^{\dagger}(I_{\mathbb{R}^m} - F'(x)F'(x)^{\dagger})F(x)\| \leq \kappa\|x - y\| \ \text{ for each } x \text{ and } y \in B(x_0,R^*),$$

where $\kappa \in [0,1)$.
(c_3) Set $\eta = \|F'(x_0)^{\dagger}F(x_0)\| > 0,\ F'(x_0) \neq 0$.

$$rank(F'(x)) \leq rank(F'(x_0)) \neq 0 \text{ for each } \ x \in B(x_0,R^*).$$

(c_4)

$$f_0(0) = f(0) = 0,\ f'(0) = f_0'(0) = -1$$
$$f_0(t) \leq f(t) \text{ and } f_0'(t) \leq f'(t) \text{ for each } \ t \in [0,R^*).$$

(c_5) f_0', f' are convex and strictly increasing.
Let $\mu \geq 0$ be such that $\mu \geq -\kappa f'(\eta)$ and define $\varphi_{\eta,\mu} : [0,R^*) \to \mathbb{R}$ by

$$\varphi_{\eta,\mu}(t) = \eta + \mu t + f(t).$$

(c_6) $\varphi_{\eta,\mu}(t) = 0$ for some $t \in [0,R^*)$.
(c_7) For each $s,t,u \in [0,R^*)$ with $s \leq t \leq u$

$$t + \frac{\varphi_{\eta,\mu}(u)}{f_0'(u)} \leq u + \frac{\varphi_{\eta,\mu}(t) - \varphi_{\eta,\mu}(s) - \varphi_{\eta,\mu}'(s)(t-s)}{f_0'(t)}$$

The majorizing iteration $\{r_k\}$ for $\{x_k\}$ is given by

$$r_0 = 0,\ r_{k+1} = r_k - \frac{\varphi_{\eta,\mu}(r_k)}{f_0'(r_k)}. \tag{2.1}$$

The corresponding iteration $\{t_n\}$ used in [14] is given by

$$t_0 = 0,\ t_{k+1} = t_k - \frac{\bar{\varphi}_{\eta,\mu}(t_k)}{g'(t_k)}, \tag{2.2}$$

where $\bar{\varphi}_{\eta,\mu}(t) = \eta + \mu t + g(t)$, continuously differentiable function $g : [0,R) \longrightarrow \mathbb{R}$ is such that

$$\|F'(x_0)^{+}\|\|F'(x) - F'(y)\| \leq g'(\|y - x\| + \|x - x_0\|) - g'(\|x - x_0\|)$$

for each $x,y \in B(x_0,R)$. Moreover, define iterations $\{s_k\}$ by

$$s_0 = 0, s_{k+1} \quad = \quad s_k - \frac{\varphi_{\eta,\mu}(s_k)}{f_0'(s_k)}.$$

This iteration was used by us in [5]. In view of these conditions, we have

$$f_0'(t) \leq g'(t) \tag{2.3}$$

and

$$f'(t) \leq g'(t) \tag{2.4}$$

for each $t \in [0,R^*)$. Next, the main semi-local convergence result for the Gauss-Newton method is presented.

Theorem 2.1. *Suppose that the $(\mathscr{C})$ conditions hold and $f_0'(t) \le f'(t)$ for each $t \in [0,R^*]$. Then, the following hold: $\varphi_{\eta,\mu}(t)$ has a smallest zero $r^* \in (0,R^*)$, the sequences $\{r_k\}$ and $\{x_k\}$ for solving $\varphi_{\eta,\mu}(t) = 0$ and $F(x) = 0$, with starting point $t_0 = 0$ and x_0, respectively given by (1.2) and (2.3) are well defined, $\{r_k\}$ is strictly increasing, remains in $[0,r^*)$, and converges to r^*, $\{x_k\}$ remains in $B(x_0,r^*)$, converges to a point $x^* \in B(x_0,r^*)$ such that $F'(x^*)^\dagger F(x^*) = 0$. Moreover, the following estimates hold:*

$$\|x_{k+1} - x_k\| \le r_{k+1} - r_k \text{ for each } k = 0,1,2,\cdots,$$

$$\|x^* - x_k\| \le r^* - r_k \text{ for each } k = 0,1,2,\cdots,$$

and

$$\|x_{k+1} - x_k\| \le \frac{r_{k+1} - r_k}{(r_k - r_{k-1})^2}\|x_k - x_{k-1}\|^2 \text{ for each } k = 0,1,2,\cdots.$$

Furthermore, if $\mu = 0$($\mu = 0$ and $f_0'(r^*) < 0$), the sequence $\{r_k\}$, $\{x_k\}$ converge $Q-$linearly and $R-$linearly ($Q-$ quadratically and $R-$ quadratically) to r^* and x^*, respectively.

Proof. Simply repeat the proof of Theorem 3.9 in [5] (or the proof in [14]) with f replacing g. Notice also that the iterates x_n remain in $B(x_0,R_0)$ which is a more precise location than $B(x_0,R^*)$ used in [5, 14].

Remark 2.2. *(i) As noted in [14] the best choice for μ is given by $\mu = -\kappa f'(\kappa)$.*

(ii) If $f(t) = g(t) = f_0(t)$ for each $t \in [0,R_0)$ and $R_0 = R$, then Theorem 2.1 reduces to the corresponding Theorem in [8]. Moreover, if $f_0'(t) \le f't) = g'(t)$ we obtain the results in [5]. If

$$f_0'(t) \le f'(t) \le g'(t) \text{ for each } t \in [0,R^*) \tag{2.5}$$

then the following advantages denoted by $(\mathscr{A})$ are obtained: weaker sufficient convergence criteria, tighter error bounds on the distances $\|x_n - x^*\|, \|x_{n+1} - x_n\|$ and an at least as precise information on the location of the solution x^*. These advantages are obtained using less computational cost, since in practice the computation of function g requires the computation of functions f_0 and f as special cases. It is also worth noticing that under (c_1) function f_0' is defined and therefore R^* which is at least as small as R.

We have that, if function $\bar{\varphi}_{\eta,\mu}$ has a solution t^*, then, since $\varphi_{\eta,\mu}(t^*) \le \bar{\varphi}_{\eta,\mu}(t^*) = 0$ and $\varphi_{\eta,\mu}(0) = \bar{\varphi}_{\eta,\mu}(0) = \eta > 0$, we get that function $\varphi_{\eta,\mu}$ has a solution r^* such that

$$r^* \le t^* \tag{2.6}$$

but not necessarily vice versa. It also follows from (2.6) that the new information about the location of the solution x^* is at least as precise as the one given in [14, 5].

Let us specialize conditions $(\mathscr{C})$ even further in the case when f_0, f and g are constant functions L_0, K, L, respectively. Then, (for $\mu = 0$) we have that:

$$\bar{\varphi}_{\eta,\mu}(t) = \frac{L}{2}t^2 - t + \eta \tag{2.7}$$

and

$$\varphi_{\eta,\mu}(t) = \frac{K}{2}t^2 - t + \eta, \tag{2.8}$$

respectively. In this case the convergence criteria become, respectively

$$h = L\eta \le \frac{1}{2}$$

and

$$h_1 = K\eta \le \frac{1}{2}.$$

Notice that

$$h \le \frac{1}{2} \Longrightarrow h_1 \le \frac{1}{2}$$

but not vice versa unless, $K = L$. Criterion (2.8) is famous for its simplicity and clarity Kantorovich hypothesis for the semilocal convergence of Newton's method to a solution x^* of nonlinear equation $F(x) = 0$ [7, 16]. In the case of Wang's conditions [20] we have for $\mu = 0$:

$$g(t) = \frac{\gamma t^2}{1-\gamma t} - t,\ f(t) = \frac{\beta t^2}{1-\beta t} - t,\ f_0(t) = \frac{\gamma_0 t^2}{1-\gamma_0 t} - t,$$

$$\bar{\varphi}_{\eta,\mu}(t) = \frac{\gamma t^2}{1-\gamma t} - t + \eta, \tag{2.9}$$

$$\varphi_{\eta,\mu}(t) = \frac{\beta t^2}{1-\beta t} - t + \eta \tag{2.10}$$

with convergence criteria, given respectively by

$$H = \gamma\eta \le 3 - 2\sqrt{2} \tag{2.11}$$

$$H_1 = \beta\eta \le 3 - 2\sqrt{2}. \tag{2.12}$$

Then, again we have that

$$H \leq 3-2\sqrt{2} \Longrightarrow H_1 \leq 3-2\sqrt{2}$$

but not necessarily vice versa, unless if $\beta=\gamma$.
Concerning the error bounds and the limit of majorizing sequence, suppose that

$$-\frac{\varphi_{\eta,\mu}(r)}{f_0'(r)} \leq -\frac{\varphi_{\eta,\mu}(s)}{f_0'(s)}$$

for each $r,s \in [0,R^*]$ with $r \leq s$. According to the proof of Theorem 2.1, sequence $\{r_n\}$ is also a majorizing sequence for (1.2). Moreover, a simple induction argument shows that

$$r_n \leq s_n, r_{n+1}-r_n \leq s_{n+1}-s_n$$

and

$$r^* = \lim_{n\longrightarrow\infty} r_n \leq s^*.$$

Furthermore, the first two preceding inequalities are strict, for $n \geq 2$ if $f_0'(t) < f'(t)$ for each $t \in [0,R^*]$. Similarly, suppose that

$$-\frac{\varphi_{\eta,\mu}(s)}{f_0'(s)} \leq -\frac{\varphi_{\eta,\mu}(t)}{f_0'(t)}$$

for each $s,t \in [0,R^*]$ with $s \leq t$. Then, we have that

$$s_n \leq t_n, s_{n+1}-s_n \leq t_{n+1}-t_n.$$

The first two preceding inequalities are also strict for $n \geq 2$, if strict inequality holds in (2.12).

Finally, the rest of the results in [5, 14] can be improved along the same lines by also using K instead of L. We leave the details to the motivated reader.

3. Numerical examples

We present a simple example where we show that Wang's condition (2.11) [20] is violated but our condition (2.12) is satisfied. More examples can be found in [7] where $L_0 \leq K \leq L$ are satisfied as strict inequalities (therefore the new advantages apply) (or see also [19]).

Example 3.1. *Let $\mu=0$, $p\in(0,1)$, $x_0=1$, $\Omega=B(x_0,\frac{1}{2-p})$ and define functions on Ω by*

$$f(x)=\frac{x^4}{4}-px,\; F(x)=x^3-p. \tag{3.1}$$

Define $\Omega^*=B(x_0,1-p)$. Then, we have

$$\Omega^* \subseteq \Omega, \text{ if } p \in [0.381966,1). \tag{3.2}$$

Let $L_0=3-p$ and $L=2(2-p)$. Then, Argyros showed in [8] that for each $x,y\in\Omega$

$$|F'(x_0)^{-1}(F'(x)-F'(x_0))| \leq L_0|x-x_0| \tag{3.3}$$

and

$$|F'(x_0)^{-1}(F'(x)-F'(y))| \leq L|x-y|. \tag{3.4}$$

Consider the conditions

$$\|F'(x_0)^{-1}F''(x)\| \leq \frac{2\gamma}{(1-\gamma\|x-x_0\|)^3} \tag{3.5}$$

for each $x\in\Omega$,

$$\|F'(x_0)^{-1}(F'(x)-F'(x_0))\| \leq \frac{1}{(1-\gamma_0\|x-x_0\|)^2}-1 \tag{3.6}$$

for each $x\in\Omega$ and

$$\|F'(x_0)^{-1}F''(x)\| \leq \frac{2\beta}{(1-\beta\|x-x_0\|)^3} \tag{3.7}$$

for each $x\in\Omega^*$. Notice that functions $\bar{\varphi}_{\eta,0}$, $\varphi_{\eta,0}$ satisfy these conditions, respectively. In view of (3.4) and (3.5), we have $L\leq 2\gamma$, so we choose $\gamma=2-p$. Then, since $\eta=\frac{1}{3}(1-p)$, condition (2.11) is satisfied, if

$$0.6255179 \leq p < 1. \tag{3.8}$$

We must have

$$B(x_0,(1-\frac{1}{\sqrt{2}})\frac{1}{\gamma}) \subseteq B(x_0,1-p),$$

which is true for

$$0 < p \leq 0.7631871. \tag{3.9}$$

It follows from (3.8) and (3.9) that

$$0.6255179 < p \leq 0.7631871. \tag{3.10}$$

Set $y = \gamma_0|x - x_0|$ *and* $L_0 = d\gamma_0, d > 0, \gamma_0 > 0$. *Using (3.6) and (3.3), we must have*

$$L_0|x - x_0| \leq \frac{1}{(1 - \gamma_0|x - x_0|)^2} - 1$$

or

$$d(1-y)^2 \leq 2 - y$$

or

$$dy^2 + (1-2d)y + d - 2 \leq 0. \tag{3.11}$$

Let e.g. $d = 2$, *then* $\gamma_0 = \frac{L_0}{2} = \frac{3-p}{2}$ *and (3.11) becomes* $(p-3)(p-1) \leq 3$ *or* $p(p-4) \leq 0$, *which is true. We must show* $(1 - \frac{1}{\sqrt{2}})\frac{1}{\gamma_0} \leq 1 - p$ *or* $p^2 - 4p + 1 + \sqrt{2} \geq 0$, *which is true for*

$$0 < p \leq 0.7407199. \tag{3.12}$$

Notice that $\Omega_0 \subset \Omega$, *since* $(1 - \frac{1}{\sqrt{2}})\frac{1}{\gamma_0} < \frac{1}{\gamma}$ *or* $p \leq 3 + \sqrt{2}$, *which is true, so*

$$\Omega \cap \Omega_0 = \Omega_0. \tag{3.13}$$

Then, for $x \in \Omega_0$

$$\begin{aligned} |F'(x_0)^{-1}F''(x)| &= 2|x| \leq 2(|x - x_0| + |x_0|) \\ &\leq 2((1 - \frac{1}{\sqrt{2}})\frac{2}{3-p} + 1) \end{aligned}$$

must be smaller than 2β, *so we can choose*

$$\beta = 1 + (1 - \frac{1}{\sqrt{2}})\frac{2}{3-p} = 1 + \frac{2-\sqrt{2}}{3-p}.$$

Notice that $\beta < \gamma$, *if (3.12) holds. We also have that* $\gamma_0 < \beta$, *if*

$$\frac{3-p}{2} < 1 + \frac{2-\sqrt{2}}{3-p}$$

or if

$$p^2 - 4p - 1 + 2\sqrt{2} < 0$$

or, if

$$0.5263741 < p < 1. \tag{3.14}$$

We also must have

$$(1 - \frac{1}{\sqrt{2}})\frac{1}{\beta} \leq 1 - p$$

or

$$2p^2 + (\sqrt{2} - 10)p + 4 + \sqrt{2} \leq 0,$$

which is true for

$$p \leq 0.767996. \tag{3.15}$$

Then, notice that

$$1 - p \leq \frac{1}{\gamma},$$

if $p^2 - 3p + 1 \leq 0$, *which is true for*

$$0.381966 \leq p < 1. \tag{3.16}$$

Then, we have that $\alpha_0 \leq 3 - 2\sqrt{2} = q$, *if* $(1 + \frac{2-\sqrt{2}}{3-p})\frac{1}{3}(1-p) \leq q$ *or if*

$$p^2 + (\sqrt{2} - 6 + 3q)p + 5 - \sqrt{2} - 9q \leq 0,$$

which is true for

$$0.5857931 \leq p < 1. \tag{3.17}$$

In view of (3.12), (3.14), (3.15) and (3.17) we must have

$$0.5857931 \leq p \leq 0.7407199. \tag{3.18}$$

Define intervals I and I_1 by

$$I = [0.5857931, 0.6255179) \tag{3.19}$$

and

$$I_1 = (0.7407199, 0.7631871]. \tag{3.20}$$

In view of (3.10), (3.19) and (3.20), we see that for $p \in I$ [20] cannot guarantee the convergence of x_n to $x^* = \sqrt[3]{p}$. However, our Theorem 2.1 guarantees the convergence of x_n to x^*. Notice that, if $p \in I_1$, then we can set $\beta = \gamma = \gamma_0$.
Next, we compare the error bounds. Choose $p = 0.623$. Then, we have the following comparison table, which shows that the new error bounds are more precise than the ones in [20].

n	$r_{n+1} - r_n$	$t_{n+1} - t_n$
1	0.1257	0.1257
2	0.0268	0.0333
3	0.0013	0.0027
4	3.3384e-06	1.8199e-05
5	2.0876e-11	8.2197e-10

Table 1: Comparison table.

References

[1] Argyros, I.: On the semilocal convergence of the Gauss-Newton method. Adv. Nonlinear Var.Inequal. 8(2), 93–99, 2005.
[2] Argyros, I., Hilout, S.: On the local convergence of the Gauss-Newton method. Punjab Univ. J.Math. 41, 23–33, 2009.
[3] Argyros, I., Hilout, S.: On the Gauss-Newton method. J. Appl. Math. Comput. 1–14, 2010.
[4] Argyros, I. K, Hilout, S.: Extending the applicability of the Gauss-Newton method under average Lipschitz-type conditions. Numer. Algorithms 58(1), 23–52, 2011.
[5] Argyros, I. K, S. George, Expanding the applicability of the Gauss-Newton method for a certain class of systems of equations, J. Numer.Anal. Approx. Theory, vol., 45(1), 3–13, (2016).
[6] Argyros, I. K., Hilout, S.: Improved local convergence of Newton's method under weak majorant condition, Journal of Computational and Applied Mathematics, 236(7), 1892–1902, 2012.
[7] Argyros, I., Hilout, S.: Numerical methods in nonlinear analysis, World Scientific Publ. Comp. New Jersey, USA, 2013.
[8] Ben-Israel, A., Greville, T.N.E.: Generalized inverses. CMS Books in Mathematics/Ouvrages de Mathematiques de la SMC, 15. Springer-Verlag, New York, second edition, Theory and Applications, 2003.
[9] Catinas, E.: The inexact, inexact perturbed, and quasi-Newton methods are equivalent models, Math. Comput. 74, 249, (2005), 291-301.
[10] Dedieu, J.P., Kim, M.H.: Newton's method for analytic systems of equations with constant rank derivatives. J. Complexity, 18(1): 187-209, 2002.
[11] Ferreira, O.P., Gonçalves, M.L.N, Oliveira, P.R.:, Local convergence analysis of inexact Gauss–Newton like methods under majorant condition, J. Complexity, 27(1), 111-125, 2011.
[12] Ferreira, O.P., Svaiter, B.F.: Kantorovich's majorants principle for Newton's method. Comput.Optim. Appl. 42(2), 213–229, 2009.
[13] Häussler, W.M.: A Kantorovich-type convergence analysis for the Gauss-Newton-method. Numer. Math. 48(1), 119–125, 1986.
[14] Gonçalves, M.L.N, Oliveira, P.R.:, Convergence of the Gauss- Newton method for a special class of systems of equations under a majorant condition, Optimization, 64, 3(2015), 577–594.
[15] Hu, N., Shen, W. and Li, C.: Kantorovich's type theorems for systems of equations with constant rank derivatives, J. Comput. Appl.Math., 219(1): 110-122, 2008.
[16] Kantorovich, L.V., Akilov, G.P., Functional Analysis, Pergamon Press, Oxford, 1982.
[17] Li, C., Hu, N., Wang, J.: Convergence behavior of Gauss-Newton's method and extensions of the Smale point estimate theory. J. Complex. 26(3), 268–295, 2010.
[18] Potra, F.A., Ptak, V.: Nondiscrete induction and iterative processes. Research notes in Mathematics, 103, Pitman(Aóvanced Publishing Program), Boston, MA, 1984.
[19] Smale, S., Newton's method estimates from data at one point. The merging of disciplines: new directions in pure, applied, and computational mathematics (Laramie, Wyo., 1985), 185-196, Springer, New York, 1986.
[20] Wang, X.H., Convergence of Newton's method and uniqueness of the solution of equations in Banach spaces, IMA J. Numer. Anal., 20 , 123–134, 2000.

Journal of Mathematical Sciences and Modelling, 1 (2) (2018) 86-92

Journal of Mathematical Sciences and Modelling

Journal Homepage: www.dergipark.gov.tr/jmsm
ISSN 2636-8692

On convolution surfaces in Euclidean 3-space

Selin Aydöner[a] and Kadri Arslan[b*]

[a]*Department of Mathematics, Institute of Natural and Applied Science, Uludağ University, Bursa, Turkey*
[b]*Department of Mathematics, Faculty of Science and Arts, Uludağ University, Bursa, Turkey*
[*]*Corresponding author E-mail: arslan@uludag.edu.tr*

Article Info

Keywords: *Convolution of surfaces, Flat surfaces, Gaussian curvature, Minkowski sum, Second fundamental form*
2010 AMS: *53C40, 53C42*
Received: *18 May 2018*
Accepted: *24 September 2018*
Available online: *30 September 2018*

Abstract

In the present paper we study with the convolution surface $C = M \star N$ of a paraboloid $M \subset \mathbb{E}^3$ and a parametric surface $N \subset \mathbb{E}^3$. We take some spacial surfaces for N such as, surface of revolution, Monge patch and ruled surface and calculate the Gaussian curvature of the convolution surface C. Further, we give necessary and sufficient conditions for a convolution surface C to become flat.

1. Introduction

Given two objects A and B in $\mathbb{R}^3$, their *Minkowski sum* $A \oplus B$ is defined to be the set

$$A \oplus B := \{a + b : a \in A, b \in B\}, \tag{1.1}$$

where a and b denote position vectors of arbitrary points in A and B. Minkowski sums in two and three dimensions are used in various fields, for example mathematical morphology, computer graphics, convex geometry, computational geometry motion planning. The algorithmic problem for polynomial and polyhedral shapes as well as approximations of the convolution and Minkowski sum have been studied, see for instance ([3], [5]) and the references therein. Let $M = \partial A$ and $N = \partial B$ be boundaries of A and B respectively. Then, the computation of the boundary $\partial(A \oplus B)$ is related to the computation of the *convolution surface* $M \star N$ of the two boundary surfaces M and N. We always assume in the following that M and N are smooth surfaces with normal vector fields $\overrightarrow{n_M}$ and $\overrightarrow{n_N}$, respectively. The convolution surface is defined to be

$$M \star N := \{x + y : x \in M, y \in N, \text{ and } \overrightarrow{n_M} \parallel \overrightarrow{n_N}\}, \tag{1.2}$$

where $\overrightarrow{n_M}(x)$ and $\overrightarrow{n_N}(y)$ are mutually parallel normal vectors at points x and y ([4], [2]). In particular, if A and B are convex objects, the boundary $\partial(A \oplus B)$ of the Minkowski sum $A \oplus B$ is exactly given by the convolution surface $M \star N$. Unfortunately, for non-convex objects this property is no longer true. In general, the boundary $\partial(A \oplus B)$ of the Minkowski sum is contained in the convolution surface $M \star N$, formed by the boundaries $M = \partial A$ and $N = \partial B$, respectively. The boundary $\partial(A \oplus B)$ of the Minkowski sum $A \oplus B$ is contained in the envelope of B with respect to the translations $x' = a + x, a \in A$ (see, [1]).
In general, the computation of the convolution surface $M \star N$ of two smooth surfaces M and N results in the following way. Assume that the surfaces M and N are parametrized by $x = x(u,v)$ and $y = y(s,t)$, respectively and that the normal vectors are denoted by $\overrightarrow{n_M}(u,v)$ and $\overrightarrow{n_N}(s,t)$. The convolution surface $M \star N$ is formed by the sums of the position vectors x, y of the surfaces M and N whose normal vectors $\overrightarrow{n_M}$ and $\overrightarrow{n_N}$ are parallel. Thus, we have to find parametrization

$$x(u(s,t); v(s,t)) = x(s,t) \tag{1.3}$$

and $y(s,t)$ of parts of M and N over a common parameter domain of the st-plane with the property that the normal vectors $\overrightarrow{n_M}(s,t)$ and $\overrightarrow{n_N}(s,t)$ at x and y are parallel. Let us point out that in case of an arbitrary surface N there is no one-one correspondence between points $x \in M$ and $y \in N$ with $\overrightarrow{n_M}(x) \parallel \overrightarrow{n_N}(y)$ (see, [4]).

Email addresses: **selinaydoner@gmail.com (S. Aydöner), arslan@uludag.edu.tr (K. Arslan)**

2. Convolution of the surfaces

Let M be a surface given with the regular patch

$$M : x(u,v) = \left(u, v, u^2 + cv^2\right), \quad u,v,c \in \mathbb{R}, \tag{2.1}$$

which is either an elliptic or hyperbolic paraboloid depending on whether $c > 0$ or $c < 0$. The surface N assumed to admit a local parametrization

$$N : y(s,t) = (y_1(s,t), y_2(s,t), y_3(s,t)), \quad s,t \in \mathbb{R}, \tag{2.2}$$

which is a smooth mapping. The points $x(u,v) = p$ and $y(s,t) = q$ are corresponding if the normal vectors $\overrightarrow{n_M}$ and $\overrightarrow{n_N}$ at p and q, respectively, are linearly dependent. That is;

$$\overrightarrow{n_M} = \lambda \overrightarrow{n_N}, \quad 0 \neq \lambda \in \mathbb{R}. \tag{2.3}$$

Then $p+q$ is a point of the convolution surface $M \star N$ (see, [4]). Assume that the normal vector of N is given with the parametrization of the form

$$\overrightarrow{n_N} = (n_1(s,t), n_2(s,t), n_3(s,t)). \tag{2.4}$$

So, the condition (2.3) gives

$$\begin{pmatrix} -2u \\ -2cv \\ 1 \end{pmatrix} = \lambda \begin{pmatrix} n_1(s,t) \\ n_2(s,t) \\ n_3(s,t) \end{pmatrix}. \tag{2.5}$$

In the case of $n_3(s,t) \neq 0$ we have

$$\begin{aligned} \lambda &= \frac{1}{n_3(s,t)}, \\ u(s,t) &= \frac{-n_1(s,t)}{2n_3(s,t)}, \\ v(s,t) &= \frac{-n_2(s,t)}{2cn_3(s,t)}, \end{aligned} \tag{2.6}$$

(see, [4]).
Denoting this reparametrization by the mapping

$$\phi : (s,t) \to (u(s,t), v(s,t)),$$

the surface patch $x(\phi(s,t))$ represents in general the only part of M. If the determinant of the Jacobian matrix of ϕ does not vanish, then the equation (2.6) represents a regular parametrization. Consequently, we have the following results;

Proposition 2.1. *The determinant of the Jacobian matrix of ϕ is given by*

$$det(J\phi) = \frac{1}{4cn_3} \det(n_N(s,t), n_{N_s}(s,t), n_{N_t}(s,t)). \tag{2.7}$$

Proof. By the definition of the Jacobian matrix

$$\det(J\phi) = \begin{vmatrix} \frac{\partial u}{\partial s} & \frac{\partial u}{\partial t} \\ \frac{\partial v}{\partial s} & \frac{\partial v}{\partial t} \end{vmatrix}.$$

By the use of (2.6), we get

$$\begin{aligned} \det(J\phi) &= \begin{vmatrix} \frac{(n_3)_s n_1 - n_3 (n_1)_s}{2n_3^2} & \frac{(n_3)_t n_1 - n_3 (n_1)_t}{2n_3^2} \\ \frac{(n_3)_s n_2 - n_3 (n_2)_s}{2cn_3^2} & \frac{(n_3)_t n_2 - n_3 (n_2)_t}{2cn_3^2} \end{vmatrix} \\ &= \frac{1}{4cn_3} \det(n_N(s,t), n_{N_s}(s,t), n_{N_t}(s,t)). \end{aligned}$$

This completes the proof of the Proposition 2.1. □

Proposition 2.2. *The Gaussian curvature of the surface N is given by*

$$\widetilde{K} = \frac{1}{\widetilde{W}^4} \det(n_N(s,t), n_{N_s}(s,t), n_{N_t}(s,t)) \tag{2.8}$$

where $\widetilde{W}^2 = \widetilde{E}\widetilde{G} - \widetilde{F}^2$ is the area element of the surface N.

Proof. Let $\widetilde{e},\widetilde{f},\widetilde{g}$ be the coefficients of the second fundamental form of the surface N

$$\begin{aligned} e^* &= \langle y_{ss}, n_N\rangle = -\langle y_s, (n_N)_s\rangle \\ f^* &= \langle y_{st}, n_N\rangle = -\langle y_s, (n_N)_t\rangle \\ g^* &= \langle y_{tt}, n_N\rangle = -\langle y_t, (n_N)_t\rangle \end{aligned}$$

then

$$\begin{aligned} e^*g^*-f^{*2} &= \langle y_s, (n_N)_s\rangle\langle y_t, (n_N)_t\rangle - \langle y_s, (n_N)_t\rangle\langle y_t, (n_N)_s\rangle \\ &= \langle y_s\times y_t, (n_N)_s\times (n_N)_t\rangle \\ &= \langle n_N, (n_N)_s\times (n_N)_t\rangle (s,t) \\ &= \det(n_N(s,t), (n_N)_s(s,t), (n_N)_t(s,t)). \end{aligned}$$

Hence,

$$\begin{aligned} \widetilde{e} &= \frac{e^*}{\widetilde{W}}, \\ \widetilde{f} &= \frac{f^*}{\widetilde{W}}, \\ \widetilde{g} &= \frac{g^*}{\widetilde{W}}, \end{aligned}$$

implies that

$$\begin{aligned} \widetilde{K} &= \frac{1}{\widetilde{W}^2}(\widetilde{e}\widetilde{g}-\widetilde{f}^2) \\ &= \frac{1}{\widetilde{W}^4}(e^*g^*-f^{*2}) \\ &= \frac{1}{\widetilde{W}^4}\det(n_N(s,t), n_{N_s}(s,t), n_{N_t}(s,t)). \end{aligned} \tag{2.9}$$

This completes the proof of the Proposition 2.2. □

As a consequence of Proposition 2.1 and Proposition 2.2, we get

Corollary 2.3. *The determinant of the Jacobian matrix of the mapping ϕ is given by*

$$\begin{aligned} \det(J\phi) &= \frac{1}{4cn_3}\det(n_N(s,t), n_{N_s}(s,t), n_{N_t}(s,t)) \\ &= \frac{1}{4cn_3}\widetilde{W}^4\widetilde{K}. \end{aligned} \tag{2.10}$$

From Corollary 2.3, it is easy to see that the reparametrization (2.6) is not invertible if N is a developable surface.
The final representation of the convolution surface $M\star N$ has the parametrization

$$(x+y)(s,t) = (\frac{-n_1(s,t)}{2n_3(s,t)}+y_1(s,t), \frac{-n_2(s,t)}{2cn_3(s,t)}+y_2(s,t), \frac{1}{4cn_3^2}(cn_1^2+n_2^2)+y_3(s,t)). \tag{2.11}$$

The convolution surface $M\star N$ of a paraboloid M and a parametrized surface N consists of the explicit parametrization (2.11).

3. Some particular surfaces

In the present section we consider the convolution surface of some special surfaces.

I) Assume that N is a local surface given with the *Monge patch*

$$N: y(s,t) = (s,t,h(s,t)), \tag{3.1}$$

then the parametrization (2.6) is obtained by

$$\begin{aligned} \lambda &= 1, \\ u &= \frac{h_s}{2}, \\ v &= \frac{h_t}{2c}, \end{aligned} \tag{3.2}$$

where h_s and h_t denote the partial derivatives of h with respect to s and t. So, the convolution surface $M\star N$ has the parametrization

$$(x+y)(s,t) = (\frac{h_s}{2}+s, \frac{h_t}{2c}+t, \frac{1}{4}h_s^2+\frac{1}{4c}h_t^2+h)(s,t). \tag{3.3}$$

If $n_3(s,t)=0$, then there exists a curve $\gamma\in N$ such that γ is a shadow boundary of N. In this case the convolution surface $M\star N$ consists of non-connected parts.

Definition 3.1. *In the Monge patch (3.1), if we take $h(s,t) = f(s)+g(t)$, then the resultant surface given with*

$$N : y(s,t) = (s,t, f(s)+g(t)) \tag{3.4}$$

is called a translation surface.

We obtain the following result.

Theorem 3.2. *Let $M \star N$ be a convolution surface of a paraboloid M and a translation surface N given with the parametrization (3.4). Then the Gaussian curvature of the convolution surface is*

$$K_{M\star N} = \frac{8c\left(-f'''f' + (f'')^2 + 2f''\right)(f''+2)g''}{(g''+2c)\left(4(f')^2 + (g')^2(f'')^2 + 4(g')^2 f'' + 4(g')^2 + (f'')^2 + 4f'' + 4\right)^2}.$$

Proof. Let $M \star N$ be a convolution surface of a paraboloid M and a translation surface N given with the parametrization (3.4) For simplicity we define $z = x+y$. Then the tangent space of $M \star N$ is spanned by

$$\begin{aligned} x_s &= \left(\frac{f''}{2}+1, 0, f'\right) \\ x_t &= \left(0, \frac{g''}{2c}+1, \frac{g'g''}{2c}+g'\right) \end{aligned}$$

Hence the coefficients of first and second fundamental forms of the convolution surface $M \star N$ are

$$\begin{aligned} E &= \langle x_s, x_s\rangle = \left(\frac{f''}{2}+1\right)^2 + (f')^2 \\ F &= \langle x_s, x_t\rangle = f'\left(\frac{g'g''}{2c}+g'\right) \\ G &= \langle x_t, x_t\rangle = \left(\frac{g''}{2c}+1\right)^2 + \left(\frac{g'g''}{2c}+g'\right)^2 \end{aligned} \tag{3.5}$$

and

$$\begin{aligned} e &= \frac{\langle x_{ss}, x_s \times x_t\rangle}{\sqrt{EG-F^2}} = \frac{(g''+2c)\left(-f'''f' + (f'')^2 + 2f''\right)}{c\sqrt{EG-F^2}} \\ f &= \frac{\langle x_{st}, x_s \times x_t\rangle}{\sqrt{EG-F^2}} = 0, \\ e &= \frac{\langle x_{tt}, x_s \times x_t\rangle}{\sqrt{EG-F^2}} = \frac{g''(f''+2)\left(g''+2c^2\right)}{c^2\sqrt{EG-F^2}} \end{aligned} \tag{3.6}$$

respectively. By definition the Gaussian curvature of the convolution surface $M \star N$ is given by

$$K_{M\star N} = \frac{eg - f^2}{EG - F^2} \tag{3.7}$$

So, substituting (3.5) and (3.6) into (3.7) we get the result. □

Corollary 3.3. *Let $M \star N$ be a convolution surface of a paraboloid M and a translation surface (3.4). If the convolution $M \star N$ is a flat surface, then at least one of the following cases occur;*

$$\begin{aligned} g(t) &= b_1 t + b_2, \\ f(s) &= -s^2 + d_1 s + d_2, \ or \\ f(s) &= \frac{e^{c_1(s+c_2)}}{c_1^2} + \frac{2}{c_1}s + c_2 \end{aligned}$$

where b_i, c_j, d_k are real constants.

Proof. If $M \star N$ is a flat surface, then

$$(-f'''(s)f'(s) + (f''(s))^2 + 2f''(s))(f''(s)+2)g''(t) = 0$$

holds. So, we have the three possible cases;
i) $g''(t) = 0$,
ii) $f''(s) + 2 = 0$,
iii) $-f'''(s)f'(s) + (f''(s))^2 + 2f''(s) = 0$.
Solving these differential equations we get the result. This completes the proof of the corollary. □

Corollary 3.4. *The convolution surface $M \star N$ given with $g(t) = b_1 t + b_2$ is a part of a plane.*

II) Assume that N is a *surface of revolution* given with the surface patch

$$N : y(s,t) = (f(s)\cos t, f(s)\sin t, h(s)), \tag{3.8}$$

then the equations in (2.6) turns into

$$\begin{aligned} \lambda &= \frac{1}{ff'} \\ u &= \frac{h'}{2f'}\cos t \\ v &= \frac{h'}{2cf'}\sin t. \end{aligned} \tag{3.9}$$

Finally, convolution surface $M \star N$ has the parametrization

$$(x+y)(s,t) = (\frac{h'+2ff'}{2f'}\cos t, \frac{h'+2cff'}{2cf'}\sin t, \frac{h'}{2c(f')^2}(c\cos^2 t + \sin^2 t) + h(s)). \tag{3.10}$$

Theorem 3.5. *Let $M \star N$ be a convolution surface of a paraboloid M and a surface of revolution given with the parametrization (3.8). Then the Gaussian curvature of the convolution surface is*

$$K_{M\star N} = \frac{4c(f')^4 h'(f'h'' - f''h')}{\Psi(s,t)}; \;\; f' \neq 0. \tag{3.11}$$

where $\Psi(s,t)$ is a real valued non-zero differentiable function of the parameters s and t.

Proof. Similar to the proof of Theorem 3.2, we get the result. □

Corollary 3.6. *Let $M \star N$ be a convolution surface of a paraboloid M and a surface of revolution (3.8). If the convolution surface $M \star N$ is a flat surface, then one of the following cases occur;*
i) N is a part of a plane, or
ii) N is a part of a cone, or
iii) N is a part of a paraboloid.

Proof. If $M \star N$ is a flat surface, then

$$(f')^4 h'(f'h'' - f''h') = 0, \; f' \neq 0 \tag{3.12}$$

holds. So, we have two possible cases;
i) $h' = 0$, or
ii) $f'h'' - f''h' = 0$.
If $h' = 0$ then N is a part of a plane. Further, if $h'' = 0$ and $f'' = 0$ then N is a part of a cone. Finally for the $f'h'' - f''h' = 0$ case with $h'' \neq 0$ and $f'' \neq 0$ the surface N is a part of a paraboloid. □

III) Assume that N is a *conoidal surface* given with the parametrization

$$N : y(s,t) = \begin{pmatrix} p(s)\sin s + p'(s)\cos s + t\cos s \\ -p(s)\cos s + p'(s)\sin s + t\sin s \\ z(s) \end{pmatrix} \tag{3.13}$$

where p and z are real valued differentiable functions. Then, the parametrization (2.6) is obtained by

$$\begin{aligned} \lambda &= \frac{-1}{t} \\ u &= \frac{-z'(s)}{2t}\sin s \\ v &= \frac{z'(s)}{2ct}\cos s. \end{aligned} \tag{3.14}$$

Finally, the sum $M \star N$ has the parametrization

$$(x+y)(s,t) = \begin{pmatrix} \left(\frac{2tp(s) - z'(s)}{2t}\right)\sin s + (p'(s)+t)\cos s \\ \left(\frac{z'(s) - 2ctp(s)}{2ct}\right)\cos s + (p'(s)+t)\sin s \\ \left(\frac{z'(s)^2}{4ct^2}\right)(c\sin^2 s + \cos^2 s) \end{pmatrix} \tag{3.15}$$

If we assume that $p(s) = p$ is a constant function and $z(s) = ks$, $k \neq 0$ then the conoidal surface N has the parametrization

$$N : y(s,t) = \begin{pmatrix} p\sin s + t\cos s \\ -p\cos s + t\sin s \\ ks \end{pmatrix} \tag{3.16}$$

Consequently, if $p(s)=0$, then the N is a right helicoid

$$y(s,t)=\begin{pmatrix} t\cos s \\ t\sin s \\ ks \end{pmatrix} \tag{3.17}$$

which is a minimal surface. We obtain the following result.

Theorem 3.7. *Let $M\star N$ be a convolution surface of a paraboloid M and a right helicoid given with the parametrization (3.17). Then, the Gaussian curvature of the convolution surface is*

$$K_{M\star N}=\frac{4t^4k^2}{(k^4+k^2t^2-4k^2t^4-4t^6)(k^2+t^2)}. \tag{3.18}$$

Proof. Similar to the proof of Theorem 3.2, we get the result. □

4. Visualization

Example 4.1. *For $f(s):=cos(s), g(t):=cos(t); c:=-3$; we obtain the following graphs of the Monge patch and the convolute surface given the parametrization (3.3);*

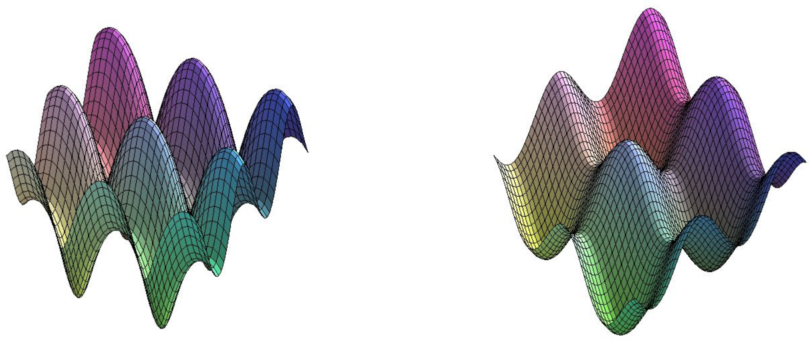

Figure 4.1: Monge patch and its convolute surface

Example 4.2. *For $f(s):=s, h(s):=3s-5; c:=-3$; we obtain the following graph of the surface of revolution and the convolute surface given the parametrization (3.10);*

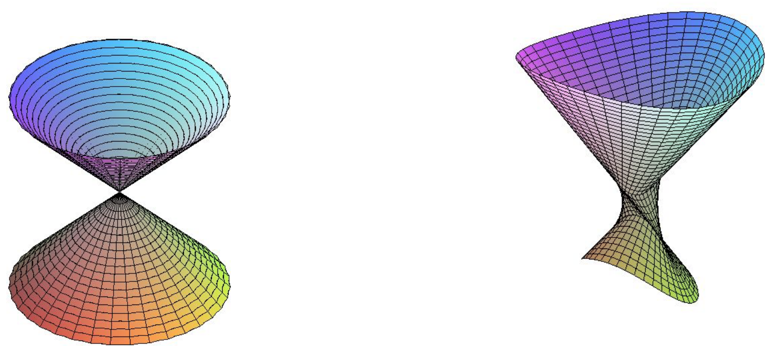

Figure 4.2: Surface of revolution and its convolute surface

Example 4.3. *For $p(s):=0, z(s):=2s$; we obtain the following graph of the conoidal surface and the convolute surface given the parametrization (3.15);*

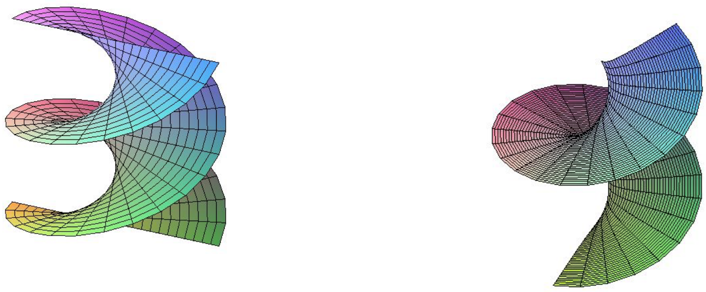

Figure 4.3: The conoidal surface and its convolute surface

5. Conclusion

Modelling with curves and surfaces are important area in applied differential geometry. In the present study we consider Minkowski sum of two smooth surfaces in 3-dimensional Euclidean space. This process is also called the convolution of two surfaces. We obtain some nice convolution surfaces by taking some particular surfaces such as Monge patch, surface of revolution and conoidal surfaces. We also plot the graph of the surfaces.

References

[1] J. Bloomenthal, K. Shoemake, *Convolution surfaces*, Computer Graphics **25(4)** (1991), 251–256.
[2] M. Lavicka, B. Bastl, Z. Sir, *Reparameterization of curves and surfaces with respect to convolutions*, in: Dæhlen, M., et al.(Eds.), MMCS 2008. In: Lecture Notes in Computer Science, 5862, 2010, 285-298.
[3] M. Peternell, T. Steiner, *Minkowski sum boundary surfaces of 3D-objects*, Graphical Models **69** (2007), 180–190.
[4] M. Peternell, F. Manhart, *The Convolution of a Paraboloid and a Parametrized Surface*, www.dmg.tuwien.ac.at/geom/peternell/parsurf_article.pdf
[5] Z. Sir, J. Gravesen, B. Jüttler, *Computing Convolutions and Minkowski sums via Support Functions*, Industrial Geometry, FSP Report **29**, 2006.
[6] J. Vrsek, M. Lavicka, *On convolutions of algebraic curves*, J. Sym. Comp. **45** (2010), 657–676.

Journal of Mathematical Sciences and Modelling, *1 (2) (2018) 93-104*

Journal of Mathematical Sciences and Modelling

Journal Homepage: www.dergipark.gov.tr/jmsm
ISSN 2636-8692

On the influence of far-field model reduction techniques using a coupled FEM-SBFEM approach in time domain

Marco Schauer[a*]

[a]*Technische Universität Braunschweig, Institut für Statik, Beethovenstraße 51, 38106 Braunschweig, Germany*
[*]*Corresponding author E-mail: m.schauer@tu-braunschweig.de*

Article Info

Keywords: *Finite element method, Geometrical decoupling, Model reduction, Scaled boundary finite element method, Soil-structure interaction, Substructuring, Unbounded domain*
2010 AMS:
Received: *20 June 2018*
Accepted: *21 August 2018*
Available online: *30 September 2018*

Abstract

To analyse soil-structure-interaction problems, often unbounded domain has to be taken into account. Since the finite element method (FEM) does not provide open boundary itself the scaled boundary finite element method (SBFEM) which fulfils the radiation condition for wave propagation to infinity is used. The coupling of FEM and SBFEM in time domain is very time and memory consuming, due to the almost fully populated acceleration unit-impulse matrices and the convolution integral, which has to be solved at every time step. This paper studies ways to overcome this drawback and describes the influence of different model reduction techniques: like extrapolated acceleration unit-impulse response matrices, geometric far-field decoupling and sub-structured far-fields which can be applied to the far-field and also their combination. The different techniques for a FEM-SBFEM coupling in time domain are evaluated in terms of accuracy and computational effort.

1. Introduction

The major motivations in the analysis of soil-structure interaction are to construct reliable earthquake-resistant structures and to isolate a building from surrounding emissions to enhance its comfort or usability. The second one becomes increasingly important in our urban society. In both cases, it is vital to analyse the structure and also to take the surrounding into account [1, 23, 25].
Numerical soil-structure interaction analysis in time domain is challenging since wave propagation towards infinity has to be taken into account. Due to the phenomenon, two significantly different types of mechanic have to be addressed. First, there is the region of interest, the near-field, typically the structure itself and second, there is the infinite half-space, the far-field, surrounding the structures foundation. The common finite element method (FEM) is not directly applicable to such problems, since it does not fulfill radiation condition implicitly. The FEM can be supplemented by transmitting boundary conditions [22], absorbing boundary conditions [12, 21] or other types of transmitting boundaries like infinite elements [2, 7]. Those types of boundary conditions are reflected in [13, 14].
A more precise alternative is to discretize the half-space with the help of either the boundary element method (BEM) [4, 6] or the scaled boundary finite element method (SBFEM) [31, 32]. The BEM is based on the boundary integral representation of the physical problem and uses its fundamental solution which fulfills the radiation condition exactly. Here, the SBFEM is used because it combines the advantages of FEM and BEM. The spatial dimension is reduced by one and the radiation conditions are satisfied exactly as it is in the BEM. Just like FEM, SBFEM does not require a fundamental solution and the coefficient matrices are symmetric and can be added to the FEM matrices without changing their dimension [31, 32]. The major advantages of the SBFEM in comparison to the BEM are the symmetric matrices, which can be exploited in storage and solving process and the absence of singular integrals, which need a very special mathematical and numerical treatment.
Such numerical schemes have been applied to different two and three dimensional applications successfully. It is especially challenging to address 3D applications since computational time and memory consumption are increasingly significant. The original formulation of a coupled FEM SBFEM approach is global in space and time; hence, all degrees of freedom are coupled at the common interface and a convolution integral has to be solved [31, 32]. To solve the convolution integral acceleration unit-impulse response matrices $\mathbf{M}_t^\infty$ have to be provided for each time step t. How the $\mathbf{M}_t^\infty$ matrices are computed, is explained in [29] in detail.
With advance in time, the acceleration unit-impulse response matrix $\mathbf{M}^\infty$ grows from time step t_i to t_{i+1} with a constant increment [34, 33]. Hence, $\mathbf{M}^\infty$ can be extrapolated at later time steps, assuming a piece-wise constant approximation of $\mathbf{M}^\infty$ at each time step. Based on this

Email addresses: **m.schauer@tu-braunschweig.de (M. Schauer)**

approach, a recursive algorithm to speed up the convolutions integral computation significantly has been proposed [17, 18, 19]. A high performance SBFEM using different time scales applied to near field and far field is also discussed [27]. Instead of solving the convolution integral high-order local approaches based on continued-fractions have been proposed as well [3, 5, 9].
If real-world problems are to be investigated, this often results in very complex models with a large number of degrees of freedom. In order to be able to calculate these complex models within a reasonable time and, if necessary, to carry out additional parameter studies, it is important to have efficient models and algorithms. Therefore, this article discusses different ways of model reduction.
Here, the influence of model reduction techniques, like extrapolated acceleration unit-impulse response matrices, geometrical decoupling and sub-structured far-field, is investigated. The FEM-SBFEM coupling in time domain is analyzed in terms of accuracy and computational effort. These model reductions are applied to the original formulation of SBFEM. The influence is shown by conducting a numerical settlement simulations and taking different mesh refinements and sets of material parameters into account.

2. FEM-SBFEM coupling in time domain

Near-field and far-field are discretized by FEM and SBFEM, respectively. The near-field represents the region of interest, including structure foundation and parts of the surrounding if needed. The far-field represents the infinite half-space. Both methods are coupled at a defined common interface Γ, as shown in fig. 2.1.

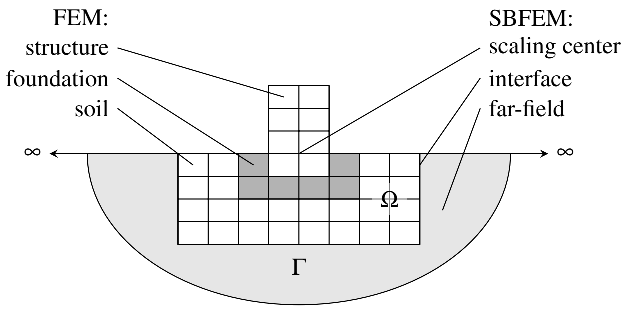

Figure 2.1: Problem definition.

The equation of motion for the displacement-based FEM is given by

$$\mathbf{M}\ddot{\mathbf{u}} + \mathbf{K}\mathbf{u} = \mathbf{p}, \tag{2.1}$$

in which $\mathbf{M}$ is the mass matrix and $\mathbf{K}$ the stiffness matrix. The vector $\mathbf{u}$ and its second derivative in time represent displacement and acceleration. Assuming that the period T can be split up into n time steps of the same size yields to a time step length $\Delta t = \frac{T}{n}$. Applying the Generalized-α scheme [10] to equation (2.1) leads to

$$(1-\alpha_{\mathrm{m}})\mathbf{M}\ddot{\mathbf{u}}_{n+1} + \alpha_{\mathrm{m}}\mathbf{M}\ddot{\mathbf{u}}_n + (1-\alpha_{\mathrm{f}})\mathbf{K}\mathbf{u}_{n+1} + \alpha_{\mathrm{f}}\mathbf{K}\mathbf{u}_n = \mathbf{p}_{n+1} - \alpha_{\mathrm{f}}\Delta t\mathbf{p}_n\,. \tag{2.2}$$

To advance in time, update rules for displacement

$$\mathbf{u}_{n+1} = \mathbf{u}_n + \Delta t\dot{\mathbf{u}}_n + \left(\frac{1}{2} - \beta\right)\Delta t^2\ddot{\mathbf{u}}_n + \beta\Delta t^2\ddot{\mathbf{u}}_{n+1}\,, \tag{2.3}$$

and velocity

$$\dot{\mathbf{u}}_{n+1} = \dot{\mathbf{u}}_n + (1-\gamma)\Delta t\ddot{\mathbf{u}}_n + \gamma\Delta t\ddot{\mathbf{u}}_{n+1} \tag{2.4}$$

are introduced. Thus, for $\alpha_m = 0$, the Generalized-α scheme is equal to the HHT$-\alpha$ [16] scheme and for $\alpha_m = 0$ and $\alpha_f = 0$ equal to the Newmark integration method [24]. The parameters α_{f}, α_{m}, β, and γ of the time step integration scheme should be set as follows

$$\alpha_{\mathrm{m}} \leq \alpha_{\mathrm{f}} \leq \frac{1}{2}, \quad \beta \geq \frac{1}{4} + \frac{1}{2}(\alpha_{\mathrm{f}} - \alpha_{\mathrm{m}}) \quad \text{and} \quad \gamma = \frac{1}{2} - \alpha_{\mathrm{m}} + \alpha_{\mathrm{f}}\,. \tag{2.5}$$

In order to couple FEM and SBFEM, the entries of the matrices in equation (2.1) have to be reordered

$$\begin{bmatrix} \mathbf{M}_{\Omega\Omega} & \mathbf{M}_{\Omega\Gamma} \\ \mathbf{M}_{\Gamma\Omega} & \mathbf{M}_{\Gamma\Gamma} \end{bmatrix}\ddot{\mathbf{u}} + \begin{bmatrix} \mathbf{K}_{\Omega\Omega} & \mathbf{K}_{\Omega\Gamma} \\ \mathbf{K}_{\Gamma\Omega} & \mathbf{K}_{\Gamma\Gamma} \end{bmatrix}\mathbf{u} = \begin{bmatrix} \mathbf{p}_{\Omega\Omega} \\ \mathbf{p}_{\Gamma\Gamma} \end{bmatrix} - \begin{bmatrix} \mathbf{0} \\ \mathbf{p}_b \end{bmatrix} \tag{2.6}$$

so that the block with the subscript "ΩΩ" contains all nodes located in the near-field while the block with subscript "ΓΓ" contains all nodes at the far-field-interface. The blocks with the subscripts "ΩΓ" and "ΓΩ" include the coupling information of near-field and far-field nodes. The vector $\mathbf{p}_b$ acts on the boundary Γ only. This additional force describes the response of the infinite half-space and can be applied to the near-field as a load.
The forces acting at the interface of near-field and far-field are given by the convolution integral

$$\mathbf{p}_b(t) = \int_0^t \mathbf{M}^{\infty}(t-\tau)\ddot{\mathbf{u}}(\tau)d\tau\,, \tag{2.7}$$

in which $\mathbf{M}^{\infty}(t)$ is the unit-impulse matrix. To solve the convolution integral (2.7), the unit-impulse matrices $\mathbf{M}_i^{\infty}$ are assumed to be constant within the time step Δt,

$$\mathbf{M}^{\infty}(t) = \begin{cases} \mathbf{M}_0^{\infty} & t \in [0;\Delta t], \\ \mathbf{M}_1^{\infty} & t \in [\Delta t; 2\Delta t], \\ \vdots & \vdots \\ \mathbf{M}_{n-j}^{\infty} & t \in [(n-j-1)\Delta t; (n-j)\Delta t], \\ \vdots & \vdots \\ \mathbf{M}_{n-1}^{\infty} & t \in [(n-2)\Delta t; (n-1)\Delta t], \\ \mathbf{M}_n^{\infty} & t \in [(n-1)\Delta t; n\Delta t]. \end{cases} \tag{2.8}$$

Due to this assumption and when applying the time step integration scheme, equation (2.7) can be rewritten as

$$\mathbf{p}_b(t_n) = \gamma \Delta t \mathbf{M}_0^{\infty} \ddot{\mathbf{u}}_n + \sum_{j=1}^{n-1} \mathbf{M}_{n-j}^{\infty} \left(\dot{\mathbf{u}}_j - \dot{\mathbf{u}}_{j-1}\right). \tag{2.9}$$

The coupling of FEM and SBFEM is realized by simply adding equation (2.9) to the resorted FEM (2.6)

$$\begin{bmatrix} \mathbf{M}_{\Omega\Omega} & \mathbf{M}_{\Omega\Gamma} \\ \mathbf{M}_{\Gamma\Omega} & \mathbf{M}_{\Gamma\Gamma} + \gamma \Delta t \mathbf{M}_0^{\infty} \end{bmatrix} \ddot{\mathbf{u}} + \begin{bmatrix} \mathbf{K}_{\Omega\Omega} & \mathbf{K}_{\Omega\Gamma} \\ \mathbf{K}_{\Gamma\Omega} & \mathbf{K}_{\Gamma\Gamma} \end{bmatrix} \mathbf{u} = \begin{bmatrix} \mathbf{p}_{\Omega\Omega} \\ \mathbf{p}_{\Gamma\Gamma} - \sum_{j=1}^{n-1} \mathbf{M}_{n-j}^{\infty} \left(\dot{\mathbf{u}}_j - \dot{\mathbf{u}}_{j-1}\right) \end{bmatrix}, \tag{2.10}$$

so the FEM-SBFEM coupling is fully described mathematically.

3. Numerical example

For the purpose of validation, a simple settlement problem is chosen and the numerical solution will be compared by analytical solutions. Therefore, an infinite half-space is loaded on a square region of $152.4 \times 152.4\text{m}^2$ by a constant load $q = 70.0\text{kNm}^{-2}$ as depicted in figure 3.1. The SBFEM scaling centre is located in the centre of the loaded area. The distance between scaling centre and boundary Γ is given by the radius $r = 190.2\text{m}$. Loosely deposited sand is chosen, the material parameters are set as follows: Young's modulus $E = 37150.0\text{kNm}^{-2}$, Poisson's ratio $\nu = 0.48$ and mass $\rho = 1800.0\text{kgm}^{-3}$.

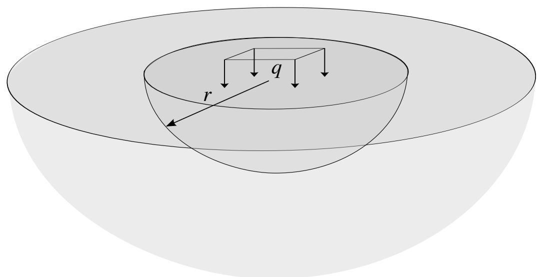

Figure 3.1: Settlement problem configuration: Near-field with radius $r = 190.2\text{m}$ and distributed load $q = 70\text{kNm}^{-2}$ on an area of $152.4 \times 152.4\text{m}^2$.

3.1. Analytical solution

The settlement and stresses underneath a loaded area at an infinite, isotropic and elastic half space can be evaluated analytically. For the given problem, the settlement at the corner of the applied load is evaluated by solving a semi-analytical approach suggested by Harr [15]. This approach can be simplified when the loaded area is perfectly square

$$s(z) = \frac{qb}{2\pi E}\left(1-\nu^2\right)\left(2\ln\left(\frac{m+1}{m-1}\right) - n\frac{1-2\nu}{1-\nu}\arctan\left(\frac{1}{nm}\right)\right) \tag{3.1}$$

with $m = \sqrt{2+n^2}$ and $n = \frac{z}{b}$. The corresponding stresses and shear stresses along the z-direction are given by analytic solutions [26], which can also be simplified, since the loaded area is perfectly square. Due to the symmetry of the given example $\sigma_x = \sigma_y$ and $\tau_{yz} = \tau_{xz} = \tau_{xy} = 0.0$ in the very centre of the loaded area, so that for validation purpose

$$\sigma_x(z) = \frac{q}{2\pi}\left(\arctan\left(\frac{b^2}{z\sqrt{2b^2+z^2}}\right) - \frac{b^2 z}{\left(b^2+z^2\right)\sqrt{2b^2+z^2}}\right), \tag{3.2}$$

$$\sigma_z(z) = \frac{q}{2\pi}\left(\arctan\left(\frac{b^2}{z\sqrt{2b^2+z^2}}\right) + \frac{2b^2 z}{\left(b^2+z^2\right)\sqrt{2b^2+z^2}}\right), \tag{3.3}$$

$$\tau_{xy} = 0.0 \tag{3.4}$$

as well as the von Mises stress

$$\sigma_{\mathrm{v}}(z)=\sqrt{\sigma_x(z)^2-2\sigma_x(z)\,\sigma_z(z)+\sigma_z(z)^2} \tag{3.5}$$

are taken into account. Thereby, b describes the physical dimension of the loaded area. To evaluate the settlement and stresses in the centre of the loaded area, the loaded region has to be subdivided into four squares of the same size and has to be evaluated separately. The outcome result of these four subregions must be superposed to get the state variables of settlement and stresses.

3.2. Numerical solution

In order to show the accuracy of the coupled FEM-SBFEM method, the meshes of near-field and far-field are refined several times, so that the geometry becomes smoother with each step of refinement. This also leads to an increasing number of degrees of freedom (DoF), as shown in Table 1. To speed up the computation, all meshes have been optimized by renumbering the containing DoF [11].

Table 1: Mesh discretization with different number of DoF. The meshes correspond to [29].

Mesh	M1	M2	M3	M4	M5	M6	M7	M8
$\mathrm{DoF}_{\mathrm{FEM}}$	396	738	1314	3096	6030	9033	14655	19818
$\mathrm{DoF}_{\mathrm{SBFEM}}$	123	219	291	480	843	1083	1515	1827

The longitudinal wave speed is $c_{\mathrm{p}}=\sqrt{\frac{E(1-\nu)}{\rho(1+\nu)(1-2\nu)}}=425.779\mathrm{ms}^{-1}$, so that the critical time step length is given by $\Delta t_{\mathrm{crit}}=\frac{r}{30c_{\mathrm{p}}}=0.0149\mathrm{s}$ as it is suggested by Borsutzky [8]. The numerical solution is carried out for a period of 6.25s with a time step length $\Delta t=0.0125\mathrm{s}\leq\Delta t_{\mathrm{crit}}$, so that 500 time steps have to be computed. Since the settlement problem is solved in time domain, the chosen period must assure that the system reaches its steady-state within this period [29]. The parameters of the Generalized-α time step integration scheme can be defined by a dissipation parameter within the range $0\leq\rho_\infty\leq1$ ($\rho_\infty=0$ asymptotic annihilation, $\rho_\infty=1$ no dissipation). Here, $\rho_\infty=0.6$ is chosen; hence, numerical damping is introduced by the time step integration scheme, this yields to integration parameters $\alpha_m=\frac{1}{8}$, $\alpha_f=\frac{3}{8}$, $\beta=\frac{25}{64}$, and $\gamma=\frac{3}{4}$.

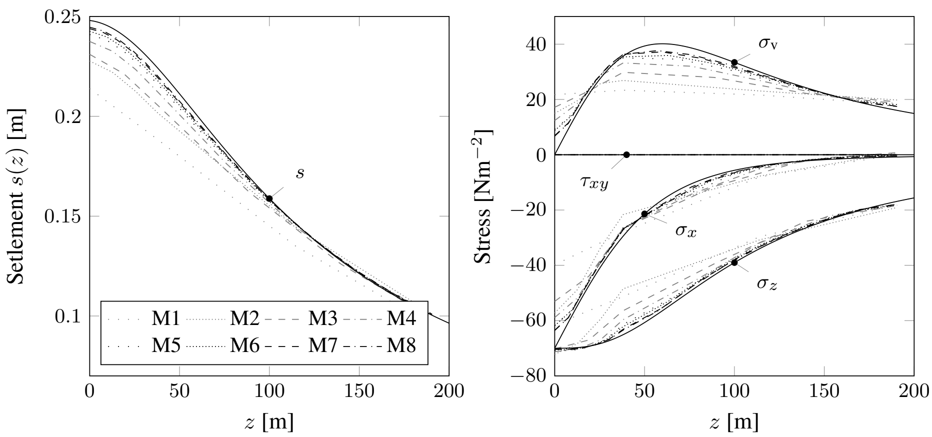

Figure 3.2: Analytic (solid black line) and numerical solutions for settlement and stresses.

In figure 3.2, the analytical solutions for settlement (eq. (3.1)) and stresses (eq. (3.2)–(3.5)) are shown. The analytical solutions and the numerical results at steady-state of the meshes M1 to M8 are depicted. Refining the meshes leads to a better accuracy of the numerical results. This is confirmed by the graphs.

4. Model reduction techniques

Computing the $\mathbf{M}^\infty$ matrices and solving the convolution integral requires a high computational effort. To simulate n time steps, for each time step a matrix which includes the N DoF at the interface Γ has to be stored in computers memory. Since the matrices are usually almost fully populated, $N\times N\times n$ values have to be stored. Additionally, there are $N\times n$ values for the nodal velocities at the interface to store. Another disadvantage is the convolution integral itself, since its computation requires more and more time with increasing time steps to conduct the matrix vector multiplications. These two disadvantages of this coupled approach cannot be cured completely, but significantly improved.
To overcome the high time and memory consumption of the coupled FEM-SBFEM approach in time domain, different model reduction techniques are discussed and evaluated in terms of accuracy and computational effort. The following sections pay attention on how the results are influenced by applying the following model reduction techniques: extrapolated acceleration unit-impulse response matrices 4.1, geometric far-field decoupling 4.2 and sub-structured far-fields 4.3 which can be applied to the far-field. Additionally, combinations of model reduction techniques are discussed 5.

4.1. Extrapolation of $\mathbf{M}^\infty$

Analysing the evolution of the $\mathbf{M}^\infty$ entries exhibit that they grow constantly after a certain time step. The simplest and fastest way to check the constant growth is to evaluate the behaviour of one arbitrary single matrix entry to find the time step t_m from which linear behaviour of

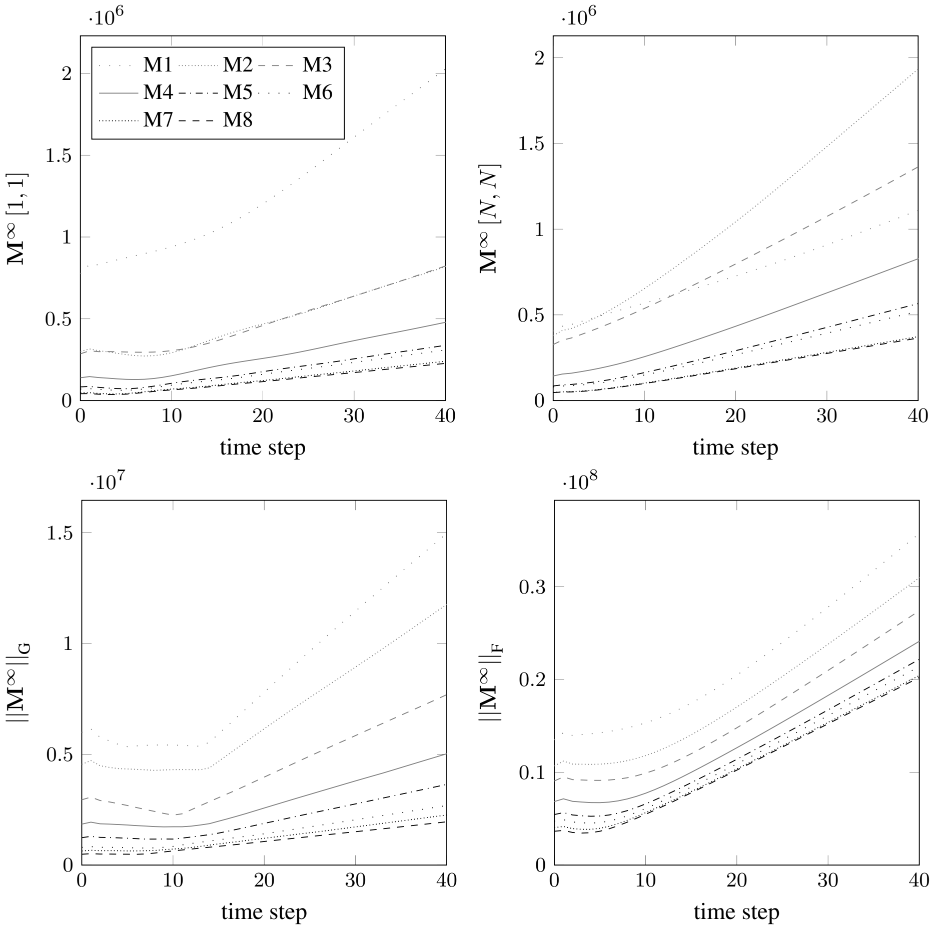

Figure 4.1: The time dependent behaviour of $\mathbf{M}^{\infty}$ evaluated by different approaches.

the matrix is assumed. Alternatively, a matrix norm can be used to check constant growth of the matrices, like the total norm

$$||\mathbf{M}^{\infty}||_{\mathrm{G}} = N \max_{i,j=1,\ldots,N} |m_{ij}| \tag{4.1}$$

or the Frobenius norm

$$||\mathbf{M}^{\infty}||_{\mathrm{F}} = \sqrt{\sum_{i=1}^{N}\sum_{j=1}^{N} m_{ij}^2}\,. \tag{4.2}$$

All three approaches lead to remarkably different data, which has to be reviewed. This also results in significantly different assumptions of the time step t_m, starting from which constant growth can be assumed and extrapolation is started for the coupled computation. The data of the first 40 time steps is shown in figure 4.1. Reviewing the graphs in figure 4.1 consequently leads to the following points:

(i) The values inside the matrix do not behave in the same manner. This is clearly depicted by the graphs $\mathbf{M}_n^{\infty}[1;1]$ and $\mathbf{M}_n^{\infty}[N;N]$. From this, it follows that the chosen matrix entry has an influence on the time step t_m and, thus, on the coupled problems solution.
(ii) The total norm $||\mathbf{M}^{\infty}||_{\mathrm{G}}$ provides usable values which are adverse for numerical treatment. Checking constant growth by algorithms might lead to improper time starting from where constant growth is assumed and consequently to wrong solutions.
(iii) The Frobenius norm $||\mathbf{M}^{\infty}||_{\mathrm{F}}$ shows the best behaviour to check constant growth. This is doubtless due to the consideration of all matrix entries. Unfortunately, this approach also is the one with the highest computational effort.

4.1.1. Algorithm

The algorithm discussed is based on [17]. For the purpose of linearising the unit-impulse matrices, these matrices have to split up for every time step t_n with $n > m$, that yields

$$\mathbf{M}_n^{\infty} = \mathbf{T}^{\infty} t_n + \mathbf{C}^{\infty}\,. \tag{4.3}$$

Here, $\mathbf{C}^{\infty}$ is a constant matrix and $\mathbf{T}^{\infty}$ describes the gradient of the unit-influence matrix $\left(\frac{\Delta \mathbf{M}^{\infty}}{\Delta t}\right)$, which is

$$\mathbf{T}^{\infty} = \mathbf{M}_{m+1}^{\infty} - \mathbf{M}_m^{\infty} \tag{4.4}$$

for an equidistant time step size Δt. Equation (2.9) has to be split up into two subtotals. The first subtotal considers the non-linear matrices for the time steps t_n, $1 \leq n \leq m$, the second subtotal represents the linear matrices for all time steps t_n, $n > m$. This yields to

$$\begin{aligned} \mathbf{p}_b(t_n) &= \gamma \Delta t \mathbf{M}_0^\infty \ddot{\mathbf{u}}_n + \mathbf{p}_b^{\mathrm{l}}(t_n) + \mathbf{p}_b^{\mathrm{nl}}(t_n), \\ &= \gamma \Delta t \mathbf{M}_0^\infty \ddot{\mathbf{u}}_n + \sum_{j=1}^{n-m+1} \mathbf{M}_{n-j+1}^\infty \left(\dot{\mathbf{u}}_j - \dot{\mathbf{u}}_{j-1}\right) + \sum_{j=n-m+2}^{n-1} \mathbf{M}_{n-j+1}^\infty \left(\dot{\mathbf{u}}_j - \dot{\mathbf{u}}_{j-1}\right). \end{aligned} \tag{4.5}$$

Solving the non-linear terms $\mathbf{p}_b^{\mathrm{nl}}(t_n)$ is analogous to equation (2.9). The linear term $\mathbf{p}_b^{\mathrm{l}}(t_n)$ is transferred into a recursive algorithm. Inserting equation (4.3) into the linear term of equation (4.5) leads to

$$\begin{aligned} \mathbf{p}_b^{\mathrm{l}}(t_n) &= \sum_{j=1}^{n-m+1} \left(\mathbf{T}^\infty t_{n-j+1} + \mathbf{C}^\infty\right) \left(\dot{\mathbf{u}}_j - \dot{\mathbf{u}}_{j-1}\right), \\ &= \left(\mathbf{T}^\infty t_m + \mathbf{C}^\infty\right) \left(\dot{\mathbf{u}}_{n-m+1} - \dot{\mathbf{u}}_{n-m}\right) + \sum_{j=1}^{n-m} \left(\mathbf{T}^\infty t_{n-j+1} + \mathbf{C}^\infty\right) \left(\dot{\mathbf{u}}_j - \dot{\mathbf{u}}_{j-1}\right), \\ &= \mathbf{M}_m^\infty \left(\dot{\mathbf{u}}_{n-m+1} - \dot{\mathbf{u}}_{n-m}\right) + \sum_{j=1}^{n-m} \left(\mathbf{T}^\infty t_{n-j+1} + \mathbf{C}^\infty\right) \left(\dot{\mathbf{u}}_j - \dot{\mathbf{u}}_{j-1}\right). \end{aligned} \tag{4.6}$$

Inside the recursive algorithm

$$\mathbf{p}_b^{\mathrm{l}}(t_{n-1}) = \sum_{j=1}^{n-m} \left(\mathbf{T}^\infty t_{n-j} + \mathbf{C}^\infty\right) \left(\dot{\mathbf{u}}_j - \dot{\mathbf{u}}_{j-1}\right) \tag{4.7}$$

is needed, hence, n has to be substituted by $n-1$ in equation (4.6). Applying the difference from $\mathbf{p}_b^{\mathrm{l}}(t_n)$ to $\mathbf{p}_b^{\mathrm{l}}(t_{n-1})$ results in the recursive formula

$$\mathbf{p}_b^{\mathrm{l}}(t_n) = \mathbf{p}_b^{\mathrm{l}}(t_{n-1}) + \mathbf{M}_m^\infty \left(\dot{\mathbf{u}}_{n-m+1} - \dot{\mathbf{u}}_{n-m}\right) + \mathbf{T}^\infty \left(\dot{\mathbf{u}}_{n-m} - \dot{\mathbf{u}}_0\right). \tag{4.8}$$

Each following time step can be computed in the same manner. Based on this linearisation, $N \times N \times m$ values are to be stored instead of the previous $N \times N \times n$ values, with $m \leq n$. The number of interface velocities $N \times n$ to be stored does not change.

4.1.2. Numerical results

The influence of matrix extrapolation to the solution of a given problem is discussed next. Therefore, two meshes (M5 and M8) from section 3 are analyzed, assuming that the unit-impulse response matrix grows constantly after a defined instant of time t_m. When constant growth of $\mathbf{M}^\infty$ is assumed, only m matrices are computed, all other matrices are extrapolated (see eq. (4.4)).

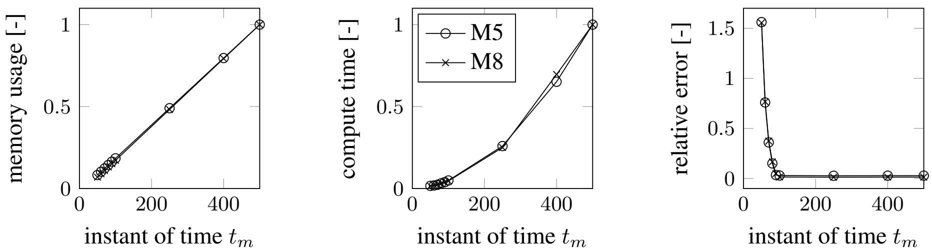

Figure 4.2: Influence of matrix extrapolation to the settlement problem: Normalized memory usage, normalized compute time and corresponding relative error.

Figure 4.2 summarizes the most important results of the examination. The normalized memory consumption, normalized compute time and relative error of the computed displacement $s(z=0)$ in the centre of the loaded area with respect to the instant of time t_m from where constant growth of $\mathbf{M}^\infty$ is assumed are shown. The memory needed to provide the $\mathbf{M}^\infty$ matrices can be reduced significantly by assuming that they grow with constant increment. In order to show the reduction of memory usage for each instant of time t_m, the memory usage is related to the memory usage when no model reduction is done and all matrices are provided, hence $t_m = 500$.

By reducing the number of $\mathbf{M}^\infty$ matrices, the computational effort is reduced as well. The corresponding normalized computing times are shown for both meshes. In both cases, the computation time of $t_m = 500$ has been used for normalization. As long as the instant of time t_m is chosen at a permissible time step, the relative error of the numerical simulation stays constant. If the number of provided matrices is too little (extrapolation it started too early), the relative error of the computation increases obviously.

Here, 100 matrices are sufficient to solve the given problem without increasing the relative error. This means a reduction of memory consumption of 81.6% and at the same time a reduction of the computational effort of 95.1% in case of mesh M5. The reductions for mesh M8 are even greater with 82.8% and 95.4%. When too few matrices are provided, consequently, the far-field leaks stiffness and the computed settlement becomes too large. If the number of matrices is reduced further, the simulation may become unstable and the near-field might float into direction of the applied forces due to insufficient far-field response.

Further numerical studies using different sets of material parameters, as summarised in table 2, have been conducted using the mesh M5. The time step Δt and the integration scheme parameters stay unchanged. All conducted simulations lead to similar results regarding the following parameters: memory consumption, compute time and relative error. Figure 4.3 shows the settlement at time step $t = 500$, 6.25s at the surface in the centre of the loaded area, when only $t_m = \{50, 60, 70, 80, 90, 100, 110, 150, 200, 250, 400, 500\}$ $\mathbf{M}^\infty$ matrices are provided and all further matrices are extrapolated as discussed before. Additionally, the corresponding relative error with respect to equation (3.1) is shown up to 10%. It is obvious that the error increases when too few matrices are provided and extrapolating of the far-fields' influence starts too early.

Table 2: Material sets.

	E kNm^{-2}	ν	ρ kgm^{-3}	c_p ms^{-1}	c_s ms^{-1}
loosely deposited sand	37150.0	0.48	1800.0	425.779	83.502
lose gravel	82000.0	0.30	1600.0	262.660	140.398
semi-stiff clay	26000.0	0.45	2200.0	211.725	63.838
crushed rock	150000.0	0.35	2100.0	338.583	162.650
rock	300000.0	0.25	2400.0	387.299	223.607

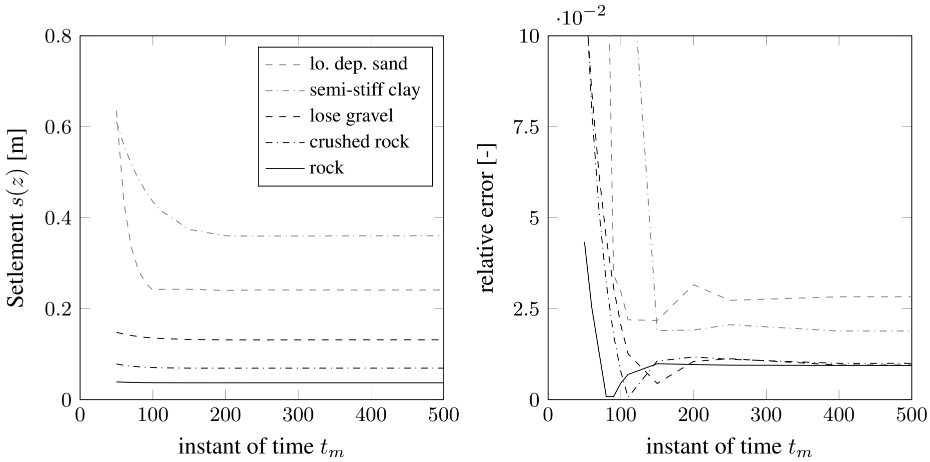

Figure 4.3: Settlements' steady-state and relative error at 6.25s, when t_m is chosen.

4.2. Far-field decoupling

The matrices are fully populated, so that all nodes at the near-field far-field interface are coupled with each other. Having a closer look to the matrix entries lead to the awareness that the geometrical distance of two nodes at the interface Γ influences the matrix entry strongly. The position of two nodes within the matrix has no influence. How strong the influence of two node turns out is determined by the corresponding entry in $\mathbf{M}^{\infty}$ matrices. The smaller the distance of two node (the closer they are), the bigger is this matrix entry. The bigger the distance of two nodes, the smaller is the matrix entry. Assuming that the influence of two very far nodes has no recognizable influence to the simulation lead to introduce a threshold ε_z, which defines the minimum value considered in the $\mathbf{M}^{\infty}$ matrices. The threshold is applied to the matrix entries after its computation, so it is some kind of a post process. Figure 4.4 shows the assignment of $\mathbf{M}_0^{\infty}$ at time step $t = 0$, all non-zero entries are pictured by a small dot. Entries containing value of zero or a value smaller then ε_z are not pictured. Here, the threshold varies within the range $1.0 \times 10^{-7} \leq \varepsilon_z \leq 1.0 \times 10^{-1}$. It is evident how the introduced threshold influences the matrix appearance. The bigger ε_z is chosen to be, the less information is stored in the matrix.

(a) $\varepsilon_z = 1.0 \times 10^{-7}$. **(b)** $\varepsilon_z = 1.0 \times 10^{-5}$. **(c)** $\varepsilon_z = 1.0 \times 10^{-3}$. **(d)** $\varepsilon_z = 1.0 \times 10^{-1}$.

Figure 4.4: M3 matrix assignment of $\mathbf{M}_0^{\infty}$ using geometrical decoupling.

The pictured matrices are generated by examining the example M3 (see Table 1). If no threshold is set, the matrices have $291 \times 291 = 84681$ entries, and are fully populated. Introducing threshold $\varepsilon_z = 1.0 \times 10^{-7}$ results in 49855 non-zero values and sparsity of 58.87%. When $\varepsilon_z = 1.0 \times 10^{-5}, 1.0 \times 10^{-3}, 1.0 \times 10^{-1}$ is set 28.6%, 8.51% and 1.2% of memory is needed, respectively. Similar reductions have been shown in [8, 20].

Since the magnitude of each matrix entry changes from one time step to another, the number of matrix entries to be stored may change as well. In order to optimize the memory needed, the sparcity pattern is not constant any more, but may change from one time step to another. That is why the implementation of the algorithm has to be done carefully.

The influence of far-field decoupling is analysed by evaluation memory usage, compute time and relative error of final displacement. Therefore, the influence matrices $\mathbf{M}_i^{\infty}$ are computed using different geometrical thresholds ε_z for M8 (see Table 1). The tolerance value lies within the range $\varepsilon_z = 1.0 \times 10^{-8}$ to $\varepsilon_z = 1.0 \times 10^{-2}$. The results are shown in figure 4.5.

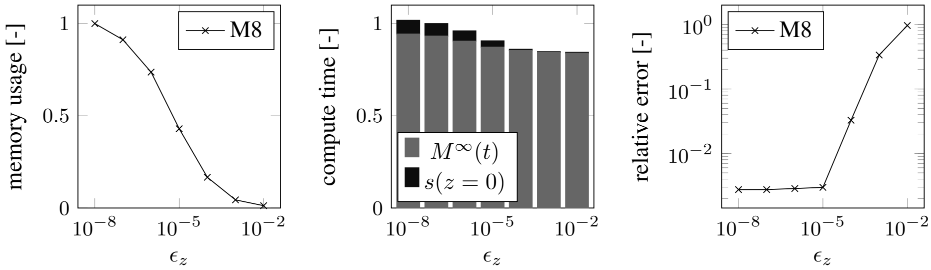

(a) Normalized memory usage. (b) Normalized compute time. (c) Relative error.

Figure 4.5: Normalized memory usage of $\mathbf{M}_0^\infty$ (a), normalized compute time (b) and relative error of final displacement (c) with respect to the chosen geometrical decoupling threshold ε_z.

Memory usage and compute time are normalized by the chosen reference solution using $\varepsilon_z = 1.0 \times 10^{-8}$. The relative error shows the computed displacement $s(z=0)$ compared to the given analytic solution in equation (3.1). It is obvious that increasing the ε_z decreases memory usage strongly and somewhat compute time, as shown in figure 4.5a and figure 4.5b, respectively. In this case, for small $1.0 \times 10^{-8} \leq \varepsilon_z \leq 1.0 \times 10^{-5}$ the relative error stays almost constant, and the advantage of less memory usage (down to 16%) should be used. When ε_z becomes too large the error increases and the user has to decide up to which error the result is still acceptable (see figure 4.5c). The other meshes M1 to M7 show very similar behaviour.

Far-field decoupling only reduces the amount of memory needed, since the entire far-field is discretized. Therefore, the far-field decoupling has no relevant influence to compute effort and time. As one can see in figure 4.5b, almost 85% of compute time is needed compared to the reference simulation also for large tolerances $\varepsilon_z \geq 1{,}0 \cdot 10^{-4}$. The reason for this behaviour is also obvious, since the system size at the interface stays constant and so the complexity of equations to solve. Only the time needed for memory access does change since matrices may be more sparse due to the far-field decoupling.

4.3. Far-field sub-structuring

As already mentioned, the geometrical far-field decoupling has no relevant influence on the compute time. Alternatively to the model reduction in post process, as described in previous section, it is possible to do a model reduction in a preprocess, before the matrices $\mathbf{M}^\infty$ are computed. For this purpose, the far-field has to be sub structured [32]. When the far-field is decomposed in sub structures artificial boundaries are introduced. These boundaries decouple nodes with large distance, which have small interaction, as described before. Each sub structure contains only a fraction of all nodes located at the interface Γ. For each sub structure $\mathbf{M}^\infty$ can be computed independently. In figure 4.6a, the interface of mesh M3 is shown. The figures 4.6b to 4.6d show sub-structured interfaces examples.

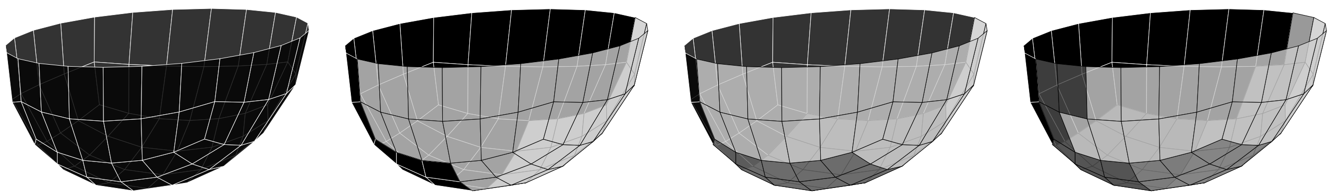

(a) No sub-structure. **(b)** Two sub-structures. **(c)** Three sub-structures. **(d)** Four sub-structures.

Figure 4.6: M3 subdivided in different numbers of sub-structures.

This is justified by the coupling of FEM and SBFEM, since the substructures have common interface nodes. This common interface nodes couple the different substructures on the boundary. Along the line from scaling center to these nodes towards infinity the substructures stay uncoupled. The coupling of sub-structured influence matrices, here $\mathbf{M}_0^\infty$, is shown in the figures 4.7b to 4.7d. The pattern of the full matrix 4.7a is also present in the pattern of sub-structured matrices. The color of matrix entries in figure 4.7 correspond to the color of substructures in figure 4.6.

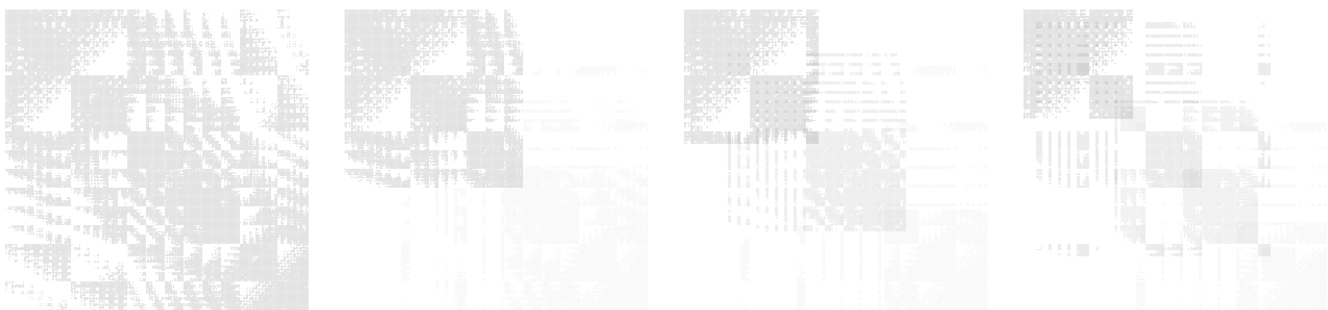

(a) No sub-structure. **(b)** Two sub-structures. **(c)** Three sub-structures. **(d)** Four sub-structures.

Figure 4.7: M3 matrix assignment of $\mathbf{M}_0^\infty$ using sub-structuring.

For each sub-structure, ε_z is set to 1.0×10^{-7} when $\mathbf{M}_0^\infty$ is computed, so that the figures 4.7a and 4.4a are identical in comparison of related figures. In contrast to the geometrical decoupling, the pattern of the influence matrix changes in a totally different way when sub-structuring is applied. The reduction of memory usage is possible and can be derived by figure 4.7 easily. It is also obvious that with an increasing number of sub-structures the size of each matrix is reduced and the ratio of matrix entries to allocated values increases. This indicates that the interaction of the nodes within one sub-structure is relatively strong. With increasing number of sub-structures the number of non-zero values within a matrix increases as well, since the nodes within a sub-structure are geometrically very close to each other. The size of $\mathbf{M}_0^\infty$ corresponding to the sub-structured domain pictured in figures 4.6 as well as the allocated number of entries and the resulting ratio compared to the full matrix without sub-structuring is summarized in table 3.

Table 3: Size and allocation of sub-structured $\mathbf{M}_0^\infty$ matrices.

sub-structures	matrix size	$\text{entries}_{\text{sub}}$	$\text{allocated}_{\text{tot}}$	ratio [%]
1	291×291	84681	84681	100.00
2	171×171	29241		
	171×171	29241	58482	69.06
3	129×129	16641		
	123×123	15129		
	129×129	16641	48411	57.17
4	105×105	11025		
	102×102	10404		
	99×99	9801		
	105×105	11025	42255	49.90

The artificial boundary does not only decouple far distant nodes, but also direct neighbor nodes, who naturally strongly interact. However, this approach leads to good results if the topology of element mesh is taken into account during sub-structuring process [30]. Theoretically, it is also possible to do the sub-structuring based on nodes instead of elements. This would reduce the amount of data even further; hence, interface nodes would appear only once. This certainly implies that information of some elements is lost, so that the influence of the half-space is not fully considered. Overlapping of sub-structures is impossible, since there are no common nodes. If the size of the neglected elements is small, this approach leads to a comparable approach. Another possibility is to use patches as discussed in [28]. The reduction of memory usage is obvious as well and can be derived by figure 4.7 easily.

In order to analyze the influence of sub-structuring technique to the solution, computations with different number of sub-structures are performed. Therefore, the far-field-interface of M8 is decomposed based on elements into n sub-structures. As already mentioned, each sub-structure represents only a part of the entire far-field and can be solved separately. By doing so, the system size of each sub-structure is reduced compared to the initial configuration, in which the entire interface is taken into account. When the given problem is computed FEM and SBFEM are coupled (cf. eq. (2.6)) and consequently the sub-structures as well:

$$\begin{bmatrix} \mathbf{M}_{\Omega\Omega} & \mathbf{M}_{\Omega\Gamma} \\ \mathbf{M}_{\Gamma\Omega} & \mathbf{M}_{\Gamma\Gamma} \end{bmatrix} \ddot{\mathbf{u}} + \begin{bmatrix} \mathbf{K}_{\Omega\Omega} & \mathbf{K}_{\Omega\Gamma} \\ \mathbf{K}_{\Gamma\Omega} & \mathbf{K}_{\Gamma\Gamma} \end{bmatrix} \mathbf{u} = \begin{bmatrix} \mathbf{p}_{\Omega\Omega} \\ \mathbf{p}_{\Gamma\Gamma} \end{bmatrix} - \sum \begin{bmatrix} \mathbf{0} \\ \mathbf{p}_b^{\text{sub}} \end{bmatrix}, \tag{4.9}$$

when $\mathbf{p}_b^{\text{sub}}$ is evaluated for each sub-structure.

In figure 4.8, the interface of mesh M8 is shown, divided into two, four and eight structures.

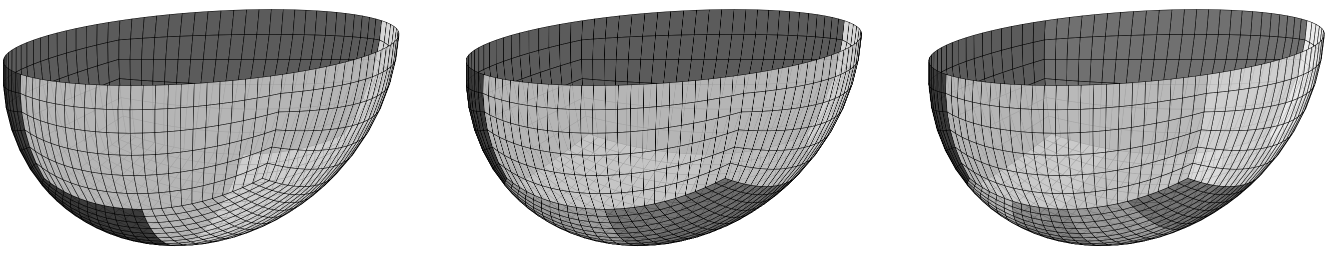

(a) Two sub-structures. **(b)** Four sub-structures. **(c)** Eight sub-structures.

Figure 4.8: M8 subdivided into different number of sub-structures.

The influence of the introduced artificial boundaries is depicted in figure 4.9. With an increasing number of sub-structures, memory usage and compute time are reduced significantly as shown in 4.9a and 4.9b. This behavior is expected, since reducing size and so the number of degrees of freedom at the interface reduces the complexity of the problem and so the time to compute it [29].

Figure 4.9c shows the relative error of the conducted settlement simulation with respect to number of sub-structures. Compared to the previous approach in section 4.2, the relative error is growing faster. The error increases clearly when 2 to 6 sub-structures are introduced, thereafter the relative error stays almost constant. If additional artificial boundaries are introduced, the far-field looses stiffness and the settlement is overestimated. From the engineering point of view, this approach leads to conservative results. The big advantage of this approach is that sub-structuring reduces memory consumption and also compute time massively (see fig. 4.9a and 4.9b). Such a massive reduction can neither be realized by extrapolation of $\mathbf{M}_0^\infty$ nor by using a far-field decomposition technique.

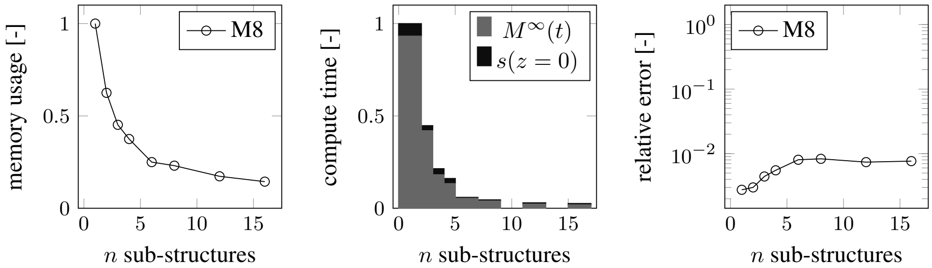

(a) Normalized memory usage. (b) Normalized compute time. (c) Relative error.

Figure 4.9: Normalized memory usage of $\mathbf{M}_0^\infty$ (a), normalized compute time (b) and relative error of final displacement (c) with respect to the number of sub-sections n.

5. Combination of model reduction techniques

Next, combinations of the presented model reduction techniques are discussed. Artificial boundaries are introduced as discussed in section 4.3 when the domain is sub-structured. This has a direct influence on the computational result, due to decoupling of neighbor nodes which normally have a strong interaction. Figure 5.1 shows a reduction of memory consumption and compute time to 62% and 45%, respectively when far-field is decomposed into three sub-structures. In this case, the relative error only increases slightly. The geometrical decoupling as discussed in section 4.2 is able to reduce memory consumption significantly, in figure 5.1 one can see that the memory usage can be reduced to 45% without increasing the relative error. Its influence to compute time is of minor importance (93%), since the problem size and so the complexity stays constant. The speed up arises from the reduction of amount of data. When extrapolation of $\mathbf{M}^\infty$ at t_m is done, as discussed in section 4.1, memory usage and computational effort can be reduced down to less than 20% and 5%, respectively without increasing the relative error.

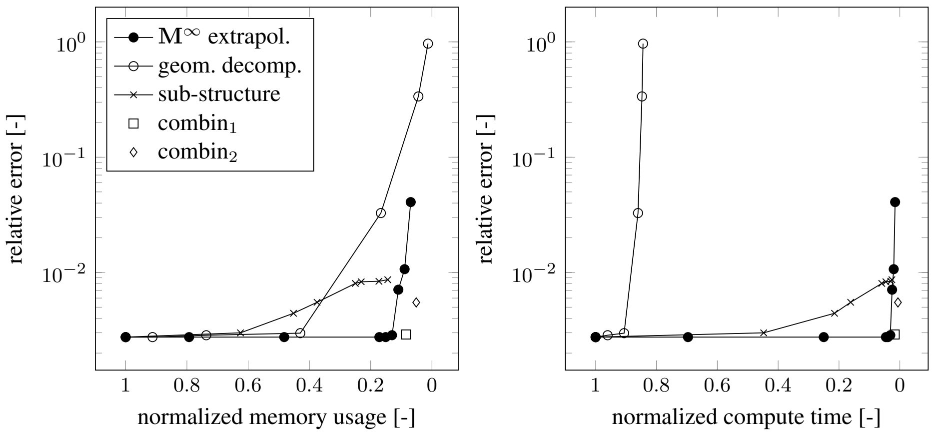

Figure 5.1: Relative error of $\mathbf{M}^\infty$ extrapolation, geometrical decoupling and sub-structuring in relation to normalized memory usage (a) and normalized compute time (b).

The strong effect of far-field sub-structuring to reduce computational time significantly is shown. Hence, it is promising to combine the far-field sub-structuring with the geometrical decoupling. Geometrical decoupling has no significant influence on the relative error but on the memory consumption cf. section 4.2. With increasing number of sub-structures, the error does not rise significantly. When sub-structuring and geometical far-field decompositions is combined and ε_z is chosen large enough, the pattern of sub-structured matrices correlates with matrices of full far-field nearly completely [8]. If ε_z is chosen to be small this is not the case. Table 4 shows the same configuration as table 3 but with taking geometric decoupling into account. Here, ε_z is chosen to be 1.0×10^{-7}. How big the further reduction is another ≈10 to ≈40%, depends strongly on the number of sub structures but without increasing the relative error.
If all three model reduction techniques are combined, the memory consumption and computational effort can be reduced even further. This can be shown by the next two examples impressively: if far-field is subdivided into two sub-structures, ε_z and t_m are chosen to be $1.0 \cdot 10^{-6}$, 60, respectively. The memory consumption and compute time can be reduced to ≈2 and ≈9%, respectively, compared to the reference solution of M8 when no model reduction is applied (cf. fig.5.1 combin$_1$). The relative error is 2.9×10^{-3} compared to the analytical solution and is dominated by the sub-structuring method, the other two model reductions have no observable influence on the solution. Subdividing the far-field into four instead of two sub-structures and setting up the same parameters for ε_z and t_m, leads to a memory consumption and compute time of ≈1 and ≈5%, respectively, compared to the reference solution (cf. fig.5.1 combin$_2$). The relative error increases to 5.5×10^{-3} which is almost twice as high. In this case, the relative error is also clearly dominated by the sub-structuring method. Similar reductions of memory usage and computational effort have been discussed in [30], in which the meshes as well as the reduction have been smaller. This leads to the awareness that the gain of model reduction techniques rises the bigger and the more complex the problems are.

6. Conclusion

A coupled approach of FEM and SBFEM is particularly well suited for applications, whenever complex structures have to be analysed and an infinite halfspace has to be taken into account, since the standard FEM can handle complex geometries with different types of material easily

Table 4: Size and allocation of sub structured $\mathbf{M}^{\infty}$ matrices of M3 with $\varepsilon_z = 1.0 \times 10^{-7}$.

sub structures	matrix size	entries	$\text{allocation}_{\text{sub}}$	$\text{allocation}_{\text{tot}}$	$\text{ratio}_{\text{sub}}$ [%]	$\text{ratio}_{\text{total}}$ [%]
1	291×291	84681	49855	49855	58.87	58.87
2	171×171	29241	19601		67.03	
	171×171	29241	19605	39206	67.05	46.30
3	129×129	16641	11665		70.10	
	123×123	15129	11567		76.46	
	129×129	16641	11673	34905	70.15	41.22
4	105×105	11025	8105		73.51	
	102×102	10404	8102		77.87	
	99×99	9801	8015		81.78	
	105×105	11025	8125	32347	73.70	38.20

and the SBFEM fulfils the radiation condition to infinity exactly. If damping needs to be considered, it can be easily added to equation (2.1), the discussed techniques are sill valid.

Since the far-field information can be computed before near-field and far-field are coupled to conduct the actual analysis, it is recommended to reduce the far-field model as discussed. When constant growth of $\mathbf{M}^{\infty}$ is observed starting from an allowed instant of time t_m, it is possible to reduce the need of memory storage and computational effort significantly. Here, it has been shown that the memory usage and the computational effort can be reduced down to less than 20% and 5%, respectively. This can be achieved without increasing the relative error of the numerical simulation. The proposed algorithms' formulation implies that the more degrees of freedom are taken into account and the more time steps have to be computed, the larger the advantage of this approach is.

Currently, the data of $\mathbf{M}^{\infty}$ is analysed to choose the time set t_m. It is revealed that picking an arbitrary matrix entry and check constant growth is not sufficient. A single entry can not state for the entire matrix and its time dependent behaviour, the entire matrix has to be taken into account. A determination of t_m a priori is challenging and will be of interest in future research. Being able to do so could allow to determine computational cost and memory consumption before running the far-field computation. Secondarily, the checking of constant growth could be skipped and additional compute time could be saved to make the approach even more effective.

Using far-field decoupling or decomposition technique is relatively simple. The geometrical decoupling technique is simple to implement, since only one algorithm is needed which assures that only values bigger than ε_z are taken into account and the matrix size is adapted to new number of non-zero values. An efficient usage of sub-structuring technique is more complex since algorithms are needed to couple an arbitrary number of far-field sub-structures to the near-field. Furthermore, the far-field has to be decomposed by the user before computing the far-fields' $\mathbf{M}^{\infty}$ matrices. Consequently, this leads to a higher effort in mesh generation. This higher effort is worthwhile since memory consumption and computation time can be reduced significantly if introducing an additional error is allowable.

It is to conclude that the studied model reduction is generally applicable to soil mechanics analysis, as long as linear material models are sufficient to describe the given problem. Hence, the different chosen sets of material parameters cover a broad range of geotechnically relevant materials. Further, it can be assumed that this approach is universally valid.

References

[1] Antes H, Spyrakos C. 1997 *Soil-Structure Interaction*, eds. Beskos DE, Anagnotopoulos SA. *Computer Analysis and Design of Earthquake Resistant Structures* Computational Mechanics Publications, Southampton.
[2] Astley RJ. 2000. *Infinite elements for wave problems: a review of current formulations and a assessment of accuracy* **49**(7):951–976 International Journal for Numerical Methods in Engineering.
[3] Bazyar MH, Sing C. 2008. *A continued fraction based high order transmitting boundary for wave propagation in unbounded domains of arbitrary geometry* **74**(2):209–237 International Journal for Numerical Methods in Engineering.
[4] Beer G. 2001. *Programming the Boundary Element Method* Wiley & Sons, Chichester, U.K.
[5] Birk C, Prempramote S, Song C. 2012. *An improved continued-fraction-based high-order transmitting boundary for time-domain analyses in unbounded domains* **89**(3):269–298 International Journal for Numerical Methods in Engineering.
[6] Brebbia CA, Telles JCF, Wrobel LC. *Boundary Element Techniques - Theory and Applications in Engineering* Springer, Berlin, Heidelberg.
[7] Bettess P. 1992. *Infinite Elements* Penshaw Press, Sunderland, U.K.
[8] Borsutzky R. 2008. *Seismic Risk Analysis of Buried Lifelines* **63** Mechanik-Zentrum Technische Universität Braunschweig.
[9] Chen D, Birk C, Song C, Du C. 2013 *A high-order approach for modelling transient wave propagation problems using the scaled boundary finite element method* **97**(13):937–959 International Journal for Numerical Methods in Engineering.
[10] Chung J, Hulbert GM. 1993. *A Time Integration Algorithm for Structural Dynamics with Improved Numerical Dissipation: The Generalized-α Method* **60**:371–375 Journal of Applied Mechanics.
[11] Cuthill E, McKee J. 1969. *Reducing the Bandwidth of Sparse Symmetric Matrices* 157–172, Proceedings of the 1969 24$^{\text{th}}$ National Conference. ACM.
[12] Engquist B, Majda A. 1977. *Absorbing boundary conditions for the numerical simulation of waves* **31**(139):629–651 Mathematics of Computation.
[13] Givoli D, 1991 *Non-reflecting Boundary Conditions* **94**:1–29 Journal of Computational Physics.
[14] Givoli D, 1992 *Numerical Methods for Problems in Infinite Domains* Elsevier Science Limited, Amsterdam.
[15] Harr ME. 1966. *Foundations of Theoretical Soil Mechanics* McGraw-Hill Book Company.
[16] Hilber H, Hughes T, Taylor R. 1977. *Improved numerical dissipation for time integration algorithms in structural dynamics* **5**:283–292, Earthquake Engineering & Structural Dynamics.
[17] Lehmann L. 2003. *Schnelles Verfahren zur Berechnung der Baugrund-Bauwerk-Interaktion im Zeitbereich* **22**:6–9, D-A-CH Mitteilungsblatt.
[18] Lehmann L, Antes H, Schanz M. 2004. *Transient analysis of soil-structure interaction problems: An effective FEM/SBFEM approach* 99–116, Advanced Numerical Analyses of Solids and Structures, and Beyond, Graz, Institute for Structural Analysis, Verlag der Technischen Universität Graz.
[19] Lehmann L. 2005. *An effective finite element approach for soil-structure analysis in the time-domain* **21**(4):37–50, Structural Engineering and Mechanics.
[20] Lehmann L. 2006. *Wave Propagation in Infinite Domains*, Springer, Berlin / Heidelberg.
[21] Liao ZP, Wong HL. 1984. *A transmitting boundary for the numerical simulation of elastic wave propagation* **3**(4):174–183 Soil Dynamics and Earthquake Engineering.
[22] Lysmer J, Kuhlmeyer RL. 1969. *Finite dynamic model for infinite media* **95**:859–875 Journal of Engineering Mechanics.
[23] Meskouris K, Hinzen KG, Butenweg C, Mistler M. 2007. *Bauwerke und Erdbeben - Grundlagen - Anwendung - Beispiele*, Vieweg+Teubner Verlag, Wiesbaden.
[24] Newmark N. 1959. *A method of computation for structural dynamics* **85**:67–94, Journal of Engineering Mechanics Division.

[25] Petersen C. 2000. *Dynamik der Baukonstruktionen* Vieweg & Sohn Verlagsgesellschaft mbH, Braunschweig/Wiesbaden.
[26] Poulos HG, Davis EH. 1974. *Elastic Solutions for Soil and Rock Mechanics* John Wiley & Sons, INC.
[27] Radmanović B, Katz C. 2010. *A High Performance Scaled Boundary Finite Element Method* **10** IOP Conf. Series: Material Science and Engineering.
[28] Schauer M, Lehmann L. 2009. *Large Scale Simulation with Scaled Boundary Finite Element Method* **9**(4) 103–106, roceedings in Applied Mathematics and Mechanics
[29] Schauer M, Roman JE, Quintana-Ortí ES, Langer S. 2012. *Parallel Computation of 3-D Soil-Structure Interaction in Time Domain with a Coupled FEM/SBFEM Approach* **52**:446–467, Journal of Scientific Computing.
[30] Schauer MM. 2015. *Ein effizienter gekoppelter FEM-SBFEM Ansatz zur Analyse von Boden-Bauwerk-Interaktionen im Zeitbereich* Dissertation, Technische Universität Braunschweig.
[31] Wolf J, Song C. 1996. *Finite-Element Modelling of Unbounded Media* John Wiley & Sons, Chichester.
[32] Wolf J. 2003. *The Scaled Boundary Finite Element Method* John Wiley & Sons, Chichester.
[33] Yan J, Zhang C, Jin F. 2004. *A coupling procedure of FE and SBFE for soil–structure interaction in the time domain* **59**1453–1471, Int. J. Numer. Meth. Engng.
[34] Zhang X, Wegner JL, Haddow JB. 1999. *Three-Dimensional Dynamic Soil-Structure Interaction Analysis in the Time Domain* **28**(10):1501–1524, Earthquake Engineering and Structural Dynamics.

Journal of Mathematical Sciences and Modelling, 1 (2) (2018) 105-130

Journal of Mathematical Sciences and Modelling

Journal Homepage: www.dergipark.gov.tr/jmsm
ISSN 2636-8692

Generalized Lie-algebraic structures related to integrable dispersionless dynamical systems and their application

Oksana E. Hentosh[a], Yarema A. Prykarpatsky[b], Denis Blackmore[c] and Anatolij Prykarpatski[d*]

[a]*The Institute for Applied Problems of Mechanics and Mathematics at the NAS, Lviv, 79060 Ukraine*
[b]*The Department of Applied Mathematics at the University of Agriculture in Krakow, 30059, Poland*
[c]*The Department of Mathematical Sciences at NJIT, University Heights, Newark, NJ 07102 USA*
[d]*The Department of Physics, Mathematics and Computer Science at the Krakow University of Technology, Krakow, 30-055, Poland*
[*]*Corresponding author E-mail: pryk.anat@cybergal.com*

Dedicated to our colleague, teacher, friend and brilliant mathematician Anatolij M. Samoilenko on his 80th Birthday Jubilee

Article Info

Keywords: *Lax–Sato equations, Heavenly equations, Lax–Sato integrability, Hamiltonian system, Torus diffeomorphisms, Loop Lie algebra, Lie-algebraic scheme, Casimir invariants, R-structure, Lie-Poisson structure, Lagrange–d'Alembert principle*

2010 AMS: *17B68,17B80,35Q53, 35G25, 35N10, 37K35, 58J70,58J72, 34A34,37K05,37K10*

Received: *21 June 2018*

Accepted: *20 September 2018*

Available online: *30 September 2018*

Abstract

Our review is devoted to Lie-algebraic structures and integrability properties of an interesting class of nonlinear dynamical systems called the dispersionless heavenly equations, which were initiated by Plebański and later analyzed in a series of articles. The AKS-algebraic and related $\mathscr{R}$-structure schemes are used to study the orbits of the corresponding co-adjoint actions, which are intimately related to the classical Lie–Poisson structures on them. It is demonstrated that their compatibility condition coincides with the corresponding heavenly equations under consideration. Moreover, all these equations originate in this way and can be represented as a Lax compatibility condition for specially constructed loop vector fields on the torus. The infinite hierarchy of conservations laws related to the heavenly equations is described, and its analytical structure connected with the Casimir invariants, is mentioned. In addition, typical examples of such equations, demonstrating in detail their integrability via the scheme devised herein, are presented. The relationship of a fascinating Lagrange–d'Alembert type mechanical interpretation of the devised integrability scheme with the Lax–Sato equations is also discussed. We pay a special attention to a generalization of the devised Lie-algebraic scheme to a case of loop Lie superalgebras of superconformal diffeomorphisms of the $1|N$-dimensional supertorus. This scheme is applied to constructing the Lax–Sato integrable supersymmetric analogs of the Liouville and Mikhalev-Pavlov heavenly equation for every $N \in \mathbb{N}\backslash\{4;5\}$.

1. Introduction

We shall discuss the Lax–Sato compatible systems, the related Lie-algebraic structures and complete integrability properties of an interesting class of nonlinear dynamical systems called the heavenly equations, introduced by Plebański [56] and analyzed in such articles as [39, 9, 46, 47, 48, 65, 66, 73, 74]. In our previous work, we employed the AKS-algebraic and related $\mathscr{R}$-structure schemes [6, 5, 7, 75, 62, 61], applied to the holomorphic Birkhoff type factorized loop Lie algebra $\tilde{\mathscr{G}} := \widetilde{diff}(\mathbb{T}^{1+n}_{\mathbb{C}})$ of vector fields on torus $\mathbb{T}^{1+n}_{\mathbb{C}} \simeq \mathbb{T}^1_{\mathbb{C}} \times \mathbb{T}^n, n \in \mathbb{Z}_+$, and reanalyzed and studied in detail the corresponding coadjoint actions on $\tilde{\mathscr{G}}^*$, closely related to the classical Lie–Poisson structures. By constructing two commuting flows on the coadjoint space $\tilde{\mathscr{G}}^*$, generated by a chosen root element $\tilde{l} \in \tilde{\mathscr{G}}^*$ and some Casimir invariants, we shall demonstrate that their compatibility condition coincides with the corresponding heavenly equations under consideration.
As a by-product of the construction devised recently in [31, 60], we prove that all the heavenly equations have a similar origin and can be represented as a Lax compatibility condition for special loop vector fields on the torus $\mathbb{T}^{1+n}_{\mathbb{C}}$. We analyze the structure of the infinite hierarchy of conservations laws related to the heavenly equations, and demonstrate that their analytical structure connected with the Casimir invariants is generated by the Lie–Poisson structure on $\tilde{\mathscr{G}}^*$. Moreover, we generalize the Lie-algebraic scheme of [31, 60] subject to the loop Lie algebra $\tilde{\mathscr{G}}^* = \widetilde{diff}(\mathbb{T}^{1|N}_{\mathbb{C}})$ of superconformal vector fields on $\mathbb{T}^{1|N}_{\mathbb{C}}$, which is the Lie algebra of the Lie group of superconformal diffeomorphisms of

Email addresses: **ohen@ukr.net (O. E. Hentosh), yarpry@gmail.com (Y. A. Prykarpatsky), denblac@gmail.com (D. Blackmore), pryk.anat@cybergal.com (A. Prykarpatski)**

the $1|N$-dimensional supertorus $\mathbb{T}^{1|N}_{\mathbb{C}} \simeq \mathbb{T}^{1}_{\mathbb{C}} \times \Lambda_1^N$, where $\Lambda := \Lambda_0 \oplus \Lambda_1$ is an infinite-dimensional Grassmann algebra over $\mathbb{C}$, $\Lambda_0 \supset \mathbb{C}$. This is applied to constructing the Lax–Sato type integrable superanalogs of the Mikhalev–Pavlov heavenly super-equation for every $N \in \mathbb{N} \setminus \{4;5\}$. Typical examples are presented for all cases of the heavenly equations and their integrability is verified using the scheme devised here. This scheme also makes it possible to construct a very natural derivation of the well-known Lax–Sato type representation [63, 64] for an infinite hierarchy of heavenly equations, related to the canonical Lie–Poisson structure on the adjoint space $\tilde{\mathscr{G}}^*$. As a result of suitably chosen superconformal mappings in the space of variables $(z;\theta_1,\dots,\theta_N) \in \mathbb{T}^{1|N}_{\mathbb{C}}$ the superanalogs of Liouville type equations are obtained. We also mention also show that an aspect of our approach to describing integrability of the heavenly dynamical systems is closely related to their classical Lagrange–d'Alembert type mechanical interpretation.

There are only a few examples of multi-dimensional integrable systems for which detailed descriptions of their mathematical structure have been given and our work is a next step in extending this list via new mathematical techniques utilizing the internal structure of heavenly nonlinear dispersionless integrable dynamical systems. We wish to mention that we have been strongly influenced both by the research of Pavlov, Bogdanov, Dryuma, Konopelchenko and Manakov [11, 9, 10, 33], as well as that of Ferapontov and Moss [26], Błaszak, Szablikowski and Sergyeyev, Krasil'shchik [7, 67, 70, 71, 68, 69, 34] wherein new effective differential-geometric and analytical methods for studying integrable degenerate multi-dimensional dispersionless heavenly type hierarchies of equations, the mathematical importance of which is still far from being fully appreciated.

2. Generalized Lie-algebraic structures and related dispersionless heavenly type quasi-Hamiltonian systems

2.1. A generalized Lie algebra of holomorphic toral vector fields

Let $\tilde{G}_{\pm} := \widetilde{Diff}_{\pm}(\mathbb{T}^{1+n}_{\mathbb{C}})$, $n \in \mathbb{Z}_+$, be subgroups of the Birkhoff type [57] loop diffeomorphisms group $\widetilde{Diff}(\mathbb{T}^{1+n}_{\mathbb{C}}) := \{\mathbb{C} \supset \mathbb{S}^1 \to Diff_{hol}(\mathbb{S}^1 \times \mathbb{T}^n)\}$, holomorphically extended in the interior $\mathbb{D}^1_+ \subset \mathbb{C}$ and in the exterior $\mathbb{D}^1_- \subset \mathbb{C}$ regions of the unit disc $\mathbb{D}^1$ with the boundary $\partial\mathbb{D}^1 = \mathbb{S}^1 \subset \mathbb{C}$, where for any $g(\lambda) \in \tilde{G}_{\pm}$, either for $\lambda \in \mathbb{D}^1_-$, $g(\infty) = 1 \in Diff(\mathbb{T}^{1+n}_{\mathbb{C}})$ or for $\lambda \in \mathbb{D}^1_+$, $g(0) = 1 \in Diff(\mathbb{T}^{1+n}_{\mathbb{C}})$. The corresponding Lie subalgebras $\tilde{\mathscr{G}}_{\pm} := \widetilde{diff}_{\pm}(\mathbb{T}^{1+n}_{\mathbb{C}})$ of the loop subgroups $\tilde{G}_{\pm}$ are vector fields on $\mathbb{T}^{1+n}_{\mathbb{C}}$ holomorphic, respectively, on $\mathbb{D}^1_{\pm} \subset \mathbb{C}$, where either for any $\tilde{a}(\lambda) \in \tilde{\mathscr{G}}_-$, $\tilde{a}(\infty) = 0$, or for any $\tilde{a}(\lambda) \in \tilde{\mathscr{G}}_+$, $\tilde{a}(0) = 0$. The loop Lie algebra $\tilde{\mathscr{G}} := \widetilde{diff}(\mathbb{T}^{1+n}_{\mathbb{C}})$ allows the direct sum splitting

$$\tilde{\mathscr{G}} = \tilde{\mathscr{G}}_+ \oplus \tilde{\mathscr{G}}_-, \tag{2.1}$$

which can be naturally identified with a dense subspace of the dual space $\tilde{\mathscr{G}}^*$ via the Sobolev type metric

$$(\tilde{l},\tilde{a})_{s;q} := \underset{\lambda\in\mathbb{C}}{res}\ \lambda^{-s} l(\lambda;\mathrm{x}), a(\lambda;\mathrm{x}))_{H^q}, \tag{2.2}$$

for some fixed $s \in \mathbb{Z}$ and $q \in \mathbb{Z}_+$. Here, by definition, a loop vector field $\tilde{a} \in \Gamma(\tilde{T}(\mathbb{T}^{1+n}_{\mathbb{C}}))$ and a loop differential 1-form $\tilde{l} \in \tilde{\Lambda}^1(\mathbb{T}^{1+n}_{\mathbb{C}})$ are given as

$$\tilde{a} \ = \sum_{j=1}^{n} a^{(j)}(\lambda;x)\frac{\partial}{\partial x_j} + a^{(0)}(\lambda;x) := \left\langle a(\mathrm{x}), \frac{\partial}{\partial \mathrm{x}}\right\rangle, \tag{2.3}$$

$$\tilde{l} \ = \sum_{j=1}^{n} l_j(\lambda;x)dx_j + l_0(\lambda;x) := \ \langle l(\mathrm{x}), d\mathrm{x}\rangle$$

for any $\mathrm{x} := (\lambda;x) \in \mathbb{T}^{1+n}_{\mathbb{C}}$, and

$$(l,a)_{H^q} = \sum_{j=0}^{n}\sum_{|\alpha|=0}^{q}\int_{\mathbb{T}^n} d\mathrm{x}\frac{\partial^{|\alpha|} l_j}{\partial \mathrm{x}^{\alpha}}\frac{\partial^{|\alpha|} a_j}{\partial \mathrm{x}^{\alpha}}. \tag{2.4}$$

In particular, for $q = 0 = s$ one has

$$(\tilde{l},\tilde{a})_0 := (\tilde{l},\tilde{a})_{0;0} = \underset{\lambda\in\mathbb{C}}{res}\int_{\mathbb{T}^n} d\mathrm{x}(\sum_{j=0}^{n} l_j\, a_j), \tag{2.5}$$

which is *the case mainly chosen in the sequel*.

It is now important to mention that the holomorphic Lie algebra $\tilde{\mathscr{G}} = diff(\mathbb{T}^{1+n}_{\mathbb{C}})$ splitting (2.1) makes it possible to introduce on the Lie algebra $\tilde{\mathscr{G}}$ the canonical $\mathscr{R}$-structure:

$$[\tilde{a},\tilde{b}]_{\mathscr{R}} := [\mathscr{R}\tilde{a},\tilde{b}] + [\tilde{a},\mathscr{R}\tilde{b}] \tag{2.6}$$

for any $\tilde{a},\tilde{b} \in \tilde{\mathscr{G}}$, where

$$\mathscr{R} := (P_+ - P_-)/2, \tag{2.7}$$

and

$$P_{\pm}\tilde{\mathscr{G}} := \tilde{\mathscr{G}}_{\pm} \subset \tilde{\mathscr{G}}. \tag{2.8}$$

Then for arbitrary smooth mappings $f,g \in \mathrm{D}(\tilde{\mathscr{G}}^*)$ one has two Lie–Poisson brackets

$$\{f,g\} := (\tilde{l},[\nabla f(\tilde{l}),\nabla g(l)]) \tag{2.9}$$

and

$$\{f,g\}_{\mathscr{R}} := (\tilde{l},[\nabla f(\tilde{l}),\nabla g(\tilde{l})]_{\mathscr{R}}), \tag{2.10}$$

where at a fixed *seed element* $\tilde{l} \in \tilde{\mathscr{G}}^*$ the gradient elements $\nabla f(\tilde{l})$ and $\nabla g(\tilde{l}) \in \tilde{\mathscr{G}}$ are calculated, in general, with respect to the metric (2.4). Now let us assume that a smooth function $h \in \mathrm{I}(\tilde{\mathscr{G}}^*)$ is a Casimir invariant, that is

$$ad^*_{\nabla h(\tilde{l})}\tilde{l} = 0 \tag{2.11}$$

for a chosen seed element $\tilde{l} \in \tilde{\mathscr{G}}^*$. As the adjoint mapping $ad^*_{\nabla h(\tilde{l})} : \tilde{\mathscr{G}}^* \to \tilde{\mathscr{G}}^*$ for any $h \in D(\tilde{\mathscr{G}}^*)$ with respect to the scalar product (2.5) can be rewritten in the reduced form as

$$ad^*_{\nabla h(\tilde{l})}\tilde{l} = \left\langle \frac{\partial}{\partial \mathrm{x}}, \circ \nabla h(l) \right\rangle \tilde{l} + \left\langle \left\langle l, \frac{\partial}{\partial \mathrm{x}} \nabla f(l) \right\rangle, dx \right\rangle, \tag{2.12}$$

where, by definition, $\nabla h(\tilde{l}) :=< \nabla h(l), \frac{\partial}{\partial \mathrm{x}} > \in \tilde{\mathscr{G}}$ and "$\circ$" denotes the composition of mappings. For a suitable Casimir function $h \in D(\tilde{\mathscr{G}}^*)$, the condition (2.11) is then equivalent to the equation

$$\left\langle \frac{\partial}{\partial \mathrm{x}}, \circ \nabla h(l) \right\rangle l + \left\langle l, (\frac{\partial}{\partial \mathrm{x}} \nabla h(l)) \right\rangle = 0, \tag{2.13}$$

which should be be solved analytically. When $\tilde{l} \in \tilde{\mathscr{G}}^*$ is chosen to be singular as $|\lambda| \to \infty$, one can consider [18] the general asymptotic expansion

$$\nabla h^{(p)}(l) \sim \lambda^p \sum_{j \in \mathbb{Z}_+} \eta_j^{(p)}(l) \lambda^{-j} \tag{2.14}$$

for some suitably chosen integers $p \in \mathbb{Z}_+$, and upon substituting (2.14) into the equation (2.13), one can solve it recurrently.
Now let $h^{(p_y)}, h^{(p_y)} \in \mathrm{I}(\tilde{\mathscr{G}}^*)$ be a Casimir functions for which the Hamiltonian vector field generators

$$\nabla h^{(y)}(\tilde{l}) := \nabla h^{(p_y)}(\tilde{l})|_+, \quad \nabla h^{(t)}(\tilde{l}) := \nabla h^{(p_t)}(\tilde{l})|_+ \tag{2.15}$$

are, respectively, defined for special integers $p_y, p_t \in \mathbb{Z}_+$. These invariants generate, owing to the Lie–Poisson bracket (2.10), (*as before for the case* $q = 0 = s$) the following commuting flows

$$\begin{aligned} \partial l/\partial t &= - \left\langle \tfrac{\partial}{\partial \mathrm{x}}, \circ \nabla h^{(t)}(l) \right\rangle l - \left\langle l, (\tfrac{\partial}{\partial \mathrm{x}} \nabla h^{(t)}(l)) \right\rangle, \\ \partial l/\partial y &= - \left\langle \tfrac{\partial}{\partial \mathrm{x}}, \circ \nabla h^{(y)}(l) \right\rangle l - \left\langle l, (\tfrac{\partial}{\partial \mathrm{x}} \nabla h^{(y)}(l)) \right\rangle, \end{aligned} \tag{2.16}$$

where $y,t \in \mathbb{R}$ are the corresponding evolution parameters. Since the invariants $h^{(p_y)}, h^{(p_y)} \in \mathrm{I}(\tilde{\mathscr{G}}^*)$ commute with respect to the Lie–Poisson bracket (2.10), the flows (2.16) also commute, implying that the corresponding Hamiltonian vector field generators

$$\nabla h^{(t)}(\tilde{l}) := \left\langle \nabla h^{(t)}(l), \frac{\partial}{\partial \mathrm{x}} \right\rangle, \quad \nabla h^{(y)}(\tilde{l}) := \left\langle \nabla h^{(y)}(l), \frac{\partial}{\partial \mathrm{x}} \right\rangle \tag{2.17}$$

satisfy the Lax–Sato compatibility condition

$$\frac{\partial}{\partial y} \nabla h^{(t)}(\tilde{l}) - \frac{\partial}{\partial t} \nabla h^{(y)}(\tilde{l}) = [\nabla h^{(t)}(\tilde{l}), \nabla h^{(y)}(\tilde{l})] \tag{2.18}$$

for all $y,t \in \mathbb{R}$. On the other hand, the condition (2.18) is equivalent to the compatibility condition of two linear equations

$$(\frac{\partial}{\partial t} + \nabla h^{(t)}(\tilde{l}))\psi = 0, \quad (\frac{\partial}{\partial y} + \nabla h^{(y)}(\tilde{l}))\psi = 0 \tag{2.19}$$

for a function $\psi \in C^2(\mathbb{R}^2 \times \mathbb{T}^{1+n}_{\mathbb{C}}; \mathbb{C})$ and all $y,t \in \mathbb{R}$.
The above can be formulated as the following key result:

Proposition 2.1. *Let a seed vector field be* $\tilde{l} \in \tilde{\mathscr{G}}^*$ *and* $h^{(p_y)}, h^{(p_y)} \in \mathrm{I}(\tilde{\mathscr{G}}^*)$ *be Casimir functions subject to the metric* $(\cdot,\cdot)_0$ *on the holomorphic Lie algebra* $\tilde{\mathscr{G}}$ *and the natural coadjoint action on the loop co-algebra* $\tilde{\mathscr{G}}^*$*. Then*

$$\partial\tilde{l}/\partial y = -ad^*_{\nabla h^{(y)}(\tilde{l})}\tilde{l}, \quad \partial\tilde{l}/\partial t = -ad^*_{\nabla h^{(t)}(\tilde{l})}\tilde{l} \tag{2.20}$$

are commuting Hamiltonian dynamical systems for all $y,t \in \mathbb{R}$*. Moreover, the compatibility condition of these flows is equivalent to the Lax–Sato vector field representation*

$$(\partial/\partial t + \nabla h^{(t)}(\tilde{l}))\psi = 0, \quad (\partial/\partial y + \nabla h^{(y)}(\tilde{l}))\psi = 0, \tag{2.21}$$

where $\psi \in C^2(\mathbb{R}^2 \times \mathbb{T}^{1+n}_{\mathbb{C}}; \mathbb{C})$ *and the vector fields* $\nabla h^{(t)}(\tilde{l}), \nabla h^{(t)}(\tilde{l}) \in \tilde{\mathscr{G}}$ *are given by the expressions (2.17) and (2.15).*

Remark 2.2. *As mentioned above, the expansion (2.14) is effective if a chosen seed element $\tilde{l} \in \tilde{\mathscr{G}}^*$ is singular as $|\lambda| \to \infty$. In the case when it is singular as $|\lambda| \to 0$, the expression (2.14) should be replaced by the expansion*

$$\nabla h^{(p)}(l) \sim \lambda^{-p} \sum_{j \in \mathbb{Z}_+} \eta_j^{(p)}(l) \lambda^j \tag{2.22}$$

for suitably chosen integers $p \in \mathbb{Z}_+$, and the reduced Casimir function gradients then are given by the Hamiltonian vector field generators

$$\nabla h^{(y)}(l) := \nabla h^{(p_y)}(l)|_-, \quad \nabla h^{(t)}(l) := \nabla h^{(p_t)}(l)|_- \tag{2.23}$$

for suitably chosen positive integers $p_y, p_t \in \mathbb{Z}_+$. Moreover, the corresponding Hamiltonian systems are, respectively, written as

$$\partial \tilde{l}/\partial t = -ad^*_{\nabla h^{(t)}(\tilde{l})} \tilde{l}, \quad \partial \tilde{l}/\partial y = -ad^*_{\nabla h^{(y)}(\tilde{l})} l, \tag{2.24}$$

where we need to mention that, owing to the analytical structure of the seed element $\tilde{l} \in \tilde{\mathscr{G}}^*$, the corresponding functional evolution equations on its coefficients are only quasi-Hamiltonian and are suitable reductions of the true Hamiltonian flows (2.24).

Remark 2.3. *It is also possible to describe the Bäcklund transformations between two special solution sets for the dispersionless heavenly equations resulting from the Lax–Sato compatibility condition (2.20). In fact, take a diffeomorphism $\xi \in \widetilde{Diff}(\mathbb{T}^{1+n}_{\mathbb{C}})$ such that a seed differential form $\tilde{l}(\lambda;x) \in \tilde{\mathscr{G}}^* \simeq \Lambda^1(\mathbb{T}^{1+n}_{\mathbb{C}})$ satisfies the invariance condition*

$$\tilde{l}(\xi(\mathrm{x}|\mu)) = k\tilde{l}(\bar{\mathrm{x}}) \tag{2.25}$$

for some non-zero constant $k \in \mathbb{C}\backslash\{0\}$, any $\mathrm{x} = (\lambda;x)$ and $\bar{\mathrm{x}} = (\mu;x) \in \mathbb{T}^{1+n}_{\mathbb{C}}$ with arbitrarily chosen parameter $\mu \in \mathbb{T}^1_{\mathbb{C}}$. As the seed element $\tilde{l}(\xi(\mathrm{x}|\mu)) \in \Lambda^1(\mathbb{T}^{1+n}_{\mathbb{C}})$ satisfies the compatible equations (2.20), the loop diffeomorphism $\xi \in \widetilde{Diff}(\mathbb{T}^{1+n}_{\mathbb{C}})$, found analytically from the invariance condition (2.25), satisfies the compatible system of vector field equations

$$\frac{\partial}{\partial t}\xi = \nabla h^{(t)}(l), \quad \frac{\partial}{\partial y}\xi = \nabla h^{(y)}(l),$$

giving rise to the Bäcklund type relationships for the coefficients of the seed differential form $\tilde{l} \in \tilde{\mathscr{G}}^* \simeq \Lambda^1(\mathbb{T}^{1+n}_{\mathbb{C}})$.

The following examples demonstrate the analytical applicability of the above Lie-algebraic scheme for constructing a wide class of nonlinear multi-dimensional heavenly integrable Hamiltonian systems on function spaces.

2.2. Example: Einstein–Weyl metric equation

Define $\tilde{\mathscr{G}} := \widetilde{diff}(\mathbb{T}^2_{\mathbb{C}})$, where for any $\tilde{a}(\lambda) \in \tilde{\mathscr{G}}_-$, $\lambda \in \mathbb{C}$, the value $\tilde{a}(\infty) = 0$, and take a seed element $\tilde{l} \in \tilde{\mathscr{G}}^*$ in the following form

$$\tilde{l} = \left(u_x\lambda - 2u_x v_x - u_y\right)dx + \left(\lambda^2 - v_x\lambda + v_y + v_x^2\right)d\lambda,$$

where $(u,v) \in C^\infty(\mathbb{R}^2 \times \mathbb{T}^1)$ and which generates with respect to the metric (2.5) (as before for $q = 0 = s$) the gradients of the Casimir invariants $h^{(1)}, h^{(2)} \in \mathrm{I}(\tilde{\mathscr{G}}^*)$ in the form

$$\begin{aligned} \nabla h^{(2)}(l) \quad &\sim \lambda^2(0,1)^\intercal + (-u_x, v_x)^\intercal\lambda + (u_y, u - v_y)^\intercal + O(\lambda^{-1}), \\ \nabla h^{(1)}(l) \quad &\sim \lambda(0,1)^\intercal + (-u_x, v_x)^\intercal + (u_y, -v_y)^\intercal\lambda^{-1} + O(\lambda^{-2}) \end{aligned} \tag{2.26}$$

as $|\lambda| \to \infty$ at $p_t = 2$, $p_y = 1$. For the gradients of the Casimir functions $h^{(1)}, h^{(2)} \in \mathrm{I}(\mathscr{G}^*)$ determined by (2.15), one can easily obtain the corresponding Hamiltonian vector field generators

$$\begin{aligned} \nabla h^{(t)}(\tilde{l}) \quad &:= \left\langle \nabla h^{(2)}(l)_+, \frac{\partial}{\partial \mathrm{x}} \right\rangle = (\lambda^2 + \lambda v_x + u - v_y)\frac{\partial}{\partial x} + (-\lambda u_x + u_y)\frac{\partial}{\partial \lambda}, \\ \nabla h^{(y)}(\tilde{l}) &= \left\langle \nabla h^{(1)}(l)_+, \frac{\partial}{\partial \mathrm{x}} \right\rangle = (\lambda + v_x)\frac{\partial}{\partial x} - u_x\frac{\partial}{\partial \lambda}, \end{aligned} \tag{2.27}$$

satisfying the compatibility condition (2.18), which is equivalent to the system

$$\begin{cases} u_{xt} + u_{yy} + (uu_x)_x + v_x u_{xy} - v_y u_{xx} = 0, \\ v_{xt} + v_{yy} + uv_{xx} + v_x v_{xy} - v_y v_{xx} = 0, \end{cases} \tag{2.28}$$

describing general integrable Einstein–Weyl metric equations [23].
As is well known [39], the invariant reduction of (2.28) at $v = 0$ gives rise to the famous dispersionless Kadomtsev–Petviashvili equation

$$(u_t + uu_x)_x + u_{yy} = 0, \tag{2.29}$$

for which the reduced vector field representation (2.19) follows from (2.27) and is given by the vector fields

$$\begin{aligned} \nabla h^{(t)}(\tilde{l}) &= (\lambda^2 + u)\frac{\partial}{\partial x} + (-\lambda u_x + u_y)\frac{\partial}{\partial \lambda}, \\ \nabla h^{(y)}(\tilde{l}) &= \lambda\frac{\partial}{\partial x} - u_x\frac{\partial}{\partial \lambda}, \end{aligned} \tag{2.30}$$

satisfying the compatibility condition (2.18), equivalent to the equation (2.29). In particular, (2.19) and (2.30) imply the vector field compatibility relationships

$$\frac{\partial\psi}{\partial t}+(\lambda^2+u)\frac{\partial\psi}{\partial x}+(-\lambda u_x+u_y)\frac{\partial\psi}{\partial\lambda}=0$$
$$\frac{\partial\psi}{\partial y}+\lambda\frac{\partial\psi}{\partial x}-u_x\frac{\partial\psi}{\partial\lambda}=0, \tag{2.31}$$

satisfied for $\psi\in C^2(\mathbb{R}^2\times\mathbb{T}^2_{\mathbb{C}};\mathbb{C})$ and any $y,t\in\mathbb{R},(\lambda;x)\in\ \mathbb{T}_{\mathbb{C}}\times\mathbb{T}^1$.

2.3. Example: The modified Einstein–Weyl metric equation

This equation system is

$$u_{xt}\quad=u_{yy}+u_xu_y+u_x^2w_x+uu_{xy}+u_{xy}w_x+u_{xx}a, \tag{2.32}$$
$$w_{xt}\qquad=uw_{xy}+u_yw_x+w_xw_{xy}+aw_{xx}-a_y,$$

where $(u,w)\in C^\infty(\mathbb{R}^2\times\mathbb{T}^1),a_x:=u_xw_x-w_{xy}$, and was recently derived in [68]. In this case we also take $\tilde{\mathscr{G}}:=\widetilde{diff}\ (\mathbb{T}^2_{\mathbb{C}})$, where for any $\tilde{a}(\lambda)\in\tilde{\mathscr{G}}_-,\lambda\in\mathbb{C}$, the value $\tilde{a}(\infty)=0$, yet for a seed element $\tilde{l}\in\tilde{\mathscr{G}}$ we choose the form

$$\tilde{l}=[\lambda^2u_x+\left(2u_xw_x+u_y+3uu_x\right)\lambda+2u_x\partial_x^{-1}u_xw_x+2u_x\partial_x^{-1}u_y+ \tag{2.33}$$
$$+3u_xw_x{}^2+2u_yw_x+6uu_xw_x+2uu_y+3u^2u_x-2au_x]dx+$$
$$+\quad[\lambda^2+(w_x+3u)\lambda+2\partial_x^{-1}u_xw_x+2\partial_x^{-1}u_y+w_x{}^2+3uw_x+3u^2-a]d\lambda,$$

which with respect to the metric (2.5) (as before for $q=0=s$) generates two Casimir invariants $h^{(1)},h^{(2)}\in\mathrm{I}(\tilde{\mathscr{G}}^*)$, whose gradients, as follows from (2.15), equal

$$\nabla h^{(2)}(l)\quad\sim\lambda^2[(u_x,-1)^\intercal+(uu_x+u_y,-u+w_x)^\intercal\lambda^{-1}+ \tag{2.34}$$
$$+(0,uw_x-a)^\intercal\lambda^{-2}]+O(\lambda^{-1}),$$
$$\nabla h^{(1)}(l)\qquad\sim\lambda[(u_x,-1)^\intercal+(0,w_x)^\intercal\ \lambda^{-1}]+O(\lambda^{-1}),$$

as $|\lambda|\to\infty$ at $p_y=1,p_t=2$. The suitable positive projections

$$\nabla h^{(y)}(l):=\nabla h^{(1)}(l)|_+=(u_x\lambda,-\lambda+w_x)^\intercal, \tag{2.35}$$
$$\nabla h^{(y)}(l)\quad:=\nabla h^{(2)}(l)|_+=(u_x\lambda^2+(uu_x+u_y)\lambda,-\lambda^2+(w_x-u)\lambda+uw_x-a)^\intercal.$$

of the gradients (2.34) generate the Hamiltonian flows (2.20), giving rise to the compatible Lax–Sato vector field system

$$\frac{\partial\psi}{\partial y}+(-\lambda+w_x)\frac{\partial\psi}{\partial x}+u_x\lambda\frac{\partial\psi}{\partial\lambda}=0, \tag{2.36}$$
$$\frac{\partial\psi}{\partial t}+\ [-\lambda^2+(\ w_x-u)\lambda+uw_x-a)\frac{\partial\psi}{\partial x}+(u_x\lambda^2+(uu_x+u_y)\lambda]\frac{\partial\psi}{\partial\lambda}=0,$$

satisfied for $\psi\in C^2(\mathbb{R}^2\times\mathbb{T}^2_{\mathbb{C}};\mathbb{C})$, any $y,t\in\mathbb{R}$ and all $(\lambda;x)\in\mathbb{T}^2_{\mathbb{C}}$.

2.4. Example: The Dunajski heavenly equations

This equation, suggested in [20], generalizes the corresponding anti-self-dual vacuum Einstein equation, which is related to the Plebański metric and the celebrated Plebański [56] second heavenly equation. To study the integrability of the Dunajski equations

$$u_{x_1t}+u_{yx_2}+u_{x_1x_1}u_{x_2x_2}-u^2_{x_1x_2}-v\quad=0, \tag{2.37}$$
$$v_{x_1t}+v_{x_2y}+u_{x_1x_1}v_{x_2x_2}-2u_{x_1x_2}v_{x_1x_2}\quad=0,$$

where $(u,v)\in C^\infty(\mathbb{R}^2\times\mathbb{T}^2;\mathbb{R}^2)$, $(y,t;x_1,x_2)\in\mathbb{R}^2\times\mathbb{T}^2$, we define $\tilde{\mathscr{G}}:=\widetilde{diff}(\mathbb{T}^3_{\mathbb{C}})$, where for any $\tilde{a}(\lambda)\in\tilde{\mathscr{G}}_-$ the value $\tilde{a}(\infty)=0$, and take the following as a seed element $\tilde{l}\in\tilde{\mathscr{G}}^*$:

$$\tilde{l}=(\lambda+v_{x_1}-u_{x_1x_1}+u_{x_1x_2})dx_1+(\lambda+v_{x_2}+u_{x_2x_2}-u_{x_1x_2})dx_2+\lambda d\lambda. \tag{2.38}$$

With respect to the metric (2.5) (as before for $q=0=s$), the gradients of two functionally independent Casimir invariants $h^{(p_y)}, h^{(p_t)} \in \mathrm{I}(\tilde{\mathscr{G}}^*)$ can be obtained as $|\lambda| \to \infty$ in the asymptotic forms

$$\nabla h^{(p_y)}(l) \sim \lambda(0,1,0)^\intercal + (-v_{x_1}, -u_{x_1x_2}, u_{x_1x_1})^\intercal + O(\lambda^{-1}), \tag{2.39}$$

$$\nabla h^{(p_t)}(l) \sim \lambda(0,0,-1)^\intercal + (v_{x_2}, u_{x_2x_2}, -u_{x_1x_2})^\intercal + O(\lambda^{-1})$$

at $p_t = 1 = p_y$. Upon calculating the Hamiltonian vector field generators

$$\nabla h^{(y)}(l) := \nabla h^{(p_y)}(l)|_+ = (-v_{x_1}, \lambda - u_{x_1x_2}, u_{x_1x_1})^\intercal, \tag{2.40}$$

$$\nabla h^{(t)}(l) := \nabla h^{(p_t)}(l)|_+ = (v_{x_2}, u_{x_2x_2}, -\lambda - u_{x_1x_2})^\intercal,$$

following from the Casimir functions gradients (2.39), one easily obtains the vector fields

$$\nabla h^{(t)}(\tilde{l}) := < \nabla h^{(t)}(l), \frac{\partial}{\partial \mathrm{x}} > = u_{x_2x_2}\frac{\partial}{\partial x_1} - (\lambda + u_{x_1x_2})\frac{\partial}{\partial x_2} + v_{x_2}\frac{\partial}{\partial \lambda}, \tag{2.41}$$

$$\nabla h^{(y)}(\tilde{l}) := < \nabla h^{(y)}(l), \frac{\partial}{\partial \mathrm{x}} > = (\lambda - u_{x_1x_2})\frac{\partial}{\partial x_1} + u_{x_1x_1}\frac{\partial}{\partial x_2} - v_{x_1}\frac{\partial}{\partial \lambda},$$

satisfying the Lax–Sato compatibility condition (2.18)

$$\begin{aligned} \frac{\partial \psi}{\partial t} + u_{x_2x_2}\frac{\partial \psi}{\partial x_1} - (\lambda + u_{x_1x_2})\frac{\partial \psi}{\partial x_2} + v_{x_2}\frac{\partial \psi}{\partial \lambda} &= 0, \\ \frac{\partial \psi}{\partial y} + (\lambda - u_{x_1x_2})\frac{\partial \psi}{\partial x_1} + u_{x_1x_1}\frac{\partial \psi}{\partial x_2} - v_{x_1}\frac{\partial \psi}{\partial \lambda} &= 0, \end{aligned} \tag{2.42}$$

equivalent to the the Dunajski [20] equation (2.37) and satisfied for $\psi \in C^2(\mathbb{R}^2 \times \mathbb{T}^3_{\mathbb{C}}; \mathbb{C})$, any $(y,t;x_1,x_2) \in \mathbb{R}^2 \times \mathbb{T}^2$ and all $\lambda \in \mathbb{T}^1_{\mathbb{C}}$. As mentioned in [9], the Dunajski equations (2.37) generalize both the dispersionless Kadomtsev–Petviashvili and Plebański second heavenly equations, and is also a Lax–Sato integrable quasi-Hamiltonian system.

2.5. Example: The Kupershmidt hydrodynamic heavenly type system

This mutually compatible hydrodynamic system [4, 36, 37, 69, 48] is given as

$$\begin{gathered} 3v_y - 6uv_x + 6u_xv + 6uu_y - 6u^2u_x - 2u_t = 0, \\ -12v_x + 6u_y - 12uu_x = 0, \\ 6uv_{xx} - 3v_{xy} - 6u_{xx}v - 6u_xu_y + 6u^2u_{xx} - 6uu_{xy} + 12uu_x{}^2 + 2u_{xt} = 0, \\ 6v_{xx} + 6uu_{xx} - 3u_{xy} + 6u_x{}^2 = 0 \end{gathered} \tag{2.43}$$

for smooth functions $(u,v) \in C^\infty(\mathbb{R}^2 \times \mathbb{T}^1; \mathbb{R}^2)$ with respect to "hidden" evolution parameters $t, y \in \mathbb{R}$ and the spatial variable $x \in \mathbb{T}^1$. Its Lax–Sato integrability stems from a seed element $\tilde{l} \in \tilde{\mathscr{G}}^*$, where $\tilde{\mathscr{G}}$ denotes the (holomorphic in $\lambda \in \mathbb{S}^1_\pm$) Lie algebra $\tilde{\mathscr{G}} := \widetilde{diff}(\mathbb{T}^2_{\mathbb{C}})$ of the loop diffeomorphism group $\widetilde{Diff}(\mathbb{T}^2_{\mathbb{C}})$, such that for any $\tilde{a}(\lambda) \in \tilde{\mathscr{G}}_-, \lambda \in \mathbb{C}$, $\tilde{a}(\infty) = 0$ and

$$\tilde{l} = [\lambda(v_x + 2uu_x) + \lambda^2 u_x]dx + [(v + u^2) + 2\lambda u + \lambda^2]d\lambda \tag{2.44}$$

for all $x \in \mathbb{T}^1$ and $\lambda \in \mathbb{T}^1_{\mathbb{C}}$. The corresponding gradients for the Casimir invariants $h^{(k)} \in \mathrm{I}(\tilde{\mathscr{G}}^*)$, $k = \overline{1,2}$, are easily constructed from the determining conditions $ad^*_{\nabla h^{(k)}(\tilde{l})}\tilde{l} = 0, k = \overline{1,2}$, as the following asymptotic expansions:

$$\nabla h^{(k)}(l) \sim \lambda^{p_k} \sum_{j \in \mathbb{Z}_+} \eta_j^{(k)}(l)\lambda^{-j}, \tag{2.45}$$

giving rise at $p_k = k, k = \overline{1,2}$, to the expressions:

$$\nabla h^{(1)}(l) \sim (2(\lambda + u), -2\lambda u_x)^\intercal + O(\lambda^{-1}), \tag{2.46}$$

$$\nabla h^{(2)}(l) \sim (3(\lambda^2 + 2\lambda u + +u^2 + v), -3\lambda(\lambda u_x + 2uu_x + v_x))^\intercal + O(\lambda^{-1}),$$

as $|\lambda| \to \infty$. Now taking into account the following Hamiltonian flows on $\tilde{\mathscr{G}}^*$

$$d\tilde{l}/dy = -ad^*_{\nabla h^{(y)}(\tilde{l})}\tilde{l}, \quad d\tilde{l}/dy = -ad^*_{\nabla h^{(t)}(\tilde{l})}\tilde{l} \tag{2.47}$$

with respect to the evolution parameters $y, t \in \mathbb{R}$, where, by definition,

$$\nabla h^{(y)}(\tilde{l}) := \nabla h^{(1)}(\tilde{l})|_+ = 2(\lambda + u)\partial/\partial x - 2\lambda u_x \partial/\partial \lambda, \tag{2.48}$$

$$\nabla h^{(t)}(\tilde{l}) := \nabla h^{(2)}(\tilde{l})|_+ = 3(\lambda^2 + 2\lambda u + u^2 + v)\partial/\partial x - 3\lambda(\lambda u_x + 2uu_x + v_x)\partial/\partial \lambda$$

are holomorphic vector fields on $\mathbb{T}^2_{\mathbb{C}}$, we can easily derive the corresponding compatible Kupershmidt hydrodynamic systems (2.43). It is also easy to check that the compatibility condition for a set of the vector fields (2.47) gives rise to the equivalent Lax–Sato vector field representation

$$\begin{gathered}\frac{\partial\psi}{\partial t}-3(\lambda^2+2\lambda u+u^2+v)\frac{\partial\psi}{\partial x}+3\lambda(\lambda u_x+2uu_x+v_x)\frac{\partial\psi}{\partial\lambda}=0,\\ \frac{\partial\psi}{\partial y}-2(\lambda+u)\frac{\partial\psi}{\partial x}+2\lambda u_x\frac{\partial\psi}{\partial\lambda}=0,\end{gathered}\tag{2.49}$$

satisfied for $\psi\in C^2(\mathbb{R}^2\times\mathbb{T}^2_{\mathbb{C}};\mathbb{C})$ for all $(y,t;x,\lambda)\in\mathbb{R}^2\times\mathbb{T}^2_{\mathbb{C}}$. The result obtained above can be formulated as the follows:

Proposition 2.4. *The Kupershmidt hydrodynamic heavenly system (2.43) is representable as commuting Hamiltonian flows (2.47) on orbits of the coadjoint action of the holomorphic loop Lie algebra $\tilde{\mathscr{G}}=\widetilde{diff}(\mathbb{T}^2_{\mathbb{C}})$ and are equivalent to the Lax–Sato vector field compatibility condition (2.49).*

2.6. Examples:New spatially $3D$-integrable heavenly systems

2.6.1. The first Sergyeyev spatially $3D$-integrable heavenly system

A new spatially $3D$-integrable heavenly system, recently constructed in [71], using techniques from contact geometry [12, 38], is given as the flow

$$\begin{aligned}u_t-v_y-vu_z-ru_x+uv_z+wv_x&=0,\\ 2u_z-r_z+w_x+2ww_z&=0,\\ 2r_x-3u_x-2w_y-v_z+2wu_z-2ww_x+2uw_z&=0,\\ w_t-r_y+2v_x-4wu_x+wr_x-rw_x-vw_z+ur_z&=0\end{aligned}\tag{2.50}$$

with respect to two evolution parameters $t,y\in\mathbb{R}$ for four smooth functions $(u,v,w,r)\in C^\infty(\mathbb{R}^2\times\mathbb{T}^2;\mathbb{R}^4)$. Let us set $\tilde{\mathscr{G}}:=\widetilde{diff}(\mathbb{T}^3_{\mathbb{C}})$ and take the corresponding seed element $\tilde{l}\in\tilde{\mathscr{G}}^*$ as

$$\begin{aligned}\tilde{l}=[&3\partial_z^{-1}(3a_{xxx}+6w_z a_{xx}+14w_{xz}w_x+(12ww_x+6r_x)\,w_z+8ww_{xx}+\\ &+\left(6w^2+6r\right)w_{xz}+16w_x^2+6r_z w_x+2v_{xz}+r_{xx}+6wr_{xz})+\\ &+6\lambda a_{xx}+\left(36\lambda a+12\lambda^2\right)a_x+6\lambda r_x]dx+\\ &+[27a_{xx}+70w_z a_x+\left(30a^2+36\lambda a+30r+12\lambda^2\right)w_z+\\ &+(64w+6\lambda)\,w_x+10v_z+(30w+6\lambda)\,r_z+9r_x]dz+\\ &+[42a_x+54w^2+48\lambda w+18r+12\lambda^2]d\lambda,\end{aligned}\tag{2.51}$$

where $w_x=(r-w^2-2u)_z$ and $a\in C^\infty(\mathbb{R}^2\times\mathbb{T}^2;\mathbb{R})$ is such that $w=a_z$, $r-w^2-2u=a_x$ for all $x,z\in\mathbb{T}^2$. The seed element (2.51) naturally generates two independent Casimir functionals $h^{(1)},h^{(2)}\in\mathrm{I}(\tilde{\mathscr{G}}^*)$, whose gradients allow as $|\lambda|\to\infty$ expansions (2.14) in the form

$$\nabla h^{(1)}(l)\sim(w_z\lambda^2+(u_z-w_x)\lambda-u_x,2\lambda+w,u-\lambda^2)^\intercal+O(\lambda^{-1}),$$

$$\begin{gathered}\nabla h^{(2)}(l)\sim(2w_z\lambda^3+(-2w_x+r_z)\lambda^2-r_x+v_z)\lambda-v_x,\\ 3\lambda^2+4w\lambda+r,-2\lambda^3-2w\lambda^2+v)^\intercal+O(\lambda^{-1}).\end{gathered}$$

Now, by defining

$$\nabla h^{(y)}(l):=\nabla h^{(1)}(l)|_+=(w_z\lambda^2+(u_z-w_x)\lambda-u_x,2\lambda+w,u-\lambda^2)^\intercal,\tag{2.52}$$

$$\begin{gathered}\nabla h^{(t)}(l):=\nabla h^{(2)}(l)|_+=(2w_z\lambda^3+(-2w_x+r_z)\lambda^2-r_x+v_z)\lambda-v_x,\\ 3\lambda^2+4w\lambda+r,-2\lambda^3-2w\lambda^2+v)^\intercal\end{gathered}$$

subject to the canonical splitting $\tilde{\mathscr{G}}=\tilde{\mathscr{G}}_+\oplus\tilde{\mathscr{G}}_-$, one obtains for the heavenly equation (2.50) the following vector field representation

$$\begin{gathered}\frac{\partial\psi}{\partial t}+(3\lambda^2+4w\lambda+r)\frac{\partial\psi}{\partial x}+(-2\lambda^3-2w\lambda^2+v)\frac{\partial\psi}{\partial z}+\\ +[2w_z\lambda^3+(-2w_x+r_z)\lambda^2+(-r_x+v_z)\lambda-v_x]\frac{\partial\psi}{\partial\lambda}=0,\\ \frac{\partial\psi}{\partial y}+[2\lambda+w]\frac{\partial\psi}{\partial x}+(3\lambda^2+4w\lambda+r)\frac{\partial\psi}{\partial z}+(u-\lambda^2)\frac{\partial\psi}{\partial\lambda}=0,\end{gathered}\tag{2.53}$$

satisfied for $\psi\in C^2(\mathbb{R}^2\times\mathbb{T}^3_{\mathbb{C}};\mathbb{C})$, any $(t,y;x,z)\in\mathbb{R}^2\times\mathbb{T}^2$ and all $\lambda\in\mathbb{T}_{\mathbb{C}}$.

2.6.2. The second Sergyeyev spatially $3D$-integrable heavenly system

The second spatially 3-D integrable heavenly system, presented in [71], is given by two separate flows

$$\begin{aligned} u_t &= 2rv_x - 2vw_z + vr_x + wu_x, \\ v_t &= vw_x + wv_x, \\ \\ w_y &= 2vr_z - 2ru_x + uw_z + rv_z, \\ r_y &= ur_z + ru_z \end{aligned} \tag{2.54}$$

with respect to two independent evolution parameters $t, y \in \mathbb{R}$ for four smooth functions $(u,v,w,r) \in C^\infty(\mathbb{R}^2 \times \mathbb{T}^2; \mathbb{R}^4)$. Inasmuch the system (2.54) is not completely specified as evolution flows and is obviously invariant with respect to the involution mapping $\mathrm{Symm}\{x \rightleftarrows z, t \rightleftarrows y; u \rightleftarrows w, r \rightleftarrows v\}$, we need to take this into account to imbed this system into our Lie-algebraic integrability scheme.
We start, as before, from the basic vector fields Lie algebra $\widetilde{diff}(\mathbb{T}^3_{\mathbb{C}})$ on the torus $\mathbb{T}^3_{\mathbb{C}}$ with coefficients from the differential-algebra $\mathbb{R}\{u,v,w,r|(x,z;\lambda)\}$, considering its splitting

$$\tilde{\mathscr{G}} := \tilde{\mathscr{G}}_+ \oplus \tilde{\mathscr{G}}_- \tag{2.55}$$

with $\tilde{\mathscr{G}}_\pm := \widetilde{diff}(\mathbb{T}^3_{\mathbb{C}})|_\pm$, naturally determining on $\tilde{\mathscr{G}}$ the canonical $\mathscr{R}$-structure $\mathscr{R} = (P_+ - P_-)/2$ with projections $P_\pm \tilde{\mathscr{G}} := \tilde{\mathscr{G}}_\pm \subset \tilde{\mathscr{G}}$. Taking into account the splitting (2.55), one can construct the adjoint with respect to the bilinear form $(\cdot,\cdot)_0$ space $\tilde{\mathscr{G}}^* = \tilde{\mathscr{G}}^*_+ \oplus \tilde{\mathscr{G}}^*_-$, where $\tilde{\mathscr{G}}^*_\pm = \widetilde{diff}^*(\mathbb{T}^3_{\mathbb{C}})|_\pm$. Now if we choose a generating seed element $\tilde{l} \in \tilde{\mathscr{G}}^*_+ \oplus \tilde{\mathscr{G}}^*_-$ to be suitably anti-symmetric subject to the system (2.54), that is

$$\mathrm{Symm}_\lambda \tilde{l} = -\tilde{l}, \tag{2.56}$$

where, by definition, the extended mapping $\mathrm{Symm}_\lambda : \tilde{\mathscr{G}}^* \to \tilde{\mathscr{G}}^*$ acts via the extended involution $\mathrm{Symm}_\lambda\{x \rightleftarrows z, t \rightleftarrows y; u \rightleftarrows w, r \rightleftarrows v; \lambda \rightleftarrows 1/\lambda$ $\}$, then one can write down, as an example, the following expression

$$\tilde{l} = l^* - \mathrm{Symm}_\lambda l^* \tag{2.57}$$

with some element $l^* \in \tilde{\mathscr{G}}^*_+$ that we take in the form

$$\begin{aligned} l^* := \; & r^4 d\lambda + +[r^2 \tfrac{\partial}{\partial z}^{-1}(3ar^6 w_z - rw_{xx} + wr_{xx} + \\ & + r^{-1}wr_x^2 + 2r^{-2}a_x) + a\lambda + r^3 r_x \lambda^2]dx + \\ & + [a - r^3 w_x + 2r^2 wr_x + r^3(w_z + r_x)\lambda + r^3 r_z \lambda^2]dz \end{aligned} \tag{2.58}$$

Here $a := r^3 \frac{\partial}{\partial z}^{-1}(3r^{-1}r_x w_z + w_{xz} + r_{xx} + 5r^{-1}r_x^2)$, with coefficients from the suitably extended differential-algebra $\mathbb{R}\{u,v,w,r|(x,z;\lambda)\}$ as it satisfies the Casimir determining equation (2.5) subject to the vector field

$$\nabla h(l^*) \sim \nabla h^{(t)}(l^*)_+ + \sum_{j\in\mathbb{Z}_+} \nabla h_j(l^*)\lambda^{-(j+1)}, \tag{2.59}$$

where

$$\nabla h^{(t)}(l^*) = [r_z\lambda^3 + (w_z - r_x)\lambda^2 - w_x\lambda]\partial/\partial\lambda + (2\lambda r + w)\partial/\partial x - r\lambda^2\partial/\partial z. \tag{2.60}$$

Based on the projected gradient element (2.60) one can construct on $\tilde{\mathscr{G}}^*$ the Hamiltonian flow

$$\partial l^*/\partial t = -ad^*_{\nabla h^{(t)}(l^*)} l^* \tag{2.61}$$

with respect to the temporal evolution parameter $t \in \mathbb{R}$. Recalling now the symmetry property (2.56), one can apply the mapping Symm_λ to (2.60) and obtain, as a result, the evolution flow

$$\partial l^*/\partial y = -ad^*_{\nabla h^{(y)}(l^*)} l^* \tag{2.62}$$

with respect to the evolution parameter $y \in \mathbb{R}$, which is compatible with the flow (2.61), where we define

$$\nabla h^{(y}(l^*) := \mathrm{Symm}_\lambda \nabla h^{(t)}(l^*) = (\lambda u_z - u_x + v_z - v_x\lambda^{-1})\partial/\partial\lambda - v\lambda^{-2}\partial/\partial x + (u + 2v\lambda^{-1})\partial/\partial z. \tag{2.63}$$

Having applied now the mapping Symm_λ to both sides of the relationship (2.62), we obtain the flow

$$\frac{\partial}{\partial t}(\mathrm{Symm}_\lambda l^*) = -ad^*_{\nabla h^{(t)}(l^*)}(\mathrm{Symm}_\lambda l^*). \tag{2.64}$$

Combining this with (2.61) gives rise to the flow

$$\partial \tilde{l}/\partial t = -ad^*_{\nabla h^{(t)}(l^*)} \tilde{l}\,, \tag{2.65}$$

which is a priori compatible with its symmetry Symm_λ image:

$$\partial\tilde{l}/\partial y = -ad^*_{\nabla h^{(y)}(l^*)}\tilde{l}. \tag{2.66}$$

As the evolution parameters are mutually independent, from flows (2.61) and (2.62) one obtains their natural compatibility condition, which is equivalent to the following vector field expression:

$$\frac{\partial}{\partial t}\nabla h^{(y)}(l^*) - \frac{\partial}{\partial y}\nabla h^{(t)}(l^*) + [\nabla h^{(t)}(l^*), \nabla h^{(y)}(l^*)] = 0, \tag{2.67}$$

giving rise to the initial heavenly system of equations of equations (2.54). As a simple consequence of (2.67), we obtain for the heavenly system (2.54) its Lax–Sato compatible vector fields representation

$$\begin{aligned} &\partial\psi/\partial t + [r_z\lambda^3 + (w_z - r_x)\lambda^2 - w_x\lambda]\partial\psi/\partial\lambda + (2\lambda r + w)\partial\psi/\partial x - r\lambda^2\partial\psi/\partial z = 0, \\ &\partial\psi/\partial y + (\lambda u_z - u_x + v_z - v_x\lambda^{-1})\partial\psi/\partial\lambda - v\lambda^{-2}\partial\psi/\partial x + (u + 2v\lambda^{-1})\partial\psi/\partial z = 0, \end{aligned} \tag{2.68}$$

satisfied for an invariant $\psi \in C^2(\mathbb{R}^2 \times \mathbb{T}^3_{\mathbb{C}};\mathbb{C})$, any $(t,y;x,z) \in \mathbb{R}^2 \times \mathbb{T}^2$ and all $\lambda \in \mathbb{T}_{\mathbb{C}}$.

Remark 2.5. *It must be mentioned that the vector field $\nabla h^{(y}(l^*) \in \tilde{\mathscr{G}}$ as devised above, possesses no proto-Casimir functionals $h^{(y)}_j \in \mathrm{D}(\tilde{\mathscr{G}}^*), j = \overline{1,2}$, whose gradients projections $\nabla h^{(y)}_j(l^*)|_\pm \in \tilde{\mathscr{G}}_\pm, j = \overline{1,2}$, would be generated. That is $\nabla h^{(y}(l^*) \neq \nabla h^{(y)}_1(l^*)|_+ + \nabla h^{(y)}_2(l^*)|_-$ for any smooth functionals $h^{(y)}_j \in \mathrm{D}(\tilde{\mathscr{G}}^*), j = \overline{1,2}$.*

2.7. Example: A generalized Liouville type equation

In [10], devoted to studying Grassmannians, closed differential forms and related N-dimensional integrable systems, the authors presented a Lax–Sato type representation for the well-known Liouville equation

$$\frac{\partial^2\varphi}{\partial y\partial t} = \exp\varphi, \tag{2.69}$$

written in the so called "laboratory" coordinates $y,t \in \mathbb{R}^2$ for a function $\varphi \in C^2(\mathbb{R}^2;\mathbb{R})$ and having different geometric interpretations. Their related result, obtained via some completely formal calculations, reads as follows: a system of the linear vector field equations

$$\begin{aligned} \partial\psi/\partial y + (\lambda^2 + v\lambda + 1)\partial\psi/\partial\lambda &= 0, \\ \partial\psi/\partial t - u\partial\psi/\partial\lambda &= 0 \end{aligned} \tag{2.70}$$

for a function $\psi \in C^2(\mathbb{R}^2 \times \mathbb{T}^1_{\mathbb{C}};\mathbb{C})$ is compatible for all $y,t \in \mathbb{R}^2$, where $u,v \in C^2(\mathbb{R}^2;\mathbb{R})$ are functional coefficients and $\lambda \in \mathbb{T}^1_{\mathbb{C}}$ is a complex parameter. Under the simple reduction $u = 1/2\exp\varphi$ the compatibility condition for (2.70) coincides with the Liouville equation (2.69).

This section is devoted to unveiling the Lie-algebraic structure of a generalized Liouville type heavenly equation, whose Lax–Sato integrability was shown in [10] using geometric analysis of Grassmanians and related closed differential forms.

As our interest is in the Lie-algebraic nature of the Lax-Sato representation (2.70) for the Liouville equation (2.69), we define the torus diffeomorphism Lie group $\tilde{G} := \widetilde{Diff}(\mathbb{T}^1_{\mathbb{C}})$, holomorphically extended in the interior $\mathbb{D}^1_+ \subset \mathbb{C}$ and in the exterior $\mathbb{D}^1_- \subset \mathbb{C}$ regions of the unit disc $\mathbb{D}^1 \subset \mathbb{C}^1$, such that for any $g(z) \in \bar{G}|_{\mathbb{D}^1_-}, z \in \mathbb{D}^1_-, g(\infty) = 1 \in \widetilde{Diff}(\mathbb{T}^1_{\mathbb{C}})$. Then we study specially chosen coadjoint orbits, which are related to the compatible system of linear vector field equations (2.70).

As a first step,one needs to consider the corresponding Lie algebra $\tilde{\mathscr{G}} := \widetilde{diff}(\mathbb{T}^1_{\mathbb{C}})$ and its decomposition into the direct sum of subalgebras

$$\tilde{\mathscr{G}} = \tilde{\mathscr{G}}_+ \oplus \tilde{\mathscr{G}}_- \tag{2.71}$$

of Laurent series with positive as $|z| \to 0$ and strongly negative as $|z| \to \infty$ degrees, respectively. Then, owing to classical Adler-Kostant-Symes theory, for any element $\tilde{l} \in \tilde{\mathscr{G}}^* \simeq \Lambda^1(\mathbb{T}^1_{\mathbb{C}})$ the following formally constructed flows

$$d\tilde{l}/dy = -ad^*_{\nabla h^{(y)}(\tilde{l})}\tilde{l}, \quad d\tilde{l}/dt = -ad^*_{\nabla h^{(t)}(\tilde{l})}\tilde{l} \tag{2.72}$$

along the evolution parameters $y,t \in \mathbb{R}^2$ are always compatible, if $h^{(p_y)}$ and $h^{(p_t)} \in \mathrm{I}(\tilde{\mathscr{G}}^*)$ are arbitrarily chosen functionally independent Casimir functionals on the adjoint space $\tilde{\mathscr{G}}^*$, and $\nabla h^{(y)}(\tilde{l}) := \nabla h^{(p_y)}(\tilde{l})_+, \nabla h^{(t)}(\tilde{l}) := \nabla h^{(p_t)}(\tilde{l})_+$ are their gradients, suitably projected on the subalgebra $\tilde{\mathscr{G}}_+$. Keeping in mind the above result, consider the Casimir functional $h^{(p_y)}$ on $\tilde{\mathscr{G}}^*$, whose gradient $\nabla h^{(p_y)}(\tilde{l}) := \nabla h^{(p_y)}(l)\partial/\partial z$ as $|z| \to \infty$ is taken, for simplicity, in the asymptotic form

$$\nabla h^{(p_y)}(\tilde{l}) \simeq (v_2 z^2 + v_1 z + v_0 + v_{-1}z^{-1} + v_{-2}z^{-2} + \ldots)\partial/\partial z, \tag{2.73}$$

where $p_y = 2$. This gives rise to the gradient projection $\nabla h^{(y)}(\tilde{l}) = (v_2 z^2 + v_1 z + v_0)\partial/\partial z \in \tilde{\mathscr{G}}_+$, where $z \in \mathbb{T}^1_{\mathbb{C}}$, $|z| \to \infty$, and $v_j \in C^2(\mathbb{R}^2;\mathbb{R}), j \in \mathbb{Z}, j \leq 2$, are some functional parameters. As the element $\tilde{l} = l(y,t;z)dz \in \Lambda^1(\mathbb{T}^1_{\mathbb{C}})$ satisfies, by definition, the differential equation

$$\frac{d}{dz}[l(y,t;z)(\nabla h^{(p_y)}(l))^2] = 0, \tag{2.74}$$

we obtain from (2.74) that the element

$$l(y,t;z)=\sigma(y,t)^2(\nabla h^{(p_y)}(\tilde{l}))^{-2}, \tag{2.75}$$

where $\sigma\in C^2(\mathbb{R}^2;\mathbb{R})$ is an arbitrary function. If for brevity we set $\sigma(y,t):=1$ and $v_2:=1$, the element (2.75) becomes

$$l(y,t;z)=z^{-4}[1-2v_1z^{-1}+(3v_1^2-2v_0)z^{-2}] \tag{2.76}$$

Observe now that the relationship (2.74) verifies the following lemma:

Lemma 2.6. *The set $\mathrm{I}(\tilde{\mathscr{G}}^*)$ of the functionally independent Casimir invariants is one-dimensional.*

As a consequence, it follows that for the element $\tilde{l}=l(y,t;z)dz\in\Lambda^1(\mathbb{T}^1_{\mathbb{C}})$ generated by the expression (2.75), there exists only the flow on $\tilde{\mathscr{G}}^*$ from (2.72) with respect to the evolution variable $y\in\mathbb{R}$:

$$dl/dy=\nabla h^{(y)}(l)^{-1}\frac{\partial}{\partial z}[l(y,t;z)\nabla h^{(y)}(l)]^2. \tag{2.77}$$

For the flow from (2.72) with respect to the evolution variable $t\in\mathbb{R}$ one can take the constant functional $h^{(p_t)}:=const\in\mathrm{I}(\tilde{\mathscr{G}}^*), p_t=0, \nabla h^{(p_t)}(l)=0$, and construct the trivial flow on $\tilde{\mathscr{G}}^*$ as

$$dl/dt=-\nabla h^{(t)}(l)\frac{\partial l}{\partial z}-2l\frac{\partial}{\partial z}(\nabla h^{(t)}(l))=0, \tag{2.78}$$

where, by definition, $\nabla h^{(t)}(l):=\nabla h^{(p_t)}(l)_+\in\tilde{\mathscr{G}}$.It is now important to observe that the compatibility condition of these two flows for all $y,t\in\mathbb{R}$ is equivalent to the following system of two *a priori* compatible linear vector field equations

$$\frac{\partial\psi}{\partial y}+\nabla h^{(y)}(l)\,\frac{\partial\psi}{\partial z}=0,\quad \frac{\partial\psi}{\partial t}+\nabla h^{(t)}(l)\frac{\partial\psi}{\partial z}=0, \tag{2.79}$$

or

$$\frac{\partial\psi}{\partial y}+\,(z^2+v_1z+v_0)\frac{\partial\psi}{\partial z}=0,\quad \frac{\partial\psi}{\partial t}+0\frac{\partial\psi}{\partial z}=0 \tag{2.80}$$

for a smooth function $\psi\in C^2(\mathbb{R}^2\times\mathbb{T}^1_{\mathbb{C}};\mathbb{C})$, meaning, in particular, that the complex parameter $z\in\mathbb{T}^1_{\mathbb{C}}$ is constant with respect to the evolution parameter $t\in\mathbb{R}$. The linear equations (2.80) are clearly equivalent to the *a priori* compatible system of the vector fields

$$dz/dy=\nabla h^{(y)}(l)=\,z^2+v_1z+v_0,\quad dz/dt=\nabla h^{(t)}(l)=0 \tag{2.81}$$

on the complex torus $\mathbb{T}^1_{\mathbb{C}}$, which can be rewritten subject to the following diffeomorphism $\mathbb{T}^1_{\mathbb{C}}\ni z\mapsto z-\alpha(t,y):=\lambda\in\mathbb{T}^1_{\mathbb{C}}$, generated by an arbitrary smooth function $\alpha\in C^3(\mathbb{R}^2;\mathbb{R})$:

$$d\lambda/dy=\,\lambda^2+\lambda(2\alpha+v_1)+(\alpha^2+\alpha v_1+v_0-\partial\alpha/\partial y),\quad d\lambda/dt=-\partial\alpha/\partial t. \tag{2.82}$$

The latter system is evidently also compatible for all $y,t\in\mathbb{R}$ and can be expressed as

$$d\lambda/dy=\,\lambda^2+\lambda v+w,\;\; d\lambda/dt=-u, \tag{2.83}$$

where

$$2\alpha+v_1:=v,\;\;\alpha^2+\alpha v_1+v_0-\partial\alpha/\partial y:=w,\;\;\partial\alpha/\partial t:=u. \tag{2.84}$$

Moreover, the *a priori* compatible system (2.80) can be recast as

$$\frac{\partial\psi}{\partial y}+\,(z^2+vz+w)\frac{\partial\psi}{\partial\lambda}=0,\quad \frac{\partial\psi}{\partial y}-u\frac{\partial\psi}{\partial\lambda}=0 \tag{2.85}$$

for the corresponding function $\psi\in C^2(\mathbb{R}^2\times\mathbb{T}^1_{\mathbb{C}};\mathbb{C})$, giving rise to the following system of heavenly equations:

$$v_t-2u=0,\quad u_y-uv+w_t=0. \tag{2.86}$$

The latter can be parameterized by means of the substitution $u:=1/2\exp\varphi$ as follows:

$$\varphi_{yt}=\exp\varphi-[2w_t\exp(-\varphi)]_t. \tag{2.87}$$

Then the reductions $w:=const=1$ or $w:=-\frac{1}{2}\exp\varphi$ give rise to the well-known Liouville equations

$$\varphi_{yt}=\exp\varphi,\quad \varphi_{yt}-\varphi_{tt}=\exp\varphi, \tag{2.88}$$

which are known to possess standard [6, 44, 59] Lax type isospectral representations. The above analysis leads directly to the following result.

Proposition 2.7. *The system (2.86) of heavenly nonlinear equations possesses Lax–Sato type compatible vector field representation (2.85), whose Lie-algebraic structure is governed by the classical Lie-algebraic Adler–Kostant–Symes theory.*

Remark 2.8. *In a manner like the above, one can describe in detail the Lie-algebraic structure for other generalized Liouville type heavenly equations, presented in [10] for a higher order in $\lambda\in\mathbb{T}^1_{\mathbb{C}}$ system of linear vector field equations (2.79).*

3. The linearization covering method and its applications

3.1. Introductory notions and examples

Some three years ago I. Krasilshchik [34] analyzed a so called Gibbon–Tsarev equation

$$z_{yy}+z_t z_{ty}-z_y z_{tt}+1=0. \tag{3.1}$$

and its so called nonlinear first-order differential *covering*

$$\frac{\partial w}{\partial t}-\frac{1}{z_y+z_t w-w^2}=0,\ \frac{\partial w}{\partial y}+\frac{z_t-w}{u_y+z_t w-w^2}=0, \tag{3.2}$$

which for any solution $z:\mathbb{R}^2\to\mathbb{R}$ to equation (3.1) is compatible for all $(t,y)\in\mathbb{R}^2$. He showed this makes it possible to determine for any smooth solution $w:\mathbb{R}^2\to\mathbb{R}$ to the equation (3.2) a suitable smooth function $\psi:\mathbb{R}\times\mathbb{R}^2\to\mathbb{R}$, satisfying the corresponding Lax–Sato type linear representation:

$$\frac{\partial\psi}{\partial t}+\frac{1}{z_y+z_t\lambda-\lambda^2}\frac{\partial\psi}{\partial\lambda}=0,\ \frac{\partial\psi}{\partial y}-\frac{z_t-\lambda}{z_y+z_t\lambda-\lambda^2}\frac{\partial\psi}{\partial\lambda}=0, \tag{3.3}$$

which for any solution to the equation (3.1) is also compatible for all $(t,y)\in\mathbb{R}^2$ and an arbitrary parameter $\lambda\in\mathbb{R}$.
Krasilshchik [34] also posed the interesting problem of providing a differential-geometric explanation of the linearization procedure for a given nonlinear differential-geometric relationship $J^1(\mathbb{R}^n\times\mathbb{R}^2;\mathbb{R})|_{\mathscr{E}}$ in the jet-manifold $J^1(\mathbb{R}^n\times\mathbb{R}^2;\mathbb{R})$, $n\in\mathbb{Z}_+$, realizing a compatible *covering* for the corresponding nonlinear differential equation $\mathscr{E}[x,\tau;u]=0$, imbedded into some adjacent jet-manifold $J^k(\mathbb{R}^n\times\mathbb{R}^2;\mathbb{R}^m)$ for some $k,m\in\mathbb{Z}_+$. His extended version of this procedure, presented in [34], was quite hard to decipher and offered no new example demonstrating its application. One of our goals is to explain some important points of this linearization procedure in the framework of the classical nonuniform vector field equations and present new and important applications. We consider the jet manifold $J^k(\mathbb{R}^n\times\mathbb{R}^2;\mathbb{R}^m)$ for some fixed $k,m\in\mathbb{Z}_+$ and a differential relationship [30] in a general form $\mathscr{E}[x,\tau;u]=0$, satisfied for all $(x;\tau)\in\mathbb{R}^n\times\mathbb{R}^2$ and suitable smooth mappings $u:\mathbb{R}^n\times\mathbb{R}^2\to\mathbb{R}^m$.
As a new example, we can take $n=1=m, k=2$ and choose a differential relationship $\mathscr{E}[x;y,t;u]=0$ in the form

$$u_t u_{xy}-k_1 u_x u_{ty}-k_2 u_y u_{tx}=0; \tag{3.4}$$

the so called ABC-equation, first discussed in [76], where $u:\mathbb{R}\times\mathbb{R}^2\to\mathbb{R}$ and $k_1,k_2\in\mathbb{R}$ are arbitrary parameters, satisfying the conditions

$$k_1+k_2-1=0\ \vee k_1+k_2-1\neq 0. \tag{3.5}$$

The first case $k_1+k_2-1=0$ was investigated in [22, 42, 76] and recently in [31], where its Lax–Sato type linearization was found along with many other its interesting properties. For the second case $k_1+k_2-1\neq 0$ the following crucial result was stated in equivalent form by P.A. Burovskiy, E.V. Ferapontov, S.P. Tsarev in [16, 35] and recently by I. Krasilshchik, A. Sergyeyev and O. Morozov in [35].

Proposition 3.1. *A dual to (3.4) covering system $J^1(\mathbb{R}\times\mathbb{R}^2;\mathbb{R})|_{\mathscr{E}}$ of quasi-linear first order differential relationships*

$$\begin{aligned}\frac{\partial w}{\partial t}+\frac{u_t w}{u_x k_1(k_1+k_2-1)}\frac{\partial w}{\partial x}-\frac{w(w+k_1+k_2-1)u_{tx}}{u_x k_1}&=0,\\ \frac{\partial w}{\partial y}+\frac{u_y w}{u_x k_1(w+k_1+k_2-1)}\frac{\partial w}{\partial x}-\frac{w(k_1+k_2-1)u_{yx}}{u_x k_1}&=0\end{aligned} \tag{3.6}$$

on the jet-manifold $J^1(\mathbb{R}\times\mathbb{R}^2;\mathbb{R})$ is compatible; that is, it holds for any its smooth solution $w:\mathbb{R}\times\mathbb{R}^2\to\mathbb{R}$ at all points $(x;y,t)\in\mathbb{R}\times\mathbb{R}^2$ iff the function $u:\mathbb{R}\times\mathbb{R}^2\to\mathbb{R}$ satisfies the ABC-equation (3.4).

Moreover, this result was recently generalized in [35] to the following "*linearizing*" proposition.

Proposition 3.2. *A system $J^1_{lin}(\mathbb{R}^2\times\mathbb{R}^2;\mathbb{R})|_{\mathscr{E}}$ of linear first order differential relationships*

$$\begin{aligned}&\frac{\partial\psi}{\partial t}+\frac{\lambda u_x^{\frac{k_2-1}{k_1}}u_t}{k_1(k_1+k_2-1)}\frac{\partial\psi}{\partial x}-\frac{\lambda^2 u_x^{\frac{k_2-k_1-1}{k_1}}(u_t u_{xx}-k_1 u_{xx}u_{xt})}{k_1^2}\frac{\partial\psi}{\partial\lambda}=0,\\ &\frac{\partial\psi}{\partial y}+\frac{k_2\lambda u_x^{\frac{k_2-1}{k_1}}u_y}{k_1(\lambda u_x^{\frac{k_2-k_1-1}{k_1}}+k_1+k_2-1)}\frac{\partial\psi}{\partial x}-\frac{\lambda^2 k_2(k_1+k_2-1)u_x^{\frac{k_2-k_1-1}{k_1}}u_y u_{xx}}{k_1^2(\lambda u_x^{\frac{k_2-k_1-1}{k_1}}+k_1+k_2-1)}\frac{\partial\psi}{\partial\lambda}=0\end{aligned} \tag{3.7}$$

on the covering jet-manifold $J^1(\mathbb{R}^2\times\mathbb{R}^2;\mathbb{R})$is compatible; that is, it holds for any its smooth solution $\psi:\mathbb{R}^2\times\mathbb{R}^2\to\mathbb{R}$ at all points $(x,\lambda;y,t)\in\mathbb{R}^2\times\mathbb{R}^2$ iff the function $u:\mathbb{R}\times\mathbb{R}^2\to\mathbb{R}$ satisfies the generalized ABC-equation (3.4).

A similar result, when $n=1,\ m,k=2$, was proved for the Manakov-Santini equations

$$\begin{aligned}u_{tx}+u_{yy}+(uu_x)_x+v_x u_{xy}-v_y u_{xx}&=0,\\ v_{xt}+v_{yy}+uv_{xx}+v_x u_{xy}-v_y v_{xx}&=0,\end{aligned} \tag{3.8}$$

whose Lax–Sato integrability was extensively studied in [21, 24, 39, 11, 31]. The system (3.8) as a jet-submanifold $J^1(\mathbb{R}\times\mathbb{R}^2;\mathbb{R})|_{\mathscr{E}}\subset J^1(\mathbb{R}\times\mathbb{R}^2;\mathbb{R})$ allows the following nonlinear first order differential representation

$$\begin{gathered}\frac{\partial w}{\partial t}+(w^2-wv_x+u-v_y)\frac{\partial w}{\partial x}+u_xw-u_y+v_{yy}+v_x(v_y-u)_x=0,\\ \frac{\partial w}{\partial y}+w\frac{\partial w}{\partial x}-v_{xx}w+(u-v_y)_x=0,\end{gathered}\tag{3.9}$$

compatible on solutions to the nonlinear differential relationship $\mathscr{E}[x,\tau;u]=0$ (3.8) on $J^2(\mathbb{R}\times\mathbb{R}^2;\mathbb{R}^2)$. The existence of the compatible representation (3.9) makes it possible to verify the following proposition.

Proposition 3.3. *A covering system $J^1_{lin}(\mathbb{R}^2\times\mathbb{R}^2;\mathbb{R})|_{\mathscr{E}}$ of linear first order differential relationships*

$$\begin{gathered}\frac{\partial\psi}{\partial t}+(\lambda^2+\lambda v_x+u-v_y)\frac{\partial\psi}{\partial x}+(u_y-\lambda u_x)\frac{\partial\psi}{\partial\lambda}=0,\\ \frac{\partial\psi}{\partial y}+(v_x+\lambda)\frac{\partial\psi}{\partial x}-u_x\frac{\partial\psi}{\partial\lambda}=0\end{gathered}\tag{3.10}$$

on the jet-manifold $J^1(\mathbb{R}^2\times\mathbb{R}^2;\mathbb{R})$ is compatible; that is, it holds for any its smooth solution $\psi:\mathbb{R}^2\times\mathbb{R}^2\to\mathbb{R}$ at all points $(x,\lambda;y,t)\in\mathbb{R}^2\times\mathbb{R}^2$ iff the function $u:\mathbb{R}\times\mathbb{R}^2\to\mathbb{R}$ satisfies the generalized Khokhlov–Zabolotska equation (3.8).

From the point of view of the propositions above, the main essence of our present analysis, similarly to that in [34], is to recover the intrinsic mathematical structure responsible for the existence of the "*linearizing*" covering jet-manifold mappings

$$J^1_{lin}(\mathbb{R}^{n+1}\times\mathbb{R}^2;\mathbb{R})|_{\mathscr{E}}\quad\rightleftharpoons\quad J^1(\mathbb{R}^n\times\mathbb{R}^2;\mathbb{R})|_{\mathscr{E}}\tag{3.11}$$

for any dimension $n\in\mathbb{Z}_+$, compatible with our differential relationship $\mathscr{E}[x,\tau;u]=0$, as it was presented above in the form (3.6) and (3.7) for the relationships (3.4). Thus, for a given nonlinear differential relationship $\mathscr{E}[x,\tau;u]=0$ on the jet-manifold $J^k(\mathbb{R}^n\times\mathbb{R}^2;\mathbb{R}^m)$ for some $k\in\mathbb{Z}_+$ one can formulate the following **problem:**
If there is a compatible system $J^1(\mathbb{R}^n\times\mathbb{R}^2;\mathbb{R}^m)|_{\mathscr{E}}\subset J^1(\mathbb{R}^n\times\mathbb{R}^2;\mathbb{R}^m)$ of quasi-linear first order differential relationships, how can construct a linearizing first order differential system $J^1_{lin}(\mathbb{R}^{(1+n)+2};\mathbb{R})|_{\mathscr{E}}\subset J^1(\mathbb{R}^{(1+n)+2};\mathbb{R})$ in a vector field equations form on the covering space $\mathbb{R}^{n+1}\times\mathbb{R}^2$, realizing the implications (3.11). The latter is interpreted as the corresponding Lax–Sato representation [8, 9, 10, 24, 25, 73, 74] for the given differential relationship $\mathscr{E}[x,\tau;u]=0$ on the jet-manifold $J^k(\mathbb{R}^n\times\mathbb{R}^2;\mathbb{R}^m)$.
As a dual approach to this linearization covering scheme, we present also the so called contact geometry linearization, suggested recently in [71] and slightly generalizing the well-known [69] Hamiltonian linearization covering method. As an example, we have proved the following proposition.

Proposition 3.4. *The following [16] nonlinear singular manifold Toda differential relationship*

$$u_{xy}sh^2u_t=u_xu_yu_{tt}\tag{3.12}$$

on the jet manifold $J^2(\mathbb{R}^2\times\mathbb{R}^2;\mathbb{R})$ allows the Lax–Sato type linearization covering

$$\begin{aligned}\frac{\partial\psi}{\partial t}+\frac{(e^{-2u_t}-1)}{2u_x}\frac{\partial\psi}{\partial x}-\left[\lambda\left(\frac{e^{-2u_t}-1}{2u_x}\right)_x+\lambda^2\left(\frac{e^{-2u_t}-1}{2u_x}\right)_z\right]\frac{\partial\psi}{\partial\lambda}&=0,\\ \frac{\partial\psi}{\partial y}-\frac{u_ye^{-2u_t}}{u_x}\frac{\partial\psi}{\partial x}+\left[\lambda\left(\frac{u_ye^{-2u_t}}{u_x}\right)_x+\lambda^2\left(\frac{u_ye^{-2u_t}}{u_x}\right)_z\right]\frac{\partial\psi}{\partial\lambda}&=0\end{aligned}\tag{3.13}$$

for smooth invariant functions $\psi\in C^2(\mathbb{R}^3\times\mathbb{R}^2;\mathbb{R})$, all $(x,z,\lambda;\tau)\in\mathbb{R}^3\times\mathbb{R}^2$ and any smooth solution $u:\mathbb{R}^2\times\mathbb{R}^2\to\mathbb{R}$ to the relationship (3.12).

3.2. The linearization covering scheme

A realization of the scheme (3.11) is based on the notion of invariants of suitably specified vector fields on the extended base space $\mathbb{R}^{n+1}\times\mathbb{R}^2$, whose definition suitable for our needs is as follows: a smooth mapping $\psi:\mathbb{R}^{n+1}\times\mathbb{R}^2\to\mathbb{R}$ is, subject to parameters $\tau\in\mathbb{R}^2$, an invariant of a set of vector fields

$$X^{(k)}:=\frac{\partial}{\partial\tau_k}+\sum_{j=\overline{1,n}}a_j^{(k)}(x,\lambda;\tau)\frac{\partial}{\partial x_j}+b^{(k)}(x,\lambda;\tau)\frac{\partial}{\partial\lambda}\tag{3.14}$$

on $\mathbb{R}^{n+1}\times\mathbb{R}^2$ with smooth coefficients $(a^{(k)},b^{(k)}):\mathbb{R}^{n+1}\times\mathbb{R}^2\to\mathbb{E}^n\times\mathbb{R}$, $k=\overline{1,2}$, if

$$X^{(k)}\psi=0\tag{3.15}$$

holds for $k=\overline{1,2}$ and all $(x,\lambda;\tau)\in\mathbb{R}^{n+1}\times\mathbb{R}^2$. The system of linear equations (3.15) is equivalently representable as a jet-submanifold $J^1_{lin}(\mathbb{R}^{n+1}\times\mathbb{R}^2;\mathbb{R})|_{\mathscr{E}}\subset J^1(\mathbb{R}^{n+1}\times\mathbb{R}^2;\mathbb{R})$. It is also well known [17] that simultaneously the following vector field flows

$$\frac{\partial x_j}{\partial\tau_k}=a_j^{(k)}(x,\lambda;\tau),\quad\frac{\partial\lambda}{\partial\tau_k}=b^{(k)}(x,\lambda;\tau)\tag{3.16}$$

are compatible for any $j=\overline{1,n}, k=\overline{1,2}$ and all $(x,\lambda;\tau)\in\mathbb{R}^{n+1}\times\mathbb{R}^2$. Taking now into account that there is such an invariant function $\psi:\mathbb{R}^{n+1}\times\mathbb{R}^2\to\mathbb{R}$ representable as $\psi(x,\lambda;\tau)=\ w(x;\tau)-\lambda:=0$ for some smooth mapping $w:\mathbb{R}^n\times\mathbb{R}^2\to\mathbb{R}$, it provides upon its substitution into (3.15) the following *a priori* compatible reduced system of quasilinear first order equations

$$\frac{\partial w}{\partial\tau_k}+\sum_{j=\overline{1,n}}a_j^{(k)}(x,w;\tau)\frac{\partial w}{\partial x_j}-b^{(k)}(x,w;\tau)=0 \tag{3.17}$$

for $k=\overline{1,2}$ on the jet-manifold $J^0(\mathbb{R}^n\times\mathbb{R}^2;\mathbb{R})$. Moreover, subject to the system (3.17) one sees [17, 29] that, modulo solutions to the equations (3.16), the expression $w(x;\tau)=\ \psi(x,\lambda(\tau);\tau)+\lambda(\tau)$ for all $(x;\tau)\in\mathbb{R}^n\times\mathbb{R}^2$, where $\psi:\mathbb{R}^{n+1}\times\mathbb{R}^2\to\mathbb{R}$ is a first integral of the vector field flows (3.16). Thus, the reduction scheme just described above provides the algorithm

$$J^1_{lin}(\mathbb{R}^{n+1}\times\mathbb{R}^2;\mathbb{R})|_{\mathscr{E}}\quad\rightarrow\quad J^1(\mathbb{R}^n\times\mathbb{R}^2;\mathbb{R})|_{\mathscr{E}} \tag{3.18}$$

from the implications (3.11) formulated above. The corresponding *inverse* implication

$$J^1_{lin}(\mathbb{R}^{n+1}\times\mathbb{R}^2;\mathbb{R})|_{\mathscr{E}}\quad\leftarrow\quad J^1(\mathbb{R}^n\times\mathbb{R}^2;\mathbb{R})|_{\mathscr{E}} \tag{3.19}$$

can be algorithmically described as follows.
Consider a compatible system $J^1(\mathbb{R}^{n+2};\mathbb{R})|_{\mathscr{E}}\subset J^1(\mathbb{R}^{n+2};\mathbb{R})$ of the first order nonlinear differential relationships

$$\frac{\partial w}{\partial\tau_k}+\sum_{j=\overline{1,n}}a_j^{(k)}(x,w;\tau)\frac{\partial w}{\partial x_j}-b^{(k)}(x,w;\tau)=0 \tag{3.20}$$

with smooth coefficients $(a^{(k)},b^{(k)}):\mathbb{R}^{n+1}\times\mathbb{R}^2\to\mathbb{E}^n\times\mathbb{R}, k=\overline{1,2}$. As the first step it is necessary to check *whether the adjacent system of vector field flows*

$$\frac{\partial x_j}{\partial\tau_k}=a_j^{(k)}(x,w;\tau) \tag{3.21}$$

on $\mathbb{R}^{n+1}$ modulo the flows (3.20) for all $j=\overline{1,n}$ and $k=\overline{1,2}$ *is also compatible.* If the answer is *yes*, it just means [17] that any solution to (3.20) as a complex function $w:\mathbb{R}^n\times\mathbb{R}^2\to\mathbb{R}$ is representable as $w(x;\tau)-\lambda=\alpha(\psi(x,\lambda;\tau))$ for any $\lambda\in\mathbb{R}$ and some smooth mapping $\alpha:\mathbb{R}\to\mathbb{R}$, where the mapping $\psi:\mathbb{R}^{n+1}\times\mathbb{R}^2\to\mathbb{R}$ is *a first integral* of the vector field equations

$$\frac{\partial\psi}{\partial\tau_k}+\sum_{j=\overline{1,n}}a_j^{(k)}(x,\lambda;\tau)\frac{\partial\psi}{\partial x_j}+b^{(k)}(x,\lambda;\tau)\frac{\partial\psi}{\partial\lambda}=0 \tag{3.22}$$

on the extended space $\mathbb{R}^{n+1}\times\mathbb{R}$ for all $(x,\lambda;\tau)\in\mathbb{R}^{n+1}\times\mathbb{R}^2$. Moreover, the value $w(x(\tau);\tau)=\lambda\in\mathbb{R}$ for all $\tau\in\mathbb{R}^2$ is constant as follows from the condition $\alpha(\psi(x(\tau),w;\tau))=0$ for the $\tau\in\mathbb{R}^2$. Thus, we have shown that the equations (3.22) realize the covering linear first order differential relationships $J^1_{lin}(\mathbb{R}^{n+1}\times\mathbb{R}^2;\mathbb{R})|_{\mathscr{E}}\subset J^1(\mathbb{R}^{n+1}\times\mathbb{R}^2;\mathbb{R})$ for $k=\overline{1,2}$ and all $(x,\lambda;\tau)\in\mathbb{R}^{n+1}\times\mathbb{R}^2$, linearizing the first order nonlinear equations (3.20) and interpreting it as the corresponding Lax–Sato representation.
On the other hand, if the adjacent system of vector field flows (3.21) *is not compatible*, it is necessary to recover a hidden isomorphic transformation

$$J^1(\mathbb{R}^{n+1}\times\mathbb{R}^2;\mathbb{R})\ni(x,w;\tau)\to(x,\tilde{w};\tau)\in J^1(\mathbb{R}^{n+1}\times\mathbb{R}^2;\mathbb{R}), \tag{3.23}$$

for which the resulting *a priori compatible* first order equations

$$\frac{\partial\tilde{w}}{\partial\tau_k}+\sum_{j=\overline{1,n}}\tilde{a}_j^{(k)}(x,\tilde{w};\tau)\frac{\partial\tilde{w}}{\partial x_j}-\tilde{b}^{(k)}(x,\tilde{w};\tau)=0 \tag{3.24}$$

already possess *a compatible adjacent system* of the corresponding flows

$$\frac{\partial x_j}{\partial\tau_k}=\tilde{a}_j^{(k)}(x,\tilde{w};\tau) \tag{3.25}$$

on the space $\mathbb{R}^n\times\mathbb{R}$, for which any solution $\tilde{w}:\mathbb{R}^{n+2}\to\mathbb{R}$ generates a first integral $\tilde{\psi}:\mathbb{R}^{n+1}\times\mathbb{R}^2\to\mathbb{R}$ of an adjacent compatible system of the linear vector field equations

$$\frac{\partial\tilde{\psi}}{\partial\tau_k}+\sum_{j=\overline{1,n}}\tilde{a}_j^{(k)}(x,\lambda;\tau)\frac{\partial\tilde{\psi}}{\partial x_j}+\tilde{b}^{(k)}(x,\lambda;\tau)\frac{\partial\tilde{\psi}}{\partial\lambda}=0 \tag{3.26}$$

on the space $\mathbb{R}^{n+1}\times\mathbb{R}^2\to\mathbb{R}$ for $k=\overline{1,2}$. Here $\tilde{\psi}(x,\lambda;\tau):=\tilde{\alpha}(\tilde{w}(x;\tau)-\lambda)$ for all $(x,\lambda;\tau)\in\mathbb{R}^{n+1}\times\mathbb{R}$ and some smooth mapping $\tilde{\alpha}:\mathbb{R}\to\mathbb{R}$. From this one easily obtains - as above - a linearized covering jet-submanifold $J^1_{lin}(\mathbb{R}^{n+1}\times\mathbb{R}^2;\mathbb{R})|_{\mathscr{E}}\subset J^1(\mathbb{R}^{n+1}\times\mathbb{R}^2;\mathbb{R})$, as a compatible system of the vector field equations (3.26), generated by the nonlinear first order differential system $J^1(\mathbb{R}^n\times\mathbb{R}^2;\mathbb{R})|_{\mathscr{E}}\subset J^1(\mathbb{R}^n\times\mathbb{R}^2;\mathbb{R})$ on the space $\mathbb{R}^n\times\mathbb{R}^2$. This determines the inverse implication (3.19) as applied to general compatible first order equations (3.22), providing for the nonlinear first order system $J^1(\mathbb{R}^n\times\mathbb{R}^2;\mathbb{R})|_{\mathscr{E}}\subset J^1(\mathbb{R}^n\times\mathbb{R}^2;\mathbb{R})$ its corresponding Lax–Sato representation.

Remark 3.5. *The existence of the map (3.23) can be deduced from the following reasoning. Assume that the mapping (3.23) exists and is equivalent to*

$$w(x;\tau) := \rho(x,\tilde{w}(x;\tau);\tau) \tag{3.27}$$

for some smooth function $\rho:\mathbb{R}^{n+1}\times\mathbb{R}^2\to\mathbb{R}$ *and all* $(x;\tau)\in\mathbb{R}^n\times\mathbb{R}^2$, *where the corresponding map* $\tilde{w}:\mathbb{R}^n\times\mathbb{R}^2\to\mathbb{R}$ *satisfies the following system of differential equations:*

$$\frac{\partial\tilde{w}}{\partial\tau_k}+\sum_{j=\overline{1,n}}a_j^{(k)}(x,\rho(x,\tilde{w};\tau);\tau)\frac{\partial\tilde{w}}{\partial x_j}=\tilde{b}^{(k)}(x,\tilde{w};\tau), \tag{3.28}$$

compatible for all $\tau_k\in\mathbb{R}$, $k=\overline{1,2}$, *and* $x\in\mathbb{R}^n$. *Here functions* $\tilde{b}^{(k)}:\mathbb{R}^{n+1}\times\mathbb{R}^2\to\mathbb{R}$, $k=\overline{1,2}$, *defined as*

$$\tilde{b}^{(k)}(x,\tilde{w};\tau):=\left[b^{(k)}-\sum_{j=\overline{1,n}}\left(\frac{\partial\rho}{\partial\tau_k}+a_j^{(k)}\frac{\partial\rho}{\partial x_j}\right)\right]\left(\frac{\partial\rho}{\partial x_j}\right)^{-1}\Bigg|_{w=\rho(x,\tilde{w};\tau)}, \tag{3.29}$$

should depend on the mapping (3.27) in such a way that the vector fields

$$\frac{\partial x_j}{\partial\tau_k}=a_j^{(k)}(x,\rho(x,\tilde{w};\tau);\tau):=\tilde{a}_j^{(k)}(x,\tilde{w};\tau) \tag{3.30}$$

are also compatible for all $j=\overline{1,n}$ *and* $k=\overline{1,2}$ *modulo the flows (3.28). This means that the equation (3.28) can be equivalently represented as a compatible system of the following vector field equations*

$$\frac{\partial\tilde{\psi}}{\partial\tau_k}+\sum_{j=\overline{1,n}}\tilde{a}_j^{(k)}(x,\lambda;\tau)\frac{\partial\tilde{\psi}}{\partial x_j}+\tilde{b}^{(k)}(x,\rho(x,\lambda;\tau);\tau)\frac{\partial\tilde{\psi}}{\partial\lambda}=0 \tag{3.31}$$

on its first integral $\tilde{\psi}:\mathbb{R}^{n+1}\times\mathbb{R}^2\to\mathbb{R}$, *where* $\tilde{\psi}(x,\lambda;\tau)=\alpha(\tilde{w}(x;\tau)-\lambda)$ *for an arbitrarily chosen smooth mapping* $\alpha:\mathbb{R}\to\mathbb{R}$, *any parameter* $\lambda\in\mathbb{R}$ *and all* $(x;\tau)\in\mathbb{R}^n\times\mathbb{R}^2$. *The system (3.31) provides a suitable Lax–Sato type linearization of the compatible quasi-linear first order differential equations (3.17). Concerning the map (3.27) and its dependents on it functions* $\tilde{b}^{(k)}:\mathbb{R}^{n+1}\times\mathbb{R}^2\to\mathbb{R}$, $k=\overline{1,2}$, *one can easily observe that the compatibility condition for the vector fields (3.30) reduces to the a priori compatible equations*

$$\begin{gathered}\frac{\partial a_j^{(k)}}{\partial\rho}\frac{\partial\rho}{\partial\tau_s}-\frac{\partial a_j^{(s)}}{\partial\rho}\frac{\partial\rho}{\partial\tau_k}+\left(\frac{\partial a_j^{(k)}}{\partial\rho}\tilde{b}^{(s)}-\frac{\partial a_j^{(s)}}{\partial\rho}\tilde{b}^{(k)}\right)\frac{\partial\rho}{\partial\tilde{w}}+\\+\sum_{m=\overline{1,n}}\left(\frac{\partial a_j^{(k)}}{\partial\rho}a_m^{(s)}-\frac{\partial a_j^{(s)}}{\partial\rho}a_m^{(k)}\right)\frac{\partial\rho}{\partial x_m}=0,\end{gathered} \tag{3.32}$$

where $j=\overline{1,n}$ *and* $k\neq s=\overline{1,2}$, *and whose solution is exactly the desired map (3.27). Inasmuch as we have only two functional parameters* $b^{(s)}:\mathbb{R}^{n+1}\times\mathbb{R}^2\to\mathbb{R}$, $s=\overline{1,2}$, *the system of* $2n$ *differential relationships (3.32) can be, in general, compatible only for the case* $n=1$. *For all other cases* $n\geq2$ *the compatibility condition for (3.32) must be checked separately by calculations.*

3.3. Example: the Gibbons–Tsarev equation

As a first degenerate case of the scheme (3.19) above, we consider a compatible nonlinear first order system $J^1(\mathbb{R}^2;\mathbb{R})|_{\mathscr{E}}\subset J^1(\mathbb{R}^2;\mathbb{R})$ at $n=0$, as discussed in [34]:

$$\frac{\partial w}{\partial t}-\frac{1}{z_y+z_tw-w^2}=0,\ \frac{\partial w}{\partial y}+\frac{z_t-w}{u_y+z_tw-w^2}=0, \tag{3.33}$$

first derived in [27], where $(t,y;w)\in\mathbb{R}^2\times\mathbb{R}$ and a map $u:\mathbb{R}^2\to\mathbb{R}$ satisfies the Gibbon–Tsarev equation $\mathscr{E}[y,t;u]=0$ in the form

$$z_{yy}+z_tz_{ty}-z_yz_{tt}+1=0. \tag{3.34}$$

Since the nonlinear system (3.33) is compatible and the adjacent system of vector field flows (3.25) it follows that any solution $w:\mathbb{R}^2\to\mathbb{R}$ to (3.33) generates a first integral $\psi:\mathbb{R}\times\mathbb{R}^2\to\mathbb{R}$ of a system of equations

$$\frac{\partial\psi}{\partial t}+\frac{1}{z_y+z_t\lambda-\lambda^2}\frac{\partial\psi}{\partial\lambda}=0,\ \frac{\partial\psi}{\partial y}-\frac{z_t-\lambda}{z_y+z_t\lambda-\lambda^2}\frac{\partial\psi}{\partial\lambda}=0, \tag{3.35}$$

where $\psi(\lambda;y,t):=\alpha(w(t,y)-\lambda)$ for all $(\lambda;t,y)\in\mathbb{R}\times\mathbb{R}^2$ and some smooth map $\alpha:\mathbb{R}\to\mathbb{R}$. The compatible system (3.35) considered as the jet-submanifold $J^1_{lin}(\mathbb{R}^1\times\mathbb{R}^2;\mathbb{R})|_{\mathscr{E}}\subset J^1(\mathbb{R}^1\times\mathbb{R}^2;\mathbb{R})$ solves the problem of constructing the linearizing implication (3.19).
As was demonstrated in [28, 40], the substitution

$$u:=\frac{1}{2}(-z_t+\sqrt{z_t^2+4z_y}),\ \ v:=\frac{1}{2}(-z_t-\sqrt{z_t^2+4z_y}) \tag{3.36}$$

gives rise to the equivalent dynamical system

$$u_y=vu_t-(u-v)^{-1},\ \ v_y=uv_t+(u-v)^{-1} \tag{3.37}$$

on a functional space $M \subset C^{\infty}(\mathbb{R};\mathbb{R}^2)$ subject to the evolution parameter $y \in \mathbb{R}$ modulo evolution with respect to the joint evolution parameter $t \in \mathbb{R}$. Taking into account the Lax–Sato representation (3.35), one readily obtains the corresponding linearizing Lax–Sato representation for the dynamical system (3.37):

$$\frac{\partial \psi}{\partial t} - \frac{1}{(\lambda+u)(\lambda+v)}\frac{\partial \psi}{\partial \lambda} = 0, \frac{\partial \psi}{\partial y} - \frac{u+v+\lambda}{(\lambda+u)(\lambda+v)}\frac{\partial \psi}{\partial \lambda} = 0. \tag{3.38}$$

The above Lax–Sato representation can be now reanalyzed more deeply within the Lie-algebraic scheme devised recently in [31]. Namely, we define the complex torus diffeomorphism Lie group $\tilde{G} := Diff(\mathbb{T}^1_{\mathbb{C}})$, holomorphically extended in the interior $\mathbb{S}^1_+ \subset \mathbb{C}$ and in the exterior $\mathbb{S}^1_- \subset \mathbb{C}$ regions of the unit circle $\mathbb{S}^1 \subset \mathbb{C}^1$, such that for any $g(\lambda) \in \tilde{G}|_{\mathbb{S}^1_-}$, $\lambda \in \mathbb{S}^1_-$, $g(\infty) = 1 \in Diff(\mathbb{T}^1)$, and study its specially chosen coadjoint orbits, related to the compatible system of linear vector field equations (3.38).
As a first step for solving this problem one needs to consider the corresponding Lie algebra $\tilde{\mathscr{G}} := diff(\mathbb{T}^1_{\mathbb{C}})$ and its decomposition into the direct sum

$$\tilde{\mathscr{G}} = \tilde{\mathscr{G}}_+ \oplus \tilde{\mathscr{G}}_- \tag{3.39}$$

of Laurent series with positive as $|\lambda| \to 0$ and strongly negative as $\lambda| \to \infty$ degrees, respectively. Then, it follows from Adler–Kostant–Symes theory, that for any element $\tilde{l} \in \tilde{\mathscr{G}}^* \simeq \Lambda^1(\mathbb{T}^1_{\mathbb{C}})$ the following formally constructed flows

$$d\tilde{l}/dy = -ad^*_{\nabla h^{(y)}(\tilde{l})}\tilde{l}, \quad d\tilde{l}/dt = -ad^*_{\nabla h^{(t)}(\tilde{l})}\tilde{l} \tag{3.40}$$

along the evolution parameters $y,t \in \mathbb{R}^2$ are always compatible, if $h^{(p_y)}$ and $h^{(p_t)} \in I(\tilde{\mathscr{G}}^*)$ are arbitrarily chosen functionally independent Casimir functionals on the adjoint space $\tilde{\mathscr{G}}^*$ and $\nabla h^{(y)}(\tilde{l}) := \nabla h^{(p_y)}(\tilde{l})_-$, $\nabla h^{(t)}(\tilde{l}) := \nabla h^{(p_t)}(\tilde{l})_-$ are their gradients, suitably projected on the subalgebra $\tilde{\mathscr{G}}_-$. Keeping in mind this result, consider the Casimir functional $h^{(p_y)}$ on $\tilde{\mathscr{G}}^*$, whose gradient $\nabla h^{(p_y)}(\tilde{l}) := \nabla h^{(p_y)}(l)\partial/\partial\lambda \in \tilde{\mathscr{G}}$ as $|\lambda| \to \infty$ is taken, for simplicity, in the asymptotic form

$$\nabla h^{(p_y)}(\tilde{l}) \sim \left(\frac{\lambda+u+v}{(\lambda+u)(\lambda+v)} + \alpha_0 + \alpha_1\lambda\right)\frac{\partial}{\partial \lambda}, \tag{3.41}$$

where $\lambda \in \mathbb{T}^1_{\mathbb{C}}$, $|\lambda| \to \infty$, and the coefficients $\alpha_j \in C^{\infty}(\mathbb{R}^2;\mathbb{R})$, $j = \overline{0,1}$, are arbitrarily chosen nontrivial functional parameters, giving rise to the gradient projection

$$\nabla h^{(y)}(\tilde{l}) := \nabla h^{(p_y)}(\tilde{l})|_- = \frac{\lambda+u+v}{(\lambda+u)(\lambda+v)}, \tag{3.42}$$

generating the first flow of (3.40). As the differential 1-form $\tilde{l} = l(\lambda;y,t)d\lambda \in \Lambda^1(\mathbb{T}^1_{\mathbb{C}}) \simeq \tilde{\mathscr{G}}$ satisfies, by definition, the condition

$$ad^*_{\nabla h^{(p_y)}(\tilde{l})}\tilde{l} = 0, \tag{3.43}$$

equivalent to the differential equation

$$\frac{d}{d\lambda}[l(\lambda;y,t)(\nabla h^{(p_y)}(l))^2] = 0, \tag{3.44}$$

one readily obtains from (3.42) and (3.44) the coefficient

$$l(\lambda;y,t) = (\nabla h^{(p_y)}(l))^{-2} = \frac{(\lambda+u)^2(\lambda+v)^2}{[\lambda+u+v+(\alpha_0+\alpha_1\lambda)(\lambda+u)(\lambda+v)]^2}, \tag{3.45}$$

satisfying the relationship $l(\lambda;y,t)(\nabla h^{(p_y)}(l))^2 = 1$ for all $(t,y) \in \mathbb{R}^2$.
Now we prove the following useful observation.

Lemma 3.6. *The set* $\mathrm{I}(\tilde{\mathscr{G}}^*)$ *of functionally independent Casimir invariants is one-dimensional.*

Proof. Any asymptotic solution to the determining equation (3.47) satisfies the symmetry invariance with respect to the multiplication $\nabla h^{(p_t)}(\tilde{l}) \to \sigma(t,y)\nabla h^{(p_t)}(\tilde{l})$ by an arbitrary smooth function $\sigma : \mathbb{R}^2 \to \mathbb{R}$, which proves the lemma. □

Consider now the gradient $\nabla h^{(p_t)}(\tilde{l}) \in \tilde{\mathscr{G}}$ of the Casimir functional $h^{(p_t)} \in \mathrm{D}(\tilde{\mathscr{G}}^*)$, which satisfies, as does (3.43), the condition

$$ad^*_{\nabla h^{(p_t)}(\tilde{l})}\tilde{l} = 0, \tag{3.46}$$

which is equivalent to the following linear differential equation

$$2l(\lambda;y,t)\frac{\partial}{\partial\lambda}\nabla h^{(p_t)}(\tilde{l}) + \nabla h^{(p_t)}(\tilde{l})\frac{\partial}{\partial\lambda}l(\lambda;y,t) = 0. \tag{3.47}$$

Its solution can be naturally represented as the asymptotic series

$$\nabla h^{(p_t)}(\tilde{l}) \sim \frac{1}{(\lambda+u)(\lambda+v)} + \sum_{j\in\mathbb{Z}_+}\beta_j\lambda^j \tag{3.48}$$

for some nontrivial coefficients $\beta_j \in C^{\infty}(\mathbb{R}^2;\mathbb{R})$, successively determined from the equation (3.47).
From Lemma 3.6, we see that the solution (3.48) to the determining equation (3.47) is unique owing to its natural symmetry invariance with respect to the multiplication $\nabla h^{(p_t)}(\tilde{l}) \to \sigma(t,y)\nabla h^{(p_t)}(\tilde{l})$ by an arbitrary smooth function $\sigma : \mathbb{R}^2 \to \mathbb{R}$. In particular, this means that

asymptotically as $\lambda \to \infty$ the product $l(\lambda;y,t)(\nabla h^{(p_t)}(l))^2 \sim 0$, for otherwise if $l(\lambda;y,t)(\nabla h^{(p_t)}(l))^2 \nrightarrow 0$, this product becomes, owing to (3.44), a nonzero constant subject to the parameter $\lambda \in \mathbb{C}$. This means that $\nabla h^{(p_t)}(l) = \nabla h^{(p_y)}(\tilde{l})\sigma(t,y)$ for any smooth arbitrary function $\sigma \in C^\infty(\mathbb{R}^2;\mathbb{R})$, producing no new flow with respect to the evolution parameter $t \in \mathbb{R}$.
Consider now the gradient projection

$$\nabla h^{(t)}(\tilde{l}) := \nabla h^{(p_t)}(\tilde{l})|_- = \frac{1}{(\lambda+u)(\lambda+v)}, \tag{3.49}$$

generating the second flow of (3.40). As a consequence of the results above we can easily derive the following compatibility condition for the flows (3.40):

$$[\frac{\partial}{\partial y} - \nabla h^{(y)}(\tilde{l}), \frac{\partial}{\partial y} - \nabla h^{(ty)}(\tilde{l})] = 0, \tag{3.50}$$

which is equivalent modulo the dynamical system (3.37) to the following system of two *a priori* compatible linear vector field equations:

$$\frac{\partial \psi}{\partial y} - \frac{\lambda+u+v}{(\lambda+u)(\lambda+v)}\frac{\partial \psi}{\partial \lambda} = 0, \quad \frac{\partial \psi}{\partial t} - \frac{1}{(\lambda+u)(\lambda+v)}\frac{\partial \psi}{\partial \lambda} = 0 \tag{3.51}$$

for $\psi \in C^2(\mathbb{R};\mathbb{R})$ and all $(\lambda;t,y) \in \mathbb{C}\times\mathbb{R}^2$. Thus, we can formulate the results, obtained above, as the following proposition.

Proposition 3.7. *A system $J^1_{lin}(\mathbb{R}\times\mathbb{R}^2;\mathbb{R})|_{\mathscr{E}}$ of the linear first order equations (3.51) on the covering jet-manifold $J^1(\mathbb{R}\times\mathbb{R}^2;\mathbb{R})$ is compatible; that is, it holds for any its smooth solution $\psi : \mathbb{R}\times\mathbb{R}^2 \to \mathbb{R}$ at all points $(\lambda;y,t) \in \mathbb{R}\times\mathbb{R}^2$ iff the function $u : \mathbb{R}^2 \to \mathbb{R}$ satisfies the Gibbons–Tsarev equation (3.34).*

Moreover, taking into account that the flows (3.40) are Hamiltonian systems on the coadjoint space $\tilde{\mathscr{G}}^*$, their reductions on the space of functional variables $(u,v) \in C^\infty(\mathbb{R}^2;\mathbb{R}^2)$ are also Hamiltonian. This reduction scheme is now under study and shall be presented elsewhere.

3.4. Example: the ABC-equation

As the second example we consider a compatible system $J^1(\mathbb{R}\times\mathbb{R}^2;\mathbb{R})|_{\mathscr{E}}$ of the nonlinear first order differential equations (3.6) on the jet-manifold $J^1(\mathbb{R}\times\mathbb{R}^2;\mathbb{R})$. It is easy to check that the adjacent system of vector field flows

$$\frac{\partial x}{\partial t} = \frac{u_t w}{u_x k_1(k_1+k_2-1)}, \quad \frac{\partial x}{\partial y} = \frac{u_y w}{u_x k_1(w+k_1+k_2-1)}, \tag{3.52}$$

modulo the relationships (3.6), is not compatible for all $(w;t,y) \in \mathbb{R}\times\mathbb{R}^2$. Thus, we need to construct a map (3.23) such that the resulting system (3.24) will possess an adjacent system of vector field flows already compatible for all $(\tilde{w};t,y) \in \mathbb{R}\times\mathbb{R}^2$. To do this let us get rid of to begin with the strictly linear part of the equations (3.6), giving rise to the representation of its solution as $w(x;t,y) = (u_x(x;t,y))^\alpha \tilde{w}(x;t,y)$ for $\alpha = (k_1+k_2-1)/k_1$ and all $(x;t,y) \in \mathbb{R}\times\mathbb{R}^2$. Its corresponding substitution into (3.6) yields the following *a priori* compatible system $J^1(\mathbb{R}\times\mathbb{R}^2;\mathbb{R})|_{\mathscr{E}}$ of the first order equations

$$\begin{aligned} &\frac{\partial \tilde{w}}{\partial t} + \frac{\tilde{w}u_x^{\alpha-1}u_t}{k_1\alpha}\frac{\partial \tilde{w}}{\partial x} + \frac{\tilde{w}^2 u_x^\alpha(u_t u_{xx} - k_1 u_{xx}u_{xt})}{k_1^2} = 0, \\ &\frac{\partial \tilde{w}}{\partial y} + \frac{k_2\tilde{w}u_x^{\alpha-1}u_y}{k_1(\tilde{w}u_x^\alpha+\alpha)}\frac{\partial \tilde{w}}{\partial x} + \frac{k_2\alpha\tilde{w}^2u_x^\alpha u_y u_{xx}}{k_1^2(\tilde{w}u_x^\alpha+\alpha)} = 0 \end{aligned} \tag{3.53}$$

on the jet-manifold $J^1(\mathbb{R}\times\mathbb{R}^2;\mathbb{R})$. We can now easily check that the above expression $\tilde{w}(x;t,y) = (u_x(x;t,y))^{-\alpha}w(x;t,y)$ for all $(x;t,y) \in \mathbb{R}\times\mathbb{R}^2$, determining the map (3.23), is exactly the one searched for, inasmuch the corresponding adjacent system of vector field flows

$$\frac{\partial x}{\partial t} = \frac{\tilde{w}u_x^{\alpha-1}u_t}{k_1\alpha}, \quad \frac{\partial x}{\partial y} = \frac{k_2\tilde{w}u_x^{\alpha-1}u_y}{k_1(\tilde{w}u_x^\alpha+\alpha)} \tag{3.54}$$

on $\mathbb{R}\times\mathbb{R}^2$ proves to be compatible modulo the system $J^1(\mathbb{R}\times\mathbb{R}^2;\mathbb{R})|_{\mathscr{E}}$ of *a priori* compatible differential relationships (3.53) on $J^1(\mathbb{R}\times\mathbb{R}^2;\mathbb{R})$. Based on this compatibility result, one can easily construct the corresponding linearizing system $J^1_{lin}(\mathbb{R}^2\times\mathbb{R}^2;\mathbb{R})|_{\mathscr{E}}$ on the covering jet-manifold $J^1(\mathbb{R}^2\times\mathbb{R}^2;\mathbb{R})$, realizing the inverse implication (3.19) as the Lax–Sato representation

$$\begin{aligned} &\frac{\partial \psi}{\partial t} + \frac{\lambda u_x^{\alpha-1}u_t}{k_1\alpha}\frac{\partial \psi}{\partial x} - \frac{\lambda^2 u_x^\alpha(u_t u_{xx} - k_1 u_{xx}u_{xt})}{k_1^2}\frac{\partial \psi}{\partial \lambda} = 0, \\ &\frac{\partial \psi}{\partial y} + \frac{k_2\lambda u_x^{\alpha-1}u_y}{k_1(\lambda u_x^\alpha+\alpha)}\frac{\partial \psi}{\partial x} - \frac{\lambda^2 k_2\alpha u_x^{\alpha-1}u_y u_{xx}}{k_1^2(\lambda u_x^\alpha+\alpha)}\frac{\partial \psi}{\partial \lambda} = 0, \end{aligned} \tag{3.55}$$

exactly coinciding with (3.7), where $\psi(x,\lambda;t,y) := \alpha(\tilde{w}(x;t,y)-\lambda)$ for all $(x,\lambda;t,y) \in \mathbb{R}^2\times\mathbb{R}^2$ and any smooth mapping $\alpha : \mathbb{R}\to\mathbb{R}$. Thus, the linear differential system (3.55) solves the above problem of constructing the inverse implication (3.19) for the compatible nonlinear differential system $J^1(\mathbb{R}\times\mathbb{R}^2;\mathbb{R})|_{\mathscr{E}}$ (3.6), thereby proving Proposition 3.4.

3.5. Example: the Manakov-Santini equations

The Manakov–Santini equations

$$u_{tx}+u_{yy}+(uu_x)_x+v_xu_{xy}-v_yu_{xx} \quad =0, \tag{3.56}$$

$$v_{xt}+v_{yy}+uv_{xx}+v_xv_{xy}-v_yv_{xx} \quad =0,$$

where $(u,v)\in C^{\infty}(\mathbb{R}\times\mathbb{R}^2;\mathbb{R}^2)$, as well known [39], are obtained as some generalization of the dispersionless reduction for the Kadomtsev-Petviashvili equation. It possesses the following compatible nonlinear first order differential covering $J^1(\mathbb{R}\times\mathbb{R}^2;\mathbb{R})|_{\mathscr{E}}\subset J^1(\mathbb{R}\times\mathbb{R}^2;\mathbb{R})$ as

$$\begin{gathered}\frac{\partial w}{\partial t}+(w^2-wv_x+u-v_y)\frac{\partial w}{\partial x}+(w-v_x)(u_x-wv_{xx})-u_y+v_{yy}+v_xv_{xy}=0,\\ \frac{\partial w}{\partial y}+w\frac{\partial w}{\partial x}-v_{xx}w+(u-v_y)_x=0,\end{gathered} \tag{3.57}$$

giving rise for all $(x;t,y)\in\mathbb{R}\times\mathbb{R}^2$ to the Manakov–Santini differential relationship $\mathscr{E}[x;y,t;u,v]=0$ (3.56) as a submanifold on the adjacent jet-manifold $J^2(\mathbb{R}\times\mathbb{R}^2;\mathbb{R}^2)$. It is now easy to check that the naturally related to (3.57) system of vector field flows

$$\frac{\partial x}{\partial t}=w^2-wv_x+u-v_y,\quad \frac{\partial x}{\partial y}=w \tag{3.58}$$

is for all $(t,y)\in\mathbb{R}^2$ not compatible modulo these differential relationships (3.57). Thus, one needs to construct such an isomorphic transformation

$$J^1(\mathbb{R}^2\times\mathbb{R}^2;\mathbb{R})\ni(x,w;t,y)\to(x,\tilde{w};t,y)\in J^1(\mathbb{R}^2\times\mathbb{R}^2;\mathbb{R}) \tag{3.59}$$

that the expression $w(x;y,t)=\beta(x,\tilde{w};y,t)$ for some, in general nonlinear, smooth mapping $\beta:\mathbb{R}^2\times\mathbb{R}^2\to\mathbb{R}$ transforms the first order differential covering (3.57) into an equivalent compatible first order differential covering (3.24), for which the corresponding vector field flows (3.25) become also compatible. This problem is easily enough solved, giving rise to the simple mapping:

$$w=\tilde{w}+v_x \tag{3.60}$$

from which one ensues the following compatible first order differential covering:

$$\begin{gathered}\frac{\partial\tilde{w}}{\partial t}+(\tilde{w}^2+\tilde{w}v_x+u-v_y)\frac{\partial\tilde{w}}{\partial x}-u_y+\tilde{w}u_x=0,\\ \frac{\partial\tilde{w}}{\partial y}+(v_x+\tilde{w})\frac{\partial\tilde{w}}{\partial x}+u_x=0.\end{gathered} \tag{3.61}$$

It is easy to check that the naturally related to (3.61) system of vector field flows

$$\frac{\partial x}{\partial t}=\tilde{w}^2+\tilde{w}v_x+u-v_y,\quad \frac{\partial x}{\partial y}=v_x+\tilde{w} \tag{3.62}$$

is already compatible for all $(t,y)\in\mathbb{R}^2$ modulo these differential relationships (3.61). Based on this compatibility result, stated above, one can easily construct the corresponding linearizing first order differential system $J^1_{lin}(\mathbb{R}^2\times\mathbb{R}^2;\mathbb{R})|_{\mathscr{E}}$ on the covering jet-manifold $J^1(\mathbb{R}^2\times\mathbb{R}^2;\mathbb{R})$, realizing the inverse implication (3.19) as the Lax-Sato representation

$$\begin{gathered}\frac{\partial\psi}{\partial t}+(\lambda^2+\lambda v_x+u-v_y)\frac{\partial\psi}{\partial x}+(u_y-\lambda u_x)\frac{\partial\psi}{\partial\lambda}=0,\\ \frac{\partial\psi}{\partial y}+(v_x+\lambda)\frac{\partial\psi}{\partial x}-u_x\frac{\partial\psi}{\partial\lambda}=0,\end{gathered} \tag{3.63}$$

thus proving proposition 3.3.

3.6. The contact geometry linearization covering scheme

3.7. Short setting

We consider two Hamilton–Jacobi type compatible for all $(x;\tau):=(x;t,y)\in\mathbb{R}\times\mathbb{R}^2$ first order differential relationships:

$$\frac{\partial z}{\partial t}+\tilde{H}^{(t)}(x,z,\partial z/\partial x;t,y)=0,\ \frac{\partial z}{\partial y}+\tilde{H}^{(y)}(x,z,\partial z/\partial x;t,y)=0, \tag{3.64}$$

where $z:\mathbb{R}^3\to\mathbb{R}$ is a so called "*action function*" and $\tilde{H}^{(t)},\tilde{H}^{(y)}:\mathbb{R}^3\times\mathbb{R}^2\to\mathbb{R}$ are smooth generalized Hamiltonian functions. The relationships 3.64 follow from the contact geometry [12, 19] interpretation of some mechanical systems, generated by vector fields. Namely, a differential one-form $\alpha^{(1)}\in\Lambda^1(\mathbb{R}^3\times\mathbb{R})$, defined by the expression

$$\alpha^{(1)}:=dz-\lambda dx, \tag{3.65}$$

is called *contact* and vector fields $X_{H^{(t)}}, X_{H^{(y)}} \in \Gamma(T(\mathbb{R}^3\times\mathbb{R}))$ are called *contact vector fields*, if there exist functions $\mu^{(t)}, \mu^{(y)}:\mathbb{R}^3\times\mathbb{R}\to\mathbb{R}$, such that for all $(x,z;\tau)\in\mathbb{R}^2\times\mathbb{R}^2$ the following equalities

$$
\begin{aligned}
-i_{X_{H^{(t)}}}\alpha^{(1)} &= H^{(t)} := \tilde{H}^{(t)}|_{\partial z/\partial x=\lambda}, \quad -i_{X_{H^{(y)}}}\alpha^{(1)} = H^{(y)} := \tilde{H}^{(y)}|_{\partial z/\partial x=\lambda}, \\
\mathscr{L}_{H^{(t)}}\alpha^{(t)} &= \mu^{(t)}\alpha^{(t)}, \qquad \mathscr{L}_{H^{(y)}}\alpha^{(y)} = \mu^{(y)}\alpha^{(y)}
\end{aligned}
\tag{3.66}
$$

hold, where $\mathscr{L}_{H^{(t)}}, \mathscr{L}_{H^{(y)}}$ are the corresponding Lie derivatives [17, 29, 19] with respect to the vector fields $X_{H^{(t)}}, X_{H^{(y)}} \in \Gamma(T(\mathbb{R}^3\times\mathbb{R}))$. From the conditions (3.66) one finds [32, 58] easily that

$$
\begin{aligned}
X_{H^{(t)}} &= \frac{\partial H^{(t)}}{\partial\lambda}\frac{\partial}{\partial x} - \left(\frac{\partial H^{(t)}}{\partial x} + \lambda\frac{\partial H^{(t)}}{\partial z}\right)\frac{\partial}{\partial\lambda} + \left(-H^{(t)} + \lambda\frac{\partial H^{(t)}}{\partial\lambda}\right)\frac{\partial}{\partial z}, \\
X_{H^{(y)}} &= \frac{\partial H^{(y)}}{\partial\lambda}\frac{\partial}{\partial x} - \left(\frac{\partial H^{(y)}}{\partial x} + \lambda\frac{\partial H^{(y)}}{\partial z}\right)\frac{\partial}{\partial\lambda} + \left(-H^{(y)} + \lambda\frac{\partial H^{(y)}}{\partial\lambda}\right)\frac{\partial}{\partial z},
\end{aligned}
\tag{3.67}
$$

where $H^{(t)} := \tilde{H}^{(t)}|_{\partial z/\partial x=\lambda}, H^{(y)} := \tilde{H}^{(y)}|_{\partial z/\partial x=\lambda}$, and the compatibility of the nonlinear relationships (3.64) is equivalent to the commutativity of the following vector fields:

$$
\left[\frac{\partial}{\partial t} + X_{H^{(t)}}, \frac{\partial}{\partial y} + X_{H^{(y)}}\right] = 0 \tag{3.68}
$$

for all $(x,z,\lambda;\tau)\in\mathbb{R}^3\times\mathbb{R}^2$, depending parametrically on $\lambda\in\mathbb{R}$. The latter can be rewritten as a compatible Lax–Sato representation for the vector field equations

$$
\frac{\partial\psi}{\partial t} + X_{H^{(t)}}\psi = 0, \quad \frac{\partial\psi}{\partial y} + X_{H^{(y)}}\psi = 0 \tag{3.69}
$$

for smooth invariant functions $\psi\in C^2(\mathbb{R}^3\times\mathbb{R}^2;\mathbb{R})$ and all $(x,z,\lambda;\tau)\in\mathbb{R}^3\times\mathbb{R}^2$.

Remark 3.8. *It is worth mentioning that when the Hamiltonian functions in (3.64) do not depend on the "action function" $z:\mathbb{R}^3\to\mathbb{R}$, the contact vector fields naturally reduce to the classical Hamiltonian ones:*

$$
X_{H^{(t)}} = \frac{\partial H^{(t)}}{\partial\lambda}\frac{\partial}{\partial x} - \frac{\partial H^{(t)}}{\partial x}\frac{\partial}{\partial\lambda}, \quad X_{H^{(y)}} = \frac{\partial H^{(y)}}{\partial\lambda}\frac{\partial}{\partial x} - \frac{\partial H^{(y)}}{\partial x}\frac{\partial}{\partial\lambda}, \tag{3.70}
$$

well known [19] from symplectic geometry.

3.8. Example: the differential Toda singular manifold equation

Some examples of applying this contact geometry linearization scheme to integrable $3D$-dispersionless equations were recently presented by A. Sergyeyev [71]. We shall apply this scheme to a degenerate case when the system (3.64) is given by the following linear equations

$$
\frac{\partial z}{\partial t} + \frac{(e^{-2u_t}-1)}{2u_x}\frac{\partial z}{\partial x} = 0, \quad \frac{\partial z}{\partial y} - u_y u_x^{-1} e^{-2u_t}\frac{\partial z}{\partial x} = 0 \tag{3.71}
$$

for a smooth map $z:\mathbb{R}\times\mathbb{R}^2\to\mathbb{R}$, whose compatibility condition is the interesting [16] differential Toda singular manifold equation (3.12) on a smooth function $u:\mathbb{R}\times\mathbb{R}^2\to\mathbb{R}$ for all $(x;y,t)\in\mathbb{R}\times\mathbb{R}^2$, which defines a differential relationship $J^2(\mathbb{R}^2\times\mathbb{R}^2;\mathbb{R})|_{\mathscr{E}} \subset J^2(\mathbb{R}^2\times\mathbb{R}^2;\mathbb{R})$ on the jet-manifold $J^2(\mathbb{R}^2\times\mathbb{R}^2;\mathbb{R})$

$$
u_{xy} sh^2 u_t = u_x u_y u_{tt}\ . \tag{3.72}
$$

Even though the equations (3.71) are linear, they contain no "spectral" parameter $\lambda\in\mathbb{R}$ subject to which one can construct the related conservation laws for (3.17) and apply the modified inverse scattering transform to construct exact special solutions.
Nevertheless, the above contact geometry linearization scheme makes it possible present the system as a set of compatible Hamilton–Jacobi equations

$$
\frac{\partial z}{\partial t} + \frac{(e^{-2u_t}-1)}{2u_x}\lambda = 0, \quad \frac{\partial z}{\partial y} - \frac{u_y e^{-2u_t}}{u_x}\lambda = 0 \tag{3.73}
$$

with the contact Hamiltonians

$$
H^{(t)} := \frac{(e^{-2u_t}-1)}{2u_x}\lambda, \quad H^{(y)} := -\frac{u_y e^{-2u_t}}{u_x}\lambda, \tag{3.74}
$$

where the function $u:\mathbb{R}^2\times\mathbb{R}^2\to\mathbb{R}$ depends here on the additional variable $z\in\mathbb{R}$. Taking into account (3.67), one can construct the corresponding extended contact vector fields

$$
\begin{aligned}
\tilde{X}_{H^{(t)}} &:= \frac{\partial}{\partial t} + X_{H^{(t)}} = \frac{\partial}{\partial t} + \frac{(e^{-2u_t}-1)}{2u_x}\frac{\partial}{\partial x} - \left[\lambda\left(\frac{e^{-2u_t}-1}{2u_x}\right)_x + \lambda^2\left(\frac{e^{-2u_t}-1}{2u_x}\right)_z\right]\frac{\partial}{\partial\lambda}, \\
\tilde{X}_{H^{(y)}} &:= \frac{\partial}{\partial y} + X_{H^{(y)}} = \frac{\partial}{\partial y} - \frac{u_y e^{-2u_t}}{u_x}\frac{\partial}{\partial x} + \left[\lambda\left(\frac{u_y e^{-2u_t}}{u_x}\right)_x + \lambda^2\left(\frac{u_y e^{-2u_t}}{u_x}\right)_z\right]\frac{\partial}{\partial\lambda}\ ,
\end{aligned}
\tag{3.75}
$$

compatible on the solution set to the equation (3.72) on $J^2(\mathbb{R}^2\times\mathbb{R}^2;\mathbb{R})$. This makes it possible to verify our final proposition on the contact geometry linearization covering of the system (3.72).

Proposition 3.9. *The linear first order differential equation (3.71) on $J^2(\mathbb{R}^2\times\mathbb{R}^2;\mathbb{R})$ allows the following, dual quadratic in the parameter $\lambda\in\mathbb{R}$, Lax–Sato linearization covering*

$$\frac{\partial\psi}{\partial t}+\frac{(e^{-2u_t}-1)}{2u_x}\frac{\partial\psi}{\partial x}-\left[\lambda\left(\frac{e^{-2u_t}-1}{2u_x}\right)_x+\lambda^2\left(\frac{e^{-2u_t}-1}{2u_x}\right)_z\right]\frac{\partial\psi}{\partial\lambda}=0, \tag{3.76}$$
$$\frac{\partial\psi}{\partial y}-\frac{u_ye^{-2u_t}}{u_x}\frac{\partial\psi}{\partial x}+\left[\lambda\left(\frac{u_ye^{-2u_t}}{u_x}\right)_x+\lambda^2\left(\frac{u_ye^{-2u_t}}{u_x}\right)_z\right]\frac{\partial\psi}{\partial\lambda}=0$$

for smooth invariant functions $\psi\in C^2(\mathbb{R}^3\times\mathbb{R}^2;\mathbb{R})$, all $(x,z,\lambda;\tau)\in\mathbb{R}^3\times\mathbb{R}^2$ and any smooth solution $u:\mathbb{R}^2\times\mathbb{R}^2\to\mathbb{R}$ to the differential equation (3.72).

4. Integrable heavenly type superflows and their Lie-algebraic structure

4.1. Introductory notions and notations

We begin from preliminaries for the superconformal loop diffeomorphism groups and their superconformal loop algebras. Let $\tilde{G}$ be the superconformal group of smooth loops $\{\mathbb{C}\supset\mathbb{S}^1\to G\}$, where $G:=Diff(\mathbb{T}^{1|N})$ is the group of superconformal diffeomorphisms of the $1|N$-dimensional supertorus $\mathbb{T}^{1|N}$, $N\in\mathbb{N}$, with coordinates $(x,\vartheta)\in\mathbb{T}^{1|N}\simeq\Lambda_0\times\Lambda_1^N$ from the infinite-dimensional Grassmann algebra $\Lambda=\Lambda_0\oplus\Lambda_1$. A superconformal vector field is

$$\tilde{a}:=a\frac{\partial}{\partial x}+\frac{1}{2}<Da,D>, \tag{4.1}$$

where $D:=(D_{\vartheta_1},D_{\vartheta_2},\cdots,D_{\vartheta_N})^\intercal, D_{\vartheta_j}:=\frac{\partial}{\partial\vartheta_j}+\vartheta_j\frac{\partial}{\partial x}$, $j=\overline{1,N}$, $\vartheta:=(\vartheta_1,\dots,\vartheta_N)^\top$, $a\in C^\infty(\mathbb{T}^{1|N};\Lambda_0)$, and is defined by the condition that the Lie superderivation $\mathscr{L}_{\tilde{a}}:\Lambda^1(\mathbb{T}^{1|N})\to\Lambda^1(\mathbb{T}^{1|N})$ of the superdifferential 1-form

$$\omega^{(1)}=dx+\sum_{j=1}^N\vartheta_jd\vartheta_j \tag{4.2}$$

is conformal, that is

$$\mathscr{L}_{\tilde{a}}\omega^{(1)}=\mu_{\tilde{a}}\omega^{(1)} \tag{4.3}$$

for some $\mu_{\tilde{a}}\in C^\infty(\mathbb{T}^{1|N};\Lambda_0)$. As a simple consequence of the condition (4.3), one also has the commutator of any two vector fields $\tilde{a},\tilde{b}\in\tilde{\mathscr{G}}$:

$$[\tilde{a},\tilde{b}]:=\tilde{c}=c\frac{\partial}{\partial x}+\frac{1}{2}<Dc,D>, \tag{4.4}$$

$$c=a\frac{\partial b}{\partial x}-b\frac{\partial a}{\partial x}+\frac{1}{2}<Da,Db>,$$

verifying that the set $\tilde{\mathscr{G}}:=\widetilde{diff}(\mathbb{T}^{1|N})$ of loop superconformal vector fields is a Lie algebra. One can naturally identify this loop Lie algebra $\tilde{\mathscr{G}}$ with a dense subspace of the dual space $\tilde{\mathscr{G}}^*$ through the parity

$$(\tilde{l},\tilde{a})_0:=\underset{\lambda\in\mathbb{C}}{res}(l,a)_H, \tag{4.5}$$

where $\tilde{l}:=ldx\in\tilde{\mathscr{G}}^*$.
For $p\in\mathbb{Z}$ and for any superconformal vector field $\tilde{a}\in\tilde{\mathscr{G}}$ and element $\tilde{l}\in\tilde{\mathscr{G}}^*$

$$\tilde{a}:=a\frac{\partial}{\partial x}+\frac{1}{2}<Da,D>,\quad\tilde{l}:=ldx, \tag{4.6}$$

and the bilinear form

$$(l,a)_H:=\int_{\mathbb{T}^{1|N}}l(x,\vartheta)a(x,\vartheta)dxd^N\vartheta \tag{4.7}$$

is determined by means of the integration with respect to the Berezin measures

$$\int_{\mathbb{T}^{1|1}}\alpha(x)dxd\vartheta_j=0,\quad\int_{\mathbb{T}^{1|1}}\alpha(x)dx\vartheta_jd\vartheta_j=\int_{\mathbb{T}^1}\alpha(x)dx,$$

where $\alpha\in C^\infty(\mathbb{T}^1;\mathbb{R})$, $j\in\overline{1,N}$. There are two cases: the first one when $N=2k-1$, $a\in C^\infty(\mathbb{T}^{1|(2k-1)};\Lambda_0)$, $l\in C^\infty(\mathbb{T}^{1|(2k-1)};\Lambda_1)$ and the second one, when $N=2k$, $a\in C^\infty(\mathbb{T}^{1|2k};\Lambda_0)$, $l\in C^\infty(\mathbb{T}^{1|2k};\Lambda_0)$, where $k\in\mathbb{N}$.
The constructed loop Lie algebra $\mathscr{G}^*$ of superconformal vector fields on the supertorus $\mathbb{T}^{1|N}$ allows the following natural splitting

$$\tilde{\mathscr{G}}=\tilde{\mathscr{G}}_+\oplus\tilde{\mathscr{G}}_-, \tag{4.8}$$

where $\tilde{\mathscr{G}}_+$ and $\tilde{\mathscr{G}}_-$ are also loop Lie algebras, that is

$$[\tilde{\mathscr{G}}_+,\tilde{\mathscr{G}}_+]\subset\tilde{\mathscr{G}}_+,\quad [\tilde{\mathscr{G}}_-,\tilde{\mathscr{G}}_-]\subset\tilde{\mathscr{G}}_-. \tag{4.9}$$

This fact makes it possible to apply to the Lie algebra $\tilde{\mathscr{G}}$ the known Lie algebraic AKS-scheme of constructing integrable Hamiltonian flows on the coadjoint space $\tilde{\mathscr{G}}^*$. Namely, let a $\mathscr{R}$-structure endomorphism $\mathscr{R}:\tilde{\mathscr{G}}\to\tilde{\mathscr{G}}$ be defined as

$$\mathscr{R}=(P_+-P_-)/2, \tag{4.10}$$

where, by definition, the projections

$$P_\pm\tilde{\mathscr{G}}:=\tilde{\mathscr{G}}_\pm\subset\tilde{\mathscr{G}}. \tag{4.11}$$

Then the following commutator

$$[\tilde{a},\tilde{b}]_{\mathscr{R}}:=[\mathscr{R}\tilde{a},\tilde{b}]+[\tilde{a},\mathscr{R}\tilde{b}], \tag{4.12}$$

where $\tilde{a},\tilde{b}\in\tilde{\mathscr{G}}$ defines, on the linear space $\tilde{\mathscr{G}}$ a new Lie structure, satisfying the Jacobi identity, and generating the deformed Lie–Poisson bracket

$$\{f,g\}_{\mathscr{R}}:=(\tilde{l},[\nabla f(\tilde{l}),\nabla g(\tilde{l})]_{\mathscr{R}}), \tag{4.13}$$

where $f,g\in \mathrm{D}(\tilde{\mathscr{G}}^*)$. The corresponding set of Casimir invariants $\mathrm{I}(\tilde{\mathscr{G}}^*)$ is generated by the functional $h\in\mathrm{D}(\tilde{\mathscr{G}}^*)$, satisfying

$$ad^*_{\nabla h(\tilde{l})}\tilde{l}=0, \tag{4.14}$$

where

$$ad^*_a l=\partial l/\partial x\, a+\frac{4-N}{2}l\,\partial a/\partial x+\frac{(-1)^{N+1}}{2}<Dl,Da> \tag{4.15}$$

for any superconformal vector field $\tilde{a}\in\tilde{\mathscr{G}}$ and a fixed element $\tilde{l}\in\tilde{\mathscr{G}}^*$. Here

$$\tilde{a}=a\frac{\partial}{\partial x}+\frac{1}{2}<Da,D>,\quad \tilde{l}=ldx. \tag{4.16}$$

The Adler-Kostant-Symes theorem allows us to construct an infinite hierarchy of mutually commuting Hamiltonian flows

$$d\tilde{l}/dt_p=-ad^*_{\nabla h^{(p)}(\tilde{l})_+}\tilde{l}, \tag{4.17}$$

where $\nabla h^{(p)}(l)=\lambda^p\nabla h(l)$, $t_p\in\mathbb{R}$, $p\in\mathbb{Z}_+$, by means of the asymptotic as $|\lambda|\to\infty$ expansion

$$\nabla h(l)\sim\sum_{j\in\mathbb{Z}_+}\nabla h_j(x,\vartheta)\lambda^{-j} \tag{4.18}$$

for the gradient of a generating functional $h\in\mathscr{D}(\tilde{\mathscr{G}}^*)$. The evolution equations (4.17) take the following forms

$$\begin{aligned} dl/dt_p=&\left(-\nabla h^{(p)}(l)_+\tfrac{\partial}{\partial x}+\tfrac{1}{2}<D\nabla h^{(p)}(l)_+,D>+\right.\\ &\left.+\left(2-\tfrac{N}{2}\right)\tfrac{\partial\nabla h^{(p)}(l)_+}{\partial x}\right)l=\\ &=-(\tilde{A}_{\nabla h^{(p)}(l)_+}+B_{\nabla h^{(p)}(l)_+})l, \end{aligned} \tag{4.19}$$

where

$$\tilde{A}_{\nabla h^{(p)}(\tilde{l})_+}:=(\nabla h^{(p)}(l)_+\frac{\partial}{\partial x}+\frac{1}{2}<D\nabla h^{(p)}(l)_+,D> \tag{4.20}$$

for all $p\in\mathbb{Z}_+$. Thus, as the flows (4.19) are commuting, the following proposition automatically holds.

Proposition 4.1. *The commuting condition for any two flows d/dt_{p_1} and d/dt_{p_2}, $p_1\neq p_2\in\mathbb{Z}_+$, from the hierarchy (4.17) is equivalent to the equality*

$$\frac{\partial}{\partial t_{p_2}}\tilde{A}_{\nabla h^{(p_1)}(\tilde{l})_+}-\frac{\partial}{\partial t_{p_1}}\tilde{A}_{\nabla h^{(p_2)}(\tilde{l})_+}=[\tilde{A}_{\nabla h^{(p_1)}(\tilde{l})_+},\tilde{A}_{\nabla h^{(p_1)}(\tilde{l})_+}], \tag{4.21}$$

or

$$\frac{\partial}{\partial t_{p_2}}\nabla h^{(p_1)}(\tilde{l})_+-\frac{\partial}{\partial t_{p_1}}\nabla h^{(p_2)}(\tilde{l})_+=[\nabla h^{(p_1)}(\tilde{l})_+,\nabla h^{(p_2)}(\tilde{l})_+]. \tag{4.22}$$

Moreover, the relationship (4.22) is a compatibility condition for the first order partial differential equations

$$\left(\frac{\partial}{\partial t_{p_1}}+\nabla h^{(p_1)}(\tilde{l})_+\right)\psi=0,\ \left(\frac{\partial}{\partial t_{p_2}}+\nabla h^{(p_2)}(\tilde{l})_+\right)\psi=0, \tag{4.23}$$

where $\psi\in C^2(\mathbb{R}^2\times\mathbb{T}^{1|N};\Lambda_0)$.

The procedure for reducing the relationship (4.22) on the corresponding coadjoint action orbits for different p_1 and $p_2\in\mathbb{Z}_+$ allows us to obtain integrable superanalogs of known integrable two-dimensional systems of heavenly equations with the Lax–Sato representations in the forms (4.21).

4.2. Example: The superanalogs of the generalized Mikhalev–Pavlov equations and their Lax–Sato integrability

We now consider the well-known Mikhalev–Pavlov [43, 48] heavenly equation

$$u_{xt}+u_{yy}=u_yu_{xx}-u_xu_{xy}, \tag{4.24}$$

where $u\in C^\infty(\mathbb{R}^2\times\mathbb{T}^1;\mathbb{R})$ and $(t,y;x)\in\mathbb{R}^2\times\mathbb{T}^1$, which is the compatibility condition for the vector fields

$$\frac{\partial\psi}{\partial t}+(\lambda^2+\lambda u_x-u_y)\frac{\partial\psi}{\partial x}=0,\quad \frac{\partial\psi}{\partial y}+(\lambda+u_y)\frac{\partial\psi}{\partial x}=0, \tag{4.25}$$

for a function $\psi\in C^\infty(\mathbb{R}^2\times\mathbb{T}^1;\mathbb{R})$ and arbitrary evolution parameters $y,t\in\mathbb{R}$ and construct its Lax–Sato integrable superanalogs for different $N\in\mathbb{N}$.
When $N\in\mathbb{Z}_+$ is odd, $N\neq 5$ and $l=\vartheta_N((N-5)u_x/2+\lambda)-\xi/2$, $u=u(x,\vartheta_1,\ldots,\vartheta_{N-1})$, $\xi=\xi(x,\vartheta_1,\ldots,\vartheta_{N-1})$, the asymptotic expansion for the gradient of the generating functional $h\in\mathrm{D}(\tilde{\mathscr{G}}^*)$ as $|\lambda|\to\infty$ has the form

$$\nabla h(l)\sim 1+(u_x+\vartheta_N\xi_x)\lambda^{-1}-(u_y+\vartheta_N\xi_y)\lambda^{-2}+\ldots\,. \tag{4.26}$$

If $p_1=1$ and $p_2=2$, one obtains from the equality (4.22) the system

$$\begin{aligned} u_{xt}+u_{yy}&=u_yu_{xx}-u_xu_{yx}-\xi_x\xi_y/2-\textstyle\sum_{i=1}^{N-1}(D_{\vartheta_i}u_x)(D_{\vartheta_i}u_y)/2,\\ \xi_{xt}+\xi_{yy}&=u_y\xi_{xx}-u_x\xi_{yx}+u_{xx}\xi_y/2-u_{yx}\xi_x/2+\\ &+\textstyle\sum_{i=1}^{N-1}(D_{\vartheta_i}u_y)(D_{\vartheta_i}\xi_x)/2-\sum_{i=1}^{N-1}(D_{\vartheta_i}u_x)(D_{\vartheta_i}\xi_y)/2,\end{aligned} \tag{4.27}$$

where $t_{p_1}:=y$, $t_{p_2}:=t$ and $(u,\xi)^\top\in C^\infty(\mathbb{R}^2\times\mathbb{T}^{1|(N-1)};\Lambda_0\times\Lambda_1)$. The compatibility condition for the first order partial differential equations such as

$$\begin{aligned} &\psi_y+((\lambda+u_x)+\vartheta_N\xi_x)\psi_x+\\ &+\textstyle\sum_{i=1}^{N-1}((D_{\vartheta_i}u_x)-\vartheta_N(D_{\vartheta_i}\xi_x))(D_{\vartheta_i}\psi)/2+\\ &+(\xi_x+\vartheta_Nu_{xx})(D_{\vartheta_N}\psi)/2=0,\end{aligned} \tag{4.28}$$

$$\begin{aligned} &\tfrac{\partial\psi}{\partial t}+[(\lambda^2+u_x\lambda-u_y)+\vartheta_N(\xi_x\lambda-\xi_y)]\tfrac{\partial\psi}{\partial x}+\\ &+\textstyle\sum_{i=1}^{N-1}(((D_{\vartheta_i}u_x)\lambda-(D_{\vartheta_i}u_y))-\\ &-\vartheta_N((D_{\vartheta_i}\xi_x)\lambda-(D_{\vartheta_i}\xi_y)))(D_{\vartheta_i}\psi)/2+\\ &+((\xi_x\lambda-\xi_y)+\vartheta_N(u_{xx}\lambda-u_{yx}))(D_{\vartheta_N}\psi)/2=0,\end{aligned}$$

where $\psi\in C^2(\mathbb{R}^2\times\mathbb{T}^{1|N};\Lambda_0)$, are Lax–Sato representation for the system (4.27).
When $N\in\mathbb{Z}_+$ is even, $N\neq 4$ and $l=((N-4)u_x/2+\lambda)+\vartheta_N(N-4)\xi_x/2$, $u=u(x,\vartheta_1,\ldots,\vartheta_{N-1})$, $\xi=\xi(x,\vartheta_1,\ldots,\vartheta_{N-1})$, the asymptotic expansion for the gradient of the generating functional $h\in\mathscr{D}(\tilde{\mathscr{G}}^*)$ as $|\lambda|\to\infty$ also has the form (4.26). For $p_1=1$ and $p_2=2$ one obtains from (4.22) the system (4.27), in which $t_{p_1}:=y$, $t_{p_2}:=t$ and $(u,\xi)^\top\in C^\infty(\mathbb{R}^2\times\mathbb{T}^{1|(N-1)};\Lambda_0\times\Lambda_1)$.
The system (4.27) can be considered as a superconformal analog of the Mikhalev–Pavlov heavenly equation for every $N\in N\backslash\{4;5\}$. Namely, for $N=1$ and $N=2$ one obtains easily the systems

$$\begin{aligned} u_{xt}+u_{yy}&=u_yu_{xx}-u_xu_{yx}-\xi_x\xi_y/2,\\ \xi_{xt}+\xi_{yy}&=u_y\xi_{xx}-u_x\xi_{yx}+u_{xx}\xi_y/2-u_{yx}\xi_x/2\end{aligned} \tag{4.29}$$

and

$$\begin{aligned} u_{xt}+u_{yy}&=u_yu_{xx}-u_xu_{yx}-\xi_x\xi_y/2-(D_{\vartheta_1}u_x)(D_{\vartheta_1}u_y)/2,\\ \xi_{xt}+\xi_{yy}&=u_y\xi_{xx}-u_x\xi_{yx}+u_{xx}\xi_y/2-u_{yx}\xi_x/2+\\ &+(D_{\vartheta_1}u_y)(D_{\vartheta_1}\xi_x)/2-(D_{\vartheta_1}u_x)(D_{\vartheta_1}\xi_y)/2,\end{aligned} \tag{4.30}$$

respectively.
It should be noted that for $N=4$ and $N=5$ one cannot find the asymptotic expansions for gradients of the generating functional $h\in\mathrm{D}(\tilde{\mathscr{G}}^*)$ as $|\lambda|\to\infty$ by means of the relationship (4.14) and as a consequence construct integrable superanalogs in the framework of the proposed Lie-algebraic approach.

4.3. Example: The superanalogs of the generalized Liouville equations and their Lax–Sato integrability

We now show using the Lie superalgebra $\tilde{\mathscr{G}}_{(1|N)}:=\widetilde{diff}(\mathbb{T}^{1|N}_{\mathbb{C}})$ of the superconformal vector fields on $\mathbb{T}^{1|N}_{\mathbb{C}}\simeq\mathbb{T}^1_{\mathbb{C}}\times\Lambda_1^N$, that the Lax–Sato integrable superanalogs of the Liouville heavenly equations can be obtained as a result of a diffeomorphism in the space of variables $(z,\vartheta)\in\mathbb{T}^{1|N}_{\mathbb{C}}$.
First one introduces the superderivatives $D_{\vartheta_j}:=\partial/\partial\vartheta_j+\vartheta_j\partial/\partial z$, $z\in\mathbb{T}^1_{\mathbb{C}}$, $\vartheta_j\in\Lambda_1$, $j=\overline{1,N}$, in the superspace $\Lambda_0\times\Lambda_1^N$. The loop Lie algebra $\tilde{\mathscr{G}}_{(1|N)}$ is generated by the superconformal vector fields

$$\tilde{a}:=a\frac{\partial}{\partial z}+\frac{1}{2}<Da,D>, \tag{4.31}$$

where $D := (D_{\vartheta_1}, D_{\vartheta_2}, \cdots, D_{\vartheta_N})^\intercal$, $i = \overline{1,N}$, $\vartheta := (\vartheta_1, \ldots, \vartheta_N)^\top$, $a \in C^\infty(\mathbb{T}^{1|N}_{\mathbb{C}}; \Lambda_0)$, with the commutator

$$[\tilde{a}, \tilde{b}] := \tilde{c} = c\frac{\partial}{\partial z} + \frac{1}{2} < Dc, D >, \tag{4.32}$$

$$c = a\frac{\partial b}{\partial z} - b\frac{\partial a}{\partial z} + \frac{1}{2} < Da, Db >,$$

This loop Lie algebra allows the following splitting:

$$\tilde{\mathscr{G}}_{(1|N)} = \tilde{\mathscr{G}}_{(1|N)+} \oplus \tilde{\mathscr{G}}_{(1|N)-}.$$

A nontrivial Casimir invariant $h^{(p_y)} \in \mathrm{I}(\tilde{\mathscr{G}}^*_{(1|N)})$ satisfies the relationship

$$(l(\nabla h^{(p_y)}(l))^2)_z - \frac{N}{4} l((\nabla h^{(p_y)}(l))^2)_z = \frac{(-1)^N}{4} < Dl, D(\nabla h^{(p_y)}(l))^2 >, \tag{4.33}$$

where $\tilde{l} := l dz \in \tilde{\mathscr{G}}^*_{(1|N)}, \nabla h^{(y)}(\tilde{l}) := \nabla h^{(y)}(l)\partial/\partial z \in \tilde{\mathscr{G}}_{(1|N)}$. If the corresponding gradient has the asymptotic expansion as $|z| \to \infty$

$$\nabla h^{(p_y)}(\tilde{l}) \simeq (V_2 z^2 + V_1 z + V_0 + V_{-1}z^{-1} + V_{-2}z^{-2} + \ldots)\partial/\partial z, \tag{4.34}$$

where $p_y = 2, V_j \in C^2(\mathbb{R}^2 \times \Lambda_1^N; \Lambda_0), j \in \mathbb{Z}, j \leq 2$, are functional parameters, we can construct the Hamiltonian flow

$$dl/dy = -l_z \nabla h^{(y)}(l) - \frac{4-N}{2} l(\nabla h^{(y)}(l))_z + \frac{(-1)^N}{2} < Dl, D\nabla h^{(y)}(l) > \tag{4.35}$$

in the framework of the classical AKS-theory. The constant Casimir invariant $h^{(p_t)} \in \mathrm{I}(\tilde{\mathscr{G}}^*_{(1|N)}), p_t = 0$, generates the trivial flow

$$dl/dt = 0. \tag{4.36}$$

The compatibility condition of these two flows for all $y, t \in \mathbb{R}$ is equivalent to the following system of two *a priori* compatible linear vector field equations

$$\frac{\partial \psi}{\partial y} + \nabla h^{(y)}(l)\frac{\partial \psi}{\partial z} + \frac{1}{2} < D\nabla h^{(y)}(l), D\psi >= 0,$$

$$\frac{\partial \psi}{\partial t} + \nabla h^{(t)}(l)\frac{\partial \psi}{\partial z} + \frac{1}{2} < D\nabla h^{(t)}(l), D\psi >= 0, \tag{4.37}$$

or

$$\frac{\partial \psi}{\partial y} + V\frac{\partial \psi}{\partial z} + \frac{1}{2} < DV, D\psi >= 0, \quad \frac{\partial \psi}{\partial t} = 0, \tag{4.38}$$

where $\nabla h^{(y)}(l) := V$, $V = V(y,t,\vartheta; z) = V_2 z^2 + V_1 z + V_0$, and $\nabla h^{(t)}(l) = 0$, for a smooth function $\psi \in C^2(\mathbb{R}^2 \times \Lambda_1^N; \Lambda_0)$. In this case we have the evolutions

$$\frac{dz}{dy} = V - \frac{1}{2} < \theta, DV >, \quad \frac{d\vartheta}{dy} = \frac{1}{2}(DV),$$
$$\frac{dz}{dt} = 0, \quad \frac{d\theta}{dt} = 0. \tag{4.39}$$

Under the diffeomorphism $z \mapsto z - \alpha - < \theta, \eta > := \lambda$ and $\vartheta \mapsto \vartheta + \eta := \tilde{\vartheta}$, $\eta := (\eta_1, \ldots, \eta_N)^\top$, $\tilde{\vartheta} := (\tilde{\vartheta}_1, \ldots, \tilde{\vartheta}_N)^\top$, on $\mathbb{T}^{1|N}_{\mathbb{C}}$, generated by the functions $\alpha := \alpha(y,t) \in C^3(\mathbb{R}^2; \Lambda_0)$ and $\eta := \eta(y,t) \in C^3(\mathbb{R}^2; \Lambda_1^N)$, the equations (4.38) are rewritten as

$$\frac{\partial \psi}{\partial y} + W\frac{\partial \psi}{\partial \lambda} + \frac{1}{2} < \tilde{D}W, \tilde{D}\psi >= 0,$$

$$\frac{\partial \psi}{\partial t} - U\frac{\partial \psi}{\partial \lambda} - \frac{1}{2} < \tilde{D}U, \tilde{D}\psi >= 0, \tag{4.40}$$

where $W := W(y,t,\tilde{\vartheta};\lambda) = W_2\lambda^2 + W_1\lambda + W_0$, $U := U(y,t,\tilde{\vartheta})$, $\tilde{D} := (D_{\vartheta_1}, \ldots, D_{\vartheta_N})^\top$ and $D_{\tilde{\vartheta}_i} := \frac{\partial}{\partial \tilde{\vartheta}_i} + \tilde{\vartheta}_i\frac{\partial}{\partial \lambda}$, $i = \overline{1,N}$. Taking into account the equations (4.39) and

$$\frac{d\lambda}{dy} = W - \frac{1}{2} < \tilde{\theta}, \tilde{D}W >, \quad \frac{d\tilde{\vartheta}}{dy} = \frac{1}{2}(\tilde{D}W), \tag{4.41}$$
$$\frac{d\lambda}{dt} = -U + \frac{1}{2} < \tilde{\theta}, \tilde{D}U >, \quad \frac{d\tilde{\vartheta}}{dt} = -\frac{1}{2}(\tilde{D}U),$$

one obtains the function W in the following form

$$W = \tilde{V} + < \eta, \tilde{D}\tilde{V} > - \frac{\partial \alpha}{\partial y} + < \eta, \frac{\partial \eta}{\partial y} >, \tag{4.42}$$
$$\tilde{V} := \tilde{V}(y,t,\tilde{\vartheta};\lambda) = V(y,t,\vartheta;z)|_{z=\lambda+\alpha+<\theta,\eta>,\ \vartheta=\tilde{\vartheta}-\eta}.$$

Here the superderivatives transform by the rules

$$D_{\vartheta_i} = D_{\tilde{\vartheta}_i} - 2\eta_i\partial/\partial\lambda, \quad i = \overline{1,N},$$

and the functions α and η obey the relationships

$$\frac{\partial\alpha}{\partial t} - <\eta, \frac{\partial\eta}{\partial t}> = U, \quad \frac{\partial\eta}{\partial t} = -\frac{1}{2}(\tilde{D}U). \tag{4.43}$$

If $W_2 := 1$ and $U := 1/2\exp\varphi$, $\varphi := \varphi(y,t,\vartheta)$, the compatibility condition for the first order partial differential equations (4.40) leads to the following Lax–Sato integrable superanalogs of the Liouville heavenly type equations:

$$\varphi_{yt} = \exp\varphi - \frac{1}{4}\sum_{i=1}^{N}\left(\frac{\partial}{\partial\tilde{\vartheta}_i}\varphi_y\right)\left(\frac{\partial}{\partial\tilde{\vartheta}_i}\exp\varphi\right) \tag{4.44}$$

for $W_0 = 1$, and

$$\begin{aligned}\varphi_{yt} - \varphi_{tt} = \exp\varphi - \\ -\frac{1}{4}\sum_{i=1}^{N}\left(\frac{\partial}{\partial\tilde{\vartheta}_i}(\varphi_y - \varphi_t)\right)\left(\frac{\partial}{\partial\tilde{\vartheta}_i}\exp\varphi\right),\end{aligned} \tag{4.45}$$

for $W_0 = -1/2\exp\varphi$. Owing to the relationship (4.33), the element $\tilde{l} \in \tilde{\mathscr{G}}^*_{(1|N)}$ can be found explicitly. For example, in the case of $N = 1$ it has the form

$$\begin{aligned}l(y,t,\vartheta_1;z) = z^{-4}(\vartheta_1(1 - 2v_1z^{-1} + (3v_1^2 - 2v_0)z^{-2}) + \\ +\beta_1/2 + (\beta_0/4 - 9\beta_1v_1/8)z^{-1}),\end{aligned}$$

where $V_2 := 1$ and $V_j := v_j + \vartheta_1\beta_j$, $j = \overline{0,1}$. Whence, one has the following proposition.

Proposition 4.2. *The super Liouville equations (4.44) and (4.45) are Hamiltonian flows on the co-adjoint space $\tilde{\mathscr{G}}^*_{(1|N)}$, generated by the seed element (4.41) and is equivalently representable as the Lax–Sato compatible linear system (4.40) on the space $C^2(\mathbb{R}^2 \times \Lambda_1^N;\Lambda_0)$.*

5. Integrability, bi-Hamiltonian structures and the classical Lagrange–d'Alembert principle

It is evident that all evolution flows like (2.16) or (2.20) are Hamiltonian with respect to the second Lie–Poisson bracket (2.10) on the adjoint loop space $\tilde{\mathscr{G}}^* = \widetilde{diff}^*(\mathbb{T}^n_{\mathbb{C}})$. Moreover, they are poly-Hamiltonian on the corresponding functional manifolds, as the related bilinear form (2.2) is marked by integers $s \in \mathbb{Z}$. This leads to [75] an infinite hierarchy of compatible Poisson structures on the phase spaces, isomorphic, respectively, to the orbits of a chosen seed element $\tilde{l} \in \tilde{\mathscr{G}}^*$ or of a seed element $\tilde{l} \in \tilde{\mathscr{G}}^*$. Since all these Hamiltonian flows possess an infinite hierarchy of commuting nontrivial conservation laws, one can prove their formal complete integrability under naturally formulated constraints. The corresponding analytical expressions for the infinite hierarchy of conservation laws can be retrieved from the asymptotic expansion (2.14) for Casimir functional gradients by employing the well-known [6, 5, 45, 75] formal homotopy technique.

In his book "*Mecanique analytique*", v.1-2, published in 1788 in Paris, Lagrange formulated *one of the basic, most general, differential variational principles of classical mechanics*, *expressing necessary and sufficient conditions for the correspondence of the real motion of a system of material points, subjected to ideal constraints and applied active forces*. Within the d'Alembert–Lagrange principle the positions of the system in its real motion are compared with infinitely close positions permitted by the constraints at a given time.

According to the d'Alembert–Lagrange principle, during a real motion of a system of $N \in \mathbb{Z}_+$ particles with masses $m_j \in \mathbb{R}_+, j = \overline{1,N}$, the totality elementary work performed by the given active forces $F^{(j)}, j = \overline{1,N}$, and by the forces of inertia for all *the possible particle displacements $\delta x^{(j)} \in \mathbb{E}^3, j = \overline{1,N}$, is equal to or less than zero:*

$$\sum_{j=\overline{1,N}} <F^{(j)} - m_j\frac{d^2x^{(j)}}{dt^2}, \delta x^{(j)}> \leq 0 \tag{5.1}$$

at any moment of time $t \in \mathbb{R}$, where $<\cdot,\cdot>$ denotes the standard scalar product in the three-dimensional Euclidean space $\mathbb{E}^3$. *Equality in (5.1) is valid for the possible reversible displacements*, the symbol $\leq$ is valid for *the possible irreversible displacements* $\delta x^{(j)} \in \mathbb{E}^3, j = \overline{1,N}$. Equation (5.1) is *the general equation of the dynamics of systems with ideal constraints*; it comprises all the equations and laws of motion, so that one can say that all dynamics is reduced to this single general formula.

This principle was established by J.L. Lagrange by generalizing the principle of virtual displacements with the aid of the classical d'Alembert principle. For systems subject to bilateral constraints, Lagrange used the formula (5.1) to deduce the general properties and laws of motion of bodies, as well as the equations of motion, which he applied to solve a number of problems in dynamics *including the problems of motions of non-compressible, compressible and elastic liquids, thus combining "dynamics and hydrodynamics as branches of the same principle and as conclusions drawn from a single general formula"*.

As was first demonstrated in [31], in the last case of *generalized reversible motions* of a compressible elastic liquid in a simply-connected open domain $\Omega_t \subset \mathbb{R}^n$ with the smooth boundary $\partial\Omega_t$, $t \in \mathbb{R}$, in space $\mathbb{R}^n, n \in \mathbb{Z}_+$, the expression (5.1) can be rewritten as

$$\delta W(t) := \int_{\Omega_t} <l(x(t);\lambda), \delta x(t)> d^nx(t) = 0 \tag{5.2}$$

for all $t \in \mathbb{R}$. Here $l(x(t);\lambda) \in \tilde{T}^*(\mathbb{R}^n) \simeq \tilde{\mathscr{G}}^*$ is the corresponding virtual vector "*reaction force*", exerted by the ambient medium on the liquid and called a *seed element*, which is here assumed to depend meromorphically on a *constant* complex parameter $\lambda \in \mathbb{C}$. If we suppose that the evolution of liquid points $x(t) \in \Omega_t$ is determined for any parameters $\lambda \neq \mu \in \mathbb{C}$ by the generating *gradient type vector field*

$$\frac{dx(t)}{dt} = \frac{\mu}{\mu - \lambda}\nabla h(\,l(\mu))(t;x(t)) \tag{5.3}$$

and the Cauchy data

$$x(t)|_{t=0} = x^{(0)} \in \Omega_0$$

for an arbitrarily chosen open one-connected domain $\Omega_0 \subset \mathbb{T}^n$ with the smooth boundary $\partial\Omega_0 \subset \mathbb{R}^n$ and a smooth functional $h: \tilde{T}^*(\mathbb{R}^n) \to \mathbb{R}$, the Lagrange–d'Alembert principle says: the infinitesimal virtual work (5.2) equals zero for all moments of time, that is $\delta W(t) = 0 = \delta W(0)$ for all $t \in \mathbb{R}$. To check this, let us calculate the temporal derivative of the expression (5.2):

$$\begin{gathered} \frac{d}{dt}\delta W(t) = \frac{d}{dt}\int_{\Omega_t} < l(x(t);\lambda), \delta x(t) > d^n x(t) = \\ = \frac{d}{dt}\int_{\Omega_0} < l(x(t);\lambda), \delta x(t) > |\frac{\partial(x(t)}{\partial x_0}| d^n x^{(0)} = \int_{\Omega_0} \frac{d}{dt}(< l(x(t);\lambda), \delta x(t) > |\frac{\partial(x(t)}{\partial x_0}|) d^n x^{(0)} = \\ = \int_{\Omega_0} [\frac{d}{dt} < l(x(t);\lambda), \delta x(t) > + < l(x(t);\lambda), \delta x(t) > \operatorname{div} \tilde{K}(\mu)] |\frac{\partial(x(t)}{\partial x_0}| d^n x^{(0)} = \\ = \int_{\Omega_t} [\frac{d}{dt} < l(x(t);\lambda), \delta x(t) > + < l(x(t);\lambda), \delta x(t) > \operatorname{div} \tilde{K}(\mu)] d^n x(t) = 0, \end{gathered} \tag{5.4}$$

if the condition

$$\frac{d}{dt} < l(x(t);\lambda), \delta x(t) > + < l(x(t);\lambda), \delta x(t) > \operatorname{div} \tilde{K}(\mu;\lambda) = 0 \tag{5.5}$$

holds for all $t \in \mathbb{R}$, where

$$\tilde{K}(\mu;\lambda) := \frac{\mu}{\mu - \lambda} \nabla h(\,\tilde{l}(\mu)) = \frac{\mu}{\mu - \lambda} < \nabla h(\,l(\mu)), \frac{d}{dx} > \tag{5.6}$$

is a vector field on $\mathbb{R}^n$, corresponding to the evolution equations (5.3). Taking into account that the full temporal derivative $d/dt := \partial/\partial t + L_{\tilde{K}(\mu;\lambda)}$, where $L_{\tilde{K}(\mu;\lambda)} = i_{\tilde{K}(\mu;\lambda)} d + d i_{\tilde{K}(\mu;\lambda)}$ denotes the well known [1, 5, 29] Cartan expression for the Lie derivation along the vector field (5.6), can be represented as $\mu, \lambda \to \infty, |\lambda/\mu| < 1$ in the asymptotic form

$$\frac{d}{dt} \sim \sum_{j \in \mathbb{Z}_+} \mu^{-j} \frac{\partial}{\partial t_j} + \sum_{j \in \mathbb{Z}_+} \mu^{-j} L_{\tilde{K}_j(\lambda}, \tag{5.7}$$

the equality (5.5) can be *equivalently rewritten* as an infinite hierarchy of the following evolution equations

$$\partial\, \tilde{l}(\lambda)/\partial t_j := -ad^*_{\tilde{K}_j(\lambda)_+}\, \tilde{l}(\lambda) \tag{5.8}$$

for every $j \in \mathbb{Z}_+$ on the space of differential 1-forms $\tilde{\Lambda}^1(\mathbb{R}^n) \simeq \tilde{\mathscr{G}}^*$, where $\tilde{l}(\lambda) :=< l(x;\lambda), dx > \in \tilde{\Lambda}^1(\mathbb{R}^n) \simeq \tilde{\mathscr{G}}^*, \tilde{\mathscr{G}} := \widetilde{diff}(\mathbb{R}^n)$ is the Lie algebra of the corresponding loop diffeomorphism group $\widetilde{Diff}(\mathbb{R}^n)$. From (5.6) one easily finds that

$$\tilde{K}_j(\lambda) = \nabla h^{(j)}(\,\tilde{l}) \tag{5.9}$$

for $\lambda \in \mathbb{C}$ and any $j \in \mathbb{Z}_+$, the evolution equations (5.8) transform equivalently into

$$\partial\, \tilde{l}(\lambda)/\partial t_j := -ad^*_{\nabla h^{(j)}(\,\tilde{l})_+}\, \tilde{l}(\lambda), \tag{5.10}$$

allowing to formulate the following important Adler–Kostant–Symes type [6, 5, 7, 75, 62, 61] proposition.

Proposition 5.1. *The evolution equations (5.10) are completely integrable mutually commuting Hamiltonian flows on the adjoint loop space* $\tilde{\mathscr{G}}^*$ *for a seed element* $\tilde{l}(\lambda) \in \tilde{\mathscr{G}}^*$, *generated by Casimir functionals* $h^{(j)} \in \mathrm{I}(\tilde{\mathscr{G}}^*)$, *naturally determined by conditions* $ad^*_{\nabla h^{(j)}(\,\tilde{l})}\, \tilde{l}(\lambda) = 0$, $j \in \mathbb{Z}_+$, *with respect to the modified Lie-Poisson bracket on the adjoint space* $\tilde{\mathscr{G}}^*$

$$\{(\tilde{l}, \tilde{X}), (\tilde{l}, \tilde{Y})\} := (\tilde{l}, [\tilde{X}, \tilde{Y}]_{\mathscr{R}}),$$

defined for any $\tilde{X}, \tilde{Y} \in \tilde{\mathscr{G}}$ *by means of the canonical* $\mathscr{R}$*-structure on the loop Lie algebra* $\tilde{\mathscr{G}}$:

$$[\tilde{X}, \tilde{Y}]_{\mathscr{R}} := [\tilde{X}_+, \tilde{Y}_+] - [\tilde{X}_-, \tilde{Y}_-], \tag{5.11}$$

where "$\tilde{Z}_\pm$*" means the positive (+)/(-)-negative part of a loop Lie algebra element* $\tilde{Z} \in \tilde{\mathscr{G}}$ *subject to the loop parameter* $\lambda \in \mathbb{C}$.

If, for instance, we consider the first two flows from (5.10) in the form

$$\begin{aligned} \partial\, \tilde{l}(\lambda)/\partial t_1 \quad &:= \partial\, \tilde{l}(\lambda)/\partial y = -ad^*_{\nabla h^{(y)}(\,\tilde{l})}\, \tilde{l}(\lambda), \\ \partial\, \tilde{l}(\lambda)/\partial t_2 \quad &:= \partial\, \tilde{l}(\lambda)/\partial t = -ad^*_{\nabla h^{(t)}(\,\tilde{l})}\, \tilde{l}(\lambda), \end{aligned} \tag{5.12}$$

where

$$\nabla h^{(y)}(\tilde{l}) := \nabla h^{(1)}(\tilde{l})|_+, \;\; \nabla h^{(t)}(\tilde{l}) := \nabla h^{(t)}(\tilde{l})|_+,$$

which are by construction commuting, from their compatibility condition one obtains a system of nonlinear partial differential equations for the coefficients of the seed element $\tilde{l}(\lambda) \in \tilde{\mathscr{G}}^*$. As this system is equivalent to the Lax–Sato compatibility condition for the corresponding vector fields $\nabla h^{(y)}(\tilde{l})$ and $\nabla h^{(t)}(\tilde{l}) \in \tilde{\mathscr{G}}$:

$$[\partial/\partial y + \nabla h^{(y)}(\,\tilde{l}),\, \partial/\partial t + \nabla h^{(t)}(\,\tilde{l})] = 0, \tag{5.13}$$

from (5.13) we obtain a system of nonlinear equations in partial derivatives (often called heavenly) that was analyzed in a series of articles [39, 9, 46, 47, 48, 65, 66, 42, 73, 74] and more recently in [11, 9, 10, 33]. These works are closely related to the problem of constructing a hierarchy of commuting vector fields, analytically depending on a complex parameter $\lambda \in \mathbb{C}$, which was posed in 1928 by the French mathematician M.A. Buhl [13, 14, 15] and in general form studied and completely solved by M.G. Pfeiffer in [50, 51, 52, 53, 54, 55].

6. Acknowledgements

The authors cordially thank Prof. M. Błaszak, Prof. J. Cieślinski, Prof. A. Sym and Prof. A. Samoilenko for their cooperation and useful discussions of the results in this paper during the Workshop "Nonlinearity and Geometry" , 20-23 January, 2017 in Warsaw, Poland, and the International Conference in Functional Analysis dedicated to the 125^{th} anniversary of Stefan Banach, 18 - 23 September, 2017 in Lviv, Ukraine. A.P. is especially indebted to Prof. M. Pavlov, Prof. W.K. Schief and Prof. Ya. G. Prytula for mentioning important references, which were very helpful in preparing the manuscript. He is also greatly indebted to Prof. V.E. Zakharov (University of Arizona, Tucson) and Prof. J. Szmigelski (University of Saskatchewan, Saskatoon) for their interest in the work and instructive discussions during the XXXV Workshop on Geometric Methods in Physics, 26.06-2.07.2016 in Białowieża, Poland. A.P.'s last but not least thanks go also to the Department of Mathematical Sciences of the NJIT (Newark NJ, USA) for the invitation to visit the NJIT during the Summer of 2017, where an essential part of this paper was completed.

References

[1] R. Abraham and J. Marsden, Foundations of Mechanics, Second Edition, Benjamin Cummings, NY
[2] L.M. Alonso, A.B. Shabat, Hydrodynamic reductions and solutions of a universal hierarchy, Theor. Math. Phys,104 (2004), 1073-1085
[3] V.I. Arnold, Mathematical Methods of Classical Mechanics., Springer, NY, 1978
[4] D. Blackmore, A.K. Prykarpatsky, Dark Equations and Their Light Integrability, Journal of Nonlinear Mathematical Physics, Vol. 21, No. 3 (2014), 407-428
[5] D. Blackmore, A.K. Prykarpatsky and V.H. Samoylenko, Nonlinear dynamical systems of mathematical physics, World Scientific Publisher, NJ, USA, 2011
[6] M. Błaszak, Classical R-matrices on Poisson algebras and related dispersionless systems, Phys. Lett. A 297(3-4) (2002) 191–195
[7] M. Błaszak and B.M. Szablikowski, Classical R-matrix theory of dispersionless systems: II. (2 + 1) dimension theory, J. Phys. A: Math. Gen. 35 (2002), 10345
[8] L.V. Bogdanov, Interpolating differential reductions of multidimensional integrable hierarchies, TMF, 2011, Volume 167, Number 3, 354–363
[9] L.V. Bogdanov, V.S. Dryuma, S.V. Manakov, Dunajski generalization of the second heavenly equation: dressing method and the hierarchy, J. Phys. A: Math. Theor. 40 (2007), 14383-14393
[10] L.V. Bogdanov, B.G. Konopelchenko, On the heavenly equation and its reductions, J. Phys. A, Math. Gen. 39 (2006), 11793-11802
[11] L.V. Bogdanov, M.V. Pavlov, Linearly degenerate hierarchies of quasiclassical SDYM type, arXiv:1603.00238v2 [nlin.SI] 15 Mar 2016
[12] A.J. Bruce, K. Grabowska, J. Grabowski, Remarks on contact and Jacobi geometry. SIGMA 13, 059 (2017);(arXiv:1507.05405)
[13] M.A. Buhl, Surles operateurs differentieles permutables ou non, Bull. des Sc.Math.,1928, S.2, t. LII, p. 353-361
[14] M.A. Buhl, Apercus modernes sur la theorie des groupes continue et finis, Mem. des Sc. Math., fasc. XXXIII, Paris, 1928
[15] M.A. Buhl, Apercus modernes sur la theorie des groupes continue et finis, Mem. des Sc. Math., fasc. XXXIII, Paris, 1928
[16] P.A. Burovskiy, E.V. Ferapontov, S.P. Tsarev, Second order quasilinear PDEs and conformal structures in projective space, Int. J. Math. 21 (2010), no. 6, 799–841, arXiv:0802.2626
[17] A. Cartan, Differential Forms. Dover Publisher, USA, 1971
[18] Earl A. Coddington, Norman Levinson, Theory of ordinary differential equations, International series in pure and applied mathematics, McGraw-Hill, 1955
[19] B.A. Dubrovin, S.P. Novikov and A.T. Fomenko, Modern Geometry - Methods and Applications: Part I: The Geometry of Surfaces, Transformation Groups, and Fields (Graduate Texts in Mathematics) 2nd ed., Springer, Berlin, 1992
[20] M. Dunajski, Anti-self-dual four-manifolds with a parallel real spinor, Proc. Roy. Soc. A, 458 (2002), 1205
[21] M. Dunajski, E.V. Ferapontov and B. Kruglikov, On the Einstein-Weyl and conformal self-duality equations. arXiv:1406.0018v3 [nlin.SI] 29 Jun 2015
[22] M. Dunajski, W. Kryński, Einstein-Weyl geometry, dispersionless Hirota equation and Veronese webs, arXiv:1301.0621
[23] M. Dunajski, L.J. Mason, P. Tod, Einstein–Weyl geometry, the dKP equation and twistor theory, J. Geom. Phys. 37 (2001), N1-2, 63-93
[24] E.V. Ferapontov and B. Kruglikov, Dispersionless integrable systems in 3D and Einstein-Weyl geometry. arXiv:1208.2728v3 [math-ph] 9 May 2013
[25] E.V. Ferapontov, B. Kruglikov, V. Novikov, Integrability of dispersionless Hirota type equations and the symplectic Monge-Amp'ere property. rXiv:1707.08070v2 [nlin.SI] 9 Jan 2018
[26] E.V. Ferapontov and J. Moss, Linearly degenerate PDEs and quadratic line complexes, arXiv:1204.2777v1 [math.DG] 12 Apr 2012
[27] J. Gibbons and S.P. Tsarev, Reductions of the Benney Equations, Physics Letters A, Vol. 211, Issue 1, Pages 19–24, 1996
[28] J. Gibbons, S.P. Tsarev, Conformal maps and reductions of the Benney equations, Phys. Lett. A, 258 (1999) 263-270.
[29] C. Godbillon, Geometrie Differentielle et Mecanique Analytique. Hermann Publ., Paris, 1969
[30] M. Gromov, Partial differential relations, Ergebnisse der Mathematik und ihrer Grenzgebiete, Vol. 9, Springer-Verlag, Berlin, Heidelberg, New York, 363p.
[31] O.E. Hentosh, Y.A. Prykarpatsky, D. Blackmore and A.K. Prykarpatski, Lie-algebraic structure of Lax–Sato integrable heavenly equations and the Lagrange–d'Alembert principle, Journal of Geometry and Physics, 120 (2017), 208–227
[32] A. A. Kirillov, Local Lie algebras, Uspekhi Mat. Nauk, 31 (1976), N4(190), 57–76
[33] B.G. Konopelchenko, Grassmanians $Gr(N-1,N+1)$, closed differential $N-1$ forms and N-dimensional integrable systems. arXiv:1208.6129v2 [nlin.SI] 5 Mar 2013
[34] I. Krasil'shchik, A natural geometric construction underlying a class of Lax pairs, Lobachevskii J. of Math., 37 (2016) no. 1, 61–66; arXiv:1401.0612
[35] I.S. Krasil'shchik1, A. Sergyeyev, O.I. Morozov, Infinitely many nonlocal conservation laws for the ABC equation with $A+B+C\neq 0$, arXiv:1511.09430v1 [nlin.SI] 30 Nov 2015
[36] B.A. Kupershmidt, Dark equations, J. Nonlin. Math. Phys. 8 (2001), 363–445
[37] B.A. Kupershmidt, Mathematics of dispersive water waves, Commun. Math. Phys., 99 (1985), 51–73
[38] A. Kushner, V. Lychagin, V. Rubtsov, Contact geometry and non-linear differential equations. Cambridge Univ. Press, Cambridge (2007)
[39] S.V. Manakov, P.M. Santini, On the solutions of the second heavenly and Pavlov equations, J. Phys. A: Math. Theor. 42 (2009), 404013 (11pp)
[40] O.I. Mokhov, Symplectic and Poissonian geometry on loop spaces of smooth manifolds and integrable equations. Institute for Computer Studies Publ., Moscow-Izhevsk, 2004 (in Ruissian)
[41] O.I. Morozov, A two-Component generalization of the integrable rd-Dym equation, SIGMA, 8 (2012), 051-056.
[42] O.I. Morozov, A. Sergyeyev, The four-dimensional Martinez-Alonso-Shabat equation: reductions, nonlocal symmetries, and a four-dimensional integrable generalization of the ABC equation, Preprint submitted to JGP, 2014, 11 p.
[43] V. G. Mikhalev, On the Hamiltonian formalism for Korteweg–de Vries type hierarchies, Funct. Anal. Appl., 26, Issue 2 (1992), 140–142
[44] S.P. Novikov (Editor), Theory of solitons: the Inverse Scattering Method. Springer, 1984
[45] P. Olver, Applications of Lie Groups to Differential Equations, Second Edition, Springer-Verlag, New York, 1993
[46] V. Ovsienko, Bi-Hamilton nature of the equation $u_{tx}=u_{xy}u_y-u_{yy}u_x$, arXiv:0802.1818v1 [math-ph] 13 Feb 2008
[47] V. Ovsienko, C. Roger, Looped Cotangent Virasoro Algebra and Non-Linear Integrable Systems in Dimension 2 + 1, Commun. Math. Phys. 273 (2007), 357–378
[48] M.V. Pavlov, Integrable hydrodynamic chains, J. Math. Phys. 44 (2003), Issue 9, 4134-4156
[49] M.V. Pavlov, Classification of integrable Egorov hydrodynamic chains, Theoret. and Math. Phys. 138 (2004), 45-58, nlin.SI/0603055
[50] G. Pfeiffer, Generalisation de la methode de Jacobi pour l'integration des systems complets des equations lineaires et homogenes, Comptes Rendues de l'Academie des Sciences de l'URSS, 1930, t. 190, p. 405-409
[51] M. G. Pfeiffer, Sur la operateurs d'un systeme complet d'equations lineaires et homogenes aux derivees partielles du premier ordre d'une fonction inconnue, Comptes Rendues de l'Academie des Sciences de l'URSS, 1930, t. 190, p. 909–911
[52] M. G. Pfeiffer, La generalization de methode de Jacobi-Mayer, Comptes Rendues de l'Academie des Sciences de l'URSS, 1930, t. 191, p. 1107-1109
[53] M. G. Pfeiffer, Sur la permutation des solutions s'une equation lineaire aux derivees partielles du premier ordre, Bull. des Sc. Math., 1928, S.2,t.LII, p. 353-361

[54] M. G. Pfeiffer, Quelques additions au probleme de M. Buhl, Atti dei Congresso Internationale dei Matematici, Bologna, 1928, t.III, p. 45-46
[55] M. G. Pfeiffer, La construction des operateurs d'une equation lineaire, homogene aux derivees partielles premier ordre, Journal du Cycle Mathematique, Academie des Sciences d'Ukraine, Kyiv, N1, 1931, p. 37-72 (in Ukrainian)
[56] J.F. Plebański, Some solutions of complex Einstein equations, J. Math. Phys. 16 (1975), Issue 12, 2395-2402
[57] A. Presley and G. Segal, Loop groups, Oxford Mathematical Monographs, Oxford Univresity Press, 1986.
[58] N.K. Prykarpatska, D. Blackmore, V.H. Samoylenko, E. Wachnicki, M. Pytel-Kudela, The Cartan-Monge geometric approach to the characteristic method for nonlinear partial differential equations of the first and higher orders. Nonlinear Oscillations, 10(1) (2007), 22-31
[59] A.K. Prykarpatsky I.V. Mykytyuk, Algebraic integrability of nonlinear dynamical systems on manifolds: classical and quantum aspects. Kluwer Academic Publishers, the Netherlands, 1998
[60] Ya.A. Prykarpatsky and A.K. Prykarpatski, The integrable heavenly type equations and their Lie-algebraic structure, arXiv:1785057 [nlin.SI] 24 Jan 2017
[61] Y.A. Prykarpatsky and A.M. Samoilenko, Algebraic - analytic aspects of integrable nonlinear dynamical systems and their perturbations. Kyiv, Inst. Mathematics Publisher, v. 41, 2002 (in Ukrainian)
[62] A.G. Reyman, M.A. Semenov-Tian-Shansky, Integrable Systems, The Computer Research Institute Publ., Moscow-Izhvek, 2003 (in Russian)
[63] M. Sato, Y. Sato, Soliton equations as dynamical systems on infinite dimensional Grassmann manifold, in Nonlinear Partial Differential Equations in Applied Science; Proceedings of the U.S.-Japan Seminar, Tokyo, 1982, Lect. Notes in Num. Anal. 5 (1982), 259–271.
[64] M. Sato, and M. Noumi, Soliton equations and the universal Grassmann manifolds, Sophia University Kokyuroku in Math. 18 (1984) (in Japanese).
[65] W.K. Schief, Self-dual Einstein spaces via a permutability theorem for the Tzitzeica equation, Phys. Lett. A, Volume 223, Issues 1–2, 25 November 1996, 55-62
[66] W.K. Schief, Self-dual Einstein spaces and a discrete Tzitzeica equation. A permutability theorem link, In Symmetries and Integrability of Difference Equations, P. Clarkson and F. Nijhoff, eds, London Mathematical Society, Lecture Note Series 255, Cambridge University Press (1999) 137-148.
[67] A. Sergyeyev and B. M. Szablikowski, Central extensions of cotangent universal hierarchy: (2+1)-dimensional bi-Hamiltonian systems, Phys. Lett. A, 372 (2008) 7016-7023
[68] B. Szablikowski, Hierarchies of Manakov–Santini Type by Means of Rota-Baxter and Other Identities, SIGMA 12 (2016), 022, 14 pages
[69] B. Szablikowski, M. Błaszak, Meromorphic Lax representations of (1+1)-dimensional multi-Hamiltonian dispersionless systems. J. Math. Phys.,47, N9, 2006, 092701
[70] A. Sergyeyev, A simple construction of recursion operators for multidimensional dispersionless integrable systems, J. Math. Anal. Appl. 454 (2017), no.2, 468–480; arXiv:1501.01955
[71] A. Sergyeyev, New integrable (3+1)-dimensional systems and contact geometry, arXiv:1401.2122v4 [math.AP] 26 Sep 2017
[72] M.B. Sheftel1, A.A. Malykh, D. Yazıcı, Recursion operators and bi-Hamiltonian structure of the general heavenly equation, arXiv:1510.03666v3 [math-ph] 25 Jun 2016
[73] K. Takasaki and T. Takebe, SDiff(2) Toda equation – Hierarchy, Tau function, and symmetries, Letters in Mathematical Physics 23(3), 205–214 (1991)
[74] K. Takasaki and T. Takebe, Integrable Hierarchies and Dispersionless Limit, Reviews in Mathematical Physics 7(05), 743–808 (1995)
[75] L.A. Takhtajan, L.D. Faddeev, Hamiltonian Approach in Soliton Theory, Springer, Berlin-Heidelberg, 1987
[76] I. Zakharevich, Nonlinear wave equation, nonlinear Riemann problem, and the twistor transform of Veronese webs, arXiv:math-ph/0006001

Journal of Mathematical Sciences and Modelling, 1 (2) (2018) 131-137

Journal of Mathematical Sciences and Modelling

Journal Homepage: www.dergipark.gov.tr/jmsm
ISSN 2636-8692

Caustics of wave fronts reflected by a surface

Alexander Yampolsky[a*] and Oleksandr Fursenko[b]

[a]*Department of Pure Mathematics, Faculty of Mathematics and Computer Science, V.N. Karazin Kharkiv National University, Kharkiv, Ukraine*
[b]*Department of Mathematics, I. Kozhedub National Air Force University,Kharkiv, Ukraine*
[*]*Corresponding author E-mail: a.yampolsky@karazin.ua, https://orcid.org/0000-0002-7215-3669*

Article Info

Keywords: *Caustic, Reflected wave front*
2010 AMS: *53A25, 53B20, 53B25*
Received: *6 June 2018*
Accepted: *20 September 2018*
Available online: *30 September 2018*

Abstract

One can often see caustic by reflection in nature but it is rather hard to understand the way of how caustic arise and which geometric properties of a mirror surface define geometry of the caustic. The caustic by reflection has complicated topology and much more complicated geometry. From engineering point of view the geometry of caustic by reflection is important for antenna's theory because it can be considered as a surface of concentration of the reflected wave front. In this paper we give purely geometric description of the caustics of wave front (flat or spherical) after reflection from mirror surface. The description clarifies the dependence of caustic on geometrical characteristics of a surface and allows rather simple and fast computer visualization of the caustics in dependence of location of the rays source or direction of the pencil of parallel rays.

Introduction

The caustic of reflected wave front is the envelope of the family of rays emitted from a given point O (source) and reflected by smooth surface S (mirror). This type of caustics are called by *catacaustics* or *caustics by reflection*. There are a number of research on caustics and catacaustics. Mostly, the authors were interested in topology of the caustic [1, 3]. Nice research concerning location of the catacaustic inside compact convex body one can find in [2]. The catacaustics of a canal surfaces were studied in [4]. The caustics of a translation surfaces were considered in [6]. The caustics on spheres and cylinders of revolution were studied in [7]. A survey on the theory of caustics and wave front propagations with applications to geometry one can found in [5]. The catacaustics from engineering viewpoint in connection with antenna's technologies have been studied in [8]. The research presented in the mentioned above papers do not use the parametric equation of the caustic.

In this paper, we show that to find the caustic of reflected rays of a surface we should consider a "virtual deformation" of the mirror and its second fundamental form under influence of the incident pencil of rays. This approach allowed to give an **explicit parameterization** of the caustic of the reflected front in geometric terms of the mirror surface (**Theorem 1**, **Theorem 2**).

1. Caustics by reflected in case of flat incident front

Let us be given a regular surface S parameterized by vector-function $\mathbf{r}: D^2(u^1,u^2) \to S \subset E^3$. Let $\mathbf{n}$ be the unit normal vector field of S oriented in such a way that the support function is positive (the origin is in positive half-space with respect to each tangent plane). Suppose $\mathbf{a}$ ($|\mathbf{a}| = 1$) is a unit normal to a flat front incident on the surface and such that the dot-product $(\mathbf{a},\mathbf{n}) < 0$. If $\mathbf{b}$ is the direction of reflected ray, then

$$\mathbf{b} = \mathbf{a} - 2(\mathbf{a},\mathbf{n})\mathbf{n}. \tag{1.1}$$

We also suppose that at initial time $t = 0$ the incident front F_0 passes through the origin. Let L be the distance that each "photon" of F_0 passes along the ray in direction of $\mathbf{a}$. The front F_t reaches the surface S if $L \geq (\mathbf{r},\mathbf{a})$. Denote by λ the distance that each "photon" of the front F_t passes after reflection. Then evidently $(\mathbf{r},\mathbf{a}) + \lambda = L$ and hence

$$\lambda = L - (\mathbf{r},\mathbf{a}). \tag{1.2}$$

Email addresses: **a.yampolsky@karazin.ua (A. Yampolsky), olfursenko@ukr.net (O. Fursenko)**

Therefore, *the parametric equation of the reflected front* is

$$\rho = \mathbf{r} + \lambda \cdot \mathbf{b} \quad (\lambda \geq 0). \tag{1.3}$$

The following assertion simplifies calculations.

Lemma 1.1. *Denote by g_{ij} and B_{ij} the matrices of the first and the second fundamental forms of a regular surface $S \subset E^3$, respectively. A caustic of the reflected front of the surface S is the same as a focal set of a surface with the first and second fundamental forms given by*

$$g^*_{ij} = g_{ij} - (\partial_j \mathbf{r}, \mathbf{a})(\partial_i \mathbf{r}, \mathbf{a}), \qquad B^*_{ij} = -2\cos\theta B_{ij}. \tag{1.4}$$

Proof. Let

$$\rho = \mathbf{r} + \lambda \cdot \mathbf{b} \quad (\lambda \geq 0) \tag{1.5}$$

be a parametric equation of the reflected front, where $\mathbf{b}$ is given by (1.1). Let us show that $\mathbf{b}$ is a unit normal vector field of the reflected front. Indeed,

$$\partial_i \rho = \partial_i \mathbf{r} + \partial_i \lambda \cdot \mathbf{b} + \lambda \cdot \partial_i \mathbf{b} \tag{1.6}$$

and hence $(\partial_i \rho, \mathbf{b}) = (\partial_i \mathbf{r}, \mathbf{b}) + \partial_i \lambda = (\partial_i \mathbf{r}, \mathbf{b}) - (\partial_i \mathbf{r}, \mathbf{a}) = 0$. Let g and B are the first and the second fundamental forms of S. Denote by g^* and B^* the first and the second fundamental forms of the reflected front. Denote, in addition, $b^*_{ij} = (\partial_i \mathbf{b}, \partial_j \mathbf{b})$ and $\cos\theta = (\mathbf{a}, \mathbf{n})$. Then

$$g^*_{ij} = g_{ij} + 4\lambda\cos\theta B_{ij} + \lambda^2 b^*_{ij} - (\partial_i \mathbf{r}, \mathbf{a})(\partial_j \mathbf{r}, \mathbf{a}), \qquad B^*_{ij} = -2\cos\theta B_{ij} + \lambda b^*_{ij}.$$

To prove this, remark that $g^*_{ij} = (\partial_i \rho, \partial_j \rho)$. From (1.1) and (1.2) it follows that

$$\partial_i \mathbf{b} = -2(\mathbf{a}, \partial_i \mathbf{n})\mathbf{n} - 2(\mathbf{a}, \mathbf{n})\partial_i \mathbf{n}, \quad \partial_i \lambda = -(\partial_i \mathbf{r}, \mathbf{a}), \quad \partial_i \rho = \partial_i \mathbf{r} - (\partial_i \mathbf{r}, \mathbf{a})\mathbf{b} + \lambda \partial_i \mathbf{b}.$$

Thus we have

$$B^*_{ij} = -\Big(\partial_i \rho, \partial_j \mathbf{b}\Big) = -\Big(\partial_i \mathbf{r} + \partial_i \lambda \cdot \mathbf{b} + \lambda \cdot \partial_i \mathbf{b}, \partial_j \mathbf{b}\Big) = -(\partial_i \mathbf{r}, \partial_j \mathbf{b}) - \lambda b^*_{ij} = -2(\mathbf{a}, \mathbf{n})B_{ij} - \lambda b^*_{ij},$$
$$g^*_{ij} = (\partial_i \rho, \partial_j \rho) = \Big(\partial_i \mathbf{r} - (\partial_i \mathbf{r}, \mathbf{a})\mathbf{b} + \lambda \partial_i \mathbf{b}, \partial_j \rho\Big) = \Big(\partial_i \mathbf{r}, \partial_j \rho\Big) + \lambda\Big(\partial_i \mathbf{b}, \partial_j \rho\Big) = g_{ij} - (\partial_j \mathbf{r}, \mathbf{a})(\partial_i \mathbf{r}, \mathbf{a}) + 2\lambda(\mathbf{a}, \mathbf{n})B_{ij} - \lambda B^*_{ij}.$$

The caustic of reflected front is nothing else but its focal surface. The latter is formed by striction lines of ruled surface generated by the unit normal vector field along lines of curvature of the reflected front. It is well known that Gaussian curvature of the latter ruled surface has to be zero. If $\mathbf{X} = X^1 \partial_1 \rho + X^2 \partial_2 \rho$ is tangent to line of curvature of the reflected front, then the condition on Gaussian curvature takes the form

$$(\partial_X \rho, \partial_X \mathbf{b}, \mathbf{b}) = (\partial_X \mathbf{r} - (X, \mathbf{a})\mathbf{b} + \lambda \partial_X \mathbf{b}, \partial_X \mathbf{b}, \mathbf{b}) = (\partial_X \mathbf{r}, \partial_X \mathbf{b}, \mathbf{b}) = 0. \tag{1.7}$$

The condition (1.7) does not depend on λ and is equivalent to the condition on $\mathbf{X}$ to be tangent to principal direction of the reflected front at the initial moment, when the reflected front and the mirror surface coincide pointwise, i.e. when $\lambda = 0$. As a consequence, the caustic can be found as a focal surface of reflected front at the moment $\lambda = 0$. Therefore, to find the caustic we can take

$$g^*_{ij} = g_{ij} - (\partial_j \mathbf{r}, \mathbf{a})(\partial_i \mathbf{r}, \mathbf{a}), \qquad B^*_{ij} = -2\cos\theta B_{ij},$$

where $\cos\theta = (\mathbf{a}, \mathbf{n})$ is the angle function between the incident rays and the unit normal vector field of the surface. □

Theorem 1.2. *Let S be a regular surface of non-zero Gaussian curvature parameterized by position-vector $\mathbf{r}$ and $\mathbf{n}$ be a the unit normal vector field of S. Denote by $\mathbf{a}$ ($|\mathbf{a}| = 1$) a direction of incident rays. Then there exist two caustics of the reflected front and their parametric equations can be given by*

$$\xi^* = \mathbf{r} + \frac{1}{k^*_i}\mathbf{b} \quad (i = 1, 2),$$

where $\mathbf{b} = \mathbf{a} - 2(\mathbf{a}, \mathbf{n})\mathbf{n}$ is a direction of reflected rays and k^*_i are the roots of the equation

$$(k^*)^2 + 2\cos\theta\big(2H + k_n(a_t)\tan^2\theta\big)k^* + 4K = 0,$$

where H is the mean curvature, K is the Gaussian curvature and $k_n(a_t)$ is the normal curvature of the surface in a direction of tangential projection of the incident rays.

Proof. Introduce on the surface the curvature coordinates (u^1, u^2). Then

$$g = \begin{pmatrix} g_{11} & 0 \\ 0 & g_{22} \end{pmatrix}, \quad B = \begin{pmatrix} k_1 g_{11} & 0 \\ 0 & k_2 g_{22} \end{pmatrix},$$

where k_1 and k_2 are the principal curvatures of the surface S. Introduce the orthonormal frame

$$\mathbf{e}_1 = \frac{1}{\sqrt{g_{11}}}\partial_1 \mathbf{r}, \quad \mathbf{e}_2 = \frac{1}{\sqrt{g_{22}}}\partial_2 \mathbf{r}, \quad \mathbf{e}_3 = \mathbf{n}. \tag{1.8}$$

Decompose $\mathbf{a} = a_1 \mathbf{e}_1 + a_2 \mathbf{e}_2 + a_3 \mathbf{e}_3 \quad (a_1^2 + a_2^2 + a_3^2 = 1)$. We have

$$B^* = -2a_3 \begin{pmatrix} k_1 g_{11} & 0 \\ 0 & k_2 g_{22} \end{pmatrix}, \qquad g^* = \begin{pmatrix} g_{11}(1 - a_1^2) & -\sqrt{g_{11}g_{22}}a_1 a_2 \\ -\sqrt{g_{11}g_{22}}a_1 a_2 & g_{22}(1 - a_2^2) \end{pmatrix}.$$

Figure 1.1: Caustic of the hemi-sphere when the rays are parallel to the hemi-sphere axis of symmetry (left) and non parallel to this axis (right)

Then, evidently,

$$\det g^* = g_{11}g_{22}(1-a_1^2-a_2^2) = g_{11}g_{22}a_3^2.$$

The Weingarten matrix is

$$A^* = -\frac{2}{a_3}\begin{pmatrix} (1-a_2^2)k_1 & a_1a_2k_2\sqrt{\frac{g_{22}}{g_{11}}} \\ a_1a_2k_1\sqrt{\frac{g_{11}}{g_{22}}} & (1-a_1^2)k_2 \end{pmatrix}.$$

Thus, the characteristic equation on k_i^* takes the form

$$(k^*)^2 + \frac{2}{a_3}\Big((a_1^2+a_3^2)k_1 + (a_2^2+a_3^2)k_2\Big)k^* + 4k_1k_2 = 0,$$

or

$$(k^*)^2 + 2a_3\Big(k_1+k_2+\frac{a_1^2k_1+a_2^2k_2}{a_3^2}\Big)k^* + 4k_1k_2 = 0.$$

It remains to notice that $k_1+k_2 = 2H$, $k_1k_2 = K$, $a_1^2k_1+a_2^2k_2 = B(a_t,a_t) = k_n(a_t)g(a_t,a_t) = k_n(a_t)\sin^2\theta$ and $a_3 = \cos\theta$. As a result, we obtain

$$(k^*)^2 + 2\cos\theta\big(2H + k_n(a_t)\tan^2\theta\big)k^* + 4K = 0.$$

If we denote by k_i^* the roots, then the equation of caustic of the reflected front takes the form

$$\xi_i^* = \mathbf{r} + \frac{1}{k_i^*}\mathbf{b}.$$

Evidently, $k_1^*k_2^* = 4K$ and hence, if $K \neq 0$, then both of caustics exit. □

Example 1.3. ***The sphere of radius*** 1. We have $k_1 = k_2 = 1$, $K = 1, H = 1$, $k_n(a_t) = 1$ and hence the equation on k^* takes the form

$$(k^*)^2 + 2\Big(\cos\theta + \frac{1}{\cos\theta}\Big)k^* + 4 = 0$$

with evident solutions $k_1^* = -2\cos\theta$, $\quad k_2^* = -\frac{2}{\cos\theta}$ So, the parametric equations of caustics of the reflected front take the forms

$$\xi_1^* = \mathbf{r} - \frac{1}{2\cos\theta}\mathbf{b}, \quad \xi_2^* = \mathbf{r} - \frac{\cos\theta}{2}\mathbf{b}.$$

Take a local parameterization for the sphere as $\mathbf{r} = \{\cos u\cos v, \cos u\sin v, \sin u\}$ and suppose $\mathbf{a} = \{0,0,1\}$. Then $\cos\theta = (\mathbf{a},\mathbf{n}) = -\sin u$ where $u \in (0,\pi/2)$. Thus, we have two caustics

$$\xi_1^* = \left\{0, 0, \frac{1}{2\sin u}\right\}, \qquad \xi_2^* = \left\{\cos^3 u\cos v, \cos^3 u\sin v, \frac{\sin u}{2}(2\cos^2 u + 1)\right\}.$$

The first caustic degenerates into a straight line, the second one is a surface of revolution generated by the caustic of plane circle (see Figure 1.1)

Example 1.4. ***General surface of revolution.*** We have

$$\mathbf{r} = \{x(u)\cos(v), x(u)\sin(v), z(u)\}, \quad \big((x')^2 + (z')^2 = 1\big)$$

and let $\mathbf{a} = \{0,0,1\}$. Then

$$\mathbf{e}_1 = \{x'\cos v, x'\sin v, z'\},$$
$$\mathbf{e}_2 = \{-\sin v, \cos v, 0\},$$
$$\mathbf{e}_3 = \{-z'\cos v, -z'\sin v, x'\}$$

and hence $\mathbf{a} = z'\mathbf{e}_1 + x'\mathbf{e}_3$, i.e. $a_1 = z', a_2 = 0, a_3 = x'$. The equation on k^* takes the form

$$(k^*)^2 + 2\Big(\frac{k_1}{a_3} + a_3k_2\Big)k^* + 4k_1k_2 = 0$$

with evident solutions $k_1^* = -\frac{2k_1}{a_3}$, $\quad k_2^* = -2a_3k_2$. The caustics are

$$\xi_1^* = r - \frac{a_3}{2k_1}\mathbf{b}, \quad \xi_2^* = r - \frac{1}{2k_2a_3}\mathbf{b},$$

where

$$\mathbf{b} = \mathbf{a} - 2a_3\mathbf{n} = z'\mathbf{e}_1 - x'\mathbf{e}_3 = \{2x'z'\cos v, 2x'z'\sin v, (z')^2 - (x')^2\}.$$

So we have

$$\xi_1^* = \left\{ \left(x - \frac{(x')^2z'}{(z''x' - z'x'')}\right)\cos v, \left(x - \frac{(x')^2z'}{(z''x' - z'x'')}\right)\sin v, z - \frac{x'((z')^2 - (x')^2)}{2(z''x' - z'x'')} \right\}, \qquad \xi_2^* = \left\{0, 0, z - \frac{x((z')^2 - (x')^2)}{2x'z'}\right\}$$

The ξ_1^* is a surface of revolution generated by caustic of curve on a plane in case when incident rays are parallel to the axis of revolution. The caustic ξ_2^* is the degenerated one.

Example 1.5. ***Translation surface***. Let us be given a translation surface $\mathbf{r} = \{x, y, f(x) + h(y)\}$ and suppose $\mathbf{a} = \{0, 0, 1\}$. Then

$$\mathbf{n} = -\frac{\partial_x\mathbf{r} \times \partial_y\mathbf{r}}{|\partial_x\mathbf{r} \times \partial_y\mathbf{r}|} = \frac{1}{\sqrt{1 + f_x^2 + h_y^2}}\{f_x, h_y, -1\}$$

and

$$\mathbf{b} = \frac{1}{1 + f_x^2 + h_y^2}\{2f_x, 2h_y, -1 + f_x^2 + h_y^2\}.$$

A direct computation show that in this case

$$g^* = \begin{pmatrix} 1 & 0 \\ 0 & 1 \end{pmatrix}, \quad B^* = \frac{2}{1 + f_x^2 + h_y^2}\begin{pmatrix} -f_{xx} & 0 \\ 0 & -h_{yy} \end{pmatrix}$$

and hence

$$\frac{1}{k_1^*} = -\frac{1 + f_x^2 + h_y^2}{2f_{xx}}, \quad \frac{1}{k_2^*} = -\frac{1 + f_x^2 + h_y^2}{2h_{yy}}.$$

Therefore, the equations of caustics take the forms

$$\xi_1^* = \{x, y, f(x) + h(y)\} - \frac{1}{2f_{xx}}\{2f_x, 2h_y, -1 + f_x^2 + h_y^2\},$$

$$\xi_2^* = \{x, y, f(x) + h(y)\} - \frac{1}{2h_{yy}}\{2f_x, 2h_y, -1 + f_x^2 + h_y^2\}.$$

In partial case of the *hyperbolic paraboloid* $\mathbf{r} = \left\{x, y, \frac{1}{2}x^2 - \frac{1}{2}y^2\right\}$ we have $f_x = x, f_{xx} = 1, h_y = -y, h_{yy} = -1$ and after simplifications we get

$$\xi_1^* = \left\{0, 2y, \frac{1}{2} - y^2\right\}, \qquad \xi_1^* = \left\{2x, 0, x^2 - \frac{1}{2}\right\}.$$

The caustics degenerate into two parabolas (See Figure 1.2). In partial case of *elliptic paraboloid* $\mathbf{r} = \left\{x, y, \frac{1}{2}x^2 + \frac{1}{2}y^2\right\}$ the both caustics degenerate into one point $\left(0, 0, \frac{1}{2}\right)$ (see Figure 1.3 for the other cases)

Figure 1.2: Reflected caustics of hyperbolic paraboloid in case of incident rays parallel to the axis of symmetry (left) and non-parallel to this axis (right)

Example 1.6. ***Cylinder over curve in a plane***. Consider a cylinder based on a naturally parameterized curve $\gamma(s)$ in xOy plane and suppose the rulings are directed along the Oz axis. Then the parametric equation of the cylinder is $\mathbf{r} = \gamma + t\,\mathbf{e}_3$. Denote by $\tau = \gamma_s'$ and ν the Frenet frame of the curve. The orthonormal tangent frame of the surface consists of τ and $\mathbf{e}_3$. The unit normal vector field of the surface is ν. Suppose $\mathbf{a} \perp \mathbf{e}_3$. Then the decomposition of $\mathbf{a}$ with respect to the frame $\tau, \mathbf{e}_3, \nu$ takes the form

$$\mathbf{a} = \sin\theta\ \tau + \cos\theta\ \nu.$$

The principal curvatures of this kind of cylinder are $k_1 = k(s)$ and $k_2 = 0$, where $k(s)$ is the curvature of γ. Hence $K = 0$, $2H = k(s)$. In addition, the first and second fundamental forms are

$$g = \begin{pmatrix} 1 & 0 \\ 0 & 1 \end{pmatrix}, \quad B = \begin{pmatrix} k(s) & 0 \\ 0 & 0 \end{pmatrix},$$

Figure 1.3: Two reflected caustics of elliptic paraboloid in case of incident rays parallel non-parallel to the axis of symmetry

respectively. Thus we have the following equation on k^*

$$(k^*)^2 + 2\left(k(s)\cos\theta + \frac{1}{\cos\theta}k(s)\sin^2\theta\right)k^* = 0.$$

We have two solutions

$$(1)\ \ k^* = 0, \quad (2)\ \ k^* = -\frac{2k(s)}{\cos\theta}.$$

The solution (1) gives rise to "caustic" at infinity. The solution (2) gives rise to cylinder over caustic of the curve γ

$$\xi^* = \mathbf{r} - \frac{\cos\theta}{2k(s)}(\sin\theta\,\tau - \cos\theta\,\nu) = \mathbf{r} + \frac{(\mathbf{a},\nu)}{2k(s)}(-(\mathbf{a},\tau)\tau + (\mathbf{a},\nu)\nu),$$

which is the same as one can find in textbooks (see, e.g. [10], p. 109).

2. Caustics by reflection in case of spherical incident front.

In this section we consider the case when the source of the rays is located at the origin.

Theorem 2.1. *Let S be a regular surface parameterized by position-vector $\mathbf{r}$ and $\mathbf{n}$ be a the unit normal vector field of S. Denote by $\mathbf{a} = \frac{\mathbf{r}}{r}$ $(r = |\mathbf{r}|)$ a direction of incident rays. Denote by k_i^* $(i = 1,2)$ the solutions of*

$$\left(k^* + \frac{1}{r}\right)^2 + 2\cos\theta\left(2H + k_n(a_t)\tan^2\theta\right)\left(k^* + \frac{1}{r}\right) + 4K = 0,$$

where H is the mean curvature, K is the Gaussian curvature and $k_n(a_t)$ is the normal curvature of the surface in a direction of tangential projection of the incident rays. Then, over each local domain where $k_i^* \neq 0$, the parametric equations of caustics of the reflected front can be given by

$$\xi_i^* = \mathbf{r} + \frac{1}{k_i^*}\mathbf{b},$$

where $\mathbf{b} = \mathbf{a} - 2(\mathbf{a},\mathbf{n})\mathbf{n}$ is a direction of the reflected rays .

Proof. By Lemma 1.1, we can restrict our research to the case $\lambda = 0$. Denote $r = |\mathbf{r}|$. After computations we get

$$g_{ij}^* = g_{ij} - (\partial_j\mathbf{r},\mathbf{a})(\partial_i\mathbf{r},\mathbf{a}), \qquad B_{ij}^* = -2\cos\theta B_{ij} - (\partial_i\mathbf{r},\partial_j\mathbf{b}) = -2\cos\theta B_{ij} - \frac{1}{r}g_{ij}^* \tag{2.1}$$

This means that in this case the Weingarten matrix W^* takes the form

$$W^* = A^* - \frac{1}{r}E,$$

where A^* is a matrix of the same structure as the Weingarten matrix of the flat front. The equation on k^* take the form

$$\det\left(A^* - \left(k^* + \frac{1}{r}\right)E\right) = 0$$

or

$$\left(k^* + \frac{1}{r}\right)^2 + 2\cos\theta\left(2H + k_n(a_t)\tan^2\theta\right)\left(k^* + \frac{1}{r}\right) + 4K = 0 \tag{2.2}$$

If we denote by k_i^* the solution for (2.2), then the parametric equation of the caustic takes the form

$$\xi_i^* = \mathbf{r} + \frac{1}{k_i^*}\mathbf{b}$$

provided that $k_i^* \neq 0$ over a local domain. □

Example 2.2. ***The sphere of radius 1 centered at the origin***. Suppose the emitting point is at the origin and hence

$$r = 1, \mathbf{a} = \mathbf{r} = -\mathbf{n}, \quad \theta = \pi, H = K = 1.$$

Then the equation on k^* takes the form $(k^*+1)^2 - 4(k^*+1) + 4 = 0$, i.e. $k^* = 1$ and hence $\xi^* = \mathbf{r} + \mathbf{n} = 0$.

Figure 2.1: Caustic inside the sphere when the source is located not far from the center (left). This caustic itself (right)

Figure 2.2: Caustic inside the three-axis ellipsoid when the source is located not far from the center of symmetry

If the source does not located at the center, the caustic of reflected front has rather complicated structure, see Figure 2.1.
Inside three-axis ellipsoid in case of source does not located at the center of symmetry (but not too far from it), the caustic can be seen at Figure 2.2.

Example 2.3. ***Cylinder over curve in a plane***. Consider a cylinder based on a naturally parameterized curve $\gamma(\mathbf{s})$ in xOy plane and suppose the rulings are directed along the Oz axis. Then the parametric equation of the cylinder is $\mathbf{r} = \gamma + t\,\mathbf{e}_3$. Denote by $\tau = \gamma_s'$ and ν the Frenet frame of the curve. The orthonormal tangent frame of the surface consists of τ and $\mathbf{e}_3$. The unit normal vector field of the surface is ν. Denote $r = |\mathbf{r}|$ and $\mathbf{a} = \frac{\mathbf{r}}{r}$. Then the decomposition of $\mathbf{a}$ with respect to the frame τ, $\mathbf{e}_3$, ν takes the form

$$\mathbf{a} = \sin\theta\,\cos\alpha\,\tau + \sin\theta\,\sin\alpha\,\mathbf{e_3} + \cos\theta\,\nu.$$

As it well known, the principal curvatures of this kind of a cylinder are $k_1 = k(s)$ and $k_2 = 0$, where $k(s)$ is the curvature of γ. Hence $K = 0,\ 2H = k(s)$. In addition, the first and second fundamental forms are

$$g = \begin{pmatrix} 1 & 0 \\ 0 & 1 \end{pmatrix} \quad \text{and} \quad B = \begin{pmatrix} k(s) & 0 \\ 0 & 0 \end{pmatrix},$$

respectively. Thus we have the equation on k^* of the following form

$$\left(k^* + \frac{1}{r}\right)^2 + 2\left(k(s)\cos\theta + \frac{1}{\cos\theta}k(s)\sin^2\theta\cos^2\alpha\right)\left(k^* + \frac{1}{r}\right) = 0.$$

We have two solutions

$$(1)\ \ k^* = -\frac{1}{r} \quad (2)\ \ k^* = -\frac{1}{r} - \frac{2k(s)}{\cos\theta}\left(\cos^2\theta + \sin^2\theta\cos^2\alpha\right).$$

The cross-section $\alpha = 0$ is the caustic of rays reflected by the curve γ in xOy- plane. The equation takes the form

$$\xi^* = \mathbf{r} - \frac{\cos\theta}{\frac{\cos\theta}{r} + 2k(s)}(\sin\theta\,\tau - \cos\theta\,\nu) = \mathbf{r} + \frac{(\mathbf{r},\nu)}{(\mathbf{r},\nu) + 2r^2k(s)}(-(\mathbf{r},\tau)\tau + (\mathbf{r},\nu)\nu),$$

which is the same as one can find in textbooks (see, e.g. [10], p. 109).

3. Conclusion

In this paper we have found exact and simple parameterization of caustics of reflected wave fronts by using purely geometric approach. Now we know which geometric characteristic of a mirror surface define geometry of the caustic, how the location of the surface with respect to incident pencil of rays changes the caustic. As a byproduct, the results allow to get fast and exact formulas for computer simulation of caustics of reflected fronts that can be used both in geometry and engineering. The examples approve the calculations and have nice visual representations.

References

[1] J. W. Bruce, P. J. Giblin, C. G. Gibson. On caustics by reflexion, Topology 21(2) (1982), 179–199.
[2] Chr. Georgiou, Th. Hasanis, D. Koutroufiotis. On the caustic of a convex mirror. Geometriae Dedicata 28 (1988), 153–169.
[3] S. Izumiya, Perestroikas of optical wave fronts and graphlike Legendrian unfoldings. J. Differential Geom. 38 (1993) 485–00.
[4] S. Izumiya, M. Takahashi. On caustics of submanifolds and canal hypersurfaces in Euclidean space. Topology and its Applications, 159 (2012) 501 – 508.
[5] S. Izumiya, M. Takahashi, Caustics and wave front propagations: Applications to differential geometry, in: Geometry and Topology of Caustics. Banach Center Publ. 82 (2008), 125–142.
[6] J. Chen, H. Liu, J. Miao. Caustics of translation surfaces in Euclidean 3-space. Nonlinear Sci. Appl., 10 (2017), 5300 – 5310. doi:10.22436/jnsa.010.10.16
[7] G. Glaeser. Refections on spheres and cylinders of revolution. Journal for Geometry and Graphics. 3(2) (1999), 121 – 139.
[8] D. R. J. Chillingworth, G. R. Danesh-Narouie, B. S. Westcott. On Ray-Tracing Via Caustic Geometry. IEEE transactions on antennas and propagation. 38(5) May 1990, 625 - 632
[9] M. Kokubu, W. Rossman, M. Umehara and K. Yamada. Flat fronts in hyperbolic 3-space and their caustics, J. Math. Soc. Japan 59(1) (2007), 265 – 299
[10] Rovenski V.: Geometry of Curves and Surfaces with MAPLE. Birkhäuser Boston, 2000.